Function of the *Synechocystis* RNA helicase, CrhR, and its cyanobacterial homologs

by

Denise Samantha Whitford

A thesis submitted in partial fulfillment of the requirements for the degree of

Doctor of Philosophy

Department of Biological Sciences

University of Alberta

Abstract

RNA helicases function in all aspects of RNA metabolism, regulating a diverse range of cellular processes by rearranging RNA structures and mediating RNA-protein interactions. Prokaryotic RNA helicases have been shown to have roles in RNA degradation, ribosome biogenesis and translation, with their effects on these processes enhanced during abiotic stress. The model cyanobacterium *Synechocystis* sp. PCC 6803 encodes a single DEAD-box RNA helicase, CrhR. CrhR expression is known to be regulated by a variety of abiotic stresses, sensed through the redox poise of the photosynthetic electron transport chain; however, the cellular role of CrhR is unknown.

Evidence is presented that is consistent with CrhR performing roles in translation and RNA processing/degradation. CrhR co-precipitates with actively translating polysomes and components of the RNA degradosome, an interaction that is RNA-dependent. CrhR was also found to localize to the thylakoid membrane space in *Synechocystis.* The helicase also enhances processing of its own dicistronic transcript, at a site with sequence and structural features sufficient for cleavage by recombinant RNase E *in vitro*. CrhR participation in translation and RNA processing/degradation, combined with prior transcriptomic and proteomic studies, suggest CrhR regulates expression of genes involved in photosynthesis, energy metabolism, carbon metabolism, and protein stability and turnover. Related to these crucial metabolic pathways, it is shown that CrhR is regulated in response to nitrogen availability. Similar to other abiotic stresses, *crhR* mutation affects growth rate and abundance of photosynthetic pigments differentially in response to various sources of fixed nitrogen. Cyanobacterial nitrogen metabolism is interconnected with photosynthetic energy transfer, enhanced reduction of which

regulates CrhR expression. This links the role of CrhR during nitrogen stress with the other characterized abiotic stresses that are sensed through the redox poise of the photosynthetic electron transport chain.

Conservation of CrhR throughout the majority of cyanobacterial diversity was also shown. These CrhR-like helicases form a separate clade, defined by a characteristic highly conserved sequence motif in the C-terminus that is unique to cyanobacterial DEAD-box proteins. It is believed that this motif may function in substrate specificity or auto-regulation of CrhR abundance.

In this thesis, a function for CrhR in regulating maintenance of photosynthesis and thylakoid membranes, particularly energy transfer, through the effects of CrhR on RNA maturation, stability and translation is proposed. This function, unique to cyanobacterial DEAD-box RNA helicases, appears to be conserved throughout cyanobacteria that encode CrhR-like helicases.

Preface

The introduction in chapter 1 and concluding analysis in chapter 6 are solely my original work. Contributions of collaborators for chapters 2-5 are detailed below.

Chapter 2: A version of this chapter has been published as A.R.R. Rosana, D.S. Whitford, R.P. Fahlman and G.W. Owttrim, 2016. "Cyanobacterial RNA helicase CrhR localizes to the thylakoid membrane region and cosediments with degradosome and polysome complexes in *Synechocystis* sp. strain PCC 6803," Journal of Bacteriology, vol. 198, no. 15, 2089-2099. I was jointly responsible for data collection and analysis, and manuscript composition with A.R.R. Rosana. R.P. Fahlman assisted with mass spectroscopy data collection and analysis. A project student, C.A. Stevens, created the CrhR-GFP fusions in Figures 2.9-2.10 and performed the microscopy under my supervision. G.W. Owttrim was the supervisory author and was involved with project design and manuscript composition.

Chapter 3: A version of this chapter has been published as A.R.R. Rosana, D.S. Whitford, A. Migur, C. Steglich, S.L. Kujat-Choy, W.R. Hess and G.W. Owttrim. 2020. "RNA helicase-regulated processing of the *Synechocystis rimO-crhR* operon results in differential cistron expression and accumulation of two sRNAs," Journal of Biological Chemistry, vol. 295, 6372-6386. Some of the research conducted for this chapter forms part of an international research collaboration, led by G.W. Owttrim at the University of Alberta, with W.R. Hess being the lead collaborator at the University of Freiburg. A.R.R. Rosana and I were jointly responsible for data acquisition, analysis and manuscript composition. A.R.R. Rosana performed the Northern analyses presented in Figures 3.3 and 3.5-3.9 and the 5' RACE in Figure 3.11. S.L. Kujat-Choy performed the S1 nuclease and primer extension analysis presented in Figure 3.11. A. Migur (University of Freiburg) performed the RNase E assay presented in Figure 3.14. W.R. Hess performed the *in silico* RNA-RNA interaction analysis presented in Table 3.3 and Figure 3.10. G.W. Owttrim, C. Steglich and W.R. Hess provided supervision, and were involved in concept formation and manuscript composition and editing.

Chapter 4: I designed and performed experiments and wrote the manuscript for Chapter 4. A project student, L.A. Brand, performed the analysis of NtcA as a transcription factor for the *slr0082-crhR* operon promoter presented in Table 4.2. G.W. Owttrim was involved with experiment design, data analysis and manuscript composition.

Chapter 5: A preliminary phylogenetic tree of 72 cyanobacterial DEAD-box RNA helicase sequences prepared by J. Georg and W.R. Hess (University of Freiburg) inspired this project. I designed and performed the bioinformatic analyses and wrote the manuscript for Chapter 5. G.W. Owttrim was involved with design and analysis.

Acknowledgements

Many individuals from within the University of Alberta community, collaborative research groups and my personal support network have supported me during my graduate program. I have tremendous gratitude to each of them for their advice, assistance, generosity and kindness. I wish to personally acknowledge a few individuals and groups who have had a significant impact on me during my graduate studies:

My supervisor, Dr. George Owttrim, who helped guide me through my research projects, mentored me in my teaching, and even collected samples for me when scheduling didn't work out. Most of all, he always had time for a cup of tea when I needed advice or encouragement. Thank you for everything!

My supervisory committee, Dr. Lisa Stein and Dr. Richard Fahlman, for their advice and feedback, as well as assistance with accessing equipment and reagents for these projects.

My fellow graduate students in the Owttrim lab, particularly Albert, Aleks, Jason, Brendan, Logan and Sean, for your assistance, advice and camaraderie. Your support made learning new techniques, interpreting confusing results and trouble-shooting problematic procedures infinitely easier!

The undergraduate project students I had the privilege of mentoring. Your expectations of me and interest in what you were doing pushed me to always keep learning and developing my knowledge and skills.

The instructors and coordinators I worked with when teaching: George, Anthony, Cec and Rich. You provided me with support and guidance when I needed it, but also pushed me to rely on myself when I was ready. Your support, both in relation to teaching, but also my project and life, was so valuable.

My parents and family for your support and your patience. The value you placed on education and lifelong learning contributed to my interest in graduate studies. You molded me into someone who wanted the opportunity to continue learning and exploring, and have supported me through every step of that process. Even when I've been busy or frazzled, I've always known you're there with me.

My partner, Jeffrey, for supporting me through a program that was initially just a two-year MSc… and then wasn't. You could always be relied on for a cup of tea or a homemade pizza when I was busy, or encouraging words when you were out of town. Thank you for being understanding and supportive of my dreams and ambitions.

And finally, to our cat, Fiona, thank you for not accidentally deleting my thesis the many times you walked across or sat on my keyboard!

Table of Contents

Chapter 1: Introduction **1**

1.1 Cyanobacteria 2

1.1.1 Phylum Cyanobacteria 2

1.1.2 Cyanobacteria in the environment 3

1.1.3 *Synechocystis* sp. PCC 6803 as a model cyanobacterium 7

1.2 DEAD-box RNA Helicases 10

1.2.1 RNA helicases 10

1.2.2 Structure and biochemistry of DEAD-box RNA helicases 11

1.2.3 DEAD-box RNA helicases in eukaryotes 13

1.2.4 Prokaryotic DEAD-box RNA helicases 14

1.2.4.1 Helicases and the bacterial ribosome 15

1.2.4.2 Helicases in the bacterial RNA degradosome 17

1.2.4.3 ncRNA metabolism in prokaryotes may also involve DEAD-box helicases 19

1.2.5 Cyanobacterial RNA helicases 19

1.3 Thesis objectives 24

Chapter 2: CrhR co-sediments with polysomes and RNA degradosomes, and localizes to the thylakoid membrane **26**

2.1 Summary 27

2.2 Introduction 27

2.3 Experimental procedures 30

2.3.1 Culture conditions and strains 30

2.3.2 Extraction of soluble and insoluble fractions of *Synechocystis* cells 32

2.3.3 Polysome isolation 32

2.3.4 Polysome fractionation 33

2.3.5 Membrane isolation 34

2.3.6 Western analysis 35

2.3.7 Mass spectrometry 35

2.3.8 ciFP and CrhR fusion expressing stains 36

2.4 Results 39
2.4.1 CrhR localizes to fractions containing both the cytoplasm and membranes 39
2.4.2 CrhR cosediments with polysomes 41
2.4.3 *crhR* truncation results in improper polysome association 46
2.4.4 CrhR cosediments with polysome- and degradosome-associated proteins 46
2.4.5 CrhR associates with the thylakoid membrane 53
2.4.6 CrhR localization *in vivo* 56
2.5 Discussion 59
Chapter 3: RNA helicase-regulated processing of the *Synechocystis rimO-crhR* operon results in differential cistron expression and accumulation of two sRNAs 64
3.1 Summary 65
3.2 Introduction 65
3.3 Experimental procedures 67
3.3.1 Cyanobacterial strains and growth conditions 67
3.3.2 RNA manipulation 68
3.3.3 Identification of operon transcripts 71
3.3.4 Primer extension and S1 nuclease protection assays 71
3.3.5 5' RACE-RCA, inverse PCR and DNA sequencing 72
3.3.6 Primary transcript analysis 73
3.3.7 Identification of RNA-RNA interactions 74
3.3.8 RNA structure prediction 74
3.3.9 RNase E cleavage assay 74
3.4 Results 75
3.4.1 Genetic organization of the *rimO-crhR* region in *Synechocystis* sp. PCC 6803 75
3.4.2 Detection of full-length operon transcripts 75
3.4.3 CrhR inactivation results in deregulated expression of the *rimO-crhR* operon 78
3.4.4 *rimO* transcript half-life is not affected by temperature downshift or *crhR* mutation 81

3.4.5 Accumulation of a stable RNA from the *rimO* ORF 81
3.4.6 Accumulation of a stable RNA from the *rimO* 5' UTR 85
3.4.7 Determination of transcript 5' ends in the *rimO-crhR* region 90
3.4.8 Identification of primary transcripts 93
3.4.9 Identification of putative RNase E processing mechanism 96
3.5 Discussion 100
3.5.1 *rimO-crhR* is expressed as a dicistronic operon 101
3.5.2 RNA processing generates monocistronic transcripts with differing fates 101
3.5.3 A role for the CrhR RNA helicase in *rimO-crhR* transcript processing 106
3.5.4 *rimO-crhR* co-transcription and cold stress 107
3.5.5 Conclusion 107
Chapter 4: Regulation of *crhR* expression by fixed nitrogen availability and source 109
4.1 Summary 110
4.2 Introduction 110
4.3 Experimental procedures 116
4.3.1 Bacterial strains and growth conditions 116
4.3.2 Experimental conditions 118
4.3.3 Protein analysis 118
4.3.4 Growth curves 119
4.3.5 Pigment analysis 119
4.3.6 ROS/RNS analysis 119
4.3.7 Inhibitor treatments 120
4.3.8 RNA analysis 121
4.3.9 DNA affinity column purification and mass spectrometry 122
4.4 Results 123
4.4.1 Nitrogen source affects growth and pigmentation 123
4.4.2 Nitrogen source effect on intracellular ROS abundance 129
4.4.3 Nitrogen source effect on CrhR abundance 131
4.4.4 CrhR abundance in response to nitrogen depletion 135
4.4.5 Nitrogen regulation: Requirement for *de novo* synthesis 138

4.4.6 MSX inhibition of nitrogen assimilation affects CrhR expression 140
4.4.7 NtcA interaction with the *rimO* promoter 146
4.5 Discussion 149
Chapter 5: Distribution of DEAD-box RNA helicases in cyanobacteria 157
5.1 Summary 158
5.2 Introduction 158
5.3 Methods 160
5.3.1 Sequence data 160
5.3.2 Sequence alignments and phylogenetic analysis 161
5.3.3 Gene context analysis 161
5.3.4 C-terminal motif identification 162
5.3.5 Pfam domain identification 162
5.3.6 *rpoC* neighbour-joining tree 162
5.4 Results 162
5.4.1 Cyanobacterial DEAD-box RNA helicases form 3 distinct clades 162
5.4.2 CrhR-like proteins are conserved across cyanobacterial diversity 173
5.4.3 A conserved sequence motif in the C-terminus of CrhR-like proteins characterizes the CrhR-like clade 180
5.4.4 CsdA-like proteins are found in primarily unicellular strains of the order *Synechococcales* 180
5.4.5 CsdA-like proteins contain a DbpA RNA binding domain in the C-terminal extension 184
5.4.6 RhlE-like helicases co-occur with another DEAD-box protein 187
5.4.7 Proteins from all three helicase clades are only encoded in four related strains of cyanobacteria 187
5.5 Discussion 191
Chapter 6: Conclusions 196
References 206

List of Tables

Table 2.1: Strains and plasmids used in this chapter. 31
Table 2.2: Oligonucleotides used in this chapter. 37
Table 2.3: Polysome pellet mass spectrometry analysis. 47
Table 3.1: Bacterial strains and plasmids used in this chapter. 69
Table 3.2: Oligonucleotides used in this chapter. 70
Table 3.3: *In silico* predicted *rimO* 5' UTR interacting mRNAs. 88
Table 3.4: Predicted RNA structures at termini of processed transcripts. 105
Table 4.1: Bacterial strains, plasmids and oligonucleotides used in this chapter. 117
Table 4.2: Mass spectrometry analysis of proteins co-purified with the *rimO* promoter. 147
Table 5.1: DEAD-box RNA helicase proteins encoded in cyanobacterial genomes. 164

List of Figures

Figure 1.1: The taxonomy of phylum Cyanobacteria. 4

Figure 1.2: Cyanobacteria in the environment. 6

Figure 1.3: *Synechocystis* sp. PCC 6803. 8

Figure 1.4: Characteristic sequence motifs of SF2 and DEAD-box RNA helicases. 12

Figure 1.5: Genomic mutants of *crhR*. 22

Figure 2.1: pMON ciFP-CrhR and pMON CrhR-ciFP constructs. 38

Figure 2.2: CrhR abundance in cytoplasmic and membrane fractions. 40

Figure 2.3: CrhR localization in soluble *Synechocystis* lysates. 43

Figure 2.4: *Synechocystis* polysome fractionation. 44

Figure 2.5: $CrhR_{TR}$ localization in soluble *Synechocystis* lysates. 45

Figure 2.6: Venn diagram of polysome-associated polypeptides. 52

Figure 2.7: CrhR localization in wild type *Synechocystis* membranes. 54

Figure 2.8: $CrhR_{TR}$ localization in *crhR*$_{TR}$ mutant *Synechocystis* membranes. 55

Figure 2.9: *In vivo* CrhR localization using fusions with citrine fluorescent protein. 57

Figure 2.10: Expression of ciFP and CrhR fusion proteins. 58

Figure 3.1: Genomic organization of the *Synechocystis rimO-crhR* operon. 76

Figure 3.2: *rimO-crhR* operon verification. 77

Figure 3.3: Time course of *rimO* transcript accumulation. 79

Figure 3.4: Time course of *rimO* transcript accumulation in Δ*crhR* cells. 80

Figure 3.5: *rimO* transcript half-life. 82

Figure 3.6: Temperature induction of *rimO* ORF expression. 83

Figure 3.7: *rimO* accumulation in response to temperature acclimation. 84

Figure 3.8: Temperature induction of *rimO* 5' UTR expression. 86

Figure 3.9: *rimO* 5' UTR accumulation at 10°C. 87

Figure 3.10: *In silico* identification of potential *Synechocystis* sequences interacting with the *rimO* 5'UTR. 89

Figure 3.11: Identification of 5' termini of transcripts. 92

Figure 3.12: Detection of primary transcripts. 94

Figure 3.13: Summary of *rimO-crhR* operon transcript start sites and products. 95

Figure 3.14: Evidence for RNase E processing of the *rimO-crhR* operon. 99
Figure 3.15: Model of *rimO-crhR* processing and transcript stability. 103
Figure 4.1: Summary of nitrogen uptake, assimilation and regulation of nitrogen metabolism in cyanobacteria. 113
Figure 4.2: Effect of fixed nitrogen on the growth rate of *Synechocystis.* 124
Figure 4.3: Concentration dependence of the effect of ammonium chloride on *Synechocystis* growth. 125
Figure 4.4: Effect of nitrogen source on *Synechocystis* pigmentation. 127
Figure 4.5: Effect of nitrogen source on the whole cell pigmentation of *Synechocystis*. 128
Figure 4.6: Effect of fixed nitrogen source on intracellular reactive oxygen species. 130
Figure 4.7: Changes in exogenous fixed nitrogen source affect CrhR expression. 132
Figure 4.8: Changes in exogenous fixed nitrogen source affect $CrhR_{TR}$ expression. 133
Figure 4.9: Effect of mixing nitrogen sources on CrhR abundance. 134
Figure 4.10: Nitrogen depletion induces nitrogen-dependent conditional proteolysis of CrhR. 136
Figure 4.11: Northern blots of *crhR* abundance during nitrogen depletion. 137
Figure 4.12: Nitrogen depletion-dependent CrhR proteolysis requires *de novo* protein synthesis. 139
Figure 4.13: MSX treatment is not sufficient to induce chlorosis in *Synechocystis.* 141
Figure 4.14: Response of canonical NtcA-regulated mRNAs *glnB* and *gifA* to MSX treatment. 142
Figure 4.15: CrhR proteolysis can be induced with an inhibitor of glutamine synthetase, MSX. 144
Figure 4.16: Northern analysis of the *rimO-crhR* operon in the presence of MSX. 145
Figure 4.17: Putative NtcA binding sites in the *rimO* promoter. 148
Figure 5.1: Cyanobacterial DEAD-box proteins cluster into three clades. 172
Figure 5.2: Maximum likelihood tree of cyanobacterial DEAD-box RNA helicase proteins. 178
Figure 5.3: Conserved gene sequence surrounding CrhR-like DEAD box RNA helicases. 179

Figure 5.4: The C-terminal extension of CrhR-like helicases contains a unique, highly conserved sequence motif. 182
Figure 5.5: *Gloeobacter violaceus* PCC 7421 DEAD box helicase lacks the CrhR-specific domain. 183
Figure 5.6: The C-terminal extension of the CsdA-like helicases contains a DpbA RNA binding domain. 186
Figure 5.7: Co-occurrence of RhlE-like helicases with CsdA- and CrhR- like proteins. 189
Figure 5.8: Conservation in the C-terminal extension of cyanobacterial DEAD-box proteins. 190
Figure 5.9: *rpoC2* neighbour-joining tree of cyanobacteria that encode CrhR-, CsdA- and RhlE-like helicases. 192
Figure 6.1: CrhR in a *Synechocystis* cell: linking stress-responsive expression through to functions in cellular adaptation. 200

Chapter 1: Introduction

1.1 Cyanobacteria

1.1.1 Phylum Cyanobacteria

Cyanobacteria are oxygenic phototrophic prokaryotes found ubiquitously in aquatic environments across the planet. These organisms may have arisen as early as 3.5 billion years ago, and contributed significantly to the Great Oxidation Event (1). Cyanobacteria were originally classified under the botanical code of nomenclature as a class of algae, referred to as Cyanophyceae or blue-green algae. Cyanophytes were characterized as photosynthetic cells with a 'primitive' cell wall structure, lacking an organized nucleus, and containing chlorophyll *a*, carotenoids and phycobiliproteins as their photosynthetic pigments. While comparisons with bacterial cell structure were ongoing in the late 19th century, particularly in the writings of Ferdinand Cohn, cyanophytes continued to be seen as distinct from bacteria due to the universal and unique nature of photosynthesis in cyanophytes compared to the organisms recognized as bacteria.

Recognition of cyanobacteria as bacteria, and thus prokaryotes, developed in the middle of the 20th century as researchers used advances in the understanding of physiological and biochemical properties of the cell to differentiate eukaryotic protists from prokaryotic bacteria (2). The murein cell wall of cyanobacteria, which stains negative by the Gram method due to the presence of an outer membrane, was one key characteristic used to identify these organisms as bacteria; however, differences exist between cyanobacterial and typical Gram negative cell walls, including a thickened peptidoglycan, increased cross-linking, a chemical composition intermediate between Gram negative and Gram positive cell walls, and the presence of external sheath layers (3). Another characteristic that defined cyanobacteria as bacteria rather than protists was the distribution of the cellular metabolism within the cytoplasm (2). While two key metabolic processes in cyanobacteria, respiration and chlorophyll *a*-dependent photosynthesis, only occur in the presence of the lamellae membranes, the lamellae are distributed throughout the cytoplasm in cyanobacteria cells, in contrast to chloroplasts, the membrane-enclosed photosynthetic organelles of true algae and plants.

While cyanobacteria are now commonly accepted as prokaryotic organisms, the taxonomy of cyanobacteria has become a significant issue for researchers. Inclusion of

cyanobacteria under the bacterial code of nomenclature was formally proposed in 1978, and discussions on harmonization of cyanobacterial nomenclature under the bacterial and botanical codes continue today (4, 5). Presently, taxonomic names used by researchers may be described following either of these systems; however, many of the names in common use are not accepted under either the bacterial or botanical code (5). Molecular phylogeny methods that have been applied to cyanobacteria also indicate that many of the traditional taxa, defined on the basis of morphology and physiology, are polyphyletic (6, 7), requiring reclassification of many species once an acceptable system of nomenclature has been developed.

Cyanobacterial phylogeny has been further complicated by the discovery of species possessing divergent characteristics, including chlorophyll *b* (8), photosynthesis in the absence of structured thylakoid membranes (9), and nitrogen fixation in unicellular cyanobacteria (10). Recently, cyanobacteria that lack the genes required for oxygenic photosynthesis have been discovered (11). Beginning in 2005, cyanobacterial-related sequences were reported in metagenomic projects examining aphotic environments, such as the intestinal microbiota (12). When the genomes of non-photosynthetic organisms closely related to cyanobacteria were reconstructed from a study of subsurface groundwater aquifers and human fecal samples in 2013, a new candidate phylum, 'Melainabacteria', was proposed (11). Based on further analyses of genomes from non-photosynthetic cyanobacteria (13-15), classification into three classes within the phylum Cyanobacteria was proposed: 'Melainabacteria' and 'Sericytochromatia' for the non-photosynthetic cyanobacteria, and 'Oxyphotobacteria' for the photosynthetic cyanobacteria (15). The taxonomical classifications that will be used in this thesis is indicated in Figure 1.1. Note that unless otherwise indicated, use of the term 'cyanobacteria' in this thesis is in reference to the cyanobacteria capable of oxygenic photosynthesis.

1.1.2 Cyanobacteria in the environment

Cyanobacteria are the primary photoautotrophs of the prokaryotic domain of life, commonly found in both fresh- and salt-water environments where they frequently constitute the basis of the food web (16, 17). The diversity of cyanobacterial habitats is

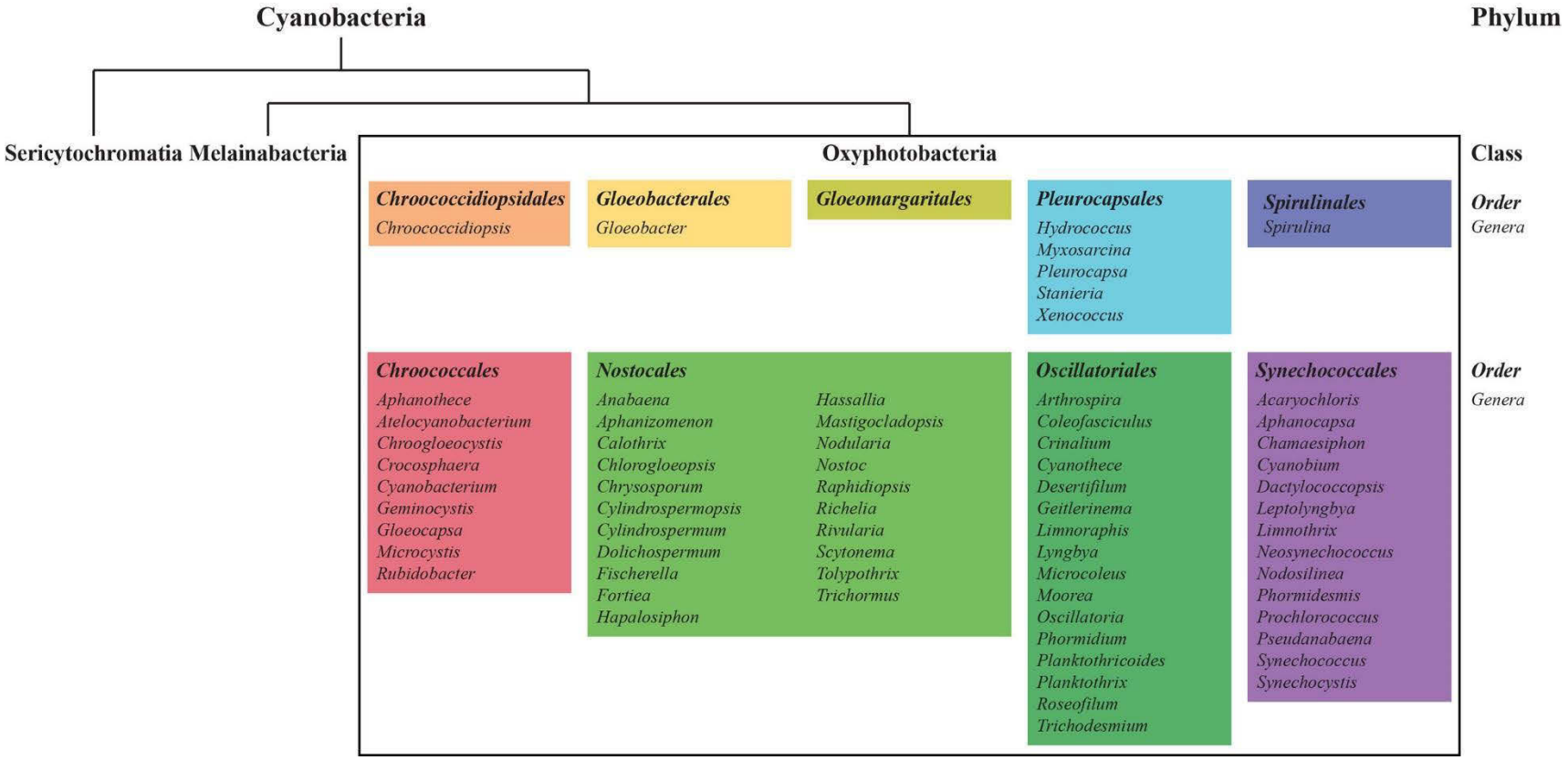

Figure 1.1: The taxonomy of phylum Cyanobacteria.

The dendrogram shows the proposed cyanobacterial classes from Soo *et al.* (15), encompassing the organisms both capable (Oxyphotobacteria) and incapable (Sericytochromatia and Melainabacteria) of performing oxygenic photosynthesis. Oxyphotobacteria, the focus of this thesis, is expanded to show the orders and genera that will be discussed.

not limited to aquatic environments (see Figure 1.2); terrestrial cyanobacteria can be found in surface-exposed layers of soils (typically alkaline), rocks, ice, vegetation and even in the hair of animals (18). In these environments, cyanobacteria influence the cycling of major nutrients, serving as a key biological source of oxygen and fixed carbon via oxygenic photosynthesis, and, in the case of diazotrophic cyanobacteria, fixed nitrogen. Cyanobacteria can also form a symbiotic association with a fungus, which directly relies on the cyanobacterial symbiont for key nutrients (19). These cyanobacteria-containing lichens can be found on the bark of trees, but also as key primary producers in biological soil crusts of arid environments (20). Through influences on biogeochemical cycling and direct interactions with other organisms, cyanobacteria have a profound influence on the biological diversity of their environments.

Cyanobacteria are not the only significant oxygenic photosynthetic organisms. Photosynthetic eukaryotes, such as higher plants and algae, utilize a unique organelle, the chloroplast, which contains all the pigments and electron transport proteins required for photosynthesis (21). The structural and functional similarities between the chloroplast of photosynthetic eukaryotes and cyanobacterial cells, as well as the presence of numerous cyanobacterial gene homologs in nuclear chromosomes of photosynthetic eukaryotes led to the development of an endosymbiotic theory for chloroplast acquisition in eukaryotic photosynthetic organisms (22, 23). The conservation of the proteins and processes in oxygenic photosynthesis between these organisms also supports the endosymbiotic theory, making cyanobacteria an ideal model organism for the study of oxygenic photosynthesis.

Unfortunately, cyanobacteria do not always have beneficial impacts on their environment. Blooms of cyanobacteria often cause a decrease in water quality in their vicinity by producing compounds that alter the taste and odour of the water, as well as a range of hepatotoxins, neurotoxins and dermatoxins (24, 25). Human uses of contaminated water, including for consumption and recreational activities, can be significantly impacted by these harmful cyanobacterial blooms. The toxins and other compounds released by the blooms also pose a major threat to the environment, with effects on the populations of zooplankton, invertebrates, fish and mammals, including humans (25, 26). Harmful effects in the immediate environment also continue following

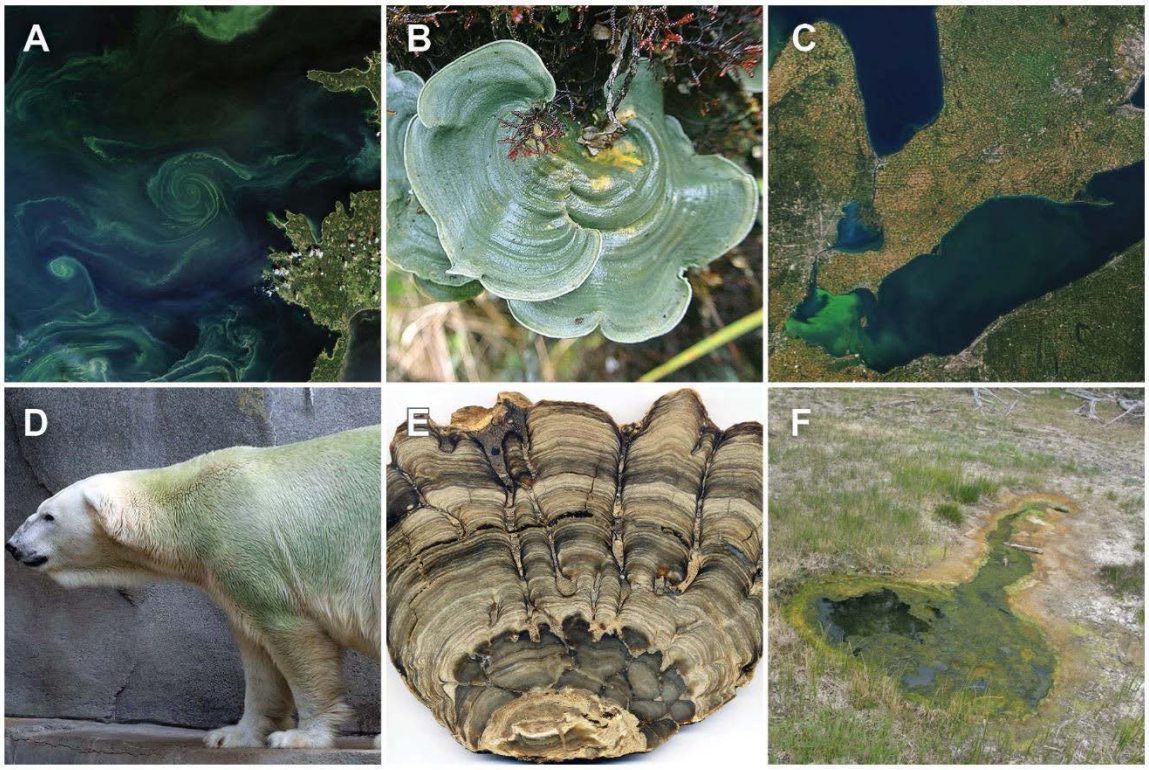

Figure 1.2: Cyanobacteria in the environment.[1]

(A) A heavy bloom of cyanobacteria that occurred off in the Baltic sea in July 2018. (B) The cyanolichen *Dictyonema glabratum*. (C) A toxic *Microcystis* bloom in Lake Erie in September 2013. (D) Cyanobacteria growing in the hair of a polar bear. (E) A stromatolite, a rock formation created by the deposit of sediment onto cyanobacterial mats. (F) Thermophilic organisms, including cyanobacteria, inhabit the hot springs at Yellowstone National Park.

[1] Images in panels A and C were obtained from the NASA Earth Observatory, and are used in accordance with the NASA image use policy. Images in panels B, D, and E were obtained from http;//www flicker.com users Dick Culbert, Asten, and James St. John, respectively. Panels B and E were used under a CC BY 2.0 licence and panel D was used under a CC BY-NC 2.0 licence.

the collapse of the bloom, when the toxins are released and the increasing metabolic activity of heterotrophic bacteria degrading the biomass of the bloom reduces localized oxygen concentrations, resulting in hypoxic zones (27).

Recently, researchers have been working to develop engineered cyanobacteria that will benefit human life, for example, as platforms for bioproduction of fuels and plastics. Introduction of the synthetic pathways for production of fuels, such as ethanol and isobutanol (28), and plastics, such as polyhydroxyalkanoates (29), into cyanobacteria has been successful, although further development of optimized carbon-fixing and regulatory elements is necessary to enhance product yields (30, 31). Cyanobacteria are an appealing platform for bioproduction due to the ability to fix carbon and, in some strains, nitrogen, reducing ongoing costs for input nutrients. They also provide industrial CO_2 emitters with a potential method to utilize waste gases, as CO_2 from flue gases can be used to supply carbon to cyanobacterial bioreactors; however, before cyanobacterial bioreactors become practical, further design work to overcome challenges with light accessibility and maintenance of a sterile environment is necessary (29). Another challenge is controlling expression of the synthetic pathways for bioproduction, with various native gene expression pathways being explored as methods to control expression of the target genes in response changes in the cyanobacterial metabolism, such as a temperature-regulated element linking product production to diurnal cycling (30).

1.1.3 *Synechocystis* sp. PCC 6803 as a model cyanobacterium

Synechocystis sp. PCC 6803 (hereafter *Synechocystis*) was first isolated from a freshwater source near Berkeley, California by R. Kunisawa in 1968 and was initially identified as *Aphanocapsa* sp. str. N-1 (32). The cell morphology (see Figure 1.3) consists of unicellular coccoid cells with division occurring along 2 or more planes (32, 33). The genome of *Synechocystis* consists of a 3.57 Mb circular chromosome (34), four large plasmids: pSYSA (103 kbp), pSYSG (44 kb), pSYSM (120 kb) and pSYSX (106 kb) (35), and 3 small cryptic plasmids: pCA (2.4 kb), pCB (2.4 kb) and pCC (5.2 kb) (36-38). This cyanobacterium is non-diazotrophic, and was initially characterized as an obligate photoautotroph with sporadic gliding motility (32). Variations in glucose-sensitivity and motility, as well as other phenotypes, have been reported for *Synechocystis*, leading to the

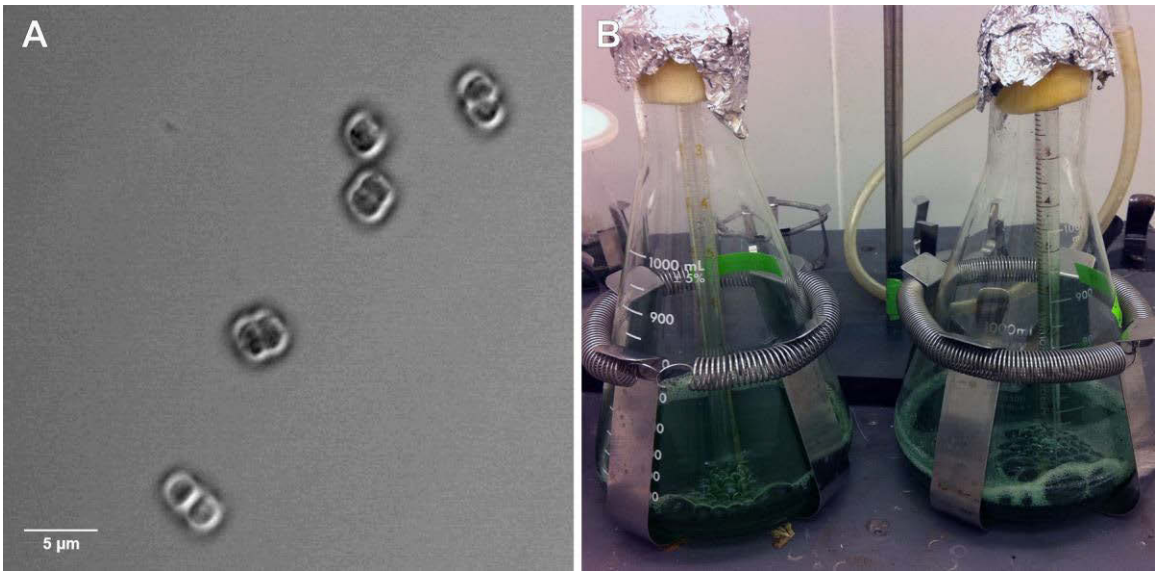

Figure 1.3: *Synechocystis* sp. PCC 6803.

(A) Confocal micrograph of *Synechocystis* sp. PCC 6803 at 63× magnification. (B) *Synechocystis* cultured in liquid BG-11 media. Cultures are supplied with sterile air and agitated to support optimal growth.

development of various sub-strain designations based on strain history and phenotype, and supported by sequence variations (39, 40). The sub-strain of *Synechocystis* used in this thesis is non-motile and capable of facultative photoheterotrophic growth on glucose (41).

Synechocystis has been widely used as a model organism for unicellular cyanobacterial research for many years due to its relative ease of genetic manipulation. It was the first photosynthetic organism to have its complete genome sequenced, which was made available online through the now defunct cyanobacteria-specific sequence database, CyanoBase (42, 43), in addition to more general databases, such as NCBI's GenBank. The original isolate, termed the Berkeley sub-strain (44), is naturally transformable, and can integrate exogenous DNA into the chromosome by homologous recombination to form genetic knockouts (45, 46). A significant challenge in working with recombinant strains of *Synechocystis* has been controlling product yield, both at the levels of DNA copy number and expression. *Synechocystis* is a polyploid organism, with genome copy number ranging from 9 to 218 under normal growth conditions (47, 48). As a result, segregation of chromosomal mutations can be time-consuming, while optimizing the copy number of replicative vectors to yield a biologically relevant quantity of product is challenging as replicative vectors used in *Synechocystis* have generally been restricted to RSF1010-based shuttle vectors (49). Expression-level control of recombinant DNA expression has also been a challenge, as commonly-used prokaryotic expression promoters exhibit unregulated expression in *Synechocystis* (50), possibly due to the differences in the composition of the cyanobacterial RNA polymerase (51). Deficiencies in current knowledge about other key points of expression regulation in cyanobacteria, such as transcription termination, transcript processing and degradation and translation initiation also contribute to challenges in regulating recombinant expression in *Synechocystis* (52). Recent advances have been made in methods for *Synechocystis* genetic manipulation, including a marker-less method for chromosomal mutation (53), CRISPR-based genome editing and knockdowns (54, 55), and development of a modular cloning system, CyanoGate (56); however, research into regulation of gene expression in cyanobacterial systems continues to be of great importance, particularly for bioproduction applications.

1.2 DEAD-box RNA Helicases

1.2.1 RNA helicases

Structured RNAs play important roles in the regulation of RNA processes, such as translation and degradation, thereby affecting expression of the products they regulate and encode. Proteins that alter the secondary structure of RNA, such as RNA helicases, are important for regulating the structure of those RNAs and their influence on cellular processes. RNA helicases are classified within the context of a larger group of proteins, the nucleic acid helicases and translocases. These proteins all share similarities in the structure and biochemical function of their core domains, containing a recombinase A-(RecA) like protein fold with ATPase activity and a binding pocket for polynucleotide duplexes (57, 58). Helicases are generally classified into six superfamilies (SFs) on the basis of conserved sequence motifs and structure, with SF1 and SF2 generally consisting of monomeric and dimeric proteins with two RecA-like domains, while SF3-6 and the translocases function as hexameric or dodecameric toroidal rings of proteins with a single RecA-like domain (57, 58). Most known helicases that act on RNA-RNA duplex substrates are found in SF2.

The SF2 helicases are generally divided into 10 major families, as well as two smaller groups (59). The proteins in several of these families act on RNA substrates and are termed RNA helicases. The largest family of RNA helicases, the DEAD-box proteins, will be discussed in more detail later. The DEAH/RHA family of RNA helicases are characterized by two conserved C-terminal domains in addition to the RecA-like domains. DEAH/RHA proteins have roles in ribosome biogenesis, mRNA splicing and processing (60-64). The Ski2-like family of RNA helicases are 3'-5' processive, with key roles in large protein complexes performing RNA processing and degradation in eukaryotes (65, 66). While Ski2-like helicases are encoded in several bacterial phyla, characterization *in vivo* has not yet occurred (67). RIG-I-like RNA helicases act as part of the innate immune system, detecting RNA ligands from viruses with ssRNA or DNA genomes (68). Viruses also encode helicases, the NS3/NPHII proteins, which aid in strand separation during replication and packaging of the viral RNA genome (69). These

proteins require a loading strand, generally consisting of a 3' ssRNA overhang, and translocate along the RNA or DNA substrate in the 3' to 5' direction (70, 71).

DEAD-box helicases are the largest family of SF2 helicases, and the only family that act solely on RNA substrates (59). They are conserved across all three domains of life. In eukaryotes, they are essential for survival and growth of the organism, with key functions in all aspects of RNA metabolism (72). In prokaryotes, DEAD-box proteins are not required for survival under optimal conditions, instead allowing the organism to adapt to a variety of changing environments and their associated stresses (73-75).

1.2.2 Structure and biochemistry of DEAD-box RNA helicases

DEAD-box helicases have a structurally conserved helicase core region, composed of two RecA-like core domains with twelve highly conserved sequence motifs (59, 72), as well as non-conserved auxiliary domains in the N- and C-termini of the protein (Figure 1.4). The name of this helicase family comes from one of its characteristic ATP-binding motifs, motif II, with the highly conserved Asp-Glu-Ala-Asp motif in the DEAD-box family of helicases (76, 77). ATP-binding and hydrolysis occur in a pocket near the linker of the two RecA-like domains of the helicase and require motifs I and II (Walker A & B), similar to other ATPases (76, 78), as well as the Q motif and motifs V and VI. The Q motif is specific to DEAD-box proteins and localized near the N-terminus of the protein (79, 80). Motif V binds with the 3' hydroxyl of the ribose, while Motif VI interacts with the tri-phosphate residue (81).

RNA interacts with the helicase in a binding cleft formed by motifs Ia, Ib and Ic on the N-terminal RecA domain and motifs IV and V on the C-terminal RecA-like domain (82). This interaction is non-specific, involving the 2' hydroxyl of the ribose group or the phosphodiester backbone (81, 83). Binding of the nucleic acid is mediated by the state of the nucleotide triphosphate, with ATP-binding causing permissive rearrangements of the RNA-binding site and hydrolysis catalysing the RNA unwinding and release (82). There are also two motifs, III and Va, which are required for coordinating the activity of the ATPase and the RNA binding motifs in DEAD-box proteins (84). Motif III interacts with motifs Ia, II, V and VI of the ATPase to couple

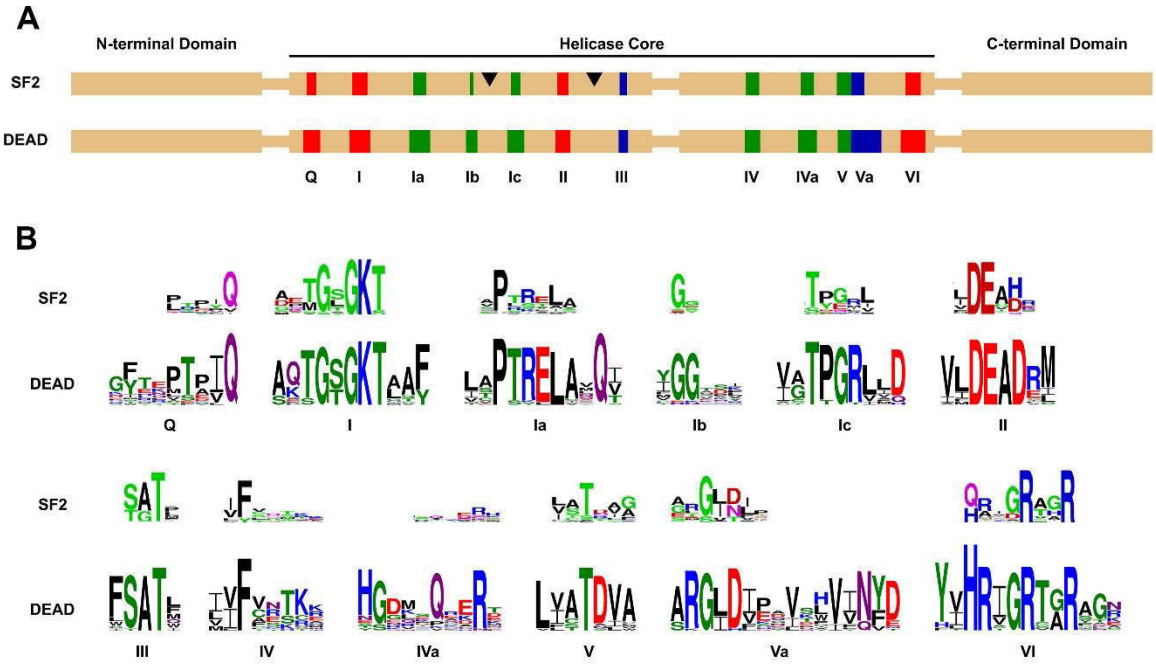

Figure 1.4: Characteristic sequence motifs of SF2 and DEAD-box RNA helicases. (A) A representation of the major domains of SF2 helicases, including the DEAD-box protein family. The helicase core region consists of twelve conserved sequence motifs distributed within two recombinase A (RecA)-like domains. Accessory domains, which can confer additional function or sequence specificity, can be found at the N- or C-terminus of the helicase core, or inserted within the first RecA-like domain (see black triangle). Locations of the twelve sequence motifs are colour-coded with the primary function of the motif: red for ATP binding and hydrolysis, green for RNA binding, and blue for coordination between ATP and RNA binding. (B) Sequence logos of the twelve conserved motifs from the DEAD-box protein family and the larger SF2 helicase superfamily. This figure is modified from Fairman-Williams *et al*. (59) and Linder and Jankowsky (72).

conformational changes in the RNA binding site with ATP-binding and hydrolysis, regulating the RNA-dependent ATPase function of the helicase (84).

The biochemical activity of the helicase core region is very similar between various DEAD-box helicases, with binding of ATP initiating structural changes that permit RNA binding by the protein, and RNA-stimulated ATP hydrolysis triggering RNA release and turnover of the complex (82, 84, 85). DEAD-box proteins cause localized unwinding of the dsRNA structure (86), shown in crystal structures of the core domains of the *Drosophila* helicase, Vasa, as a result of bending of the RNA backbone (81). Depending on the stability and persistence of the helicase on the RNA, the helicase may also serve as an RNA "clamp", recruiting other proteins and factors that act together as a complex to function (87).

1.2.3 DEAD-box RNA helicases in eukaryotes

RNA helicases from the DEAD-box family are essential to the survival of eukaryotic organisms, as they have essential roles in many cellular processes that involve RNA metabolism, starting at transcription and including RNA splicing, translation, RNA degradation and even small RNA (sRNA) metabolism (72). For many eukaryotic RNA helicases, disruption of the helicase results in a lethal phenotype. It is also important to note that eukaryotic DEAD-box helicases typically cannot complement the deletion of another RNA helicase as each has specific domains in the N- and C-termini extending beyond the helicase core domains. These regions confer functional specificity and mediate interactions with other proteins in the cell, leading to substrate and pathway specificity.

One of the first characterized eukaryotic DEAD-box RNA helicases was the mammalian translation initiation factor, eIF4A-I, a constituent of the cap-binding complex that recruits the ribosome to the mRNA in preparation for translation. eIF4A-I was shown to have roles in translation initiation as both an ATPase, transferring energy from ATP into the catalytic energy required for translation initiation, and a helicase, facilitating localized unwinding of secondary structures in the 5' cap region of the mRNA (88-90). Since eIF4A-I is required for the initiation of translation on essentially all mRNAs, the absence of eIF4A-I from the cap-binding complex results in reduced

translation initiation in the cell, particularly when inhibitory secondary structures are present in the 5' UTR (91, 92). Biochemically, eIF4A-I, within the eIF4F complex, and a second eIF4A homolog are interesting as they cooperatively are capable of bidirectional RNA unwinding, while most DEAD-box helicases unwind RNA in only a 3' to 5' or 5' to 3' direction (90).

While it would not be possible to illustrate the extent of the roles RNA helicases perform in eukaryotes, a prime example is their involvement in RNA splicing, when introns are removed from the pre-mRNA sequence during maturation of the transcript. Eight RNA helicases, three of which are DEAD-box proteins, function at various steps in the splicing pathway (93). In addition, DEAD-box RNA helicases are found in mitochondria, a result of endosymbiosis. For example, a yeast helicase, Mss116, has been extensively characterized *in vitro* and is required for the splicing and maturation of many mitochondrial mRNAs (94-96). Mss116 catalyzes localized unwinding of non-permissive RNA structures that block the recognition of the mRNA and activity of the spliceosome proteins (94, 97). This DEAD-box helicase also exhibits an ATP-independent RNA chaperone activity as well as catalyzing RNA annealing, which is a rare secondary activity found in a limited number of RNA helicases (94, 96).

The potential for organelle RNA helicases to perform multiple functions, unlike eukaryotic helicases, is exemplified by DSS1 and SUV3. These helicases have roles in RNA splicing in yeast and are also components of the mitochondrial degradosome (98-101). This degradosome is minimally formed from a DEAD-box helicase and a PNPase, and functions in both intron-dependent and intron-independent maturation and turnover of mitochondrial transcripts (99, 100). Although these roles for DEAD-box RNA helicases are just a sampling of the many roles RNA helicases perform in eukaryotic cells, it is important to highlight that there are both similarities and differences in the regulation and function of DEAD-box RNA helicases between eukaryotic and prokaryotic organisms.

1.2.4 Prokaryotic DEAD-box RNA helicases

Prokaryotic DEAD-box helicases, like in eukaryotes, can have roles in major cellular processes, such as translation, ribosome biogenesis and RNA degradation; however, the

DEAD-box RNA helicase composition in these multi-subunit protein complexes can vary in response to changing growth conditions, such as low temperature (102, 103). There is a strong relationship between low temperature stress and DEAD-box RNA helicases in prokaryotes, as many prokaryotic DEAD-box proteins are upregulated in response to cold stress and helicase deletion often results in cold-sensitive phenotypes (102, 104-106). Additionally, DEAD-box proteins are not found in all prokaryotic genomes, and their complement can vary in number from one to at least twelve in the organisms that do encode DEAD-box proteins (41, 107). In organisms with multiple DEAD-box helicases, each helicase has a defined role in the cell, but many are also capable of partially complementing the deletion of other members of the helicase complement. This is clearly demonstrated by the five DEAD-box helicases of *Escherichia coli*, as the degradosome-associated helicases RhlE and RhlB contribute to ribosome biogenesis in the absence of CsdA, DbpA and SrmB (102, 108).

1.2.4.1 Helicases and the bacterial ribosome

DEAD-box proteins interact with components of the bacterial ribosome to aid in the maturation of precursor ribosomal RNAs (rRNAs) that assemble into the 30S and 50S ribosomal subunits. In *E. coli*, four of the five DEAD-box helicases, CsdA, SrmB, DbpA and possibly RhlE, have roles in maturation of the 50S ribosomal subunit, particularly during cold temperature stress (109-112). For example, CsdA aids in processing of the 5' terminus of the 23S rRNA, with 40S intermediate particles accumulating in a *csdA* mutant (109). In addition, many of the free 50S subunits that form in *csdA* mutants are functionally inactive (113). *srmB* mutants also accumulate a 40S intermediate, containing precursors of both the 23S and 16S rRNAs, suggesting a role in rRNA processing (110). The ATPase activity of DpbA is stimulated by specific binding to hairpin 92 of the 23S rRNA transcript; however, only overexpression of the protein, rather than deletion, has a measurable effect on ribosome biogenesis (112, 114, 115). The function of RhlE is less characterized than the other *E. coli* helicases, but deletion of *rhlE* has been shown to differentially alter the cold sensitive effects of Δ*csdA* and Δ*srmB* on ribosome profiles (111). SrmB also has a role in expression of ribosomal proteins, as it has been shown to

enhance expression of the ribosomal proteins L13 and S9 by suppressing premature transcription termination (116).

A role for DEAD-box RNA helicases in bacterial ribosome biogenesis has also been demonstrated in several other organisms. The helicase Lmo1722 of *Listeria monocytogenes*, a CshA homolog, is important for the processing of the 23S rRNA precursor at low temperatures (117). Similar to its homolog, DpbA, the ATPase activity of YxiN from *Bacillus subtilis* is stimulated by interaction with hairpin 92 of the 23S rRNA precursor (118). Two other helicases in *B. subtilis,* CshA and YfmL also affect biogenesis of the 50S subunit, and the fourth, CshB, has a role in assembly of the active, 70S ribosome from the 30S and 50S subunits (119). CshA and CshB homologs in *Staphylococcus aureus* copurify with ribosomal proteins, potentially indicating a similar role in ribosome biogenesis (120).

A role in protein translation is also posited for prokaryotic DEAD-box RNA helicases, likely by resolving inhibitory secondary structures surrounding the translation initiation site to enhance translation, particularly at the colder, less kinetically favourable temperatures where increased abundance of DEAD-box proteins is often observed. While there is evidence that the ribosome itself is capable of resolving some inhibitory mRNA secondary structures within the protein coding sequence during translation (121, 122), this ribosomal activity would not be sufficient to resolve structures in the 5' UTR, such as an occluded Shine-Dalgarno sequence. There is some evidence that DEAD-box RNA helicases in *E. coli* may perform this function. Circumstantial evidence for prokaryotic RNA helicase involvement in translation initiation comes from a variety of observations. For example, when cells experience low temperature stress, expression of heat shock proteins is initially repressed, then gradually resumes; however, in a *csdA* deletion mutant, expression of the heat shock proteins remains low (106). This effect was interpreted to be independent of the role of CsdA in ribosome maturation, as the abundance of other proteins, such as EF-Tu, were unaffected (106). In another study, translation of chloramphenicol acetyltransferase (*cat*) mRNA with a synthetic structured stem-loop inserted to occlude the translation initiation region was enhanced by overexpression of CsdA (123). CsdA was also shown to enhance the translation of the *E. coli* response regulator UvrY (124). The CsdA homolog in *Pseudomonas aeruginosa* is

also believed to function in translation, as it stimulates translation of the T3SS regulator ExsA in a manner dependent on the sequences of the 5'UTR and coding region of the mRNA (125). These observations involving CsdA intimate a role for DEAD-box RNA helicases in prokaryotic translation, specifically translation initiation; however, there is currently no direct, mechanistic evidence available. DEAD-box proteins may also facilitate translation by binding to and protecting ribosome-free regions of the mRNA, thus stabilizing the transcript (126).

1.2.4.2 Helicases in the bacterial RNA degradosome

The bacterial RNA degradosome has roles in both RNA processing and turnover, both of which are essential for normal RNA metabolism in cells. The degradosome of *E. coli* has been the most extensively characterized, with studies of its components, assembly, activity and localization contributing to the understanding of RNA degradation in prokaryotes. The *E. coli* multi-subunit degradosome core is composed of an RNase E, possessing 5' endonuclease activity, a PNPase, with 3' to 5' exonuclease activity, and RhlB, a DEAD-box helicase (127, 128). Other proteins, such as the enolase, also form part of the RNA degradosome, regulating the degradation of specific mRNAs in response to cellular conditions, but are not essential for the basic function of the degradosome (127, 129).

The *E. coli* degradosome core requires RNase E for assembly, as the C-terminal domain of RNase E is a scaffolding domain with several RNA-binding and protein interaction motifs (130-133). From purified RNase E, RhlB, PNPase and, optionally, enolase, a functional degradosome can be assembled *in vitro* (128, 134). The ribonucleases that form the degradosome, RNase E and PNPase, were shown to be capable of RNA degradation independent of the complete degradosome complex, but only for RNA molecules with simple secondary structures (135, 136). The DEAD-box helicase that associates with the degradosome, RhlB, aids in degradation of mRNAs with complex secondary structures by unwinding the RNA, exposing it for cleavage by RNase E and PNPase (108, 127, 128, 137).

The structure and function of the *E. coli* degradosome is conserved in other prokaryotes that also encode an RNase E endonuclease. In the gammaproteobacterium

Pseudoalteromonas haloplanktis, the degradosome is also composed of RNase E, PNPase and a RhlB-like DEAD-box helicase, and it functions much like the *E. coli* degradosome (138). The alpha proteobacterium *Caulobacter crescentus* also has a degradosome composed of RNase E, PNPase and a DEAD-box helicase, either RhlB or RhlE, but has an aconitase as the fourth component in place of enolase (139, 140). Degradosome composition can vary more widely, as shown by the purple bacterium *Rhodobacter capsulatus*, which is composed of two DEAD-box helicases and the Rho terminator in addition to RNase E (141).

Recently, it has been discovered that degradosomes containing both a RNase and a DEAD-box helicase are not restricted to organisms encoding RNase E. The Gram positive bacterium *B. subtilis* has a degradosome composed of the endonucleases RNase J1, RNase J2 and RNase Y, as well as PNPase, enolase, phosphofructokinase and the DEAD-box helicase CshA (142). CshA interacts directly with the PNPase and RNase Y, forming a core degradosome similar to that in *E. coli* (119, 142). In association with a DEAD-box helicase, RNase J is also capable of forming an active degradosome, as has been shown in *Helicobacter pylori*, where the activity of each protein is stimulated by interaction with the other (143).

Recent evidence suggests DEAD-box RNA helicases may link translation and degradation in prokaryotes. The *E. coli* helicase RhlB has been shown to complement the activity of helicases involved in the maturation of 23S rRNA in addition to its role in the degradosome core (102, 127). Recently, a simultaneous role for RhlB in both the degradosome and active polysomes has been suggested (144). RhlB mediates interactions between the 50S ribosomal subunit and two RNA binding sites on the RNase E scaffolding domain (144). This interaction brings the degradosome into close proximity with mRNAs that are being actively translated, possibly to aid in rescue of stalled ribosomes on damaged transcripts or to catalyze mRNA processing reactions. Interactions between degradosomes and polysomes has also been observed in *H. pylori*, in which the degradosome endonuclease, RNase J, and the helicase, RhpA, are found colocalized with the *H. pylori* ribosome (143). Similarly, copurification of ribosomal proteins with both the degradosome helicase, CshA, and the endonuclease, RNase J1, was also observed in *S. aureus* (120).

1.2.4.3 ncRNA metabolism in prokaryotes may also involve DEAD-box helicases

Bacterial non-coding RNAs (ncRNAs) regulate expression of genes through interactions with mRNAs and other ncRNAs, and can also modify protein activity. In *E. coli*, ncRNA function often involves the RNA chaperone Hfq. Two of the five DEAD-box helicases of *E. coli*, CsdA and RhlB, have been shown to interact with Hfq-mediated ncRNA metabolism (145, 146). For CsdA, interaction with Hfq and the ncRNA DsrA, activates translation of the sigma factor *rpoS* mRNA at low temperature by resolving an inhibitory stem-loop structure that sequesters the ribosome binding site (146). Conversely, RhlB competes with the ncRNA-Hfq complex to bind to the RNase E C-terminal scaffold, preventing degradation of the mRNA target of the ncRNA (145). Similarly, a role for RNA helicase involvement in ncRNA metabolism in the cyanobacterium *Synechocystis* was demonstrated by CrhR helicase-dependent transcriptome changes involving a subset of both the cellular mRNAs and ncRNAs (147). These changes in ncRNA abundance could not be fully explained by altered transcript stability, indicating a possible role for the helicase in regulating ncRNA biogenesis. This could occur in a similar manner to the indirect transcriptional regulation of the *E. coli* ncRNA CsrB by the helicase CsdA (124). CsdA activates translation of a response regulator, UvrB, which then regulates the transcription of the ncRNA CsrB and other targets. At this time, the examples of bacterial DEAD-box RNA helicases interacting with ncRNAs are limited, and do not involve interaction of the ncRNA with the RNA-binding site present in the DEAD-box proteins.

1.2.5 Cyanobacterial RNA helicases

In cyanobacteria, the only DEAD-box proteins that have been characterized are from *Anabaena variabilis* UTCC 387 (hereafter *Anabaena*), *Nostoc* sp. PCC 7120 (formerly *Anabaena*, hereafter *Nostoc*) and *Synechocystis* sp. PCC 6803. The CrhA (cyanobacterial RNA helicase A) protein of *Anabaena* is a DEAD-box protein with a relatively rare amino acid substitution in the highly conserved SAT motif, motif III (see Figure 1.4), in which a phenylalanine replaces the highly conserved serine, producing an FAT box (148). Inactivation of *crhA* results in truncation of the *Anabaena* filaments (148). *Nostoc* encodes two DEAD-box RNA helicases, *crhB* and *crhC* (105). Expression of *crhB* is

sensitive to several abiotic stresses, including temperature, salt, and light, while *crhC* expression is limited to cold temperature conditions in a light dependent manner (105, 149). Temperature-responsive control of *crhC* expression occurs at several levels. At normal growth temperature, 30°C, when CrhC is undetectable, an unidentified transcriptional repressor binds in close proximity to the AT-rich and -10 elements of the *crhC* promoter (150). *crhC* expression is also controlled at the post-transcriptional level, involving a pair of temperature-responsive stem-loop structures in the 5'UTR that resemble an RNA thermometer (150). Biochemically, the CrhC protein exhibits unidirectional RNA unwinding activity in the 5' to 3' direction, with enhanced stimulation of its activity when rRNA or polysome preparations are used as substrate (151). Similar to CrhA, CrhC has a phenylalanine in motif III (105). In *Nostoc* cells, CrhC localizes to the cytoplasmic face of the plasma membrane with a bias toward the cell poles (152). It has been proposed that CrhC may facilitate coordinated translation and transertion of protein products into the septal junctions of the filaments at low temperatures, allowing for rapid adaptation of the composition of the plasma membrane or cell-to-cell communication during cold temperature stress (152).

Synechocystis encodes a single DEAD-box RNA helicase, cyanobacterial RNA helicase redox, termed *crhR* (41), which will be the focus of this thesis. *In vitro*, CrhR is an RNA-dependent ATPase, with ATP-dependent unwinding activity in both the 5'-3' and 3'-5' directions (153). Similar to other DEAD-box proteins, CrhR has a low processivity of approximately 25 bp (153). Unusually, CrhR is also capable of annealing complementary RNA strands in an ATP-dependent reaction (153). Both unwinding and annealing activities of CrhR have been shown to occur concurrently *in vitro*, indicating a possible ATP-dependent strand exchange activity (153). Helicase-catalyzed annealing and strand exchange, consistent with CrhR activities, has only been observed in a small subset of DEAD-box RNA helicases (154-156). CrhR has also been demonstrated to form a homodimer through the N-terminal RecA-like domain (157). While CrhR has been shown to possess several biochemical activities that alter RNA secondary structure *in vitro*, the physiological role of this and many other RNA helicases *in vivo* is unknown. Thus, a major challenge in understanding the role of the CrhR RNA helicase in

Synechocystis is linking the biochemical activity of the helicase with its physiological role.

Mutation of *crhR* (see Figure 1.5) has significant effects on the morphology and physiology of *Synechocystis*, particularly during low temperature stress (104, 158). *Synechocystis* deficient in CrhR exhibit a reduced growth rate, with a doubling time of 37 h for the *crhR* mutant at 30°C, compared to 30 h for wild type. At 20°C, while the growth rate of wild type does decrease, the *crhR* mutant exhibits a severe cold sensitive phenotype with essentially no growth (104). At 30°C, wild type *Synechocystis* and *crhR* mutants have a very similar ultrastructure as seen in both SEM and TEM images; however, at 20°C, *crhR* mutants show pronounced changes in that ultrastructure (104). These include a reduced size, loss of the cell surface structure, disordered thylakoid membranes, and enlargement of the carboxysomes (104). The *crhR* mutant also has a reduced quantity of the photosynthetic pigments chlorophyll *a* and phycocyanin, even at the normal growth temperature (104, 158). The photosynthetic rate is also depressed in the *crhR* mutant, as shown by significantly reduced evolution of oxygen from water splitting, and these cells exhibit problems with state transitions of photosystem II (PSII), reduction of the plastoquinone pool, and expression of the reaction center proteins for photosystem I (PSI) (158). A large intracellular pool of inorganic carbon (Ci) accumulates in *crhR* mutants, likely due to the reduced utilization of the pool for photosynthetic carbon fixation (104).

As DEAD-box helicases act at the level of RNA metabolism, the pronounced effects of crhR mutation at low temperature reflect an essential role for CrhR in regulating the expression of a subset of stress-responsive genes. A microarray study focused on mRNAs demonstrated an effect by CrhR on low temperature expression of protein chaperones, glutamine synthetase regulators, a fatty acid desaturase and the gene immediately upstream of *crhR*, *slr0082* (159). Additional mRNAs, as well as ncRNAs, whose expression is sensitive to *crhR* mutation, representing approximately 10% of annotated *Synechocystis* mRNAs and ncRNAs, were identified in an expanded microarray transcriptome, demonstrating a role for CrhR in regulating the expression of this subset of stress-responsive genes (147). Importantly, changes in general RNA half-life in the *crhR* mutant was not sufficient to account for the changes in abundance of the

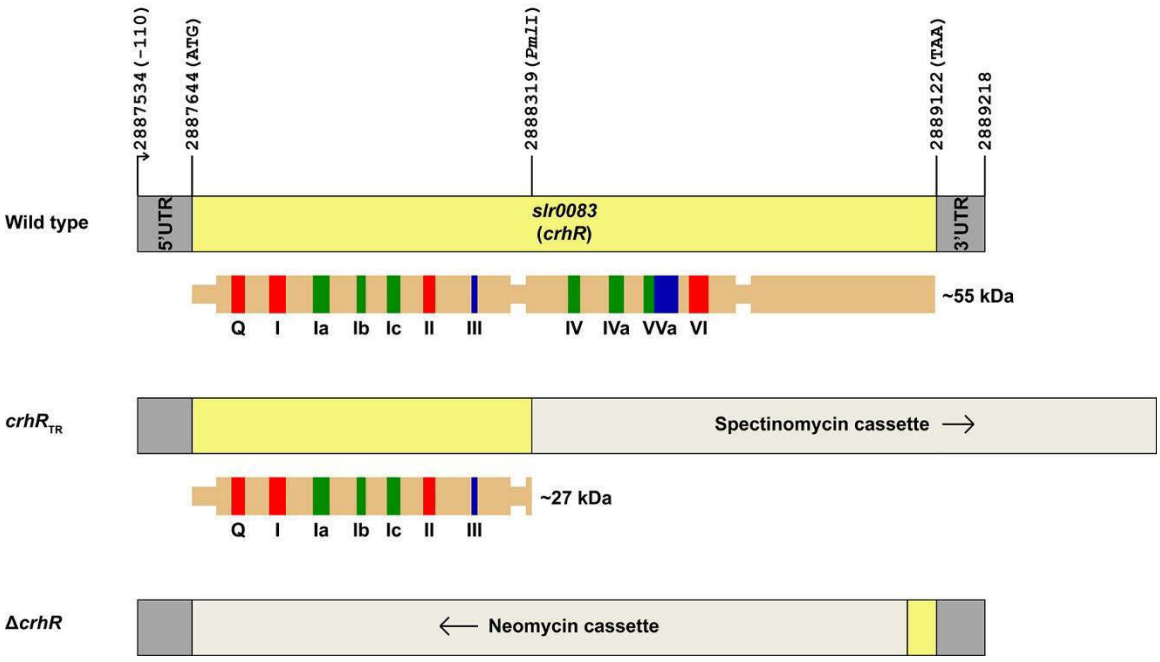

Figure 1.5: Genomic mutants of *crhR*.

Scale diagram of the wildtype *slr0083* (*crhR*) gene and CrhR protein, as well as the *crhR*$_{TR}$ and Δ*crhR* mutants. *crhR*$_{TR}$ was created by insertion of a spectinomycin cassette at the *Pml*I site between the two conserved RecA-like domains, resulting in expression of a truncated, 27 kDa protein lacking the second RecA-like domain and C-terminal extension (104). The *crhR* ORF was replaced with a neomycin cassette to create Δ*crhR*, resulting in a strain that does not express CrhR protein (160). Protein motif colours are as described in Figure 1.4.

mRNAs and ncRNAs observed in these microarrays (147). Thus, while CrhR may directly interact with some of the transcripts it regulates, it is also likely that changes in some of the transcripts are indirect, occurring further downstream in a signalling cascade that includes the activity of CrhR.

Understanding the stresses that affect the expression of *crhR* is also useful to identify a cellular function for CrhR. Three stresses were initially reported to induce expression from *crhR*: high salt/osmotic stress, light, and low temperature (41, 161, 162). An additional stress that induces CrhR expression, heavy metal stress, was recently reported (163). All four of these conditions affect the flow of electrons through the photosynthetic electron transport chain in *Synechocystis*, and their regulatory effects on induction of CrhR expression is dependent on their effects on the redox poise of quinones between Q_B in photosystem II and the plastoquinone pool (41, 163). Regulation occurs at several points in CrhR expression, with effects that can be attributed to transcriptional, post-transcriptional, and even post-translational stages of expression (41, 164). The LexA-related transcription factor encoded by *sll1626* represses expression of *crhR* in conditions favouring LexA accumulation by binding immediately downstream of the transcription start site (165). Low temperature stress causes a transient accumulation of *crhR* transcript, accompanied by an accumulation of CrhR protein to a maximal level that persists for the duration of the stress (164). Upon relief of the stress, CrhR protein undergoes a relatively rapid proteolysis by a currently unknown mechanism (160). Interestingly, some of these points of regulation are dependent on the activity of CrhR, such as the transient nature of *crhR* accumulation, indicative of auto-regulation (164). The patterns of CrhR expression indicate that it is likely involved in more general responses to abiotic stresses that affect photosynthesis in *Synechocystis*, a model that is supported by CrhR-dependent expression changes in photosynthetic genes, as well as genes encoding proteins related to cellular changes in response to the various abiotic stresses discussed above; however, the mechanism by which CrhR affects expression of these genes is still unknown.

1.3 Thesis objectives

The primary objective of this thesis is to further explore the functional role of DEAD-box RNA helicases in photosynthetic bacteria, with a focus on the protein CrhR encoded in the cyanobacterium *Synechocystis*. The research presented in this thesis is organized into four sections, with the first three providing additional insights into the function of CrhR in *Synechocystis*, and the final section demonstrating that proteins homologous to CrhR are evolutionarily conserved within and distributed widely through cyanobacterial diversity.

The first objective is to investigate the subcellular localization of CrhR and its association with protein complexes. In Chapter 2, CrhR is shown to cosediment with polysomes and RNA degradosome components during ultacentrifugation. Discontinuous sucrose gradient ultracentrifugation of *Synechocystis* membranes indicates that CrhR localizes to the thylakoid membrane. Requirements for active translation and functional CrhR in maintaining these interactions is also examined.

In Chapter 3, the genetic context of *crhR* is studied to provide insights into regulation of CrhR expression. Northern blotting and RT-PCR demonstrate that *crhR* is transcribed as the second cistron in a discistronic operon with *slr0082* (*rimO*). Transcript accumulation and half-lives in wild type *Synechocystis* and a *crhR* truncation mutant show that the *slr0082-crhR* transcript is rapidly processed after transcription, resulting in destabilization of the *slr0082* transcript. A model for cleavage of the *slr0082-crhR* transcript by RNase E is suggested by RNA secondary structure modeling and *in vitro* cleavage of the dicistronic transcript by RNase E. Two stable transcripts, likely ncRNAs, are also shown to originate from the 5' UTR and ORF of *slr0082*.

Chapter 4 involves identification of a fifth abiotic stress reponse, nitrogen, that is associated with CrhR expression. Effects on growth rate and pigmentation of *Synechocystis* cultured with several sources of fixed nitrogen are shown to be altered by *crhR* truncation. Transcript and protein abundance demonstrates that accumulation of transcripts and protein from *crhR* is induced when the molecular form of exogenous fixed nitrogen is altered. Proteolysis of CrhR upon depletion of fixed nitrogen is demonstrated. Treatment with the glutamine synthetase inhibitor MSX shows that the proteins involved in CrhR proteolysis are likely regulated by the global nitrogen transcription factor NtcA.

Based on binding of NtcA immediately upstream of the *slr0082* transcription start site, the *slr0082-crhR* operon is also shown to be within the NtcA regulon.

The fourth objective demonstrates a broader role for CrhR across cyanobacterial diversity. A preliminary phylogenetic analysis by Jens Georg (University of Freiburg) showed that cyanobacterial DEAD-box helicases can be classified into three clades, one with homology to CsdA and a second with homology to RhlE from *E. coli* (166). Here, the analysis is extended to include amino acid sequences for 461 cyanobacterial DEAD-box helicases, representing all the complete sequences that are currently available from the publicly accessible NCBI database. Helicases homologous to CrhR are found in examples from almost all cyanobacterial orders but are not found in other bacteria. Synteny of *crhR* with the methyltransferase *rimO* is also frequently observed, comprising a *rimO-crhR* operon in many species. Sequence features characteristic of each clade are also identified.

Overall, these results indicate that the likely physiological function of CrhR, the sole DEAD-box RNA helicase encoded in *Synechocystis*, is to regulate expression of proteins involved in the maintenance of oxygenic photosynthesis and electron transfer in the thylakoid membrane, particularly during abiotic stress. CrhR interacts with large complexes, such as polysomes and potentially the RNA degradosome to affect expression of these proteins. Diverse cyanobacteria encode DEAD-box RNA helicases of the CrhR-like clade, and this unique function for a DEAD-box protein may be conserved across that diversity.

Chapter 2: CrhR co-sediments with polysomes and RNA degradosomes, and localizes to the thylakoid membrane

A version of this chapter has been previously published as Rosana, A.R.R.*, Whitford, D.S.*, Fahlman, R.P., and Owttrim, G.W. (2016). Cyanobacterial RNA helicase CrhR localizes to the thylakoid membrane region and cosediments with degradosome and polysome complexes in *Synechocystis* sp. strain PCC 6803. Journal of Bacteriology. 198(15): 2089-2099.

2.1 Summary

The interaction between mRNA translation and degradation is a major determinant controlling gene expression. Regulation of RNA function through alteration of secondary structure by RNA helicases performs crucial roles, not only in both of these processes but in all aspects of RNA metabolism. The model cyanobacterium *Synechocystis* sp. strain PCC 6803 encodes a single DEAD-box RNA helicase, *crhR*, whose expression is tightly auto-regulated in response to low temperature (cold) stress. Subcellular localization and proteomic analysis indicate that CrhR localizes to both the cytoplasmic and thylakoid membrane regions, and cosediments with polysome and RNA degradosome components. Evidence is presented that either functional RNA helicase activity or a C-terminal localization signal is required for polysome but not thylakoid membrane localization. Polysome fractionation and runoff translation analysis results indicate that CrhR associates with actively translating polysomes. The data indicate a role for CrhR in translation or RNA degradation in the thylakoid region related to thylakoid biogenesis or stability, a role that is enhanced at low temperature. Furthermore, CrhR cosedimentation with polysome and RNA degradosome complexes links alteration of RNA secondary structure with a potential translation-RNA degradation complex in *Synechocystis*.

2.2 Introduction

Compartmentalization of metabolic processes is crucial for cells to avoid futile cycles. While this is efficiently achieved by lipid bilayers in eukaryotic cells, this solution does not generally apply in prokaryotes. Although prokaryotes have the ability to compartmentalize using invagination of the inner cell membrane, these compartments (e.g. magnetosomes) tend to perform one specific function and are not widely used (167). Prokaryotes can also form proteinaceous microcompartments in which specific reactions occur, the primary cyanobacterial example being that of carboxysomes (168). Prokaryotes do not compartmentalize essential, everyday anabolic and catabolic processes such as transcription and translation, or protein and RNA decay; however, there is a growing body of evidence indicating that prokaryotes spatially confine these cellular processes (169). A prime example is the localization of the RNA degradation complex,

the degradosome, to the cytoplasmic membrane (CM) in *E. coli* (170) and *B. subtilis* (171).

The *E. coli* degradosome consists of RNase E, polynucleotide phosphorylase (PNPase), enolase, and the DEAD-box RNA helicase RhlB (127). DEAD-box RNA helicases are ubiquitous enzymes that participate in all aspects of RNA metabolism (72). While eukaryotes generally encode numerous DEAD-box RNA helicases, 25 in yeast (59) and over 50 in *Arabidopsis* (172), prokaryotic genomes encode fewer members, 5 in *E. coli* (173) and 4 in *B. subtilis* (119). Structurally, RNA helicases consist of two tandem RecA-like helicase domains with N-terminal and/or C-terminal extensions that provide substrate and protein interaction domains (72). Functionally, in all organisms, RNA helicases are associated with ribonucleoprotein (RNP) complexes frequently involved in RNA degradation (120, 139, 174), translation initiation (175), and ribosome biogenesis (109, 110). While the majority of RNA helicases perform specific functions, some bacterial enzymes, including CsdA in *E. coli* (176) and CshA in *Bacillus cereus* (177), are associated with a variety of pathways. In some systems, the multifunctionality of these helicases originates from their association with different RNP complexes in response to environmental stress. For example, the degradosome-associated RNA helicase RhlB in *E. coli* can be functionally replaced by another DEAD-box helicase, either CsdA or RhlE, during low-temperature stress, forming a cold-specific degradosome (170, 178). Recently, RhlE and an uncharacterized DEAD-box helicase, CCNA_01546, have also been shown to form part of the *C. crescentus* degradosome, in addition to RhlB (140). In *B. cereus*, the four DEAD-box RNA helicases have divergent functions in response to a variety of stresses, including low temperature for three of the DEAD-box proteins (177). Thus, the reduced RNA helicase repertoire present in bacteria can perform the essential RNA metabolic processes by some helicase proteins performing multiple functions.

Divergent RNA helicase functions are also associated with specific subcellular localization. For example, four of the five *E. coli* DEAD-box RNA helicases localize with respect to their physiological function. RhlB is RNA degradosome-associated at the cytoplasmic membrane, and SrmB and DbpA are soluble and ribosome-associated, while the multifunctional helicase CsdA is associated with all three cellular compartments

(176). Although RNA helicases do not contain canonical membrane-spanning domains, they are membrane-associated in some bacteria (152, 174, 179) but not all (139, 180). For example, RNA helicases associated with RNA degradosomes localize to the cytoplasmic membrane via RNase E in *E. coli* (170, 174) and RNase Y in *B. subtilis* (171) whereas CshA and CshB colocalize with CspB and ribosomes in areas surrounding the *B. subtilis* nucleoid, the localization being dependent on active transcription (181). Localization of these RNA helicase-containing complexes to specific cellular sites therefore confines the associated processes to restricted cellular regions. Thus, understanding RNA helicase localization provides insight into how the spatial separation of synthesis and degradation contributes to an integrated mechanism regulating cellular pathways in bacteria.

The Gram-negative, photosynthetic cyanobacteria also encode limited numbers of DEAD-box RNA helicases, for example, one in *Synechocystis* (41, 153, 164) and two in *Nostoc* (105, 149, 151). In *Nostoc*, *crhB* is expressed in response to a range of environmental conditions whereas *crhC* is exclusively expressed in response to temperature downshift (105, 149). In contrast, expression of the *Synechocystis* DEAD-box RNA helicase encoded by *crhR* is regulated by abiotic stresses that alter the redox status of the electron transport chain in the thylakoid membrane (41), including temperature stress (162, 164) and salt stress (161). *crhR* expression is regulated at a number of CrhR-independent and CrhR-dependent checkpoints in response to temperature, associated with both the induction and repression of the system (164). The auto-regulatory, CrhR-dependent checkpoints include temperature regulation of *crhR* transcript and protein half-life (164). CrhR protein half-life is controlled by conditional, temperature-upshift-induced proteolysis that generates the reduction in CrhR abundance observed at the optimal growth temperature, 30°C (160, 164). A truncated mutant of *crhR*, $crhR_{TR}$, causes severe morphological and physiological aberrations in *Synechocystis*, including decreased photosynthetic electron transport, carbon fixation, and oxygen evolution, as well as significant disorganization of internal cell structures, including the thylakoid membrane (104).

Although subcellular localization is a crucial aspect required to decipher the physiological role performed by prokaryotic RNA helicases, RNA helicase localization in cyanobacteria has been reported only for CrhC in *Nostoc*, where it localizes to the

cytoplasmic membrane, primarily at the cell poles (152). In an attempt to identify the physiological pathway(s) associated with CrhR activity, we investigated the subcellular localization of this stress-induced RNA helicase and identified protein complexes with which it interacts. Here, we provide evidence that CrhR localizes to both the thylakoid membrane and cytoplasmic region, from which it cosediments with both polysome and RNA degradosome components. The results suggest that *Synechocystis* possesses a polysome-RNA degradosome complex to which CrhR localizes, linking alteration of RNA secondary structure with a translation-RNA turnover macromolecular complex in prokaryotic systems.

2.3 Experimental procedures

2.3.1 Culture conditions and strains

Wild type *Synechocystis* sp. strain PCC 6803, a truncated *crhR* mutant strain, *crhR*$_{TR}$, and a complete *crhR* deletion, Δ*crhR*, (see Table 2.1) were cultivated photoautotrophically on BG-11 medium as described previously (164). The *crhR*$_{TR}$ mutant was created by insertion of a spectinomycin resistance cassette at the *Pml*I site halfway between motifs III (SAT) and IV (FVRTK), thereby removing the second RecA domain and C-terminal extension from *crhR* (104). CrhR$_{TR}$, the 27-kDa truncated version of the CrhR polypeptide expressed in this strain (104, 164), is biochemically inactive (D. Chamot and G.W. Owttrim, unpublished data). The *crhR*$_{TR}$ mutant strain was grown on BG-11 medium containing sodium thiosulfate (0.3% w/v) that was buffered with tricine (10 mM, pH 8.0) and supplemented with 50 μg ml^{-1} each of spectinomycin and streptomycin (182). The Δ*crhR* mutant was created by insertion of a neomycin resistance cassette in place of the *crhR* ORF (160) and grown on BG-11 medium supplemented with sodium thiosulfate (0.3% w/v), tricine buffer (10 mM, pH 8.0) and 50 μg ml^{-1} of kanamycin. For liquid cultures, cell mass was increased gradually, starting at 50 ml and progressing to 300 ml and finally to 4 liters at 30°C with continuous shaking (150 rpm) coupled with bubbling with humidified air at an illumination of 50 μmol photons m^{-2} s^{-1} (182). To induce CrhR expression, mid-log-phase cells were cold stressed for 3 h at 20°C.

Table 2.1: Strains and plasmids used in this chapter.

Strain or plasmid	Relevant characteristics	Source or reference
***Synechocystis* strains**		
Wild type	glucose-tolerant strain	(41)
crhR$_{TR}$	*crhR*::spectinomycin cassette; C-terminal deletion of CrhR	(104)
Δ*crhR*	replacement of the complete *crhR* ORF with neomycin cassette	(160)
***E. coli* strains**		
DH5α	F-Φ80lacZΔM15 Δ(lacZYA-argF) U169recA1 endA1 hsdR17 (rK-, mK+) phoA supE44 λ-thi-1 gyrA96 relA1	Laboratory collection
HB101 pRL623	Carries three *ava* methyltransferases from cyanobacterial RM systems, helper plasmid in triparental mating	(183)
HB101 RP4	Conjugal plasmid in triparental mating	(184)
Plasmids		
pCambia 1303-derived plasmid	pCambia 1303 (185) digested *Nco*I/*Bst*EII to replace GUS-GFP with ciFP	N. Zhang and M. Deyholos, personal communication
pMON 36456	*E. coli – Synechocystis* hybrid cloning vector, Gen^R	(186)
pMON ciFP-CrhR	pMON 36456 containing an N-terminal fusion of ciFP onto CrhR	This study
pMON CrhR-ciFP	pMON 36456 containing a C-terminal fusion of ciFP onto CrhR	This study

Representative data from a minimum of three biological replicates for each experiment are shown.

2.3.2 Extraction of soluble and insoluble fractions of *Synechocystis* cells

Cultures of wild type *Synechocystis* and *crhR*$_{TR}$ cells were divided, with half of the culture volume maintained at 30°C and half of the culture volume maintained at 20°C for 3 h. Aliquots were collected by centrifugation at the indicated growth temperature. Cells were mechanically lysed by vortex mixing in the presence of glass beads in cyanobacterial protein extraction buffer (PEB; 20 mM Tris-HCl [pH 8], 100 mM NaCl, 1 mM $MgCl_2$, 5 mM dithiothreitol [DTT], Roche cOmplete Mini EDTA-free protease inhibitor cocktail) as described previously (153, 182). An initial centrifugation at 1,000 ×*g* for 1 min removed unlysed cells and glass beads and was followed by clarification of the lysate at 15,000 ×*g* for 15 min. Following clarification, the pellet (membrane fraction) was washed with PEB and suspended in PEB at the same volume as the soluble, cytoplasmic fraction. For the solvent and RNase A extraction of CrhR, aliquots of the membrane fraction corresponding to 60 µg cytoplasmic protein were utilized for each treatment. The STS buffer contains 0.4% w/v SDS, 0.5% v/v Triton X-100, and 0.5% w/v Sarkosyl. Solvent extractions were allowed to proceed on ice for 30 min, while the RNase A (0.4 µg µl^{-1}) treatment was performed at 37°C for 30 min. Solubilized protein were separated from remaining insoluble material by centrifugation at 15,000 ×*g* for 15 min. Supernatants were retained and pellets suspended in an equivalent volume of PEB. Protein concentrations of the cytoplasmic fractions were determined with the Bradford assay (Bio-Rad) using bovine serum albumin (BSA) as the standard. Cytoplasmic proteins (10 µg) or the equivalent volume of the insoluble fraction were resolved by 10% SDS-PAGE, electrophoretically transferred to Protran 0.45 µm pore-size nitrocellulose membranes (Amersham), and subjected to Western blotting.

2.3.3 Polysome isolation

Polysomes were isolated from cyanobacterial cytoplasmic extracts as described by Tyystjärvi *et al.* (187) with modifications. Two-liter mid-log-phase cell cultures were harvested by centrifugation at 7,500 ×*g*, and the pellet was washed with 0.1× volume

wash buffer (0.4 M sucrose; 50 mM Tris [pH 8.5], 10 mM $MgCl_2$, 30 mM EDTA [pH 8.0], 500 µg ml^{-1} chloramphenicol) and harvested by centrifugation. The resulting pellet was washed with 0.1× volume polysome isolation buffer (0.4 M sucrose, 50 mM Tris [pH 8.5], 10 mM $MgCl_2$, 500 µg ml^{-1} chloramphenicol) and harvested, and the pellets were suspended in 0.0125× polysome isolation buffer containing protease inhibitor cocktail (Roche). Cells were lysed by passage through a continuous French pressure cell press (American Instrument Company) system at 20,000 lb in^{-2} three times. The cell lysate was cleared of intact cells by centrifugation at 1,000 ×*g* and clarified twice at 18,000 ×*g*, separating the cell debris from the cytoplasmic fraction. Aliquots of both pellet and supernatant fractions were retained for Western analysis. The supernatant was equilibrated with 0.5× volume polysome isolation buffer without sucrose and treated with polyoxyethylene (10) tridecyl ether (Sigma-Aldrich) (2% v/v) (187). Samples were incubated on ice for 10 min and unsolubilized components eliminated by two centrifugations at 18,000 ×*g* for 20 min each time. Clarified supernatant was layered on a 1 M sucrose cushion (1.0 M sucrose, 50 mM Tris [pH 8.5], 10 mM $MgCl_2$, 500 µg ml^{-1} chloramphenicol) and centrifuged at 4°C for 16 h at 243,500 ×*g* in a SW40Ti rotor using a L8-60M ultracentrifuge (Beckman Coulter Inc., Pasadena, CA). Pigmented layers were individually harvested, and the polysome-containing pellet was suspended in polysome isolation buffer without sucrose. Samples of the supernatant layers (equivalent to 100 µg protein) and polysome pellet (A_{260} = 100 U) were analyzed by Western blotting. Blots were purposely overloaded to detect any CrhR in the fractions. Constituent proteins in the polysome pellet were identified by mass spectrometry. For the polysome runoff experiment, cells were grown and the lysates processed as previously described except that chloramphenicol was omitted.

2.3.4 Polysome fractionation

The cytoplasmic fraction from a wild type *Synechocystis* cell extract grown at 20°C for 3 h was overlaid on a continuous sucrose gradient (20% to 60% w/v sucrose) prepared using a gradient former (DCode system; Bio-Rad) and centrifuged at 243,500 ×*g* for 16 h at 4°C as described above. The absorbance of each fraction was measured at 254 nm

using a NanoDrop spectrophotometer (ThermoScientific). Equal volumes of each fraction were analyzed by Western blotting.

2.3.5 Membrane isolation

The three membranes present in *Synechocystis* cells were separated by discontinuous flotation sucrose gradient fractionation as initially described by Murata and Omata (188) and modified according to the method of El-Fahmawi and Owttrim (152). Cultures grown at 30°C or cold shocked at 20°C for 3 h were harvested at 7,500 ×*g* for 15 min at 4°C. The cell pellet was washed with 0.1× volume of potassium phosphate buffer (20 mM potassium phosphate, pH 7.8) and suspended in 0.1× volume potassium phosphate buffer supplemented with protease inhibitor cocktail (Roche). Cells were lysed by vortex mixing in the presence of glass beads (153, 182), and insoluble, membrane-containing material was pelleted by centrifugation at 111,000 ×*g* for 30 min at 4°C in a SW40Ti rotor as described above. The crude membrane pellet was gently washed, centrifuged, and suspended in 20 mM potassium phosphate buffer and adjusted to a final sucrose concentration of 50% w/v. A discontinuous sucrose gradient using 20 mM potassium phosphate and the indicated increasing sucrose concentrations (% w/v) and volume ratios was assembled for the wild type membrane isolation as follows: 10% (0.2×); 30% (0.09×); 39% (0.23×); and 50% (0.49×) (cell lysate adjusted with sucrose). For the *crhR*$_{TR}$ mutant membrane suspension, a finer discontinuous sucrose gradient was assembled, using 20 mM potassium phosphate buffer and the indicated increasing sucrose concentrations (wt/vol) and volume ratios as follows: 10% (0.03×); 30% (0.17×); 35% (0.17×); 38% (0.17×); 42% (0.19×) (cell lysate adjusted with sucrose); 50% (0.14×); and 60% (0.14×) (189). Membrane separation was performed by floatation ultracentrifugation at 131,500 ×*g* for 16 h at 4°C in a SW40Ti rotor as described above. A fraction from each membrane-containing layer was carefully harvested and diluted three times with 20 mM potassium phosphate. Individual membrane-containing fractions were pelleted at 188,000 ×*g* for 45 min at 4°C as described above, and the pellets were suspended in 20 mM potassium phosphate buffer. The procedure also yielded a pellet that is referred to here as the cell wall pellet.

2.3.6 Western analysis

Western analysis was performed on the fractionated samples as described previously (104, 182) with slight modifications. Proteins were separated on SDS–10% polyacrylamide gels and electroblotted onto nitrocellulose membranes using a semidry transfer apparatus (Tyler Research). Membranes were blocked with 5% w/v skimmed milk–Tris buffered saline (TBS; pH 7.4) for 3 h prior to the addition of polyclonal antisera. Anti-CrhR and anti-*E. coli* ribosomal protein S1 (S1) antibodies were used at a 1:5,000 dilution (104). For *Synechocystis* membrane-specific protein detection, anti-FtsH (raised against *Arabidopsis thaliana*) and anti-Vipp1 (immunoreactive to *Synechocystis*) were used at a 1:2,000 dilution as thylakoid and cytoplasmic membrane-specific markers, respectively. The *Synechocystis* thylakoid-specific protein PsbA (D1) antibody (1:5,000 dilution) was used to verify CrhR localization. All immunoreactive polypeptides were detected with anti-rabbit horseradish peroxidase (HRP)-conjugated secondary antibody (Sigma) (1:20,000 dilution) using enhanced chemiluminescence (ECL; Amersham).

2.3.7 Mass spectrometry

The crude polysome pellet from the first ultracentrifugation was treated with 2% v/v polyoxyethylene (10) tridecyl ether (187), layered over a 9 ml 1 M sucrose cushion, and centrifuged as described above. The resulting pellet was suspended in polysome isolation buffer without sucrose. A_{260} (100 U) fractions of this polysome pellet were resolved on an SDS–4 to 15% polyacrylamide gel (Bio-Rad) and stained with colloidal Coomassie (0.08% Coomassie brilliant blue G250, 1.6% v/v orthophosphoric acid, 8% w/v ammonium sulfate, 20% v/v methanol). Mass spectrometry analysis was performed at the Alberta Proteomics and Mass Spectrometry Facility (APM), University of Alberta as described below.

In-gel trypsin digestion was performed on the samples. Each excised lane was cut into 10 equal gel sections, destained twice in 100 mM ammonium bicarbonate/acetonitrile (ACN) (50:50), reduced (10 mM beta-mercaptoethanol [BME]–100mM bicarbonate), and alkylated (55 mM iodoacetamide–100 mM bicarbonate). After dehydration, trypsin digestion (6 ng μl^{-1}) was allowed to proceed overnight at room temperature. Tryptic peptides were extracted from the gel using 97% water–2% v/v

acetonitrile–1% v/v formic acid followed by a second extraction using 50% v/v acetonitrile in the initial extraction buffer.

Fractions containing tryptic peptides were resolved and ionized using nanoflow high-performance liquid chromatography (HPLC) (Easy-nLC II; Thermo Scientific) coupled to an LTQ XL-Orbitrap hybrid mass spectrometer (Thermo Scientific). Nanoflow chromatography and electrospray ionization were accomplished by using a Pico-Frit fused silica capillary column (ProteoPepII; C18) with a 100-µm inner diameter (New Objective) (300 Å, 5 µm pore size). Peptide mixtures were injected onto the column at a flow rate of 3,000 nl min^{-1} and resolved at 500 nl min^{-1} using 70-min linear gradients of 4% to 45% v/v aqueous ACN with 0.2% v/v formic acid. The mass spectrometer was operated in data-dependent acquisition mode, recording high-accuracy and high-resolution Orbitrap survey spectra using external mass calibration, with a resolution of 60,000 and *m/z* range of 400 to 2,000. The 10 most intensely multiply charged ions were sequentially fragmented by using collision-induced dissociation, and spectra of their fragments were recorded in the linear ion trap; after two fragmentations, all precursors selected for dissociation were dynamically excluded for 60 s.

Data were processed using Proteome Discoverer 1.4 (Thermo Scientific), and the Uniprot cyanobacteria database was searched using SEQUEST (Thermo Scientific). Search parameters included a precursor mass tolerance of 10 ppm and a fragment mass tolerance of 0.8 Da. Peptides were searched with carbamidomethyl cysteine as a static modification and oxidized methionine and deamidated glutamine and asparagine as dynamic modifications.

2.3.8 ciFP and CrhR fusion expressing stains

To create citrine fluorescent protein (ciFP)-tagged CrhR for visualization by fluorescent microscopy, ciFP and CrhR were PCR amplified from a pCambia 1303-derived plasmid containing ciFP in place of GUS-GFP (N. Zhang and M. Deyholos, personal communication) and *Synechocystis* genomic DNA, respectively, with the primers described in Table 2.2. After restriction endonuclease digestion of the PCR products with *Eco*RI, *Bam*HI or *Xba*I, dependent on the primer sequence, the PCR products were ligated into *Eco*RI and *Xba*I digested pMON 36456 (186) to generate the plasmids

Table 2.2: Oligonucleotides used in this chapter.

Restriction sites are indicated in bold and mutagenic bases are underlined.

Oligonucleotide	Sequence	Application
BL2	CACACA**GGATCC**CCTAGCTATTTACCT AGTAGG	Reverse primer for ciFP, contains *Bam*HI restriction site
BL3	GATGTA**GGATCC**ATGGTGAGCGCTG	Forward primer for ciFP, contains, *Bam*HI restriction site
BL4	CGCCGC**GAATTC**TCACCTAGCTATTTA CCTAG	Reverse primer for ciFP, contains *Eco*RI restriction site
BL5	GAAGCC**TCTAGA**ATGGTGAGCGCTG	Forward primer for ciFP, contains *Xba*I restriction site
DSW18	GAGGCCTACTAGGTTAATAGCTAGGGG ATCC	Site-directed mutagenesis primer to remove additional ciFP stop codon
DSW19	GGATCCCCTAGCTATTAACCTAGTAGG CCTC	Site-directed mutagenesis primer to remove additional ciFP stop codon
LLO6	ACTACT**GGATCC**CTGTTGGCGATCACT ATAGGC	Reverse primer for CrhR, contains *Bam*HI restriction site
LLO12	TCTTCT**GGATCC**ATGACTAATACTTTG ACTAGTACC	Forward primer for CrhR, contains *Bam*HI restriction site
LLO13	ACCATA**GAATTC**TTACTGTTGGCGATC ACTATAGGC	Reverse primer for CrhR, contains *Eco*RI restriction site
LLO18	CTCGCC**TCTAGA**ATGACTAATACTTTG ACTAGTACC	Forward primer for CrhR, contains *Xba*I restriction site

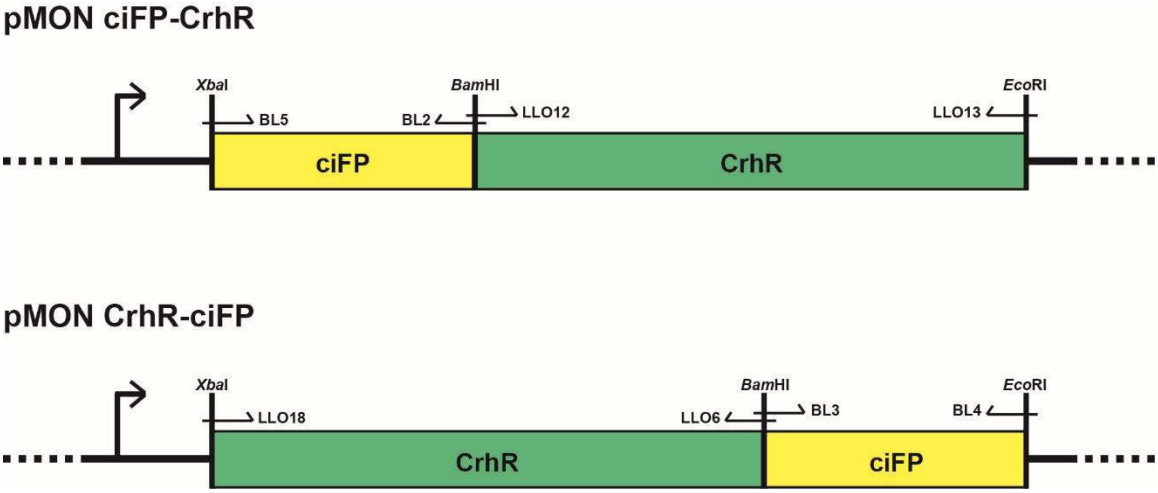

Figure 2.1: pMON ciFP-CrhR and pMON CrhR-ciFP constructs.

The *crhR* ORF was PCR amplified from *Synechocystis* genomic DNA using the indicated oligonucleotides. Citrine fluorescent protein (ciFP) was amplified from a modified pCambia 1303 vector, in which the GUS-GFP was replaced with the ciFP ORF (N. Zhang and M. Deyholos, personal communication). The PCR products were restriction digested and ligated into the *Xba*I/*Eco*RI digested pMON 36456 vector, creating an N-terminal fusion of ciFP onto CrhR, pMON ciFP-CrhR, and a C-terminal fusion, designated pMON CrhR-ciFP.

pMON ciFP-CrhR and pMON CrhR-ciFP, containing translational fusions of ciFP to either the N- or C-terminus of *crhR* (see Figure 2.1). These constructs were transformed into *E. coli* DH5α and selected on LB agar containing 10 μg ml^{-1} gentamicin. Constructs were confirmed by sequencing. An additional in-frame stop codon found in the pMON ciFP-CrhR plasmid was changed to a leucine by site-directed mutagenesis based on the method by Weiner and Costa (190) with primers DSW18 and DSW19 (Table 2.2). The plasmids, transformed into *E. coli* HB101 pRL623, were introduced to *Synechocystis* Δ*crhR* by triparental mating with *E. coli* HB101 RP4 as described previously (184). Cyanobacteria containing the plasmids were selected on BG-11 agar containing increasing concentrations of gentamicin to a final concentration of 10 μg ml^{-1}.

Laser-scanning confocal microscopy was performed on the ciFP-containing Δ*crhR* cells after cold induction for 3hr at 20°C. Cultures in liquid BG-11 were visualized using a Plan-Apochromat 63×/1.40 Oil DIC M27 objective lens mounted on a Zeiss LSM 510 Meta laser-scanning confocal microscope. Excitation was performed using 488 nm (28% intensity) and 514 nm (18% intensity) lasers. ciFP fluorescence was detected with a 520-555 nm filter, and chlorophyll *a* (Chl *a*) autofluorescence was detected in the 556 nm channel. The Zeiss Zen 2.3 SP1 (black) software was used to add scale bars to images and create the merged images prior to export as .tiff files.

2.4 Results

2.4.1 CrhR localizes to fractions containing both the cytoplasm and membranes

Differential extraction revealed that CrhR was detected in both the soluble and insoluble fractions of cell lysates, suggesting association with the cytoplasm and membrane fractions, respectively (Figure 2.2A). Previously, detection of CrhR had only been tested in soluble lysate, where it was present at background levels in cells grown at 30°C and increased in abundance by ~10-fold at 20°C (104). The same change in absolute protein abundance was observed here, with CrhR abundance increasing at 20°C in both the cytoplasmic and membrane fractions. Consistently and unexpectedly, CrhR migrated slower in the membrane fraction (Figure 2.2A), a result of excess lipid present in these

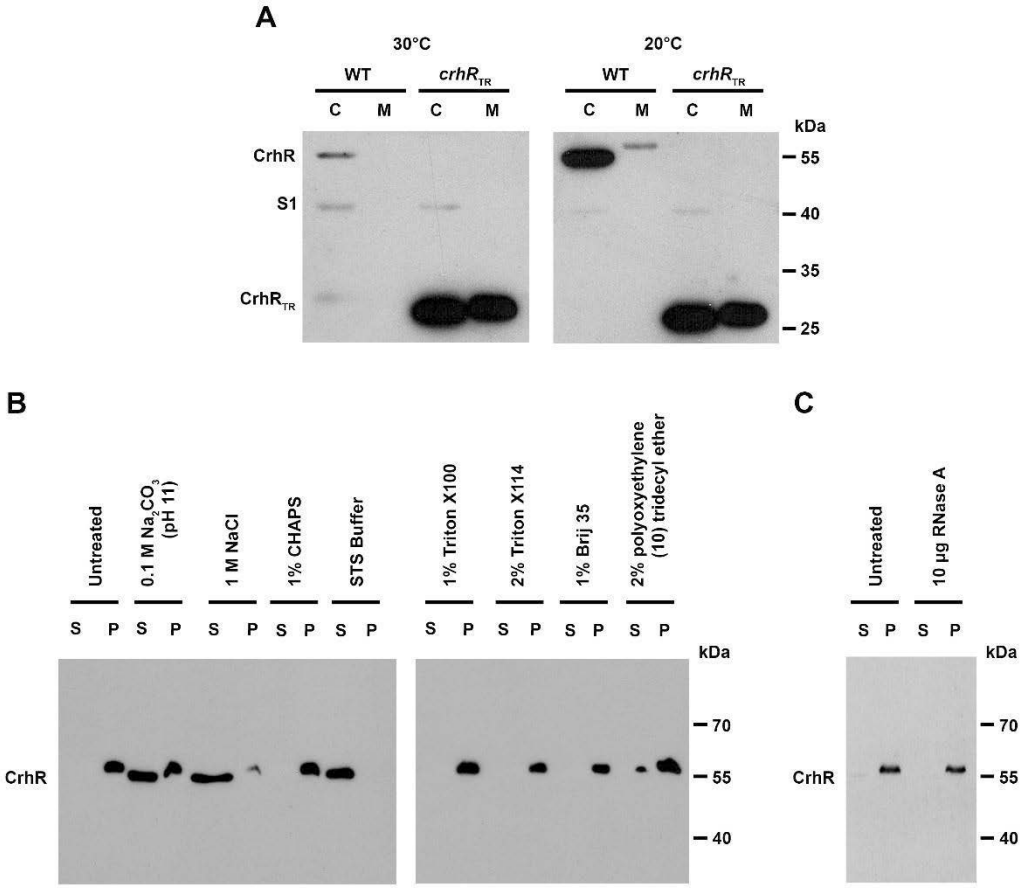

Figure 2.2: CrhR abundance in cytoplasmic and membrane fractions.

(A) Wild type (WT) and crhR$_{TR}$ mutant strains were grown at 30°C, and half of the culture was incubated at 20°C for 3h. Cells were mechanically lysed and clarified by centrifugation at 13,000 ×g to generate crude soluble cytoplasmic (lanes C) and membrane (lanes M) fractions. Soluble protein (10 µg) or an equivalent volume of the membrane fraction was subjected to Western analysis. CrhR (55 kDa), S1 (40 kDa) and CrhR$_{TR}$ (27 kDa) were detected using anti-CrhR and anti-S1 antibodies. (B and C) Extraction of CrhR from the membrane fraction. The indicated solvents (B) were tested for extraction of CrhR from *Synechocystis* membrane pellets obtained from cells that were cold-shocked at 20°C for 3 h prior to lysis. Following lysate clarification, the pellet was suspended in the presence of the indicated compounds and incubated on ice for 30 min or were treated with RNase A (C) and incubated at 37°C for 30 min. Solubilized proteins (S) were separated from the membrane pellet (P) by centrifugation. CrhR was detected in equal volumes of the soluble and pellet fractions using CrhR antibody.

samples, as only a single peptide was detected when the cytoplasmic and membrane fractions were mixed (data not shown). Although the majority of the wild type CrhR was detected in the cytoplasmic fraction, the results of extraction into this fraction were variable in our hands, likely due to the intensity of the mechanical extraction. In contrast, $CrhR_{TR}$, a truncated form of the CrhR protein, did not change with respect to either the abundance or the segregation of the protein (Figure 2.2A), consistent with the previously observed lack of expression regulation of the truncated protein (104). This suggests that $CrhR_{TR}$ is overexpressed in the mutant at 30°C and that the truncation affects $CrhR_{TR}$ localization. Localization of the control, primarily soluble ribosome-associated protein S1, was detected in supernatant fractions only under the conditions tested (Figure 2.2A). These observations led us to further analyze CrhR association with both the cytoplasmic and membrane fractions.

The degree to which CrhR associates with the membrane fraction was investigated by determining CrhR release in response to classic membrane-disrupting agents. As shown in Figure 2.2B, CrhR was relatively weakly associated with this fraction, as high-salt and/or high-pH treatments were sufficient to remove a portion of CrhR from the membrane pellet. Among the gentle, nonionic detergents tested, only polyoxyethylene (10) tridecyl ether was able to remove a portion of the CrhR from the membrane fraction. STS buffer, a mixture of ionic and nonionic detergents, was the only treatment that completely removed CrhR from the membrane fraction. RNase A treatment also did not remove CrhR from the membrane fraction (Figure 2.2C). The extraction results indicate that a portion of the cellular CrhR in *Synechocystis* is peripherally associated with membranes.

2.4.2 CrhR cosediments with polysomes

CrhR association with both cytoplasmic and membrane fractions prompted us to investigate the localization of CrhR within the *Synechocystis* cytoplasm. Sucrose ultracentrifugation separated the soluble *Synechocystis* extract into colored layers, as well into as a pellet that contained proteins capable of sedimentation through a 1 M sucrose cushion (Figure 2.3A). Western analysis detected the slower-migrating, 58-kDa CrhR in the dark green (third) layer obtained from the sucrose gradient ultracentrifugation (Figure

2.3B). This layer contained chlorophyll *a* (Chl *a*) and thus most likely contained thylakoid membranes, consistent with the membrane-associated CrhR observed (Figure 2.2A). CrhR and S1 were enriched in the pellet fraction, indicating cosedimentation of CrhR with polysome-containing material and not soluble translation components. CrhR cosedimented with this material from cells grown at both 30°C and 20°C, suggesting that temperature does not influence CrhR association with this fraction (Figure 2.3B and C). RNase A treatment was sufficient to extract CrhR from the polysome pellet (A. Rosana, personal communication).

We also localized CrhR in wild type cells that were not treated with chloramphenicol. The polysome runoff analysis indicated that CrhR distribution was dramatically altered, with CrhR being predominately detected in colored supernatant fractions 3 and 4 and less abundant in the polysome pellet obtained from cells grown at 20°C (Figure 2.3D). S1 distribution was dramatically altered, shifting from the polysome pellet to the colored supernatant fractions (Figure 2.3D). These results suggest that soluble S1 and CrhR are associated with actively translating polysomes; the absence of chloramphenicol allowed polysomes to finish translation during isolation, releasing CrhR and S1 into the supernatant fraction. These results also indicate that CrhR localization to the pellet fractions was not a result of aggregation.

In order to separate CrhR association with ribosome biogenesis from active translation, a linear sucrose gradient was used to fractionate soluble wild type *Synechocystis* extracts to isolate ribosome subunits from 70S ribosomes and polysomes. Absorbance (A_{254}) and Western analysis of the sucrose gradient fractions from cells grown at 20°C further confirmed the cosedimentation of CrhR only with the polysome fraction and not significantly with the 30S or 50S subunits or free 70S ribosomes (Figure 2.4). The slower-migrating (58-kDa) CrhR band was detected at a low level in lanes 15 to 18, at an approximate sucrose concentration of 44% to 49%. The molecular mass and sucrose banding data suggest that the detected CrhR corresponded to the membrane-localized CrhR, as total *Synechocystis* extract was utilized in the analysis. As a control, S1 was detected in all ribosome-containing fractions (Figure 2.4).

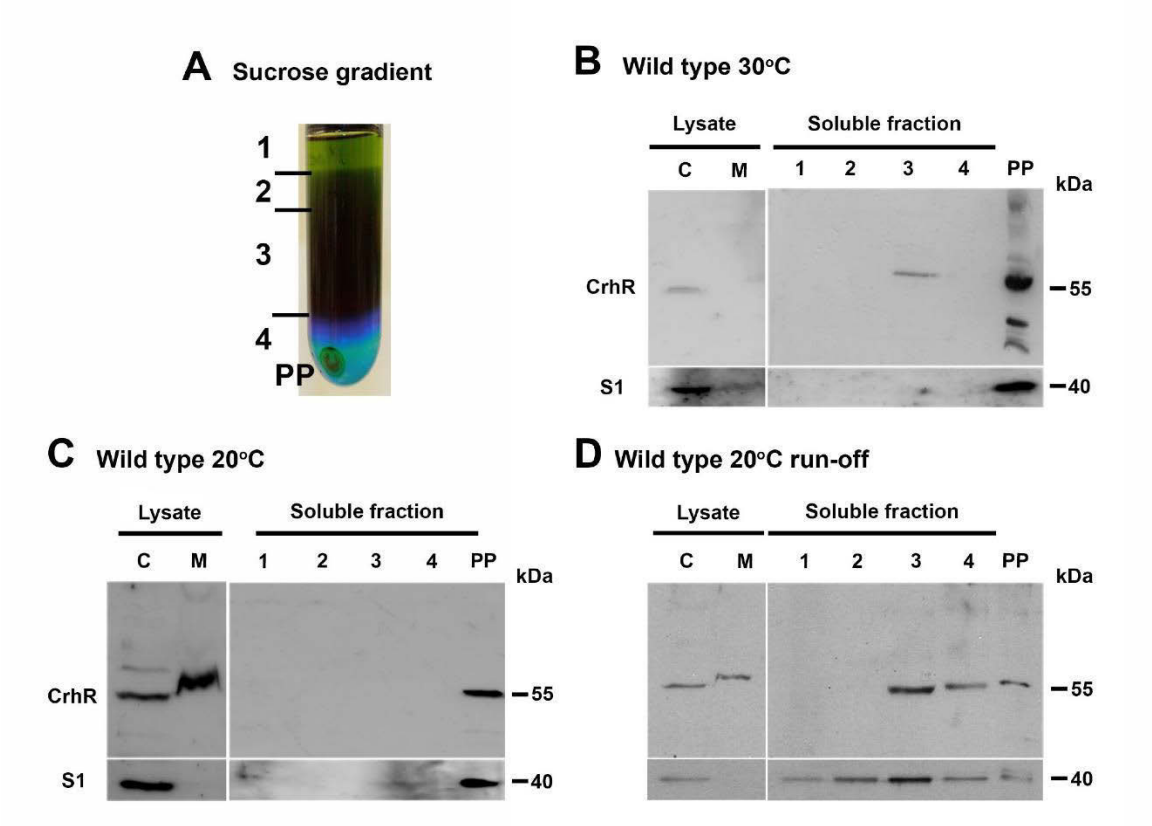

Figure 2.3: CrhR localization in soluble *Synechocystis* lysates.[2]

(A) Lysate fractionation. A soluble cell lysate was overlaid on a 1 M sucrose cushion, resulting in a crude polysome-containing pellet (PP) and colored soluble layers (layers 1 to 4) by ultracentrifugation. (B and C) CrhR localization. Wild type *Synechocystis* cells were treated with chloramphenicol to stabilize polysome complexes before lysis. CrhR and S1 were detected in the gradient fractions obtained from wild type cells grown at 30°C (B) and cold-shocked at 20°C for 3 h (C). (D) CrhR localization under translational runoff conditions. CrhR and S1 were localized in sucrose gradient fractions for wild type cells grown at 20°C that were not treated with chloramphenicol. For reference, CrhR was also detected in the cytoplasmic (lanes C) and membrane (lanes M) fractions obtained after clarification of French press lysates. CrhR and S1 were detected as described in the Figure 2.2 legend.

[2] Panels A-C were previously published in (191) and are used with permission.

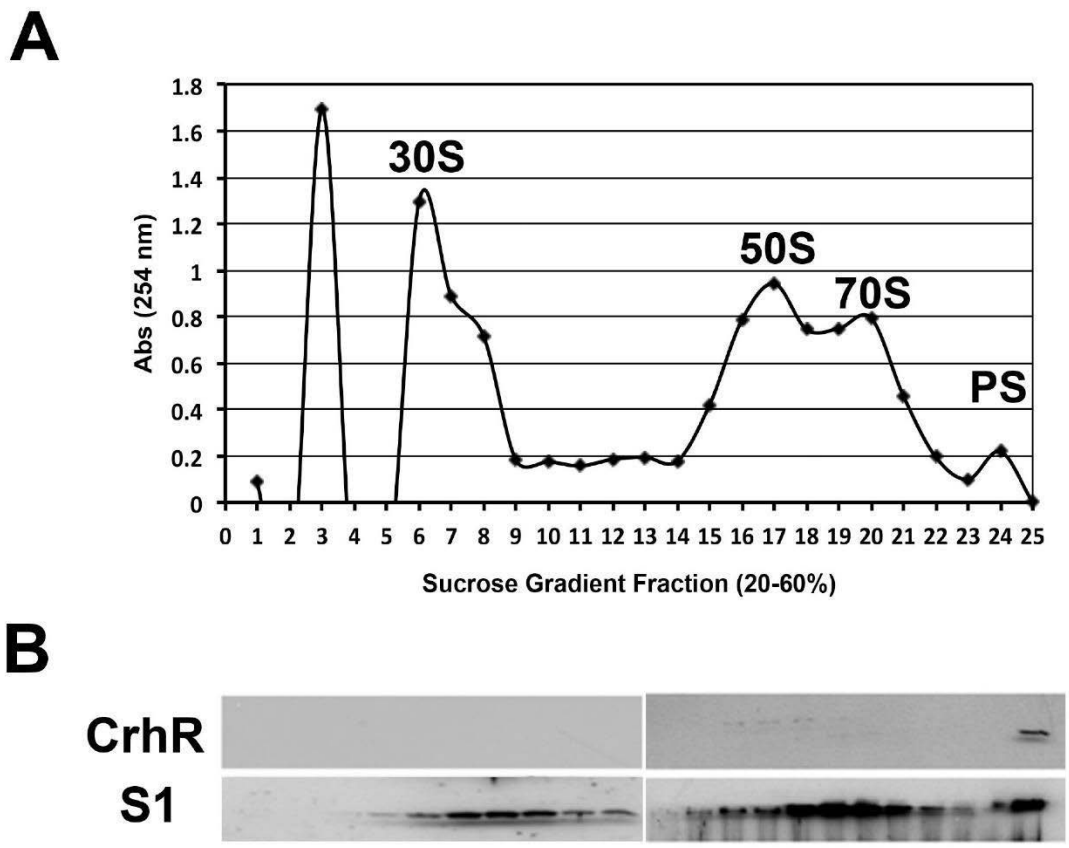

Figure 2.4: *Synechocystis* polysome fractionation.

Total soluble protein from wild type *Synechocystis* cells cold-shocked at 20°C for 3 h was fractionated on a linear 20-60% sucrose gradient. (A) Absorbance profile. The absorbance profile of the gradient fractions is shown with the ribosomal subunits and complexes indicated. (B) CrhR detection. CrhR was localized in the gradient fractions using anti-CrhR antibody. S1 was detected as a control.

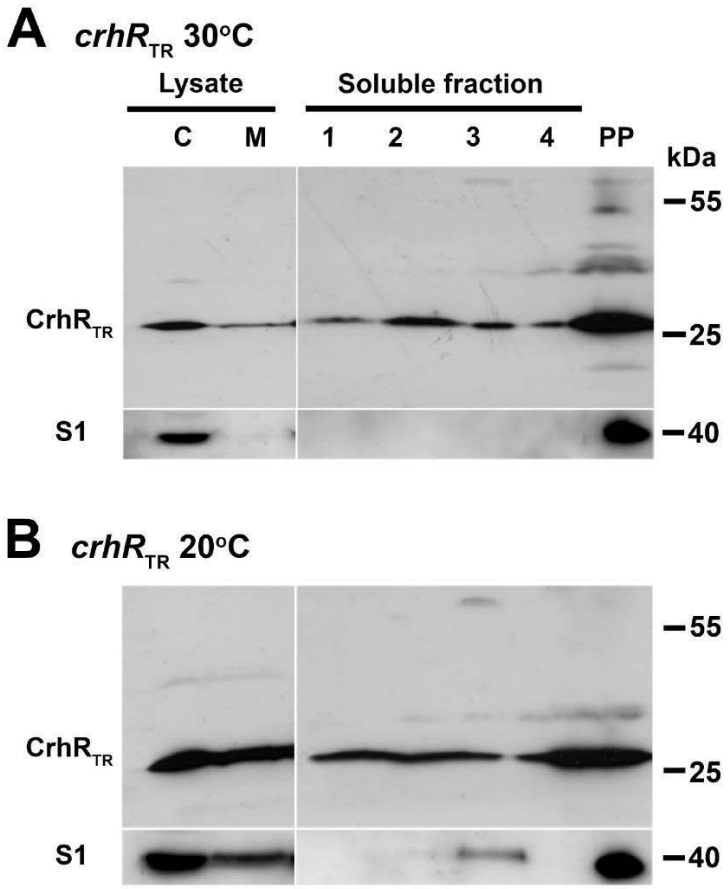

Figure 2.5: CrhR$_{TR}$ localization in soluble *Synechocystis* lysates.[3]

CrhR$_{TR}$ cells were treated with chloramphenicol to stabilize polysome complexes before lysis. Soluble cell lysate from *crhR*$_{TR}$ mutant cells was overlaid on a 1 M sucrose cushion and a polysome-containing pellet (PP) was obtained by ultracentrifugation. CrhR$_{TR}$ and S1 were detected in the gradient fractions obtained from *crhR*$_{TR}$ cells grown at 30°C (A) and cold-shocked at 20°C for 3 h (B). For reference, CrhR$_{TR}$ was also detected in the cytoplasmic (lanes C) and membrane (lanes M) fractions obtained after clarification of French press lysates. CrhR$_{TR}$ and S1 were detected as described in the Figure 2.2 legend.

[3] The images in this figure have previously been published in (191) and are used with permission.

2.4.3 *crhR* truncation results in improper polysome association

A similar polysome analysis was performed using the *crhR*$_{TR}$ mutant to determine the effect of CrhR truncation on localization. In striking contrast to the polysome-specific localization of CrhR in wild type cells, the CrhR$_{TR}$ polypeptide was detected in all sucrose layers and in the pellet, irrespective of growth temperature (Figure 2.5). In comparison, S1 localization was not altered in the *crhR*$_{TR}$ mutant (Figure 2.5). Similar to the observations in wild type cells (Figure 2.3B), S1 was detected only in the pellet fraction and also in Chl *a*-containing layer 3 of the sucrose gradient of soluble lysate obtained from cells grown at 20°C (Figure 2.5B). This suggests that full-length and/or functionally active CrhR RNA helicase is not required for S1 localization to polysomes but is required for CrhR cosedimentation with polysomes.

2.4.4 CrhR cosediments with polysome- and degradosome-associated proteins

Proteins cosedimenting with polysomes from soluble extracts of wild type and *crhR*$_{TR}$ cells grown at 30°C and 20°C were identified by mass spectrometry following a second purification through a 1 M sucrose cushion. The complete data set was organized into functional categories and is presented in Table 2.3. The major categories include subunits of the small and large ribosomal complexes, translation initiation and elongation factors, ribosome binding factors, and transcription factors. Furthermore, RNA modification enzymes involved in rRNA processing and RNA binding, and the RNase E and PNPase degradosome subunits were also detected. Proteins known to be primarily thylakoid membrane-localized, such as photosynthesis-associated proteins, including phycobilisome proteins, ATP synthase subunits, and photosystem I (PSI) and II components, were also detected. Other proteins associated with energy metabolism, primarily glycolytic enzymes, carboxysome fragments, proteins involved in regulation of transcription, including LexA and RNA polymerase components, protein degradation subunits, bacterioferritin, and a number of unknown and hypothetical proteins were also detected.

A Venn diagram depicting the polypeptides detected in the 1M cushion pellet obtained from soluble extracts of wild type and *crhR*$_{TR}$ mutants at 20°C and 30°C is presented in Figure 2.6. A total of 38% of the detected polypeptides that pelleted through

Table 2.3: Polysome pellet mass spectrometry analysis.[4]

Polypeptides are organized by gene ontology designation (modified from https://www.ebi.ac.uk/QuickGO/) and further sorted according to detected PSM value. Polypeptides were identified by mass spectrometry of polysome pellets isolated from wild type and *crhR*$_{TR}$ mutant strains grown at 30°C and 20°C. Resulting peptides were searched against and annotated using the *Synechocystis* sp. PCC 6803 Uniprot proteome SYNY3.

Locus Tag	Gene Code	Description	PSM #				Uniprot accession #
			WT 30	WT 20	*crhR*$_{TR}$ 30	*crhR*$_{TR}$ 20	
Amino acid metabolism							
sll1908	SerA	Phosphoglycerate dehydrogenase	12	26	22	22	P73821
slr0585	ArgG	Argininosuccinate synthase	4	6	3	10	P77973
sll1363	IlvC	Ketol-acid reductoisomerase	3	7		4	P29107
sll0080	ArgC	N-acetyl-gamma-glutamyl-phosphate reductase				2	P54899
slr0212	MetH	Methionine synthase				2	Q55786
slr0661	ProC	Pyrroline-5-carboxylate reductase				2	P74572
slr0710	GdhA	Glutamate dehydrogenase		2			P54386
ATP synthase subunits							
sll1326	AtpA	ATP synthase subunit alpha	49	54	45	71	P27179
sll1327	AtpG	ATP synthase gamma chain	14	25	23	32	P17253
slr1329	AtpB	ATP synthase subunit beta				6	P26527
Carbohydrate metabolism							
sll1393	GlgA	Glycogen synthase 2		6	28	36	P72623
sll1525	Prk	Phosphoribulokinase	3	8	4	35	P37101
slr1176	GlgC	Glucose-1-phosphate adenylyltransferase		11	3	24	P52415
sll0018	FbaA	Fructose-1,6-bisphosphate aldolase, class II	4	17	11	5	Q55664
sll1356	GlgP	Glycogen phosphorylase			7	8	P73511
sll0158	GlgB	1,4-alpha-glucan branching enzyme				6	P52981
sll0945	GlgA	Glycogen synthase 1			2	4	P74521
slr1857	GlgX	Glycogen operon protein homolog				6	P73608
slr1843	Zwf	Glucose-6-phosphate 1-dehydrogenase				4	P73411
slr0518	AbfB	Arabinofuranosidase				3	Q55841
slr2094	GlpX	D-fructose 1,6-bisphosphatase class 2/sedoheptulose 1,7-bisphosphatase				3	P73922
Carbon fixation							
slr0009	RbcL	Ribulose bisphosphate carboxylase large chain	218	348	206	247	P54205
sll1031	CcmM	Carbon dioxide concentrating mechanism protein	8	27	12		P72758
slr0012	RbcS	Ribulose bisphosphate carboxylase small subunit		16		5	P54206
sll0920	Ppc	Phosphoenolpyruvate carboxylase		6	4	9	P74299
Cell division associated proteins							
sll1633	FtsZ	Cell division protein ftsZ			3		P73456
Circadian Rhythm							
slr0758	KaiC	Circadian clock protein kinase		2	2	4	P74646
slr1942	KaiC3	Circadian clock protein KaiC-like protein 2		3		3	P74503
DNA metabolism							
sll1583	Lig	DNA ligase	11	27	14		P73196
sll0569	RecA	Recombinase A		20	6	8	P74737
sll0656	NucH	Extracellular nuclease			4	11	P72938
slr2058	TopA	DNA topoisomerase		6			P73810
slr0417	GyrA	DNA gyrase subunit A		4			Q55738

[4] Mass spectrometry analysis was completed with the assistance of J. Moore and R.P. Fahlman of the Alberta Proteomics and Mass Spectrometry Facility, University of Alberta.

Locus Tag	Gene Code	Description	PSM #				Uniprot accession #
			WT 30	WT 20	*crhR* $_{TR}$ 30	*crhR* $_{TR}$ 20	
Energetics							
slr0963	Sir	Ferredoxin-sulfite reductase		3		14	P72854
slr1643	PetH	Ferredoxin-NADP oxidoreductase				3	Q55318
Fatty acid biosynthesis							
slr0886	FabG	3-oxoacyl-[acyl-carrier protein] reductase			4	2	P73574
slr1051	FabI	Enoyl-[acyl-carrier-protein] reductase		3			P73016
Glycolysis							
sll1342	Gap2	Glyceraldehyde-3-phosphate dehydrogenase	117	144	158	142	P80505
sll1841	OdhB	Dihydrolipoamide acetyltransferase pyruvate dehydrogenase complex E2 component	6	46	54	34	P74510
slr1096	PhdD	Dihydrolipoyl dehydrogenase	5	34	35	29	P72740
slr0394	Pgk	Phosphoglycerate kinase	15	14	21	19	P74421
slr1934	PdhA	Pyruvate dehydrogenase E1 component, alpha subunit	3	3		4	P74490
slr0884	Gap1	Glyceraldehyde 3-phosphate dehydrogenase				3	P49433
Heme biosynthesis							
sll1994	HemB	Delta-aminolevulinic acid dehydratase	2	2			P77969
Metabolism, general							
sll0947	LrtA	Light repressed protein	12	3	13	24	P74518
sll1536	MoeB	Molybdopterin biosynthesis protein		6	15	15	P74344
sll1559		Soluble hydrogenase 42 kDa subunit		7			P74281
slr1020	SqdB	Sulfolipid biosynthesis protein		4		3	P73128
sll1070	TktA	Transketolase				2	P73282
Nitrogen metabolism							
slr1756	GlnA	Glutamine synthetase	13	20	11	55	P77961
sll1750	UreC	Urease subunit alpha				6	P73061
sll1499	GltS	Ferredoxin-dependent glutamate synthase		2			P55038
Nucleotide sugar metabolism							
sll1212	RfbD	GDP-D-mannose dehydratase		3			P72586
Nucleotide metabolism							
sll0654	PhoA	Alkaline phosphatase		11	80	24	P72939
sll0469	PrsA	Ribose-phosphate pyrophosphokinase		4		3	Q55848
sll0144	PyrH	Uridine monophosphate kinase				2	P74457
Photosynthesis related							
slr0335	ApcE	Phycobilisome LCM core-membrane linker polypeptide	193	418	631	349	Q55544
sll1580	CpcC1	Phycocyanin associated linker protein	116	153	182	210	P73203
sll1579	CpcC2	Phycocyanin associated linker protein	65	82	85	104	P73204
sll0851	PsbC	Photosystem II CP43 reaction centre protein	43	53	100	72	P09193
slr1834	PsaA	Photosystem I P700 chlorophyll a apoprotein A1	52	50	68	57	P29254
slr1835	PsaB	Photosystem I P700 chlorophyll a apoprotein A2	51	38	63	69	P29255
sll1577	CpcB	Phycocyanin b subunit	28	33	66	71	Q54714
slr2051	CpcG	Phycobilisome rod-core linker polypeptide; CpcG	9	11	59	52	P73093
sll0033	CrtH	Carotene isomerase		4	45	37	Q55455
slr1986	ApcB	Allophycocyanin b chain		13	19	42	Q01952
slr0737	PsaD	Photosystem I reaction centre subunit II	17	7	21	25	P19569
sll0849	PsbD	Photosystem II D2 protein	15	23	19	11	P09192
ssr3383	ApcC	Phycobilisome 7.8 kDa linker polypeptide, allophycocyanin-associated, core			22	29	Q02925
sll1578	CpcA	Phycocyanin a subunit	10	12	11	8	Q54715
slr2067	ApcA	Allophycocyanin a chain	4	8		7	Q01951
ssl0563	PsaC	Photosystem I iron-sulfur center	6		5		P32422
slr0506	Por	Protochlorophyllide oxido-reductase				9	Q59987
slr0261	NdhH	NADH-quinone oxidoreductase subunit H		7			P27724
slr1963	Ocp	Water-soluble carotenoid protein			3	3	P74102
sll1471	CpcG	Phycobilisome rod-core linker polypeptide		3			P74625
slr0906	PsbB	Photosystem II CP47 reaction centre protein			3		P05429
slr1808	HemA	Glutamyl-tRNA reductase		2			P28463
Polyhydroxybutyrate biosynthesis							
slr1830	PhbC	Poly(3-hydroxyalkanoate) synthase	2	2	9	6	P73390

Locus Tag	Gene Code	Description	PSM #				Uniprot accession #
			WT 30	WT 20	*crhR*$_{TR}$ 30	*crhR*$_{TR}$ 20	
Protein chaperone							
sll0170	DnaK	Chaperone protein DnaK2				2	P22358
Protein degradation							
sll0020	ClpC	ATP-dependent Clp protease regulatory subunit	16	27			Q55662
slr1604	FtsH	ATP-dependent zinc metalloprotease FtsH 3	10	17			P72991
slr0228	FtsH2	ATP-dependent zinc metalloprotease FtsH2	8	11	6		Q55700
sll1463	FtsH4	ATP-dependent zinc metalloprotease FtsH 4		11		5	P73437
slr0804	DacB	D-alanyl-D-alanine carboxypeptidase			3		P74032
slr0164	ClpR	ATP-dependent Clp protease proteolytic subunit-like				2	P74466
Protein secretion system							
slr1531	Ffh	Signal recognition particle protein	2	12	8	9	P74214
slr1277	GspD	General secretion pathway protein D	3	21			P74189
slr0063	GspE	General secretion pathway protein E	3	6			Q55155
Ribosome biogenesis							
slr0742	RimP	Ribosome maturation factor	2			4	P72687
slr0808	RimM	Ribosome maturation factor				6	P74035
RNA polymerase subunits							
slr1265	RpoC1	DNA-directed RNA polymerase subunit gamma	27	59	54	42	P74177
slr0653	RpoD	RNA polymerase sigma factor SigA	5	7	7	53	P74565
sll1787	RpoB	DNA-directed RNA polymerase subunit beta	16	32	12	11	P77965
sll1818	RpoA	DNA-directed RNA polymerase subunit alpha		15	3		P73297
sll1789	RpoC2	DNA-directed RNA polymerase subunit beta'		8	2	3	P73334
RNA modification							
sll1043	Pnp	Polyribonucleotide nucleotidyltransferase	14	33	19	18	P72659
slr0551	Rnj	Ribonuclease J	30	35		3	P54123
slr1129	Rne	Ribonuclease E	2	13	19	7	P72656
sll0754	RbfA	Ribosome-binding factor A	6	2	5	16	Q55625
sll1910	Zam	Protein conferring resistance to acetazolamide		5	15	5	Q46363
sll0708	RsmA	Ribosomal RNA small subunit methyltransferase A	3	3	10	5	P72666
slr0083	CrhR	ATP-dependent RNA helicase		9			Q55804
Transcription							
sll1626	LexA	SOS function regulatory protein homolog LexA	187	162	530	971	P73722
sll1561	PutA	Delta-1-pyrroline-5-carboxylate dehydrogenase	3	6	7		P74275
sll0998	RbcR	LysR family transcriptional regulator		5		5	P73123
Translation, ribosomal proteins							
sll1810	RplF	50S ribosomal protein L6	1031	801	1071	1510	P73306
sll1800	RplD	50S ribosomal protein L4	748	728	887	1188	P73319
sll1808	RplE	50S ribosomal protein L5	638	799	925	1035	P73308
sll1744	RplA	50S ribosomal protein L1	546	463	959	1235	P36236
sll1802	RplB	50S ribosomal protein L2	599	634	915	1018	P73317
sll1812	RpsE	30S ribosomal protein S5	679	725	751	807	P73304
sll1799	RplC	50S ribosomal protein L3	484	456	760	748	P73320
sll1244	RplI	50S ribosomal protein L9	401	478	528	725	P42352
sll1097	RpsG	30S ribosomal protein S7	339	353	339	656	P74229
slr1356	Rps1A	30S ribosomal protein S1 homolog A	345		498	676	P73530
sll1813	RplO	50S ribosomal protein L15	415		356	746	P73303
sll1260	RpsB	30S ribosomal protein S2	301	367	368	407	P74071
slr0469	RpsD	30S ribosomal protein S4	324	288	322	430	P48939
sll1817	RpsK	30S ribosomal protein S11	359	289	219	331	P73298
sll1805	RplP	50S ribosomal protein L16	381	243	198	375	P73313
sll1804	RpsC	30S ribosomal protein S3	204	147	329	452	P73314
sll1821	RplM	50S ribosomal protein L13	183	278	239	314	P73294
sll1822	RpsI	30S ribosomal protein S9	166	139	185	294	P73293
sll1816	RpsM	30S ribosomal protein S13	196	204	115	242	P73299
sll0767	RplT	50S ribosomal protein L20	153	150	118	294	P48957
sll1803	RplV	50S ribosomal protein L22	253	203	105	141	P73315
slr1678	RplU	50S ribosomal protein L21	187	122	115	222	P74266
ssr2799	RpmA	50S ribosomal protein L27	320	263	39	19	P74267
sll1801	RplW	50S ribosomal protein L23	271	283	68	10	P73318
sll1806	RplN	50S ribosomal protein L14	449	89	62	29	P73310
sll1811	RplR	50S ribosomal protein L18	225	205	86	61	P73305
sll1807	RplX	50S ribosomal protein L24	135	52	86	161	P73309
sll1767	RpsF	30S ribosomal protein S6	215	129	16	15	P73636
sll1740	RplS	50S ribosomal protein L19	125	92	77	76	P36239
sll1809	RpsH	30S ribosomal protein S8	91	77	70	100	P73307
sll1819	RplQ	50S ribosomal protein L17	117	45	45	114	P73296
ssr0482	RpsP	30S ribosomal protein S16	183	109	23		P74410

Locus Tag	Gene Code	Description	PSM #				Uniprot accession #
			WT 30	WT 20	*crhR*$_{TR}$ 30	*crhR*$_{TR}$ 20	
Translation, ribosomal proteins							
sll1101	RpsJ	30S ribosomal protein S10	83	60	68	52	P74226
ssl3437	RpsQ	30S ribosomal protein S17	128	98	19		P73311
ssr1399	RpsR	30S ribosomal protein S18	99	63	19	19	P48946
ssr1604	RpmB	50S ribosomal protein L28	48	42	37	32	P72851
ssl3432	RpsS	30S ribosomal protein S19	62	51	21	15	P73316
ssl1426	RpmI	50S ribosomal protein L35	62	45	24	9	P48959
sml0006	RpmJ	50S ribosomal protein L36	28		39	67	P73300
slr0628	RpsN	30S ribosomal protein S14	29	17	25	32	P48944
ssl1784	RpsO	30S ribosomal protein S15	43	38	10		P72866
ssl2233	RpsT	30S ribosomal protein S20	30	29	13		P73336
sll1824	RplY	50S ribosomal protein L25	25	39	7		P73289
ssl3436	RpmC	50S ribosomal protein L29	35	26	5		P73312
sll1096	RpsL	30S ribosomal protein S12	25	9	11	13	P74230
ssl0601	RpsU	30S ribosomal protein S21	28	12	6		P48949
slr1984	Rps1B	30S ribosomal protein S1 homolog B	7	23		14	P74142
sll1745	RplJ	50S ribosomal protein L10	4	3	13	14	P23350
Translation, other							
sll1099	TufA	Protein synthesis elongation factor Tu	40	69	151	183	P74227
slr0974	InfC	Translation initiation factor IF-3	33	37	38	42	P72874
slr0744	InfB	Translation initiation factor IF-2	9	37	2	6	P72689
slr1463	FusA	Elongation factor EF-G	3	11	3	5	P28371
slr0070	Fmt	Methionyl-tRNA formyltransferase				9	Q55163
slr1886	RsfS	Ribosome silencing factor	3			2	P73658
slr0877	GatA	Glutamyl-tRNA(Gln) amidotransferase subunit A				4	P73558
sll1553	PheT	Phenylalanine-tRNA ligase beta subunit		3			P74296
Transport							
sll1341	Bfr	Bacterioferritin	315	350	1077	1917	P24602
slr1890	Bfr	Bacterioferritin	285	261	752	945	P73287
slr0161	PilT	Twitching motility protein		11	20	13	P74463
slr1247	PstS	Periplasmic phosphate binding protein			7	8	P73785
slr1596	PxcA	Proton extrusion protein			2		P74028
slr1729	KdpB	Potassium-transporting ATPase B chain		2			P73867
Vitamin metabolism							
slr1109	Ank	Erythroid ankyrin			18	30	P72736
sll1282	RibH	6,7-dimethyl-8-ribityllumazine synthase				4	P73527
Unknown proteins							
sll0518		Unknown protein	31	38	38	115	Q55466
sll1971		Probable hexosyltransferase		172			P73369
slr1841		Probable porin	2	14	68	20	P73409
slr1829		putative poly(3-hydroxyalkanoate) synthase component	3	15	39	17	P73389
sll1873		Unknown protein	6	4	12	40	P74135
sll1951	HlyA	Probable hemolysin		8	31	19	P73817
slr1908		Probable porin		10	33	14	P73103
slr0451	Ski2	Putative helicase	4		4	36	P74686
slr0955		Probable tRNA/rRNA methyltransferase	5	4	11	20	P74328
sll0617	Vipp1	Plasma membrane protein essential for thylakoid formation		6	10	23	Q55707
sll1009	FrpC	Iron-regulated protein			7	17	P73019
slr0453		Probable phosphoketolase		2	5	13	P74690
slr1617		similar to UDP-glucose 4-epimerase		4	8	8	P72895
slr1768		Unknown protein			6	12	P73049
slr0909		Unknown protein			4	11	Q55375
sll1033		Probable protein phosphatase		7	2	4	P72756
slr1258		Unknown protein	2	3	5		P73798
slr1274	PilM	probable fimbrial assembly protein		4	2	2	P74186
sll2001	PepA	Probable cytosol aminopeptidase		4		3	P73971
sll0815		Unknown protein		2	4		P74042
slr0106		Unknown protein		6			Q55877
slr0361		Probable ribosomal large subunit pseudouridine synthase B		3		2	Q55578
slr1540		Probable mRNA binding protein				5	P73424
slr1616		Unknown protein		2		3	P72894
slr0915		Putative endonuclease				4	Q79D96
sll0219	Dfa4	Putative diflavin flavoprotein A4		3			P72721
sll1546	Ppx	Exopolyphosphatase				3	P74663
slr2034	Ycf48	Ycf48-like protein				3	P73069
slr1272		Probable porin			2		P74184

Locus Tag	Gene Code	Description	PSM #				Uniprot accession #
			WT 30	WT 20	*crhR*$_{TR}$ 30	*crhR*$_{TR}$ 20	
Hypothetical proteins							
sll0735		Hypothetical protein	34	73	279	581	P74630
slr1128		Hypothetical protein	68	135	140	160	P72655
sll0185		Hypothetical protein	52	61	58	49	Q55770
sll0586		Hypothetical protein	4	13	41	40	Q55864
slr0244		Hypothetical protein		4	36	20	P72700
slr0848		Hypothetical protein	20	29	10		Q55436
sll0175		Hypothetical protein			24		Q55555
sll1526		Hypothetical protein	6	9		4	P74360
slr1122		Hypothetical protein		5	10	4	P72645
sll1021		Hypothetical protein		7	4	5	P72929
slr0064		Hypothetical protein		2	6	4	Q55156
slr0404		Hypothetical protein		2	3	5	P74433
sll1336		Hypothetical protein	3	6			P74535
slr0049		Hypothetical protein		2		6	Q55131
sll0283		Hypothetical protein			2	3	Q55913
sll0822		Hypothetical protein			5		Q55432
sml0011		Hypothetical protein				5	A0A068N0P2
slr0670		Hypothetical protein			2	2	P72937
slr1541		Hypothetical protein				4	P73425
slr5023		Hypothetical protein			4		Q6ZEV7
slr0039		Hypothetical protein				2	Q55458
slr0374		Hypothetical cell division cycle protein		2			Q55589
slr1363		Hypothetical protein				2	P73537
slr1519		Hypothetical protein				2	P73963
slr1660		Hypothetical protein			2		P74661

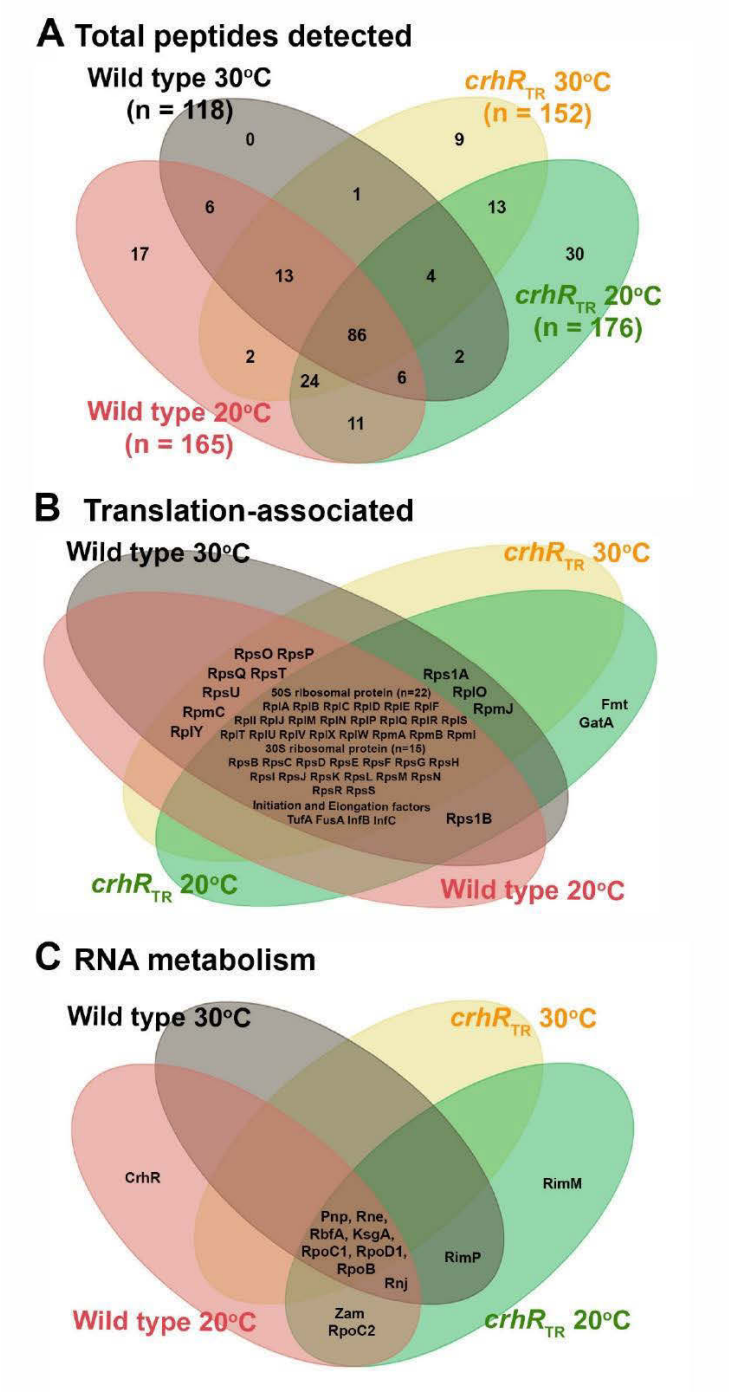

Figure 2.6: Venn diagram of polysome-associated polypeptides.

(A) The number of common and unique peptides identified by mass spectrometry that co-sediment with *Synechocystis* polysomes isolated from wild type and *crhR*TR stains at 30°C and 20°C are indicated. (B and C) Venn diagrams indicating the specific peptides that are associated with (B) translation and (C) RNA metabolism. Venn diagrams were produced using: creately.com/Draw-Venn-Diagrams-Online.

the 1 M sucrose cushion were shared among all conditions (Figure 2.6A). Differential detection of the remainder could have resulted from either temperature effects or the absence of functional CrhR RNA helicase activity. The extensive numbers of polypeptides detected in the 1 M sucrose cushion that are associated with translation and RNA metabolism, including degradation, are depicted in Figure 2.6B and C, respectively. The majority of these polysome- and degradosome-associated polypeptides were detected under all four conditions tested.

2.4.5 CrhR associates with the thylakoid membrane

The presence of the ~58-kDa polypeptide cross-reacting with the CrhR antibody from the membrane-containing pellet fractions necessitated analysis of the three distinct membranes found in *Synechocystis*. We utilized the classic flotation ultracentrifugation method using a discontinuous sucrose gradient described by Murata and Omata (188) to separate the *Synechocystis* membranes from the total cell lysate. The fractions corresponded to the outer membrane (OM; 10% sucrose), the cytoplasmic membrane (CM; 30% sucrose), the thylakoid membrane (TM; 39% sucrose), and cell wall and other material that pelleted through the 50% sucrose cushion (cell wall pellet). CrhR was detected only in the thylakoid membrane-containing 39% sucrose layer and the pellet (Figure 2.7). To verify the purity of the thylakoid membrane fraction, the thylakoid-associated integral FtsH protease and the photosystem-associated PsbA (D1) protein were used as thylakoid membrane-specific markers. As expected, the anti-FtsH and anti-PsbA antibodies detected polypeptides in the thylakoid membrane-containing 39% sucrose layer and not in the cytoplasmic membrane (Figure 2.7). Similarly, Vipp1 and S1 were detected in the cytoplasmic and thylakoid membrane fractions in which they are known to function (Figure 2.7). Vipp1 and S1 were also detected in the cell wall pellet, indicating that this fraction was contaminated with thylakoid membrane and/or membrane-associated polysomes that would pellet through the 50% sucrose cushion. Overall, the parallel detection of CrhR with FtsH and PsbA suggests colocalization of these peptides within the thylakoid membrane fraction in *Synechocystis*.

Since the truncated CrhR peptide was observed in all fractions of the polysome preparation, a finer discontinuous sucrose gradient (189) was used to isolate the three

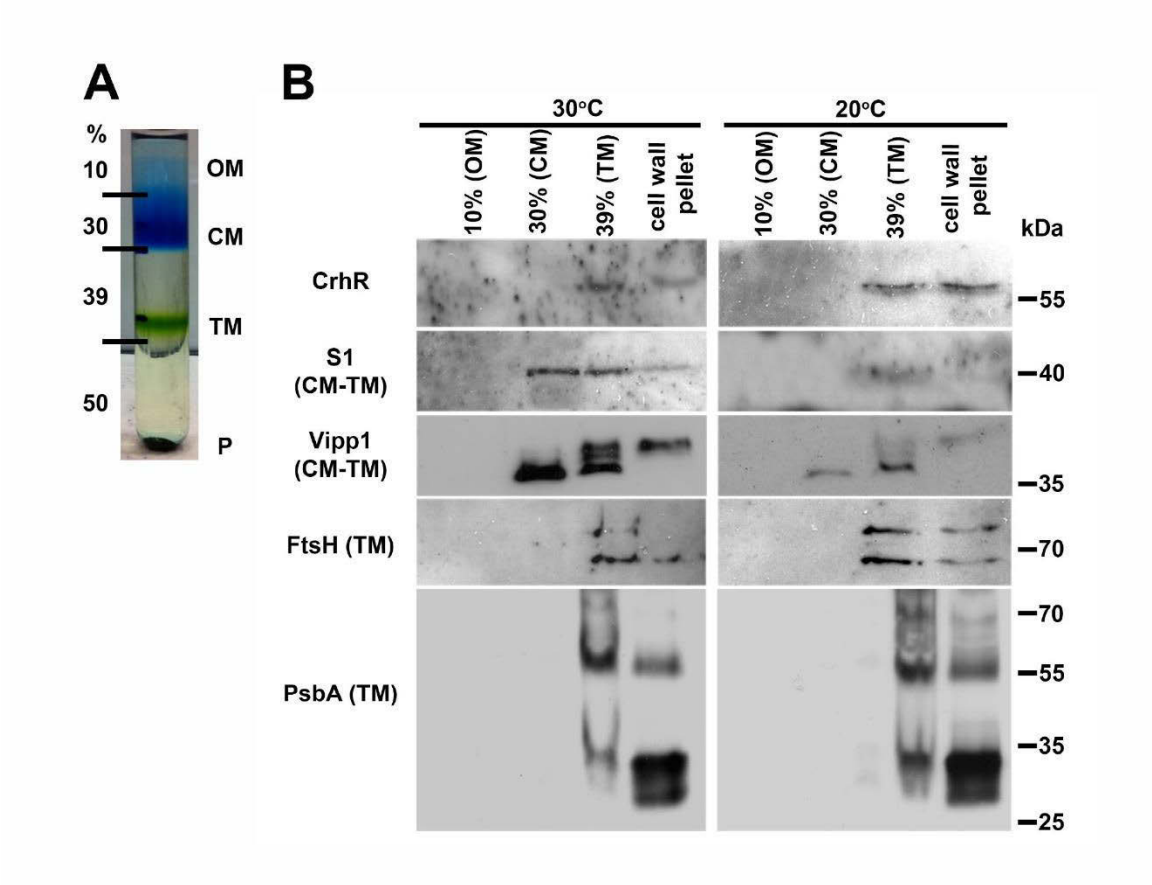

Figure 2.7: CrhR localization in wild type *Synechocystis* membranes.[5]

Total membrane pelleted from cells grown at 30°C and cold-shocked at 20°C for 3 h was adjusted to 50% sucrose, and individual membranes were isolated by flotation ultracentrifugation. (A) Sucrose gradient showing the relative positions of the membrane fractions. OM, outer membrane; CM, cytoplasmic membrane; TM, thylakoid membrane; P, cell wall pellet. (B) The indicated peptides were detected in the resolved membrane fractions using anti-CrhR, anti-FtsH, anti-S1, anti-Vipp1 and anti-PsbA antibodies.

[5] Panel B of this figure has been previously published in (191) and is used with permission.

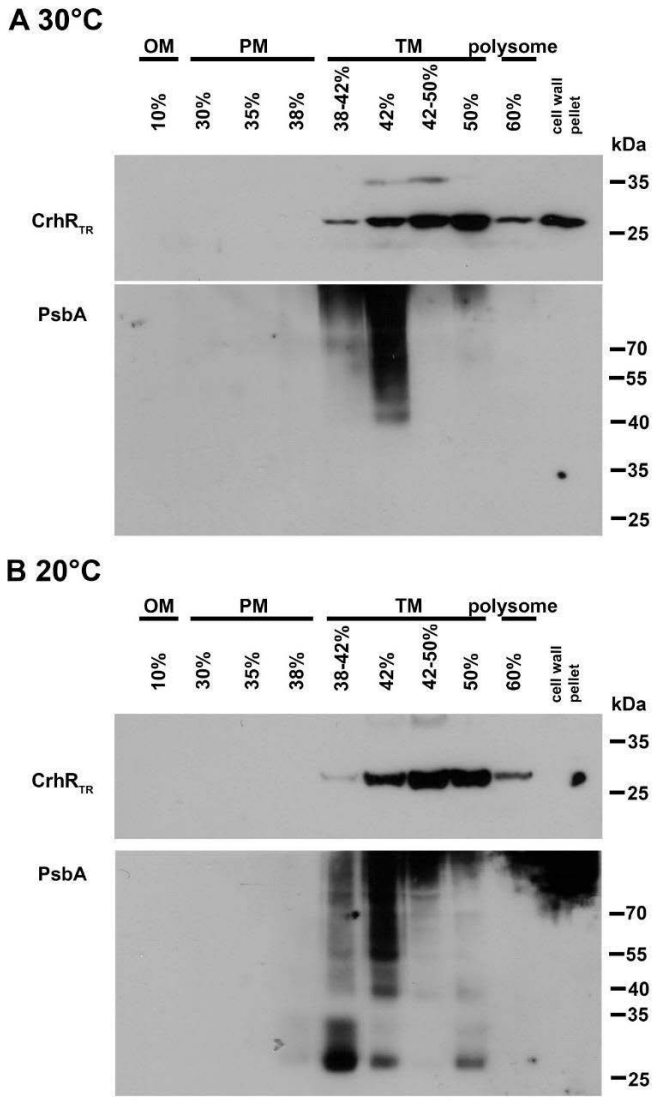

Figure 2.8: CrhR$_{TR}$ localization in *crhR*$_{TR}$ mutant *Synechocystis* membranes. Total membrane pelleted from *crhR*$_{TR}$ cells grown at 30°C (A) and 20°C (B) was adjusted to 42% sucrose, and individual membranes were purified by flotation ultracentrifugation in a discontinuous sucrose gradient. CrhR$_{TR}$ and PsbA distributions were detected in equal volumes of each of the gradient fractions using anti-CrhR and anti-PsbA antibodies. OM, outer membrane; CM, cytoplasmic membrane; TM, thylakoid membrane.

membrane types from *crhR*$_{TR}$ mutant cells. In contrast to the disrupted polysome localization shown in Figure 2.5, CrhR$_{TR}$ was primarily detected only in the thylakoid-enriched fractions at both 30°C and 20°C even though it was overexpressed at the higher temperature (Figure 2.8). Similar to the observations presented in Figure 2.7, PsbA was detected only in the sucrose layers corresponding to thylakoid membrane-containing fractions. The results suggest that the second RecA-like domain of the helicase core and the C-terminal domain are not explicitly required for CrhR or PsbA localization to the thylakoid membrane region.

2.4.6 CrhR localization *in vivo*

A preliminary fluorescence microscopy analysis using protein fusions of citrine fluorescent protein (ciFP) and CrhR (Figure 2.1) transformed into Δ*crhR* cells was also performed to visualize CrhR localization in living cells. In a fusion of ciFP to the N-terminus of CrhR, pMON ciFP-CrhR, the ciFP fluorescence was visualized in close proximity to the thylakoid membranes, as judged by the overlapping Chl *a*-based autofluorescence with ciFP-CrhR (Figure 2.9A-C). Conversely, the ciFP fluorescence was distributed throughout the center of the cells in pMON CrhR-ciFP, in which ciFP is fused to the C-terminus of CrhR, with the autofluorescence from chl *a* visible around the periphery (Figure 2.9D-F).

The high levels of ciFP fluorescence detected in cells with pMON CrhR-ciFP may occur as a result of artificially elevated expression or increased stability due to the protein fusion. This is consistent with the significantly higher levels of the fusion protein, with a predicted molecular weight of 83 kDa, detected by Western blot in this construct (Figure 2.10). A low level of fluorescence was observed in the empty vector control (pMON 36456) with the 520-555 nm filter used to detect ciFP (Figure 2.9G), and the distribution of the ciFP fluorescence is consistent with the distribution of Chl *a* autofluorescence (Figure 2.9H). Although this indicates some spectral overlap of the Chl *a* autofluorescence with ciFP likely occurs in all the *Synechocystis* samples, fluorescence due to ciFP is sufficiently pronounced to be observed above the Chl *a* autofluorescence in the range of the 520-555 nm filter. As this is a preliminary analysis, additional microscopy images will need to be captured to allow for statistical comparisons;

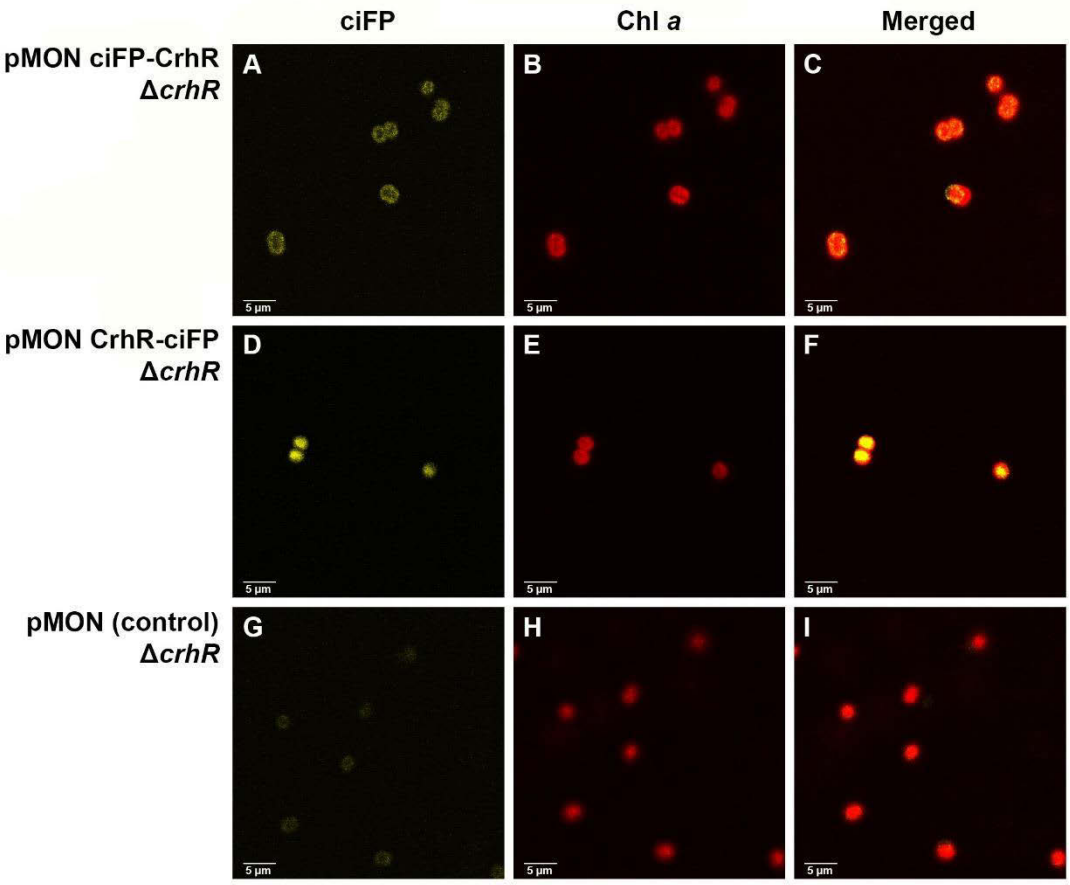

Figure 2.9: *In vivo* CrhR localization using fusions with citrine fluorescent protein.[6] Δ*crhR* cells transformed with plasmids expressing fusions of citrine fluorescent protein (ciFP) and CrhR at 20°C, and a pMON 36456 vector control were visualized with a confocal fluorescent microscope. Images shown include (A, D, G) ciFP fluorescence (ex. 514 nm, em. 520-555 nm), and (B, E, H) Chl *a* autofluorescence (ex. 488 nm, em. 556 nm). (C, F, I) Merged images of ciFP and Chl *a* fluorescence show differences in fluorescence intensity and localization between conditions.

[6] The images in this figure were captured by a project student, C.A. Stevens, under my supervision.

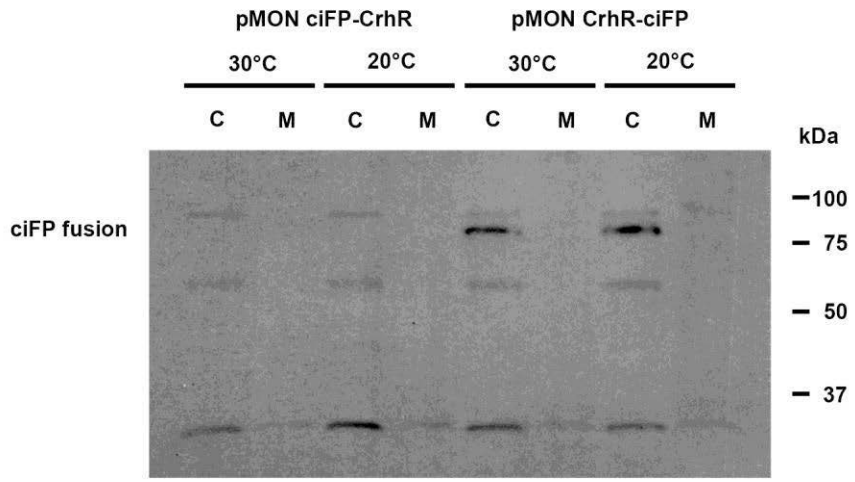

Figure 2.10: Expression of ciFP and CrhR fusion proteins.[7]

ciFP and CrhR fusion protein constructs expressed in *Synechocystis* Δ*crhR* after a cold induction for 3 hours at 20°C were analyzed by Western blotting. CrhR-containing polypeptides were detected with anti-CrhR antibodies in the crude soluble cytoplasmic (lanes C, 10 μg) and membrane pellet (lanes M) fractions after lysis, as described in the Figure 2.2 legend. This Western blot was performed shortly after the triparental mating transferring the plasmids into *Synechocystis*, resulting in additional bands that can be attributed to detection of the *E. coli* DEAD-box RNA helicases.

[7] The data in this figure was collected by a project student, C.A. Stevens, under my supervision.

however, these *in vivo* localization results suggest support for the conclusion that CrhR is thylakoid membrane-associated in *Synechocystis*.

2.5 Discussion

Prokaryotes generally compartmentalize biosynthetic pathways by sequestering processes to confined regions within the cell. A prime example is the differential localization of DEAD-box RNA helicases within RNP complexes that are associated with ribosome biogenesis, translation initiation, or RNA degradation (176). The primary objective of this investigation was to identify the pathway in which CrhR functions, utilizing a variety of cellular localization techniques. The results establish that CrhR, the single DEAD-box RNA helicase encoded in the model cyanobacterium *Synechocystis*, localizes to the cytoplasmic and thylakoid membrane regions and cosediments with translating polysome complexes. CrhR localization was temperature-independent and differentially required CrhR RNA helicase activity, as thylakoid association and polysome association were unaffected and defective, respectively.

Although many prokaryotic DEAD-box RNA helicases have roles in ribosome biogenesis (109, 110, 117, 176), our polysome fractionation results suggest that this function is unlikely in *Synechocystis*, as CrhR was detected only in the polysome-containing fraction. This, combined with the runoff polysome analysis indicated that CrhR is associated with translating polysomes. The data therefore suggest that CrhR is associated with translation, consistent with the proteomic analysis of the polysome pellet; however, the mass spectrometric analysis of the polysome pellet also detected degradosome components, such as PNPase and RNase E, that correspond to the recently identified minimal degradosome in cyanobacteria (192). Interaction with an RNA helicase such as CrhR was not tested when it was shown previously that the *Synechocystis* RNase E and PNPase interact as a complex (192). Thus, while our data indicate that CrhR cosediments with polysome and degradosome components, we cannot determine if it interacts with the degradosome complex; however, the association of CrhR with translating polysomes does not preclude association with the RNA degradosome. Thus, since CrhR is encoded by the only DEAD-box RNA helicase gene in the *Synechocystis* genome, and given the multitasking of other bacterial RNA helicases (176-

178), CrhR may be performing divergent roles and thus may associate with a range of protein complexes, possibly under different temperature conditions.

CrhR association with the translation and/or RNA degradation machinery is not unexpected, as RNA helicase association with the bacterial degradosome (120, 127, 139, 140, 170, 171, 174) and with ribosome complexes (109, 110, 175) has been well documented. How CrhR is recruited to and interacts with the thylakoid membrane and translating polysome and/or degradosome components remains unknown. The mechanisms of localization to these compartments appear to differ, as CrhR was removed from the polysome pellet but not the membrane fraction by RNase A treatment. This suggests that protein-protein and protein-RNA associations dictate CrhR localization to the thylakoid membrane and polysome, respectively. RNA- and protein-protein-dependent association of RNA helicases has been observed in other systems (120, 146, 193). The ease with which CrhR was removed from the membrane fraction also indicates that protein-protein interactions and not direct membrane interactions are involved. While RNA helicases, including CrhR, do not contain traditional membrane-spanning domains (152, 174, 179), the N-terminal and/or C-terminal amino acid extensions outside the helicase core are typically involved in specific RNA substrate recognition or protein-protein interactions (59, 72, 120). Indeed, we observed aberrant localization of $CrhR_{TR}$, which lacks the second RecA domain and C-terminal extension to the polysome pellet. These localization defects could partially result from the $CrhR_{TR}$ overexpression observed at 30°C in the truncation mutant, in addition to the loss of helicase activity. Overall, the results indicate that intact CrhR is required for proper cellular localization. This conclusion is similar to those from studies revealing similar responses to C-terminal deletion of a cold-induced RNA helicase, Lmo1722, which resulted in disassociation from the 50S ribosome in *L. monocytogenes* (117) and removal of CshA from the *S. aureus* degradosome (120).

While thylakoid membrane-associated polysomes have been reported in cyanobacteria (194), the subcellular localization of the cyanobacterial degradosome has not been determined (192). It is predicted that the *Synechocystis* degradosome is soluble, similar to that of *C. crescentus* (180), since the Rnase E in *Synechocystis* does not contain the C-terminal scaffolding domain required for membrane attachment (192), as observed

in other Gram negative bacteria (120, 139, 170, 171, 174). Although other studies investigating *Synechocystis* subcellular localization failed to detect CrhR, the lack of CrhR detection in these studies most likely resulted from growth conditions that did not induce abundant CrhR expression, as the cultures were grown at 30°C and 34°C, temperatures at which CrhR is expressed at a basal level (164). Results of those studies included the lack of detection of a DEAD-box RNA helicase in the *Synechocystis* minimal degradosome (192) and membrane (189, 195-197) or cytoplasmic (198) extracts.

CrhR localization to the thylakoid membrane is consistent with the significant morphological and physiological effects observed in response to *crhR* mutation (164). As was particularly evident when *Synechocystis* was stressed at 20°C, *crhR*$_{TR}$ cells exhibit a reduction in photosynthesis due to defects in photosynthetic carbon fixation which are associated with decreased pigmentation and alterations in electron transport chain function and thylakoid membrane structure (104). Defects in transitory adaptation of the photosynthetic apparatus to low temperature have also been observed in a *crhR* mutant which showed decreased PSII activity, a loss of PSI, and an oxidized plastoquinone pool (158). These effects are directly related to the conditions required for regulation of *crhR* expression, namely, the redox potential of the electron transport chain (41). Although CrhR function is not known, the sRNA PsrR1 regulates expression of many photosynthesis-related genes (199). CrhR mutation-mediated disruption of PsrR1 function would be expected to generate similar phenotypic alterations.

The data presented here indicate that CrhR localizes to both the cytoplasmic and thylakoid membrane regions. CrhR in the cytoplasm is associated with translation, as it cosediments with actively translating polysomes. CrhR association with and disruption of the thylakoid membrane in a *crhR* mutant suggests that CrhR performs a role in thylakoid biogenesis and/or stability. In this capacity, CrhR RNA helicase activity in the thylakoid membrane could aid translation initiation and thus transertion of proteins into the thylakoid membrane, similarly to the role proposed for the RNA helicase, CrhC, in cytoplasmic membrane protein transertion in *Nostoc* (152). Other studies have shown adjustment of thylakoid membrane polysome profiles in response to temperature and light conditions, indicating that abiotic stresses influence thylakoid function by altering translation (187, 197, 200). In this context, it would be of interest to determine if CrhR is

involved in synthesis of thylakoid membrane proteins such as the D1 photosystem II protein. D1 translation initiates on soluble ribosomes and halts in the dark (200). The stalled ribosomal complex is targeted to the thylakoid membrane in the light, D1 synthesis is completed, and D1 is cotranslationally inserted into the membrane (187).

Cosedimentation of degradosome components with the polysome indicates the possibility that a functional association between the two complexes exists in *Synechocystis*. This association is known to occur in archaea and eukarya (200-204), and polysome fractionation on sucrose gradients has recently provided evidence for polysome-RNA degradosome association in *E. coli* (144) and *H. pylori* (143). Indeed, other than the photosynthesis-associated peptides, our proteomic data set closely resembles that obtained in the *E. coli* (144) and *H. pylori* (143) studies. Similar to the results presented here, the respective RNA helicase peptides were associated with the identified polysome-RNA degradosome complexes (143, 144). In *E. coli*, the degradosome-associated RNA helicase RhlB contributes to ribosome binding and thus to formation of the polysome-RNA degradosome complex (144). Although Zhang *et al.* (192) did not detect CrhR in the minimal degradosome isolated from *Synechocystis* at 30°C, CrhR association may be seen at lower temperatures. Temperature-dependent alteration of the degradosome-associated RNA helicase has been reported in a variety of bacteria, for example, *E. coli* (178), *C. crescentus* (140) and *Psychrobacter arcticus* (205). Similarly, Redko *et al.* (143) showed that a minimal degradosome consisting of RNase J and RhpA, the only DEAD-box RNA helicase in the genome, associated with translating polysomes and not 30S or 50S subunits in *H. pylori*. Although it is different from other Gram-negative organisms in this respect, *Synechocystis* encodes an RNase J homologue that appeared in our polysome data set. The potential for CrhR to be associated with a minimal degradosome and with RNase J at low temperature deserves further investigation. Overall, these observations are similar to those we report here for CrhR, suggesting that CrhR may also contribute to the formation of a polysome-RNA degradosome complex in *Synechocystis*.

Potential roles for RNA helicase alteration of RNA secondary structure in a polysome-RNA degradosome complex include unwinding of an inhibitory RNA secondary structure that blocks RNase access and sRNA annealing to create a RNase site.

CrhR could participate in either of these scenarios, as it catalyzes both double-stranded RNA (dsRNA) unwinding and annealing reactions *in vitro* (153). In prokaryotes, related systems include termination of translation by A-site cleavage in translating ribosomes by RNase toxins in toxin-antitoxin pairs (206), and binding of the sRNA RhyB to the 5' untranslated region (UTR) of the *sodB* transcript to activate RNase E cleavage within the open reading frame (ORF) during translation (207). CrhR RNA helicase activity could be involved in similar regulatory mechanisms, as Tsai *et al.* (144) also detected Hfq in their *E. coli* polysome-degradosome preparations and speculated that Hfq contributed to RhyB binding and thus to cleavage of *sodB*. As cyanobacteria do not encode an Hfq homologue (208), this raises the possibility that CrhR replaces Hfq in a *Synechocystis* polysome-degradosome complex. In eukaryotes, RNA helicases are associated with RNA degradation of actively translating transcripts. For example, a variety of ribonucleases are targeted to the ribosome by UPF1 during nonsense-mediated decay (NMD) (203), and Dhh1 slows translation elongation and promotes decapping of polysome-associated transcripts, creating substrates for Dhh1-mediated RNA decay (204). Whether CrhR is associated with similar regulatory pathways remains to be elucidated.

Here we provide evidence that CrhR, the single DEAD-box RNA helicase encoded in the *Synechocystis* genome, localizes to both the cytoplasmic and thylakoid membrane regions and cosediments with polysome and RNA degradosome components. The results suggest that the RNA degradation machinery is coupled with translation in *Synechocystis*, contributing to the emerging picture showing that these processes are intimately linked in bacterial systems.

Chapter 3: RNA helicase-regulated processing of the *Synechocystis rimO-crhR* operon results in differential cistron expression and accumulation of two sRNAs

A version of this chapter has been published as Rosana, A.R.R.*, Whitford, D.S.*, Migur, A., Steglich, C., Kujat-Choy, S.L., Hess, W.R., and Owttrim, G.W. (2020) RNA helicase-regulated processing of the *Synechocystis rimO-crhR* operon results in differential cistron expression and accumulation of two sRNAs. Journal of Biological Chemistry 295: 6372-6386.

3.1 Summary

The arrangement of functionally related genes in operons is a fundamental element of how genetic information is organized in prokaryotes. This organization ensures coordinated gene expression by co-transcription. However, often alternative genetic responses to specific stress conditions demand the discoordination of operon expression. During cold temperature stress, accumulation of transcript from the gene encoding the sole Asp-Glu-Ala-Asp (DEAD)-box RNA helicase in *Synechocystis*, *crhR (slr0083)*, increases 15-fold. Here, we show that *crhR* is expressed from a dicistronic operon with the methylthiotransferase *rimO/miaB* (*slr0082*) gene, followed by rapid processing of the operon transcript into two monocistronic mRNAs. This cleavage event is required for and results in stabilization of the *rimO* transcript. Results from secondary structure modelling and analysis of RNase E cleavage of the *rimO-crhR* transcript *in vitro* suggested that CrhR plays a role in enhancing the rate of the processing in an auto-regulatory manner. Moreover, two putative small RNAs are generated from additional processing, degradation, or both of the *rimO* transcript. These results suggest a role for the bacterial RNA helicase CrhR in RNase E-dependent mRNA processing in *Synechocystis* and expand the known range of organisms possessing small RNAs derived from processing of mRNA transcripts.

3.2 Introduction

Differential expression of operon gene members is a major player in gene expression regulation in bacteria (209, 210). An operon is defined as a collation of two or more functional genes under the control of the same promoter that are transcribed as a primary polycistronic transcript (211). Gene clustering into operons is generally associated with their coordinated expression, involvement in functionally related processes and, in some instances, physical interactions between the encoded proteins (210). This organization provides the ability to rapidly acclimate to new growth conditions by regulating expression of a protein complex through the generation of equimolar levels of each operon member (209, 210); however, numerous studies indicate that while genes within an operon typically exhibit similar patterns of expression, co-expression can be lost in response to alteration of environmental conditions (212). Discoordinate operon

expression can result from a number of mechanisms that alter transcript stability (213, 214) associated with RNA cleavage (215-217), the formation of secondary structures (218, 219) or the binding of sRNAs (220). Regulation due to sRNA-mRNA binding can be either dependent on RNA chaperones, such as host factor for phage Qß (Hfq) (216), or chaperone-independent (220). Polycistronic transcripts can also be subject to processing events, initially by an endonuclease, such as RNase E, whose endonucleolytic cleavage generates monocistronic transcripts that subsequently undergo maturation by either 5'-3' or 3'-5' exonuclease trimming, demonstrated in *B. subtilis* (221) and *E. coli* (222), respectively. The processing event can differentially alter transcript stability of operon members, either positively or negatively (223, 224). Using RNA sequencing, Conway *et al.* (225) observed differential expression of polycistronic genes in 43% of the operons in *E.* coli. Differential regulation of operon expression is thus complex and widespread.

Operon expression has been associated with cellular response to environmental stresses, including temperature fluctuation (226, 227). The coordination of gene expression in response to temperature downshift is in part governed by co-expression of a group of operons, with genes within an operon responding more similarly to cold shock conditions than monocistronic genes randomly selected from the genome (226). A major impact of low temperature involves thermodynamic stabilization of RNA secondary structure that inhibits RNA reorganization and thus function. Stabilized RNA can be relieved by RNA chaperones whose expression is frequently regulated by low temperature, including members of the cold shock protein (Csp) (228) and RNA helicase (73, 176) gene families. RNA helicases rearrange RNA secondary structure via duplex unwinding and/or annealing, frequently involving sRNA metabolism and thereby regulating gene expression (229-231).

Cyanobacteria are Gram-negative bacteria that perform oxygenic photosynthesis and fix atmospheric carbon dioxide and thus have immense biotechnological and bioremediation potential. In response to low temperature, they induce a number of canonical cold-stress genes including RNA chaperones belonging to the RNA binding protein (Rbp) and RNA helicase families (105, 149, 232). While a diverse variety of mechanisms are known to regulate gene expression in response to temperature downshift, the molecular basis of *crhR* activation is not completely understood (233, 234). In the

model cyanobacterium, *Synechocystis*, the sensor histidine kinase, Hik33, regulates a subset of cyanobacterial cold stress genes that excludes *crhR* and other classic cold-inducible genes (162, 234, 235), while a cold-specific sigma factor has not yet been reported in cyanobacteria (236). Thus, an as yet unknown mechanism regulates the temperature-dependent expression of Hik33-independent genes. Many cold stress genes are expressed in operons in *Synechocystis*, which encodes a total of 425 predicted operons (210). While processing of mRNAs is one mechanism by which expression of multicistronic operons can be differentially regulated, the extent of RNA processing and its impact on protein expression is poorly understood. Only a few examples of differential cistron regulation due to RNA processing have been reported in cyanobacteria: the nitrogenase operons of *Anabaena variabilis* ATCC 29413 (237-240) and two mixed sRNA-protein-coding gene operons in *Synechocystis* (241).

We have previously shown that the product of the *Synechocystis slr0083* gene, the RNA helicase CrhR, auto-regulates its own expression through a complex network of interactions at the post-transcriptional level involving temperature induced alteration of both transcript and protein stability (160, 164). Here, we provide evidence that the *Synechocystis rimO-crhR* operon is expressed as a dicistronic transcript that is rapidly processed into monocistronic transcripts having different stabilities. The mechanism is auto-regulatory, as CrhR RNA helicase activity is required for the RNA processing event, and potentially catalyzed by RNase E, which correctly cleaves the polycistronic transcript *in vitro*. The results reveal a novel mechanism by which bacteria can differentially regulate suboperonic gene expression in response to temperature shift that involves auto-regulatory, RNA helicase dependent RNA processing that generates processed transcripts having divergent fates.

3.3 Experimental procedures

3.3.1 Cyanobacterial strains and growth conditions

Synechocystis was maintained on BG-11 agar supplemented with 10 mM Tricine pH 8.0 and 0.3% sodium thiosulfate (164). Two *crhR* mutant strains, a partial *crhR* deletion mutant created by insertion of a spectinomycin cassette (*crhR*$_{TR}$) (104) and a *crhR*

complete deletion mutant, created by insertion of a neomycin cassette (Δ*crhR*) (160), were grown as described below. The previously reported Δ*crhR* strain 2-76 (104) was designated as $crhR_{TR}$ to differentiate it from the complete deletion mutant, Δ*crhR*. Antibiotics were included as required, spectinomycin-streptomycin (50 μg ml^{-1} of each) for $crhR_{TR}$ and kanamycin (50 μg ml^{-1}) for Δ*crhR*. Photoautotrophic cultures were grown in liquid BG-11 at 30°C with continuous shaking (150 rpm) and bubbling with humidified air at an illumination of 50 μmol photons m^{-2} s^{-1} (41). Mixotrophic cultures were grown for an extended period in BG-11 supplemented with glucose (5 mM) to allow acclimation (182). Cold stress was induced in mid-log phase cells at 20°C for the indicated times. For temperature gradient and transcript half-life analyses, liquid cultures grown at 30°C were subjected to the indicated condition and aliquots harvested at the designated times prior to RNA isolation. Representative data is shown from a minimum of two biological replicates.

3.3.2 RNA manipulation

Total RNA was extracted from *Synechocystis* cells treated with an equal volume of 5% phenol-ethanol at the stated growth temperature as defined previously using glass bead lysis and extensive phenol-chloroform extraction (182). RNA samples were resolved in either formaldehyde 1.2% agarose gels for *rimO* transcript analysis or 8 M urea-8% polyacrylamide gels for detecting the *rimO* 5' UTR. Resolved RNA was either capillary blotted overnight from agarose gels using 2× SSC or electro-transferred from polyacrylamide gels using a semi-dry transfer (Tyler) to Hybond-N nylon membranes (Amersham). Transferred RNA was UV-crosslinked to the membrane with a Stratalinker UV Crosslinker Model 1800 (120 mJ cm^{-2}, 254 nm, Stratagene). Northern analysis was performed as previously described (164, 182) using [α-^{32}P]-labelled riboprobes corresponding to a 202 nt fragment (*Synechocystis* genomic position: 2886403-2886603 as designated in GenBank reference sequence NC_000911) internal to the *rimO* ORF, a 90 nt segment (2886040-2886129) for the detection of the *rimO* 5'UTR transcript or a 93 nt *Hinc*II-*Sac*II fragment internal to the *crhR* ORF from pBS-probeR (Table 3.1). Oligonucleotides used to create the riboprobes are indicated in Table 3.2. The constitutively expressed transcripts, *rnpB* (primers *rnpB*f and *rnpB*r; Table 3.2) or 16S

Table 3.1: Bacterial strains and plasmids used in this chapter.

Strain or plasmid	Relevant characteristic(s)	Source, reference or application
***Synechocystis* strains**		
Wild type	glucose-tolerant, non-motile strain	(41)
$crhR_{TR}$	*crhR*::spectinomycin cassette; C-terminal deletion of CrhR	(104)
Δ*crhR*	replacement of the complete *crhR* ORF with a neomycin resistance cassette	(160)
***E. coli* strains**		
DH5α	F-Φ80lacZΔM15 Δ(lacZYA-argF) U169recA1 endA1 hsdR17 (rK-, mK+) phoA supE44 λ-thi-1 gyrA96 relA1	Laboratory collection
Plasmids		
pMON 36456	*E. coli – Synechocystis* hybrid cloning vector, Gen^R	(186)
pBS CrhR	3.02 kb *Synechocystis* genomic fragment containing 1.4 kb *crhR* ORF and flanking regions cloned in pBluescript KS+	(41)
pProbeR	pBS with a 93 bp *Hinc*II-*Sac*II internal fragment of the *crhR* ORF	*crhR* (*slr0083*) riboprobe, (164)

Table 3.2: Oligonucleotides used in this chapter.

The T7 RNA polymerase promoter sequence is marked in bold.

Oligonucleotide	Sequence	Source or application
27F	GAGTTTGMTCCTGGCTCAG	16S rRNA probe
1492R	ACGGYTACCTTGTTACGACTT	16S rRNA probe
ARRR1	ATAAAGCTGCTGCTCAATGCG	5' RACE-RCA, RT-PCR
ARRR10	CCAACGCCATCAATTTGACC	RT-PCR
DCsr20f	**TAATACGACTCACTATAGG**GGTGGTGCGATAACG TGG	*slr0082* RNA probe
DCsr20r	CGTTATTTCCGGTTGCC	*slr0082* RNA probe
DCsr21f	**TAATACGACTCACTATAGGG**TGTAGGGTAGGGA CTAAAC	5' UTR RNA probe
DCsr21r	CAAATAAAAAGGGTCTGACC	5' UTR RNA probe
GWO39	TGACGATGTGAAAACC	Inverse PCR, sequencing
GWO42	AGGGGAATGGCTTCAGTTTG	Primer extension
GWO45	AAGCCAATGTCGGCCAAGAG	S1 nuclease target
LPF45	TGTTATTGACGGTTGGTTCC	RT-PCR
LPF46	CAGTTTGAATTTGGGTGGGA	Inverse PCR, sequencing
M13 FWD (pBS)	GTAAAACGACGGCCAGT	S1 nuclease target
RNaseE_CrhR_Fw	**TAATACGACTCACTATA**GGTATGACCGCCGAGGA GGCTAAGGTTTTTTAGCTATTGAA	RNase E substrate
RNaseE_CrhR_Rv	TTCAATAGCTAAAAAACCTTAGCCTCCTCGGCGGT CATACC**TATAGTGAGTCGTATTA**	RNase E substrate
rnpBf	**TAATACGACTCACTATAG**GGGGCAGGAAAAAGA CCAACC	*rnpB* RNA probe
rnpBr	TAACTGACCACTGAAAAGG	*rnpB* RNA probe

rRNA, were utilized as a control for RNA loading. Transcript half-life was determined in the presence of 400 μg ml^{-1} rifampicin to inhibit *de novo* mRNA synthesis. Transcript sizes were estimated using either the high range or low range RiboRuler RNA ladders (Thermo Fisher Scientific). Hybridized membranes were exposed to X-ray film for 3-5 exposures for each biological replicate. The exposure providing the best representation, depicting a compromise between over-and under-exposure was used for quantification to mitigate potential exposure issues. Quantitation of transcript level was performed using *rnpB* abundance as an internal control using Image J software v1.45 S (NIH, USA) as previously described (164, 242). A minimum of two biological repeats were performed for each experiment and representative data shown.

3.3.3 Identification of operon transcripts

Total RNA was extracted from cyanobacterial cultures (164) and assessed qualitatively using an RNA Nano Bioanalyzer (Agilent Genomics) and quantitively by Qubit fluorometry v2.0 (Thermo Fisher Scientific). RNA was treated twice with RNase-free rDNase I (Ambion) and residual contaminating DNA assessed by the lack of 16S rRNA amplification using the universal bacterial primer pair 27F and 1492R (243). RNA samples were reverse transcribed using random hexamer primers and Superscript III reverse transcriptase (Invitrogen). The resulting cDNA libraries (20 ng) were used as templates for the RT-PCR and controls consisted of 50 ng wild type *Synechocystis* genomic DNA and milliQ-water. PCR amplifications were performed in HF buffer with standard reaction conditions for Phusion HS II (Thermo FisherScientific) for 25 cycles. Reaction products were separated on a 1.5% agarose-0.5× TBE gel, stained with ethidium bromide and imaged on a UV transilluminator (CellBioSciences AlphaImager HP). Images shown were inverted.

3.3.4 Primer extension and S1 nuclease protection assays

Primer extension and S1 nuclease protection assays were performed as described by Ausubel *et al.* (244). PNK (Roche) was used to end label primers GWO42 and GWO45 (Table 3.2) with [γ-^{32}P] ATP (Amersham). For primer extension, the ^{32}P-GWO42 primer was annealed to total *Synechocystis* RNA (30 μg) in 1× hybridization buffer (1 M NaCl,

0.167 M HEPES-KOH [pH 7.5], 0.33 mM EDTA) with gradual cooling from 85°C to 50°C over 3.5 h. Following EtOH precipitation, DNA synthesis with AMV-RTase (25 U, Roche) and 560 μM each dNTP was performed at 44°C for 1 h. The reaction was stopped by digestion with RNase A (1 μg, 10 min, 37°C) and EtOH precipitated ssDNA fragments were suspended in Sequenase Stop Solution (Amersham).

dsDNA targets for S1 nuclease protection assays were produced by PCR from pBS-CrhR (41) using the pBS forward primer (M13 FWD) and ^{32}P-GWO45. This generated a probe homologous to the region immediately upstream of the translation start site for *crhR*, extending from the *Eco*RI site in *rimO* to 80 bp into the *crhR* coding sequence (genomic location 2887355-2887723), as well as non-homologous 5' sequence on the non-hybridizing strand. The GWO45/M13 FWD probe was annealed to total *Synechocystis* RNA (15-30 μg) by heat denaturation at 85°C for 10 min in 1× hybridization buffer followed by slow cooling to 37°C over 2 h. S1 nuclease (33 U, Amersham) digestion was performed for 30 min at 37°C. The reaction was stopped with S1 stop solution (0.8 M NH_4OAc, 8 μg ml^{-1} tRNA, 4 mM EDTA [pH 8]) and EtOH precipitated ssDNA fragments were suspended in Sequenase Stop Solution (Amersham).

Primer extension and S1 nuclease samples were separated on 6% DNA sequencing gels and signals detected by autoradiography for 3-5 d at -80°C with an intensifying screen.

3.3.5 5' RACE-RCA, inverse PCR and DNA sequencing

The 5' ends of the transcripts were determined using 5'RACE-RCA analysis as described by Polidoros *et al.* (245). Extracted total RNA, isolated from wild type cells grown under photoautotrophic conditions at 20°C, was treated with RNase-free DNase I (0.2 U per 1 μg RNA) (Invitrogen) for 15 min at 37°C. Treated RNA was purified by extensive phenol-chloroform extraction, LiCl (2 M) precipitation and finally ethanol precipitation and dissolved in RNase-free water (Invitrogen). RNA was tested for genomic DNA contamination on the basis of the absence of PCR amplification of 16S rDNA, using universal bacterial 16S rDNA primers 27F and 1492R (243) and also of the *Synechocystis rnpB* gene with primers *rnpB*f and *rnpB*r (149) (Table 3.2) for 40 cycles. *crhR* gene-specific cDNA synthesis was directed using a 5' phosphorylated primer ARRR1 (Table

3.2) targeting transcripts with *crhR*-containing mRNA sequences starting 3 bp upstream of the internal *Pml*I site, the site used to generate the *crhR*$_{TR}$ mutant (Figure 3.1). First strand cDNA synthesis was performed in a final volume of 20 µl containing 1.0 µg DNA-free RNA; 0.025 µg µl^{-1} phosphorylated ARRR1 primer; 0.5 mM dNTP (Fermentas); 40 U RNase-OUT (Ambion) and 200 U M-MLV reverse transcriptase (Superscript III, Invitrogen). Reverse transcription was performed in a Techgene Thermal Cycler (Life Sciences) using the following conditions: 37°C for 60 min, 42°C for 60 min, 70°C for 15 min. First strand cDNA was treated with 2 U RNase H (Invitrogen) for 15 min at 37°C and purified on a QiaQuick PCR purification column (Qiagen).

Purified 5' phosphorylated first strand cDNA products were circle ligated using CircLigase I (Epicentre). Ligation reactions contained 25 µl purified cDNA, 1× CircLigase buffer, 0.05 mM ATP and 150 U CircLigase I. The reaction mixture was incubated at 60°C for 1 h, heat inactivated at 80°C for 10 min and the final volume adjusted to 36.5 µl. Ligated cDNA was amplified using rolling circle amplification (RCA). The reaction mixture consisted of 36.5 µl cDNA, 11 µM modified random heptaprimer (phosphothioate blocked 3'n-1, n-2) (IDT DNA Technologies), 1.2 mM dNTP and 10 U Φ29 DNA polymerase (New England Biolabs) and incubated in a Techgene Thermal Cycler (Life Sciences) for 20 h at 30°C.

Inverse PCR was performed on RCA products using primers GWO39 and LPF46 (Table 3.2) to amplify cDNA sequencing containing *crhR* sequences. Amplified products were gel purified (QiaQuick gel purification kit, Qiagen) according to manufacturer's instructions. Gel purified PCR products were sequenced using primer GWO39 and BigDye Terminator v3.1 cycle sequencing kit (Applied Biosystems).

3.3.6 Primary transcript analysis

Total RNA was isolated from mid-log phase *Synechocystis* wild type, *crhR*$_{TR}$ and Δ*crhR* cells that were cold shocked at 20°C for 20 min to optimize *slr0082* transcript accumulation. Aliquots (20 µg) were treated with 2 U of Terminator 5'-phosphate-dependent exonuclease (Epicenter) for 60 min at 30°C, according to the manufacturers instructions. Untreated total RNA (5 µg) and Terminator treated samples were subjected

to Northern analysis using [α-^{32}P]-labelled riboprobes, as described in the RNA manipulation section above and depicted in Figure 3.1.

3.3.7 Identification of RNA-RNA interactions

Potential mRNA targets of the 75 nt sRNA originating from the *rimO* 5'UTR were predicted using the program IntaRNA – RNA-RNA interaction available from: http://rna.informatik.uni-freiburg.de/IntaRNA/ (246). The first 75 nt following the TSS upstream of *rimO* were used for the 75 nt sRNA. Sequences 100 nt upstream and 50 nt downstream of the annotated translational start sites of all protein-coding genes were used for this analysis. Hence, if the prediction covers nt positions shortly before, after or overlapping 101 to 103, it may indicate interference with initiation of translation. A functional annotation chart (246) was generated by subjecting the top 50 predicted targets to functional enrichment using the DAVID database (247).

3.3.8 RNA structure prediction

Prediction of RNA secondary structures were modelled using the RNAfold v2.4.8 WebServer (Universität Wien, Austria) with default parameters selected (248). Structures were visualized for publication in the VARNA Applet v3.93 (249).

3.3.9 RNase E cleavage assay

A 41 nt RNA containing the predicted processing sites was synthesized by *in vitro* transcription as substrate for the RNase E assay. Briefly, a DNA template was produced by annealing the ssDNA primers RNaseE_CrhR_Fw and RNaseE_CrhR_Rv (Table 3.2). The target RNA was transcribed with T7 RNA polymerase (Thermo Fisher Scientific), treated with RNA 5' polyphosphatase (Epicenter), and phosphorylated with T4 polynucleotide kinase (Thermo Fisher Scientific). The 3' end labelling of the transcipr was performed with cy3 dye (Thermo Fisher Scientific). As a control, a 5' monophosphorylated RNA oligonucleotide was synthesized that matched the sequence of the CRISPR3 repeat, a previously analyzed substrate for RNase E (250). A codon-optimized and C-terminally His-tagged version of the Synechocystis RNase E-encoding gene *slr1129* was expressed and the enzyme purified as recombinant protein as described

(250). Cleavage reactions were performed at 30°C for 30 mins in 10 µl RNase E cleavage buffer (25 mM Tris-HCl [pH 8.0], 60 mM KCl, 5 mM $MgCl_2$, 100 mM NH_4Cl, 0.1 mM DTT) and quenched with the addition of 2× RNA loading dye (95% formamide, 0.025% SDS, 0.025% bromophenol blue, 0.025% xylene cyanol FF, 0.5 mM EDTA [pH 8.0]). Following a 5 min denaturation at 95°C, reactions (80 ng RNA) were separated on a 8M urea-12% PAA gel, stained with SYBR Gold Nucleic Acid Gel Stain (Thermo Fisher Scientific; 1:10000), and visualized with a Laser Scanner Typhoon LFA 9500 (GE Healthcare; excitation 473 nm, emission filter long pass blue ≥ 510 nm, or excitation 532 nm, emission filter BPG1 560 to 580 nm in case of Cy3 labelled RNA, photomultiplier value 450 or 500).

3.4 Results

3.4.1 Genetic organization of the *rimO-crhR* region in *Synechocystis* sp. PCC 6803

The *Synechocystis slr0083* gene encodes the DEAD-box RNA helicase, CrhR, expression of which is regulated by the redox status of the electron transport chain (41, 163). Upstream of the *crhR* gene is a hypothetical gene, *slr0082*, whose putative protein product has 38% identity with RimO, a ribosomal protein S12 methylthiotransferase (UniProtKB P0AEI4) and 29% identity with the paralogous MiaB, a tRNA methylthiolase (UniProtKB P0AEI1) from *E. coli* (251, 252). The genomic organization of wild type and two *crhR* mutants, a partial deletion mutant, $crhR_{TR}$ (104), and a complete deletion mutant, Δ*crhR* (160), used in this study is shown in Figure 3.1. We utilized the two *crhR* mutants in this analysis as the $crhR_{TR}$ strain allows us to track expression and processing of the operon in the absence of RNA helicase activity (D. Chamot, personal communication) while the Δ*crhR* strain allows analysis of *rimO* expression in the absence of *crhR* (160).

3.4.2 Detection of full-length operon transcripts

Our previous study of *crhR* expression suggested *crhR* was transcribed as a monocistronic transcript whose expression is auto-regulated by the functional *crhR* gene product (164). RT-PCR was performed to determine if the tandem encoded genes, *rimO*

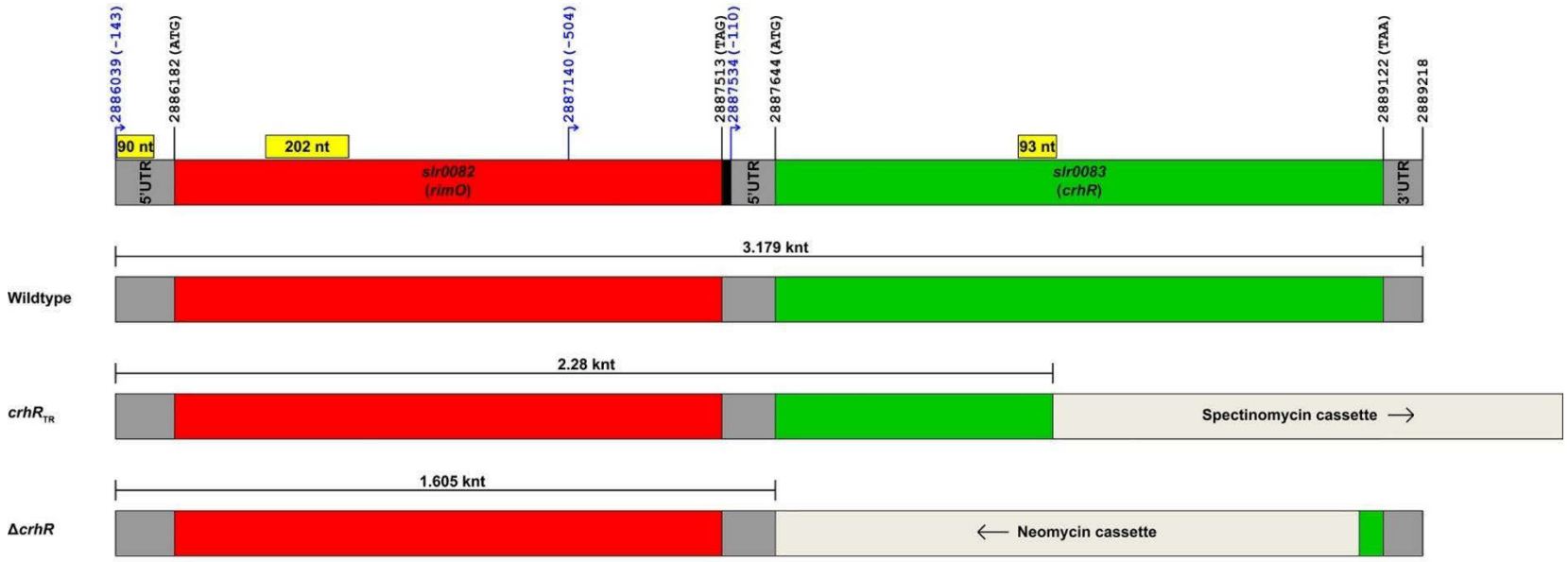

Figure 3.1: Genomic organization of the *Synechocystis rimO-crhR* operon.

Genomic organization of *rimO* (*slr0082*) and *crhR* (*slr0083*) with their respective 5' and 3' untranslated regions in wild type; $crhR_{TR}$, a partial deletion mutant which expresses a truncated *crhR* transcript and polypeptide (104, 164); and Δ*crhR*, a mutant in which the complete *crhR* ORF is deleted from the start to stop codons (160). The numbering refers to the nucleotide position in the genome (34). Indicated transcription start sites (blue) are from Kopf *et al*. (241). The relative positions and length of the riboprobes used for transcript analysis are indicated in yellow. The 93 nt probe for *crhR* was described previously (164). The predicted transcript length from the *rimO* promoter at -143 for each construct is indicated. Diagram is to scale.

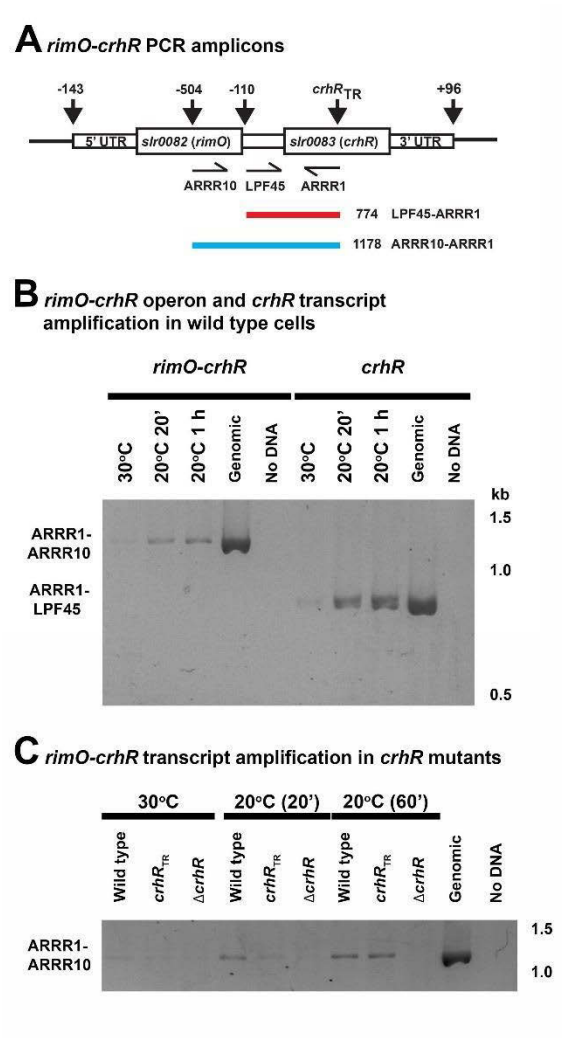

Figure 3.2: *rimO-crhR* operon verification.

(A) RT-PCR with the primers ARRR10, within the *rimO* ORF, or LPF45, between the -110 primary transcript initiation site and *crhR* ORF, in conjunction with ARRR1, within the *crhR* ORF, was used to verify the presence of operon transcripts and *crhR* transcripts, respectively. Diagram is not to scale. (B) Operon (ARRR10-ARRR1) and *crhR* (LPF45-ARRR1) transcript specific primer pairs were used to perform RT-PCR on total RNA isolated from wild type cells subjected to the indicated temperature treatments. (C) Operon specific RT-PCR (ARRR10-ARRR1) was performed on RNA extracted from wild type, *crhR*$_{TR}$ and Δ*crhR* cells. Amplification from genomic DNA and in the absence of target DNA is shown as controls. The ethidium bromide stained gel is shown.

and *crhR*, are expressed as an operon. The expected RT-PCR amplified products are shown in Figure 3.2A. A 1,178 bp product spanning the *rimO* and *crhR* genes, amplified across the transcription start site located at position -110 nt, was detected in wild type cells in addition to the 774 bp product corresponding to the *crhR* transcript (Figure 3.2B), confirming expression of *rimO-crhR* as an operon. Abundance of both amplicons was increased with low temperature, consistent with the previously observed pattern of *crhR* expression (164). Likewise, detection of an amplified PCR product spanning *rimO-crhR* in the *crhR*$_{TR}$ strain confirmed the presence of an operon transcript in the *crhR*$_{TR}$ mutant (Figure 3.2C). RT-PCR products were not detected in the Δ*crhR* strain under any condition, as this strain does not contain the ARRR1 primer binding site within *crhR* (Figure 3.2C).

3.4.3 CrhR inactivation results in deregulated expression of the *rimO-crhR* operon

The enhanced accumulation of the *crhR* transcript is transient in response to cold stress, returning to basal levels after ~3 h (164). To further examine expression of genes in this operon, transcript abundance of the upstream *rimO* ORF was determined in wild type and *crhR*$_{TR}$ strains (Figure 3.3). In wild type cells, *rimO* expression was extremely transient and unstable, with minor amounts of a ~1,450 nt transcript consistent with the 1,465 nt monocistronic *rimO* transcript and a major, stable 550 nt transcript detected (Figure 3.3A). A significant level of degraded *rimO* transcript was also detected, indicative of the rapid turnover of this transcript. Transient accumulation of *rimO* mRNA followed a similar pattern to that observed for *crhR* (164); however, the rate of accumulation and return to basal levels were significantly accelerated (Figure 3.3A and C). In contrast, detection of full-length truncated operon *rimO-crhR*$_{TR}$ (2,280 nt) and monocistronic *rimO* (1,465 nt) transcripts in the *crhR*$_{TR}$ mutant strain indicated that the *rimO-crhR* genes are expressed as an operon. Also reminiscent of *crhR* expression, the initial rate of accumulation for *rimO* was similar in both wild type and the *crhR*$_{TR}$ mutant for the first 20 min (Figure 3.3B), suggesting that the initial cold sensing and response is not affected by *crhR* inactivation. In contrast, and similar to accumulation of the *crhR* transcript (164), the subsequent repression of *rimO* accumulation is dependent on functional CrhR, as the transient nature of the accumulation of *rimO* transcripts was not observed in response to

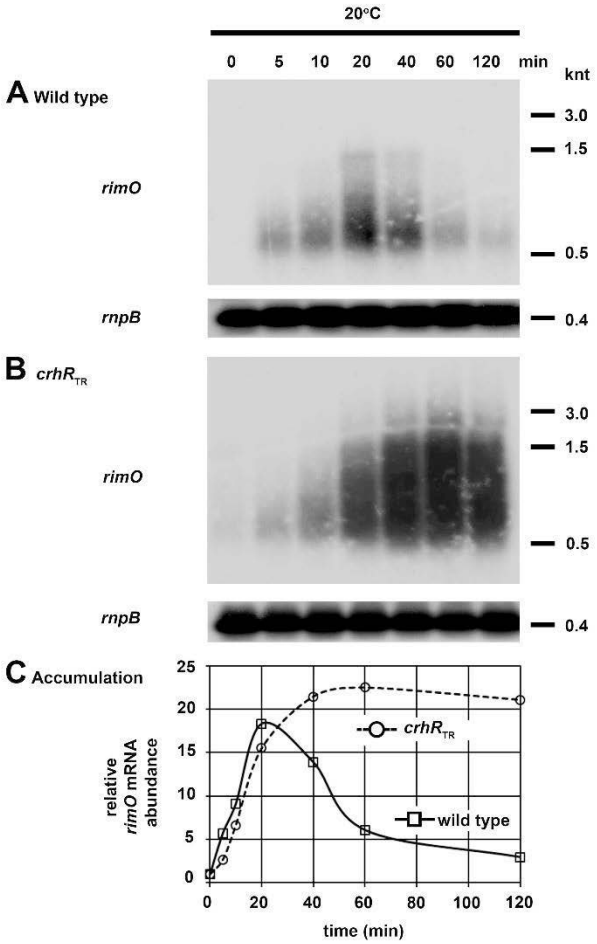

Figure 3.3: Time course of *rimO* transcript accumulation.[8]

Time courses of *rimO* transcript accumulation at 20°C in (A) wild type and (B) *crhR*$_{TR}$ *Synechocystis* strains. Cells were grown to mid-log phase at 30°C at which time the cultures were transferred to 20°C for the indicated times. *rimO* transcript was detected by Northern analysis of total RNA (5 µg) probed with a 202 nt antisense fragment internal to the *rimO* ORF as shown in Figure 3.1. Blots were stripped and probed with the *Synechocystis rnpB* gene as a control for RNA loading. (C) Quantification of *rimO* transcript levels. Transcript levels were quantified using Image J software (242) and *rimO* accumulation is expressed as accumulation relative to *rimO* abundance observed in illuminated wild type cells grown at 30°C.

[8] This figure was originally published in (191) and is used with permission.

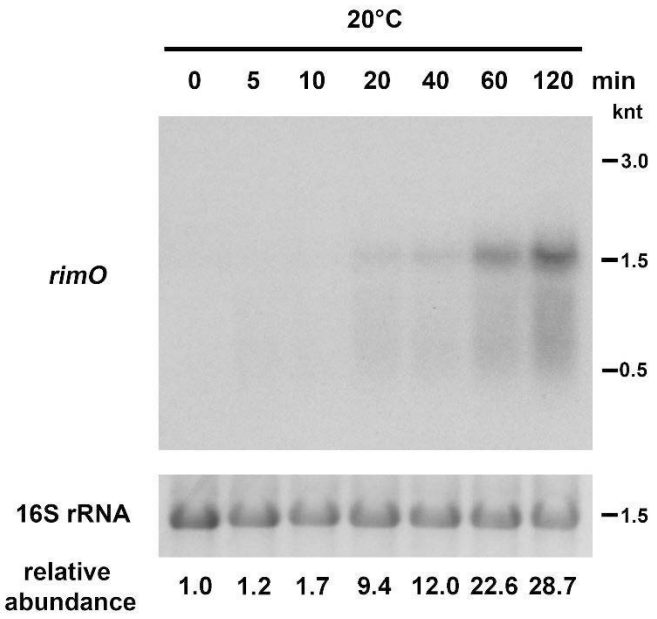

Figure 3.4: Time course of *rimO* transcript accumulation in Δ*crhR* cells.

Mid-log phase *Synechocystis* Δ*crhR* cells were grown at 30°C and cold stressed at 20°C for the indicated times. *rimO* transcript levels were detected in total RNA (20 μg), as described in Figure 3.3. The ethidium stained 16S rRNA is provided as a control for RNA loading. The relative level of *rimO* abundance is provided below each lane with abundance normalized to *rimO* levels detected from illuminated cells grown at 30°C.

cold stress in the *crhR*$_{TR}$ mutant (Figure 3.3B). In addition, *crhR* mutation altered *rimO* transcript abundance, as significantly enhanced levels of the truncated *rimO-crhR*$_{TR}$ transcript (2,280 nt) plus significant accumulation of randomly degraded transcripts, including a stable 550 nt product, were detected in the *crhR*$_{TR}$ mutant (Figure 3.3B and C). A similar expression pattern was observed in the Δ*crhR* strain, in which a transcript corresponding to the remaining 1,685 nt of the operon after insertion of the neomycin cassette used to delete the *crhR* ORF was detected (Figure 3.4). Again, significant degradation products including the 550 nt transcript were also detected. Stabilization of the *rimO* and full-length operon transcripts in the two *crhR* mutant strains suggests that CrhR is associated with regulating transcription, processing and/or degradation of the operon transcript.

3.4.4 *rimO* transcript half-life is not affected by temperature downshift or *crhR* mutation

The observed differences in transcript accumulation between wild type and *crhR*$_{TR}$ suggests that CrhR is potentially involved in the degradation of *rimO* mRNA. We therefore determined if *crhR* mutation affected *rimO* transcript half-life. In wild type cells, the *rimO* transcript half-life is temperature regulated, with half-lives of 2.5 and 6.0 min observed at 30°C and 20°C, respectively (Figure 3.5A). A similar pattern was observed in *crhR*$_{TR}$ cells; there was only a marginal alteration in *rimO* transcript half-life at both warm and cold temperatures: 5.0 and 7.5 min at 30°C and 20°C, respectively (Figure 3.5B). The results imply that turnover of *rimO* mRNA is temperature regulated by a process that does not involve a CrhR-dependent RNA degradation pathway.

3.4.5 Accumulation of a stable RNA from the *rimO* ORF

To further characterize the effect of CrhR RNA helicase activity on the temperature regulated expression of the *rimO* ORF, wild type and *crhR*$_{TR}$ cells were exposed to temperatures ranging from 10°C to 35°C for 1 h (Figure 3.6). In wild type cells, a relatively constant accumulation of the stable 550 nt transcript from the *rimO* ORF was detected at all temperatures (Figure 3.6A). This is reflective of the results shown in Figure 3.3 where only the 550 nt transcript was detectable after 1 h of cold stress. In

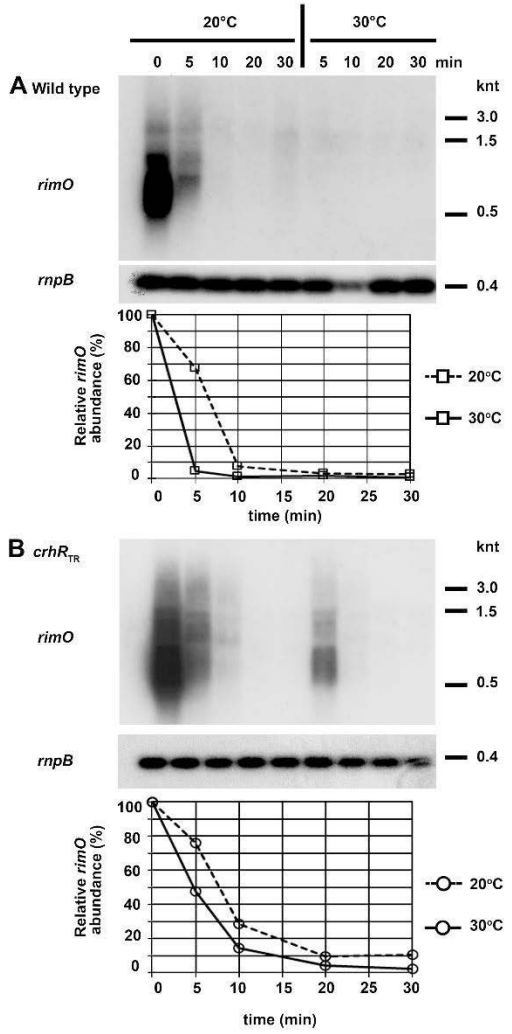

Figure 3.5: *rimO* transcript half-life.[9]

rimO transcript half-life was measured in (A) wild type and (B) *crhR*$_{TR}$ *Synechocystis* strains grown at 30°C to mid-log phase at which time the cultures were transferred to 20°C for 20 min to induce maximal *rimO* transcript accumulation. *de novo* RNA synthesis was subsequently inhibited by the addition of rifampicin (400 μg ml^{-1}) and half of each culture transferred back to 30°C. Aliquots for RNA extraction were harvested at the indicated times. *rimO* and *rnpB* transcripts were detected and quantified as indicated in Figure 3.3. Relative *rimO* transcript levels are indicated, normalized with respect to the level observed at time zero.

[9] This figure was originally published in (191) and is used with permission.

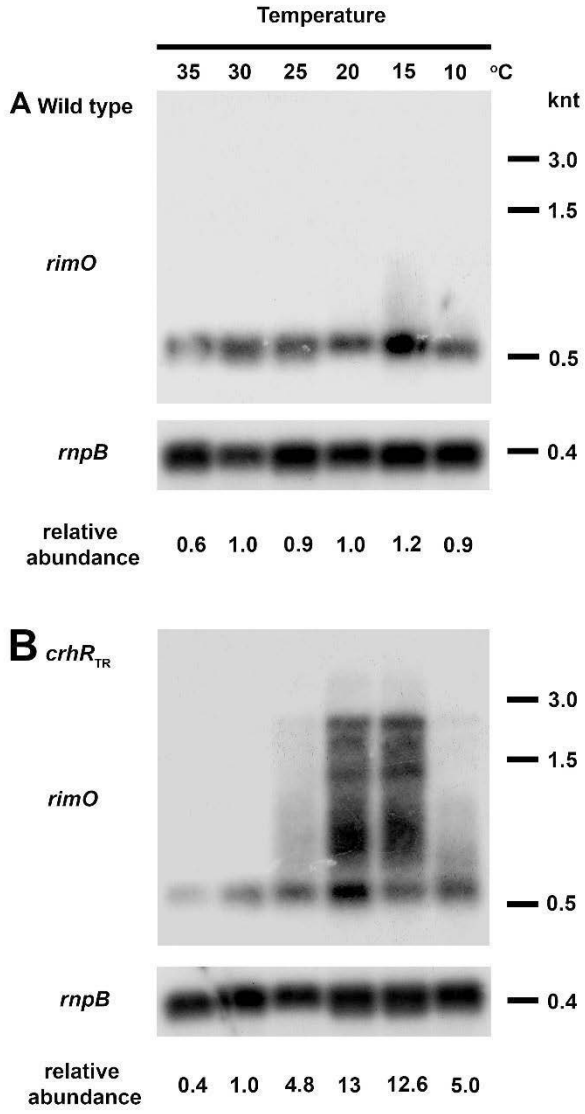

Figure 3.6: Temperature induction of *rimO* ORF expression.[10]

(A) Wild type and (B) *crhR*$_{TR}$ *Synechocystis* strains were grown to mid-log phase at 30°C and divided into 6 aliquots, each of which was incubated at the indicated temperature for 1 h. *rimO* transcript accumulation was determined in total RNA as described in Figure 3.3. The blots were stripped and probed with the *Synechocystis rnpB* gene as a control for RNA loading. The relative level of *rimO* abundance is provided below each lane with abundance normalized to *rimO* levels detected from illuminated cells grown at 30°C.

[10] This figure was originally published in (191) and is used with permission.

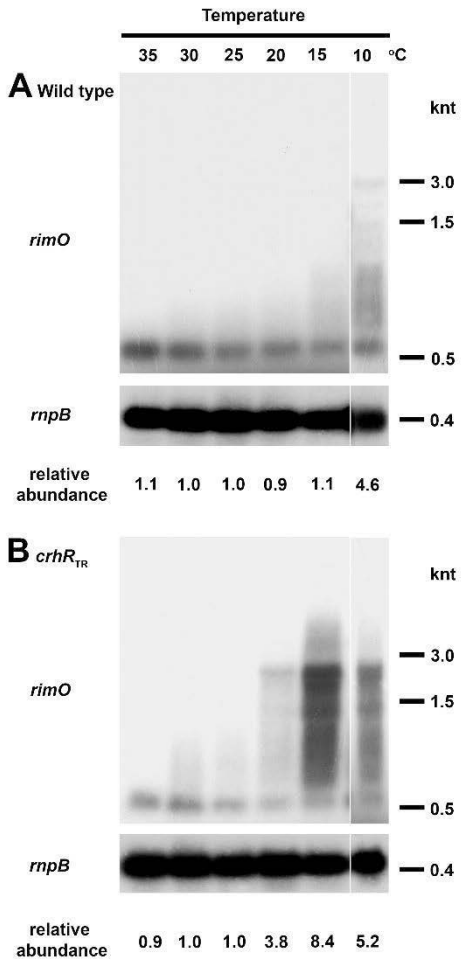

Figure 3.7: *rimO* accumulation in response to temperature acclimation.[11]

The effect of exposure to progressively lower temperatures on *rimO* accumulation was determined in (A) wild type and (B) *crhR*$_{TR}$ *Synechocystis* strains. Cultures were grown to mid-log phase at 30°C and the entire culture progressively exposed to the indicated temperature, from 35°C to 10°C, for 1 h at each temperature. Aliquots for total RNA isolation were harvested after 1 h incubation at each temperature and *rimO* transcript levels quantified in total RNA (5 µg) as described in Figure 3.3. The blots were stripped and probed with the *Synechocystis rnpB* gene as a control for RNA loading. The relative level of *rimO* accumulation, normalized to the abundance in wild type cells grown at 30°C, is provided below each lane.

[11] This figure was originally published in (191) and is used with permission.

contrast, in *crhR*$_{TR}$ cells, the *rimO* ORF probe detected both the *rimO-crhR*$_{TR}$ operon (2,280 nt) and *rimO* (1,465 nt) monocistronic transcripts, plus a smear of shorter transcripts, including the relatively constant accumulation of the 550 nt transcript (Figure 3.6B). Overall transcript abundance in *crhR*$_{TR}$ cells increased progressively as temperature decreased to 15°C, then decreased at 10°C. A similar pattern of *rimO* ORF transcript accumulation was observed when the experiment was performed by acclimation of a single culture to progressively decreasing temperatures (Figure 3.7). As in Figure 3.4, the results show a significant difference in temperature dependent transcript accumulation between wild type and mutant *crhR*$_{TR}$ strains, suggesting a role for CrhR in regulation of *rimO* expression in addition to the previously described regulation of its own transcript.

3.4.6 Accumulation of a stable RNA from the *rimO* 5' UTR

Expression of the dicistronic operon was further analyzed by determining expression of the *rimO* 5' UTR, previously mapped to start at the position -143 nt relative to the start codon of *rimO* (253). Northern analysis using a 5' UTR specific probe (Figure 3.1) detected a 75 nt stable transcript that accumulates in both wild type and *crhR*$_{TR}$ cells in a temperature-dependent manner (Figure 3.8A). Minor levels of longer products were progressively detected as temperature decreased (Figure 3.8A). Again, enhanced accumulation of the *rimO* 5' UTR transcripts was observed in the *crhR*$_{TR}$ mutant, indicating a CrhR-dependent effect on *rimO* 5' UTR processing or degradation (Figure 3.8B). It was of interest to examine the reduction in the response of *Synechocystis crhR*$_{TR}$ cells to 10°C, as shown in Figures 3.6 and 3.7, in more detail. In wild type cells, decreasing accumulation of a 75 nt and slight amounts of longer transcripts was detected by the *rimO* 5' UTR probe over time at 10°C (Figure 3.9A). In *crhR*$_{TR}$ cells, a relatively constant accumulation of the 75 nt transcript was detected at all time points following exposure to 10°C (Figure 3.9B). In addition, and in contrast to wild type cells, enhanced accumulation of longer transcripts was progressively observed in the *crhR*$_{TR}$ mutant (Figure 3.9B). Thus, a small stable RNA is generated from the *rimO* 5' UTR, independent of CrhR activity, and *crhR* mutation also affected cellular ability to process and/or degrade transcripts originating from the *rimO* 5'

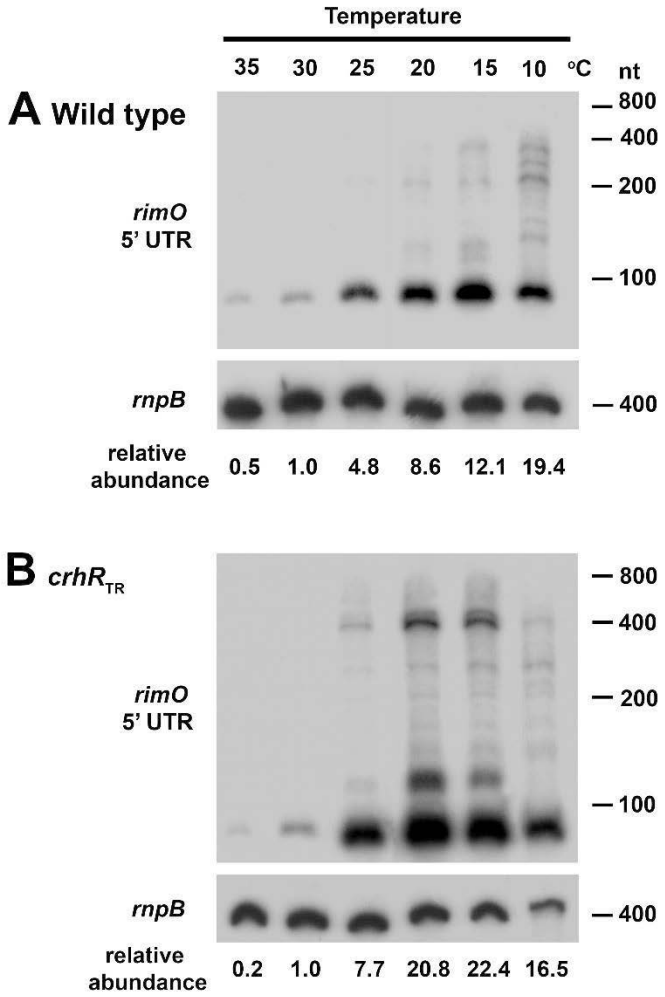

Figure 3.8: Temperature induction of *rimO* 5' UTR expression.[12]

Total RNA (5 μg) isolated from the cells grown in Figure 3.6 was separated on a 8 M urea-8% polyacrylamide gel and probed with a 90 nt riboprobe targeting the *rimO* 5' UTR. Blots show transcript detected from (A) wild type and (B) $crhR_{TR}$ *Synechocystis* strains. The blots were stripped and probed for the *Synechocystis rnpB* gene as a control for RNA loading. The relative level of *rimO* 5' UTR accumulation, normalized to the abundance in wild type cells grown at 30°C, is provided below each lane.

[12] This figure was originally published in (191) and is used with permission.

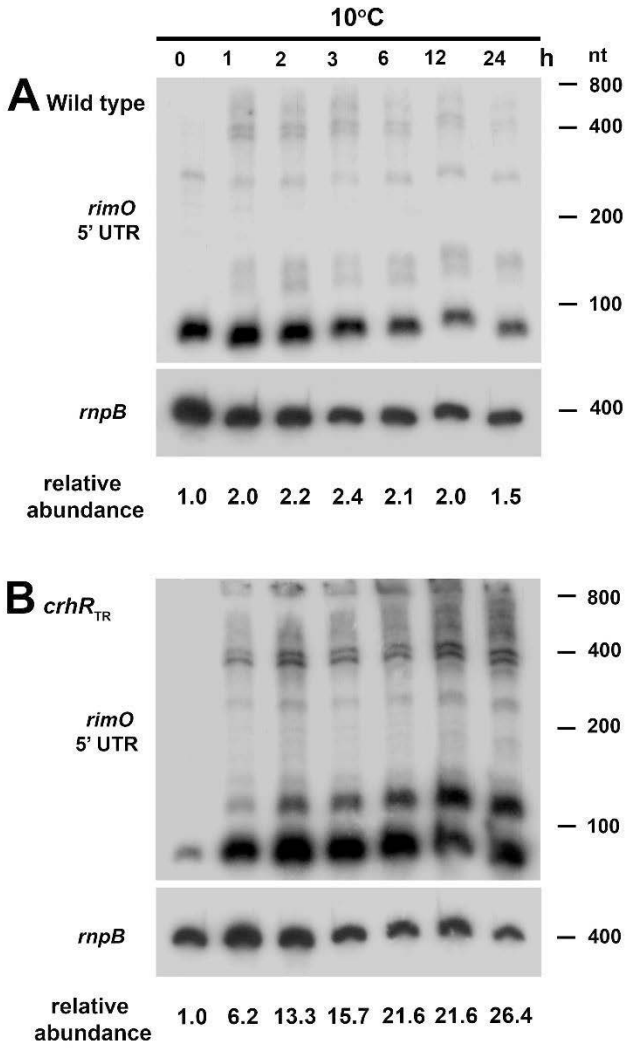

Figure 3.9: *rimO* 5' UTR accumulation at 10°C.[13]

Accumulation of the 75 nt transcript originating from the *rimO* 5' UTR was analyzed in (A) wild type and (B) *crhR*$_{TR}$ *Synechocystis* strains grown to mid-log phase at 30°C (0 time) and transferred to 10°C for the indicated times. Total RNA (5 μg) was separated on an 8 M urea-8% polyacrylamide gel and probed with a riboprobe corresponding to the *rimO* 5' UTR. The blots were stripped and probed for the *Synechocystis rnpB* gene as a control for RNA loading. The relative level of *rimO* 5'UTR accumulation is provided below each lane.

[13] This figure was originally published in (191) and is used with permission.

Table 3.3: *In silico* predicted *rimO* 5' UTR interacting mRNAs.[14]

The top ten *Synechocystis* transcripts interacting with the 75 nt *rimO* 5'UTR sRNA are shown.

Target	Start (T)	End (T)	Query	Start (Q)	End (Q)	Energy	p-value	fdr	Gene	Annotation
slr0951	116	150	75 nt	23	73	-24.94	3e-06	0.0090	*ispD*	2-C-methyl-D-erythritol-4-phosphate cytidylyl-transferase
sll1704	97	149	75 nt	17	75	-17.28	0.00088	0.8666	*csgA*	cell-cell signaling protein C-factor
sll0497	26	39	75 nt	23	35	-16.84	0.00116	0.8666		
sll1064	15	58	75 nt	19	72	-16.18	0.0017	0.8666		
sll0729	109	140	75 nt	50	75	-16.04	0.00189	0.8666		modification methylase
ssl3093	3	41	75 nt	1	32	-15.99	0.00195	0.8666	*cpcD*	phycocyanin associated linker protein
sll1558	130	147	75 nt	13	30	-15.94	0.00201	0.8666		mannose-1-phosphate guanylyl-transferase
ssl7004	128	150	75 nt	11	34	-15.45	0.00270	0.92260		probable plasmid stability protein
slr1705	87	113	75 nt	16	35	-14.82	0.0039148	0.9226052	*aspA*	asparto-acylase
slr7068	89	120	75 nt	10	35	-14.76	0.0040535	0.9226052		Cas6-2a CRISPR endonuclease

[14] The *in silico* analysis was performed by W.R. Hess, Universität de Freiburg.

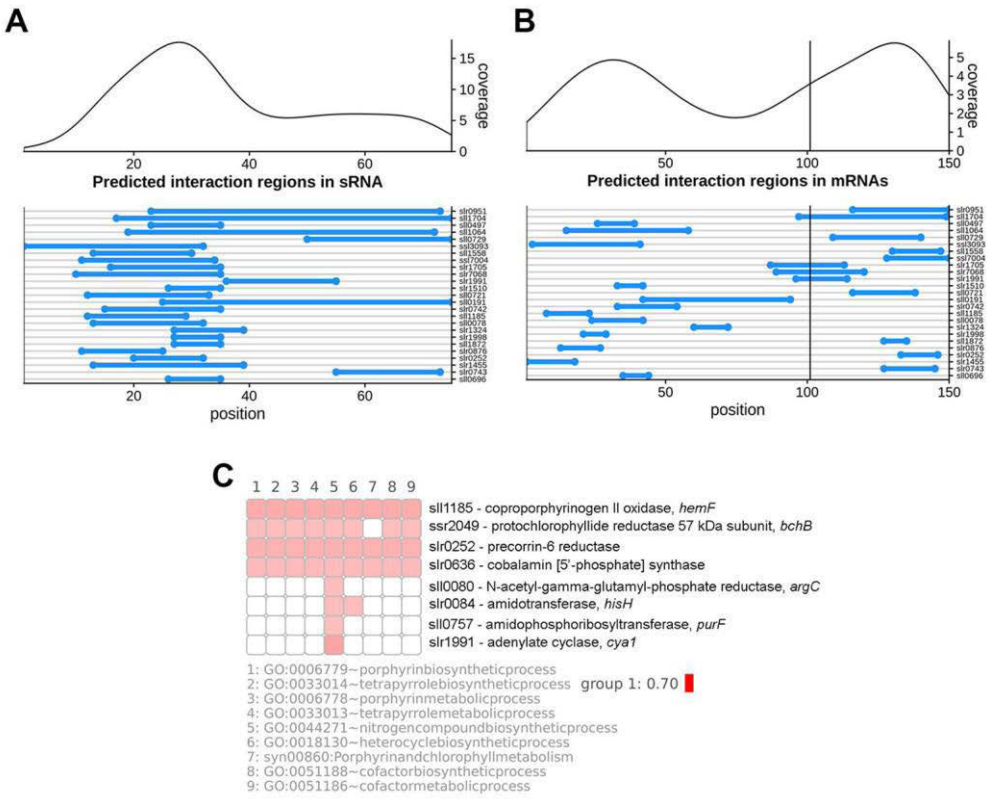

Figure 3.10: *In silico* identification of potential *Synechocystis* sequences interacting with the *rimO* 5'UTR.[15]

(A) Predicted interacting regions in the 75 nt sRNA originating from the *rimO* 5' UTR. (B) Predicted *rimO* 5' UTR interacting regions in potential target mRNAs. (C) Functional annotation chart generated by subjecting the top 50 predicted targets to functional enrichment using the DAVID database (254). The heat map shows all members of clusters with an enrichment score ≥1. Each row represents a gene and each column a specific functional term. If the gene can be assigned to a term, the corresponding square is filled. The opacity of the colour depends on the p-value of the IntaRNA prediction. A more intense colour represents a more significant p-value. Only 8 genes are detected here as functionally related. Note that the enrichment score of 0.7 for the "tetrapyrrole biosynthetic process" is below the value of 1.3 recommended (247).While a higher score represents a more statistically significant enrichment, it has been acknowledged that values below 1.3 may also contain useful information (247)

[15] The *in silico* analysis was performed by W.R. Hess, Universität de Freiburg.

UTR, an effect that progressively increased in response to exposure time at reduced temperature.

We performed *in silico* analysis to identify potential mRNA targets of the 75 nt sRNA originating from the *rimO* 5' UTR using the program IntaRNA (246). We utilized the first 75 nt following the TSS because in the previous genome-wide analysis of transcriptional start sites and 5' ends, no alternative 5' ends were found within the 5' UTR of *rimO* (241), leading to the assignment of the 75 nt sRNA as originating from the TSS of this gene. *In silico* prediction of potential mRNA targets for the 75 nt *rimO* 5' UTR-derived sRNA identified candidates that included gene products associated with tetrapyrrole metabolism (Figure 3.10 and Table 3.3). Some of these candidates have predicted interaction energies and interaction sites consistent with known mechanisms of regulation.

3.4.7 Determination of transcript 5' ends in the *rimO-crhR* region

Previous northern analysis (164) and the RT-PCR data presented above suggested that *rimO-crhR* operon expression involves an RNA processing site between the *rimO* and *crhR* cistrons in addition to the transcription start site located at position -110 nt with regard to the *crhR* initiation codon. Therefore, S1 nuclease protection and primer extension assays were employed to address all existing transcript 5' ends in this region. Both procedures identified the transcript start at position -110 or -111 nt, relative to *crhR*, in cells grown in the light (photoautotrophic) and in the presence of light + glucose (photomixotrophic) to visualize potential alterations in transcript start site use in response to growth conditions (Figure 3.11A and B). A strongly protected fragment corresponding to the entire probe was detected by S1 nuclease protection (Figure 3.11A), indicating the presence of a promoter upstream of the *Eco*RI site in *rimO* (see Figure 3.1). The *crhR* transcript was not detected by primer extension from cells grown in the dark (Figure 3.11B). Primer extension also identified a transcript 5' end 140 nt upstream of the *crhR* initiation codon in photomixotrophic cells, within the *rimO* ORF (Figure 3.11B).

To initiate analysis of the operon processing mechanism, 5' Rapid Amplification of cDNA Ends (RACE) was utilized to identify the 5' ends of the stable *crhR* ORF transcripts that accumulate in the $crhR_{TR}$ mutant at 20°C (164). The $crhR_{TR}$ inactivation

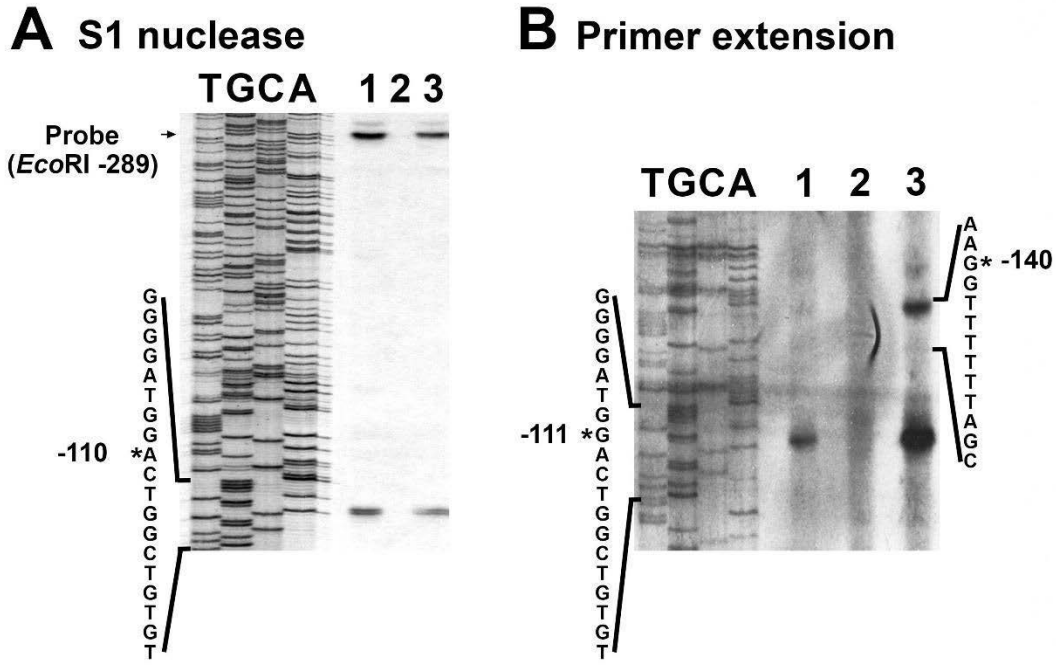

C Upstream of *slr0082* (*rimO*)

-177 AGGTTTTCTGGTGTAAATCTGTTACAATGTCTTTACAAATAAAAAGGGTCTGACCACCGT
TCCCCATCCGCAGGCTGTATTTACAGAATTTGCTGATCATTGCCTGGTTTAGTCCCTACC
CTACATCCCTTGGACTCGAACTCAGTCAATAGTCAGTTAATCCCTAGTAATTAATTTATG +3

D Upstream of *slr0083* (*crhR*)

-177 ATTATGACCTGTACGGTATGACCGCCGAGGAGGCTAAGGTTTTTTAGCTATTGAACTAAG
GGGATGGACTGGCTGTGTTATTGACGGTTGGTTCCCAGCCATTCCCGCAAACTTTTTAAT
CCTTAATTATTTGCCCACTAAACCGTCTTTTGTTATCCGAAATTATTTAACTTTTCCATG +3

Figure 3.11: Identification of 5' termini of transcripts.[16]

5' termini corresponding to *crhR* transcripts present in total RNA were determined using (A) S1 nuclease protection or (B) primer extension assays. Wild type *Synechocystis* cells were grown photoautotrophically at 30°C in the light and exposed to dark (3 h) or photomixotrophically in the presence of glucose (5 mM), as indicated. (A) S1 nuclease protection performed on cultures grown in photoautotrophic (lane 1), dark for 3 h (lane 2), and photomixotrophic (lane 3) conditions. The *Eco*RI site at the end of sequence homology within the S1 nuclease protection probe is indicated by "Probe (*Eco*RI -289)". (B) Primer extension as performed on total RNA isolated from cultures grown in photoautotrophic (lane 1), dark 3 h (lane 2) and photomixotrophic (lane 3) conditions. DNA sequencing ladders are shown for orientation. (C) The region upstream of *rimO* is depicted with the primary transcript terminus detected by both 5' RACE and deep sequencing (253) at -143 relative to *slr0082* shown in pink. (D) The region upstream of *crhR* is depicted with the sites at which detected transcripts start. A primary transcription start site identified at -110 relative to *slr0083* by primer extension, S1 nuclease protection and deep sequencing (253) is shown in blue. A second transcript terminus is also detected by primer extension under mixotrophic growth conditions (-140, pink) and 5' RACE (-138, orange). The translational stop codon for *rimO* (TAG) and the *crhR* start codon are shown in red and green, respectively.

[16] Panels A and B of this figure were originally published by Sonya Kujat-Choy in (255) and the 5' RACE analysis by Albert Remus R. Rosana in (191). This data is used with permission of the original authors.

strategy should have resulted in a 785 nt truncated *crhR* mRNA but previous northern analysis (164) also revealed three larger transcripts which, combined with the results presented above, indicates that they originate from co-transcription with the upstream *rimO* gene as a dicistronic message. Using 5' RACE-RCA, the 5' ends of the longest and shortest transcripts were mapped on RNA isolated from *crhR*$_{TR}$ cells grown under photoautotrophic conditions at 20°C. RACE identified that the 2,280 nt *rimO-crhR*$_{TR}$ transcript initiated 143 nt upstream of the *rimO* ORF and extended to the *Pml*I site within the *crhR* ORF from which the 5' RACE priming was initiated. Detection of this transcript therefore verifies that *slr0082-crhR* is expressed as a dicistronic operon in *crhR*$_{TR}$ cells grown at 20°C. The shortest mRNA identified was an 815 nt transcript that started 138 nt upstream of the *crhR* start codon, within the 3' end of the *rimO* ORF. A clone containing the shorter 785 nt transcript originating from the primary transcription start site at -110 was not detected in the clones selected for sequencing from the 5' RACE experiment. Extensive attempts to map the 5' ends of the ~1,500 and ~1,300 nt transcripts were not successful, possibly due to their reduced abundance. The identified nucleotides corresponding to the 3' termini of *rimO* and the 5' start of the *crhR* transcripts are summarized in Figure 3.11C and D.

3.4.8 Identification of primary transcripts

Terminator 5'-phosphate-dependent exonuclease was used to confirm expression of *slr0082* and *crhR* as a primary dicistronic operon, and to provide evidence that a transcript processing event created the major, ~1,700 nt *crhR* transcript detected at 20°C. Terminator 5' phosphate-dependent exonuclease destroys processed RNA transcripts containing a 5' mono-phosphate, leaving primary, 5' tri-phosphate transcripts intact. In wild type cells, the *crhR* ORF probe detected a major ~1,700 nt transcript while a transcript corresponding to the full-length *slr0082-crhR* operon (3,180 nt) was not detected (Figure 3.12A). Terminator depletion substantially reduced the abundance of the ~1,700 nt *crhR* transcript (*, Figure 3.12A). This indicates that the majority of this RNA is composed of a processed transcript starting at -138, with a basal level of a primary transcript that starting at -110. A ~2,100 nt transcript weakly detected in the untreated RNA was detected after Terminator depletion in wild type cells (**, Figure 3.12A), the

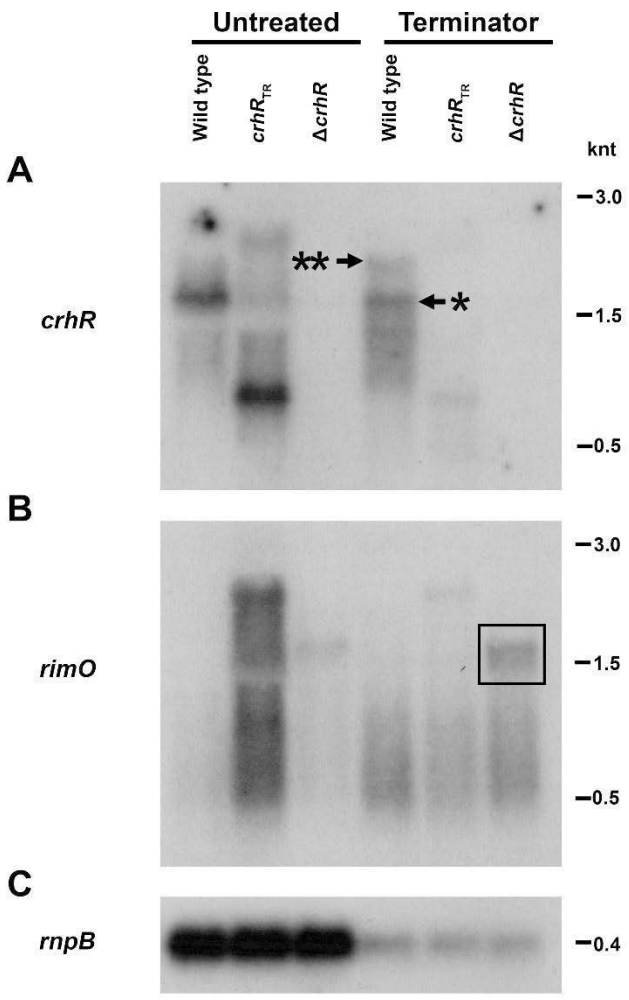

Figure 3.12: Detection of primary transcripts.

Total RNA was isolated from mid-log phase *Synechocystis* wild type, *crhR*$_{TR}$ and Δ*crhR* cells cold shocked at 20°C for 20 min. Aliquots of either untreated RNA (5 μg) or RNA treated with Terminator 5'monophospate-dependent exonuclease (20 μg), were subjected to Northern analysis to detect the *slr0083* (*crhR*) (A) or *slr0082* (B) ORF transcripts. Abundance of the *rnpB* transcript (C) was used as an RNA loading control and indicator for activity of the Terminator exonuclease. A significant proportion of the ~1700 nt *crhR* transcripts (*) have processed 5' termini, while the primary, 2000 nt transcript (**) originating at the -504 transcription start site internal to *slr0082* is enriched. A doublet of *slr0082* transcripts (outlined with a box) ~1500 nt can be detected in Δ*crhR*.

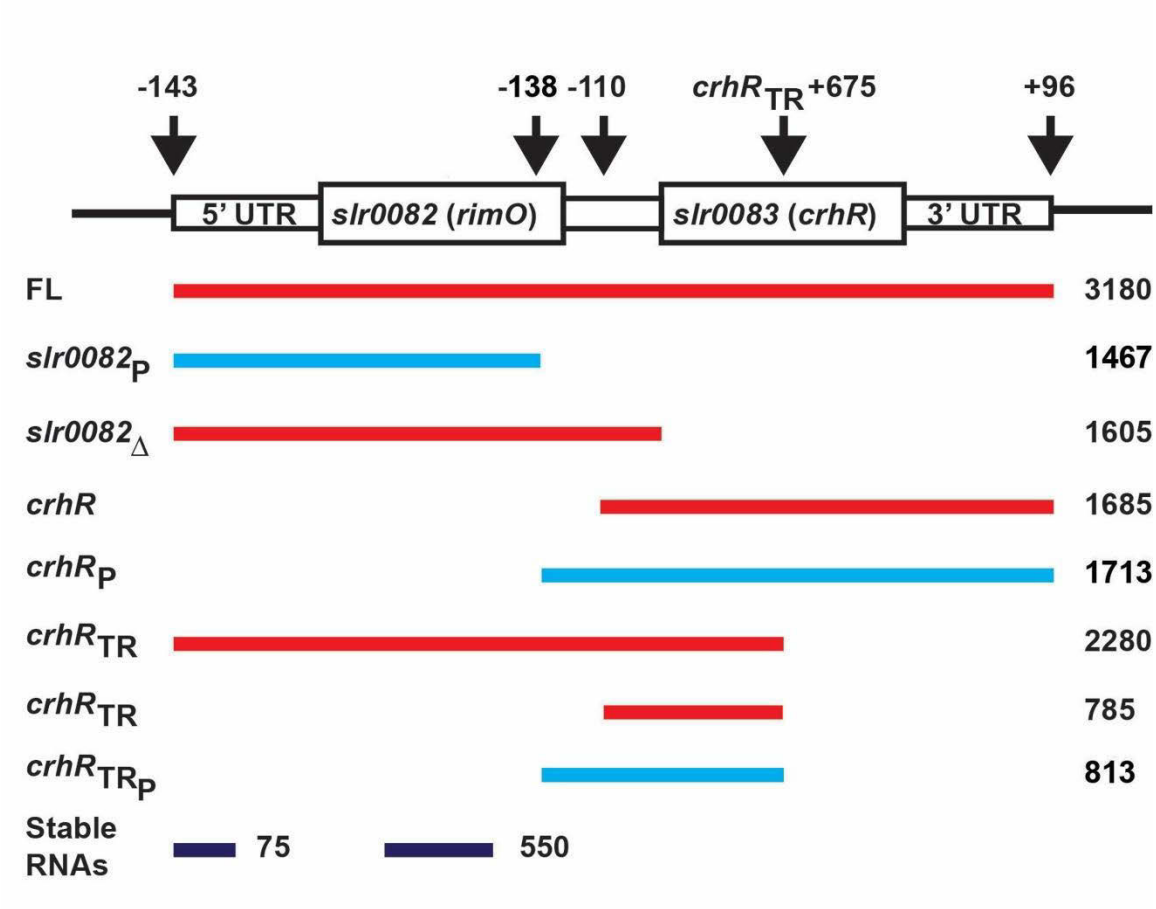

Figure 3.13: Summary of *rimO-crhR* operon transcript start sites and products. The detected transcripts produced from the *rimO-crhR* operon and their predicted lengths are shown in a genomic context. Known primary transcripts are depicted in red and transcripts originating from the proposed processing event are indicated in blue. The stable 75 and 550 nt transcripts originating from the *rimO* 5' UTR and ORF, respectively, are shown in purple. FL, full length operon transcript; P, processed operon transcript; Δ, complete *crhR* deletion mutant; TR, truncated *crhR*.

size corresponding to the internal transcript initiation site identified by Kopf *et al*. (241). In the *crhR*$_{TR}$ partial deletion mutant, four transcripts (~2,300, 1,500, 1,300 and 800 nt) were detected, as previously shown (164), with the 800 nt transcript predominating (Figure 3.12A). Terminator depletion substantially removed these transcripts, indicating that the majority of these transcripts originate from processing events except for a basal level of primary transcript. Transcripts were not detected by the *crhR* ORF probe in the complete *crhR* deletion mutant, Δ*crhR* (Figure 3.12A).

Similar analysis of the *slr0082* ORF detected a slight smear of transcript in wild type cells, again indicative of the basal level of expression and rapidity of turnover of this transcript (see Figure 3.3). In contrast, an intense smear is detected below the abundant ~2,300 nt *slr0082-crhR*$_{TR}$ operon (2,280 nt) transcript in *crhR*$_{TR}$ cells, indicating enhanced stability, and possibly reduced processing of this transcript (Figure 3.12B). The smearing is not indicative of problems with the RNA preparation, as the same RNA samples were utilized for all the analyses shown in Figure 3.12. Terminator treatment removes all of these transcripts, indicating the ~2,300 nt *slr0082-crhR*$_{TR}$ operon transcript ending at the *slr0083 Pml*I deletion site, detected in *crhR*$_{TR}$ cells, was processed at the 5' end, presumably during generation of the 75 nt stable transcript (see Figure 3.8). A doublet of ~1,600 and 1,500 nt transcripts is detected in untreated and Terminator treated RNA isolated from Δ*crhR* cells (□, Figure 3.12B). The 1,600 nt transcript is indicative of *slr0082* expression up to the translation initiation codon of *slr0083,* where the neomycin cassette was inserted to construct Δ*crhR*. The 1,500 nt transcript represents the expected transcript originating from RNA processing of the 1,600 nt transcript at the predicted RNA processing site. The extent of the Terminator depletion of processed RNA was indicated by the extensive, but not complete, reduction in *rnpB* transcript detected in 5' exonuclease treated samples (Figure 3.12C). A schematic summarizing the major transcripts observed is provided in Figure 3.13, with primary transcripts shown in red and processed transcripts shown in blue.

3.4.9 Identification of putative RNase E processing mechanism

Since the data above suggested that the transcript initiating -138 nt upstream of *crhR* is likely a processed transcript, the sequence and predicted structure of the RNA

surrounding the -138 nt site were analysed to identify a processing mechanism (Figure 3.14A). The secondary structure of a 41 nt fragment (genomic position 2887481-2887521) was predicted using the RNAfold web server (248). The resulting structure has a 3 bp hairpin within the 5' sequence, and contains the observed potential processing site at -138 nt, as well as the -140 nt site identified by primer extension within an unpaired region (Figure 3.14A). The short, upstream hairpin, and the presence of a uridylate-rich region immediately downstream of the predicted processing sites are consistent with the sequence and structure elements previously identified as required for RNase E cleavage in *Salmonella enterica* (256), and in *Synechocystis* within the *psbA* 5'UTR (257) and the crRNA maturation site in a CRISPR-Cas subtype III-Bv system (250). This sequence and structure conservation prompted us to experimentally test cleavage of this RNA by RNase E.

RNase E cleavage assays were performed *in vitro* on the 41 nt *rimO-crhR* RNA fragment shown in Figure 3.14B. After incubation with the recombinant *Synechocystis* RNase E, this RNA was processed into major products with lengths of 26/27 and minor products at 35/36 ± 1 nt (Figure 3.14B, left panel). In order to prove that the fragments were cleaved from the 5' end, the 3' end of the 41 nt RNA was labelled with Cy3 and used as a substrate in the RNase E cleavage assay. The resulting Cy3-labelled products were shorter than 26 nt, confirming the 26/27 and 35/36 nt fragments originated from the 5' end of the transcript (Figure 3.14B, right panel). Comparison of the RNase E-treated RNA to a sample of the same 41 nt transcript incubated with hydroxide confirmed that the cleavage of the *rimO-crhR* RNA fragment by RNase E occurred in a site-specific manner, while the CRISPR3 repeat as substrate (250) was included as a control for RNase E activity and showed the expected cleavage fragments (Figure 3.14B, left panel). The CRISPR3 control consists of a 36 nt 5'-monophosphorylated synthetic RNA oligonucleotide with a sequence identical to the repeats within the CRISPR3 repeat-spacer array of *Synechocystis*. RNase E cleaves 22 and 23 nt from the 5' end of these repeats *in vitro* and *in vivo* as the major maturation endonuclease for this CRISPR-Cas system (250). The 26 nt RNase E cleavage product generated from the *rimO-crhR* RNA fragment is consistent with the location of the identified -138 nt processing site and demonstrates that it is suitable for RNase E-dependent RNA processing. The sequence

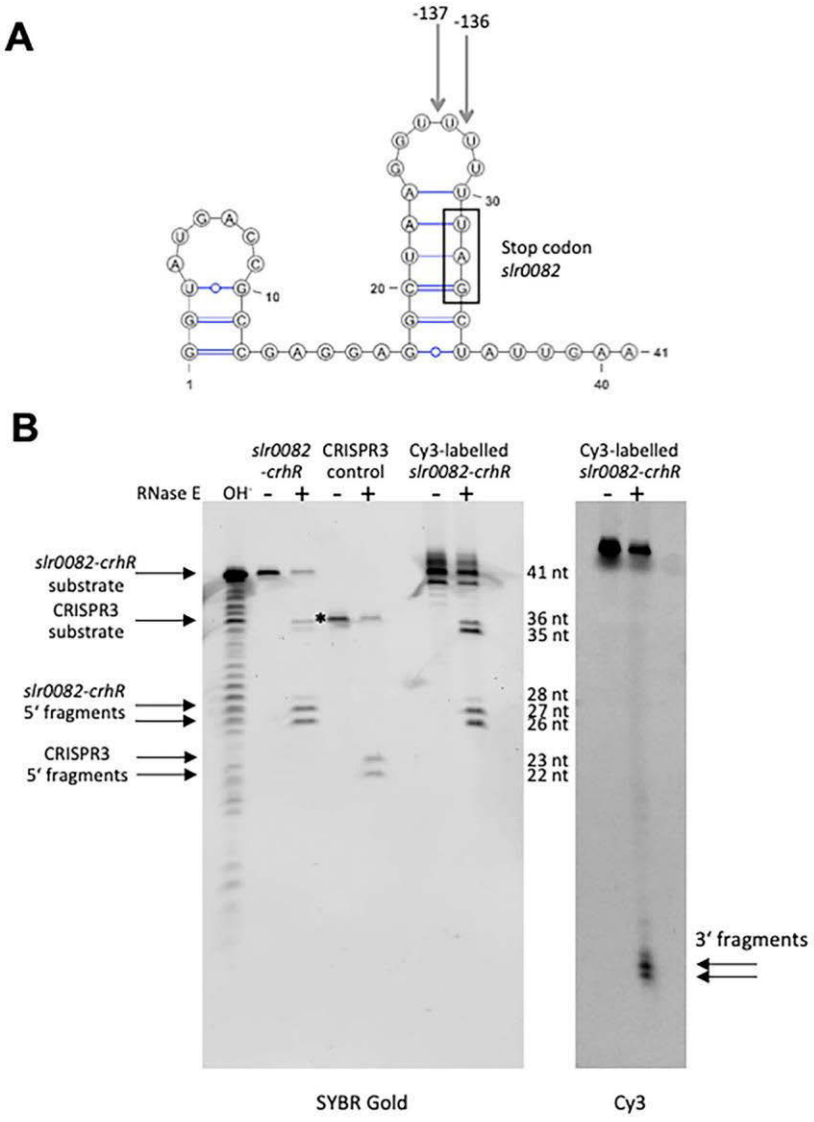
A
-137
-136
Stop codon
slr0082
B
slr0082
-crhR
CRISPR3
control
Cy3-labelled
slr0082-crhR
Cy3-labelled
slr0082-crhR
RNase E
OH⁻
slr0082-crhR
substrate
CRISPR3
substrate
slr0082-crhR
5′ fragments
CRISPR3
5′ fragments
41 nt
36 nt
35 nt
28 nt
27 nt
26 nt
23 nt
22 nt
3′ fragments
SYBR Gold
Cy3

Figure 3.14: Evidence for RNase E processing of the *rimO-crhR* operon.[17]
(A) Sequence and predicted secondary structure of the *rimO-crhR* transcript used in the RNase E cleavage assay. The secondary structure of the RNA fragment is similar to those identified for the RNase E substrates in the CRISPR3 repeat (250) and within the *psbA* 5' UTR in *Synechocystis* (257). The two major RNase E processed 5' transcript termini identified at -137 and -136 nt upstream of *crhR* are indicated by arrows, and the stop codon of *rimO* is boxed. (B) RNase E processing. Left panel: Products of the RNase E cleavage assay using the 41 nt *in vitro* transcript as substrate. Cleavage of the CRISPR3 repeat substrate (labeled with an asterisk) according to Behler *et al.* (250), as well as hydroxide degradation of the *rimO-crhR* fragment, are provided as controls. The cleavage assay was repeated for the 41 nt fragment labelled with Cy3 at the 3' end. Substrates and major 26 and 27 nt processing products are marked by arrows. A T7 RNA polymerase generated *in vitro* RNA fragment or a synthetic RNA oligonucleotide (CRISPR3 repeat) were incubated with recombinant *Synechocystis* RNase E for 30 min at 30°C. Reaction products (80 ng RNA) were separated on an 8 M urea-12% PAA gel and stained with SYBR Gold. Right panel: Same 8 M urea-12% PAA gel, but only signals from Cy3 were detected.

[17] The RNase E assay was performed by A. Migur, Universität de Freiburg (258) and is used with permission.

and structural features (Figure 3.14A) as this site (GGU↓U↓U) as well as at the minor 35/36 site (CU↓A↓UU) are consistent with the strong preference for a uridine in the +2 position as previously identified by Chao *et al*. (256). Thus, the minor 35/36 nt products also resulted from cleavage consistent with known RNase E substrate specificities, although they do not match the identified transcript termini *in vivo*. There products may represent either additional processing sites that were not identified during the 5' RACE, or sites that are cleaved by RNase E *in vitro* but not *in vivo*. The sequence of the -140 nt putative processing site, AA↓GGU, lacks the uridine in the +2 position and was not confirmed in the RNase E assay, indicating that it may be processed by a different endoribonuclease.

3.5 Discussion

Here, evidence is provided for a suboperonic gene regulatory mechanism in which RNase E-dependent processing generates differential expression of monocistronic transcripts from the dicistronic *rimO-crhR* operon in *Synechocystis*. Thus, the discoordinate expression of the *rimO-crhR* operon varies from that observed for operons in other bacterial systems, in which member transcripts are equally expressed (212) or where expression decreases with distance from the 5' end (259, 260). Previous RNA sequencing evidence suggested that *rimO* and *crhR*, encoding a methylthiotransferase and the DEAD-box RNA helicase CrhR, are potentially expressed from a major promoter upstream of *rimO* (253), while *rimO* and *crhR* were also detected as monocistronic transcripts (241). These analyses failed to explain how the observed differential accumulation of *rimO* versus *crhR* monocistronic transcripts was achieved. Here we show that the dicistronic message is rapidly processed to generate monocistronic mRNAs with differing half-lives. Interestingly, although CrhR is not necessary and sufficient for RNA processing, it is auto-regulatory, as the rate of RNA processing is enhanced by CrhR RNA helicase activity. RNA processing occurs at a site with an RNase E consensus motif that is cleaved by recombinant RNase E *in vitro*. Predicted secondary structures at the 5' and 3' termini of the *crhR* and *rimO* transcripts, generated by RNA processing, are consistent with protection of *crhR* from ribonucleases, leaving the vulnerable *rimO* transcript to be rapidly degraded. The proposed scenario will result in efficient generation

of cistron transcripts with differing stability while maintaining co-transcription of *rimO* and *crhR*. A model outlining regulation of *rimO-crhR* operon expression, including transcription, RNA processing and consequences for the respective transcripts, is shown in Figure 3.15.

3.5.1 *rimO-crhR* is expressed as a dicistronic operon

Evidence for the dicistronic expression of *rimO* and crhR was provided by northern, 5'RACE and RT-PCR results, indicating that expression of *rimO* and *crhR* is complex, involving transcription from at least two promoters. In wild type cells, the promoter upstream of *rimO* produces a primary dicistronic transcript during cold stress that is rapidly processed into two monocistronic transcripts. The second transcription start site is located between *rimO* and *crhR*, at the previously identified -110 position (41, 253), and presumably generates basal levels of CrhR at all temperatures.

3.5.2 RNA processing generates monocistronic transcripts with differing fates

Here we show that in wild type cells, both *rimO* and *crhR* are primarily detectable as monocistronic transcripts with minimal levels of the full-length dicistronic message detected. In the absence of CrhR RNA helicase activity, stabilized, full-length operon transcripts extensively accumulate, in addition to transcripts that correspond to either the *rimO* or *crhR* monocistronic ORFs. This observation is crucial, as it indicates that: i) CrhR RNA helicase activity is associated but not absolutely required for the RNA processing event, and ii) that the full-length operon transcript is stable until the processing event occurs. The latter point is associated with our observation that the two monocistronic transcripts have significantly disparate half-lives. The wild type half-lives are dramatically affected by temperature and are significantly shorter for *rimO*; *rimO* exhibits half-lives of 6 min and 2.5 min and *crhR* >30 min and 10 min at 20°C and 30°C, respectively (164). This is in distinct contrast to the observation that the *rimO* or *crhR* half-lives were not dramatically altered by *crhR* inactivation, suggesting that CrhR is not directly involved in further degradation of these monocistronic RNAs. Rather, the enhanced accumulation and stabilization of the full-length operon transcript in the *crhR*

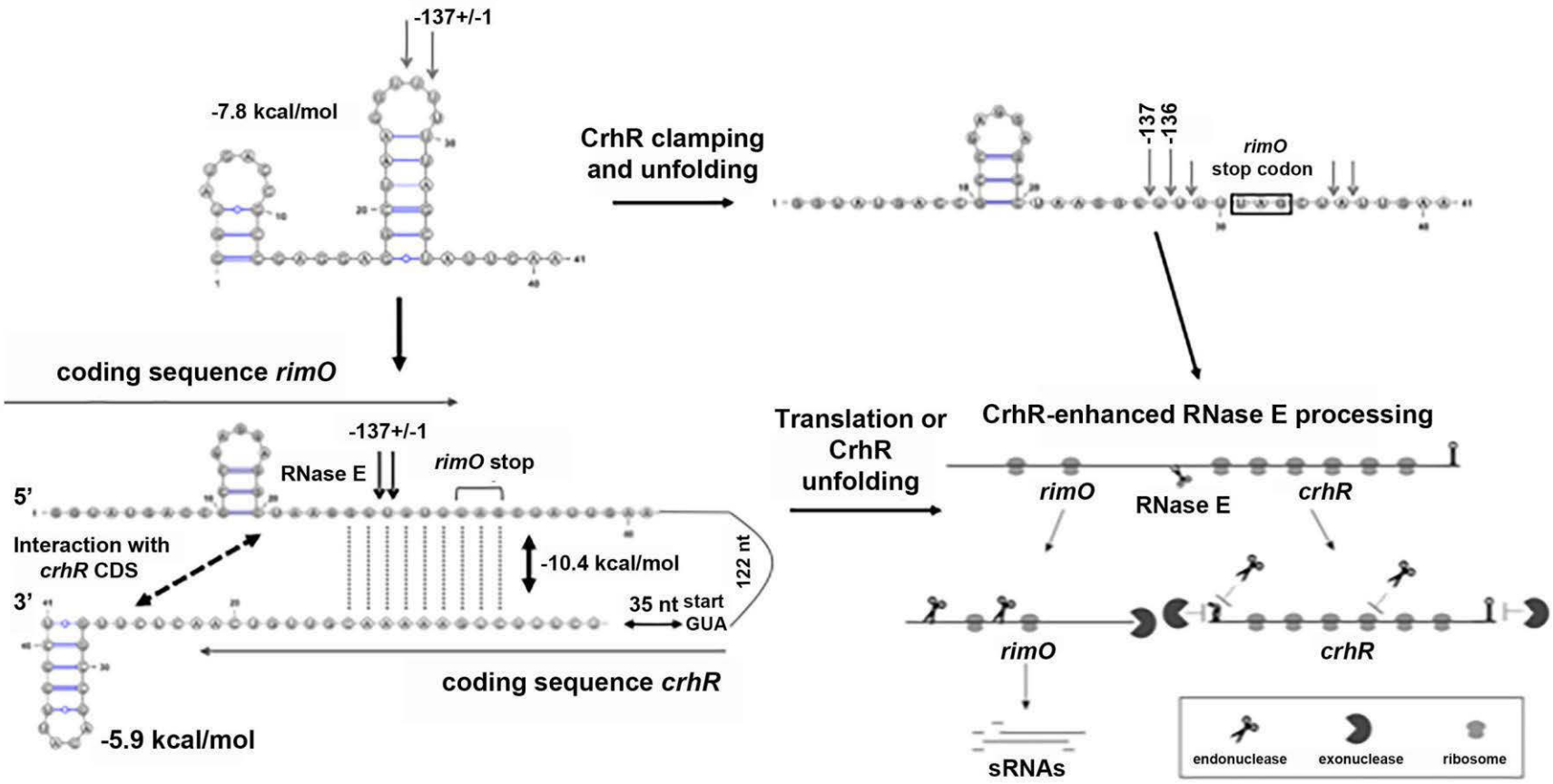
-137+/-1
-7.8 kcal/mol
CrhR clamping
and unfolding
-137
-136
rimO
stop codon
coding sequence rimO
-137+/-1
RNase E
rimO stop
5'
Interaction with
crhR CDS
3'
-10.4 kcal/mol
122 nt
35 nt start
GUA
coding sequence crhR
-5.9 kcal/mol
Translation or
CrhR
unfolding
CrhR-enhanced RNase E processing
rimO
RNase E
crhR
rimO
crhR
sRNAs
endonuclease
exonuclease
ribosome

Figure 3.15: Model of *rimO-crhR* processing and transcript stability.[18]

The RNA processing region can fold into the two structures shown. As transcription proceeds, the CrhR DEAD-box RNA helicase could bind and stabilize the double-stem loop RNA, acting as a protein scaffold for recruitment of the endonuclease and/or unwinding of the stem-loop to convert the cleavage sites into ssRNA required for RNase E cleavage. Alternatively, the cleavage site sequence could also be masked by base pairing with the *crhR* coding sequence forming a duplex structure that could be removed either by translation or CrhR binding and unwinding in a positive feedback mechanism, as described above. Subsequently, after processing by RNase E, stable RNA structures at the termini of *crhR*, as well as translating ribosomes, protect the transcript from degradation by ribonucleases, similar to suggestions by Dar and Sorek (224) for the programmed mRNA decay in *E. coli*. The *rimO* transcript is rapidly degraded from a destabilized 3' terminus created by the RNA processing event. Additional *rimO* transcript processing and/or degradation generates two stable sRNAs of 75 and 550 nt.

[18] This model includes contributions from A. Migur and W.R. Hess.

mutant indicates that RNA processing selectively destabilizes the *rimO* transcript, a process that is associated with functional CrhR RNA helicase activity.

While not all sites suitable for cleavage by RNase E *in vitro* are significant *in vivo* (261), processing at the -138 nt site in *rimO-crhR* is potentially critical for the observed differential stability of the *rimO* and *crhR* transcripts. After processing, the upstream gene product in the *rimO-crhR* operon is predicted to have a relatively unstructured 3' terminus, the most stable structure (ΔG = -4.7 kcal mol^{-1}) consisting of a single 3 bp hairpin with a 5 nt loop (Table 3.4) within the final 45 nt of the transcript. This unstructured 3' end potentially allows 3'-5' exonucleases to efficiently access and perform the observed rapid degradation of the *rimO* transcript. In contrast, the 3' terminus of the downstream gene product, encoding *crhR*, is predicted to have a more stable (ΔG = -17.0 kcal mol^{-1}) hairpin with an 11 bp stem and 10 nt loop, which potentially confers protection from 3'-5' exonucleases. In addition, three stable stem-loop structures, with a combined ΔG = -23.1 kcal mol^{-1}, are predicted to form at the 5' end of the processed *crhR* transcript (Table 3.4). These structures likely perform the same protective function as the 5' structures identified by Dar and Sorek (224) in processed *E. coli* transcripts, and perhaps extend to protection from the homolog for the 5'-3' exonuclease, RNase J, in *Synechocystis* (262).

Interestingly, further processing and/or degradation of the *rimO-crhR* operon generates two candidate sRNAs that originate from the 5'UTR and the coding sequence of *rimO*. It should be noticed that the processing events that generate these stable transcripts do not appear to be regulated by CrhR activity. A function cannot be proposed for these sRNAs yet; however, computational analyses predicted mRNAs encoding enzymes involved in pigment biosynthesis, signaling proteins and others as possible targets indicating potentially interesting regulatory relationships (Figure 3.10 and Table 3.3). NsiR4 illustrates the possible functional relevance of such sRNAs, since cells lacking it are out-selected during periods of low nitrogen, consistent with its targets in the machinery controlling nitrogen assimilation (263). In addition, a 98 nt sRNA, Nc117, originating from the *slr0550-slr0551* intergenic spacer was described by Pei *et al*. (264). Since there is not a transcription start site in this region, Nc117 derives from the 5' UTR of *slr0551*, encoding RNase J. Hence, this arrangement is similar to the situation with the

Table 3.4: Predicted RNA structures at termini of processed transcripts.

The sequences of the processed transcripts of *rimO* and *crhR* were used to predict RNA structures with the RNAfold Web Server (http://rna.tbi.univie.ac.at/cgi-bin/RNAWebSuite/RNAfold.cgi). The sequence and structure for 45 nt at the 3' terminus of each transcript was extracted from the predicted structure of the full processed transcript. For structures at the 5' terminus of the *crhR* transcript, the extracted sequence and structure was from the processing site to the start codon of *crhR*. The Gibbs free energy calculation is based on the extracted sequence and structure. Structures are shown in dot-bracket notation.

Gene	Terminus	RNA sequence & structure	ΔG (kcal/mol)
-138 nt processing site			
rimO	3'	CCGACGAUUAUGACCUGUACGGUAUGACCGCCGAGGAGGCUAAGG .....(((.....))).....	-4.7
crhR	5'	UUUUUUAGCUAUUGAACUAAGGGGAUGGACUGGCUGUGUUAUUGA .....(((((((.(((((((.....) CGGUUGGUUCCCAGCCAUUCCCGCAAACUUUUUAAUCCUUAAUUA))).....)))))))))))(((((....((((...)))). UUUGCCCACUAAACCGUCUUUUGUUAUCCGAAAUUAUUUAACUUU)))))..........(((.....)) UCCAUG))....	-23.1
crhR	3'	GGAAAAAAAUAACUCCUCCAGAACUAAGACCCUGGGGGAGUUUUA .....(((((((((.....)))))))))...	-17.0
-140 nt processing site			
rimO	3'	CACCGACGAUUAUGACCUGUACGGUAUGACCGCCGAGGAGGCUAA .....(((.....)))...	-4.7
crhR	5'	GGUUUUUUAGCUAUUGAACUAAGGGGAUGGACUGGCUGUGUUAUU .....(((((((.(((((((..... GACGGUUGGUUCCCAGCCAUUCCCGCAAACUUUUUAAUCCUUAAU .))))).....)))))))))))(((((....((((...)))). UAUUUGCCCACUAAACCGUCUUUUGUUAUCCGAAAUUAUUUAACU ..)))))..........(((..... UUUCCAUG))))....	-23.1
crhR	3'	GGAAAAAAAUAACUCCUCCAGAACUAAGACCCUGGGGGAGUUUUA .....(((((((((.....)))))))))...	-17.0

75 nt sRNA described here as originating from the 5' UTR of *slr0082*. Overexpression of Nc117 led to an improved tolerance to exogenous biofuel stress by an unknown mechanism (264), supporting the biological functionality of such transcripts in *Synechoystis* further. Moreover, hundreds of candidate sRNAs derived from processing of mRNA coding sequences and 3'UTRs have been identified in *E. coli* (265, 266). Overall, our data further extends the range of bacterial lineages that host this new class of sRNAs, suggesting they perform an important role in the regulation of gene expression in cyanobacteria. Similar examples of RNA processing associated with differential suboperonic gene expression were reported for the two nitrogenase gene clusters in the cyanobacterium *Anabaena variabilis* ATCC 29413 (237-240). Processing of the *nifBSUHDKEN-1* gene cluster, immediately upstream of *nifH1* (237) generates an extended transcript half-life for *nifH1, nifD1* and *nifK1* relative to the other nitrogenase genes (239). This effect is associated with multiple processing events and two stem-loop structures upstream of *nifH1* which convey stability to the processed *nifH1* transcript (240) Although details of the processing mechanism were not identified in these studies, the findings clearly resemble the mechanism investigated here that regulates the discoordinate expression of the *rimO-crhR* operon.

3.5.3 A role for the CrhR RNA helicase in *rimO-crhR* transcript processing

In vitro cleavage of the *rimO-crhR* transcript at the -138 nt site upstream of *crhR* is consistent with an RNase E-dependent processing mechanism, as both the RNA sequence, GG↓UUU, which conserves the strong preference for a uridine in the +2 position, and the secondary structure in the vicinity of the processing site fit the "ruler and cut" mechanism for RNase E proposed by Chao *et al*. (256) (Figure 3.15). As RNase E and CrhR have previously been reported to cosediment with polysomes from *Synechocystis* (Chapter 2), the difference in the rates of *rimO-crhR* processing between wild type and $crhR_{TR}$ cells may identify a role for CrhR in the processing event. Functionally, the ability of CrhR to both unwind and anneal RNA duplexes *in vitro* (153) could be intimately associated with the *rimO-crhR* processing mechanism. During transcription, CrhR could interact with the operon transcript directly at the processing site stem loop and function as an RNA clamp, recruiting RNase E, which will cleave after

CrhR-mediated secondary structure restructuring occurs, as depicted in Figure 3.15. Alternatively, the processing site could also base pair with the *crhR* ORF thereby masking the processing site. CrhR could rearrange this RNA secondary structure to generate ssRNA required for RNase E cleavage (Figure 3.15).

Two similar examples of bacterial RNA helicase involvement in RNA processing involving differential regulation of suboperonic gene expression have been reported. The *E. coli* DEAH-box RNA helicase, HrpA, is required for efficient endonucleolytic cleavage of the *daaA-E* polycistronic mRNA via an unknown mechanism (61). The processing event stabilizes *daaE* while destabilizing the *daaA-D* transcript upstream of the cleavage site (61). In the *Salmonella pldB-yigL* dicistronic operon, *yigL* is stabilized after processing by binding of the sRNA SgrS, an interaction mediated by the RNA chaperone Hfq (216). Thus, a common theme appears to be emerging in which an RNA chaperone, either an RNA helicase or Hfq, is required for RNA processing that generates differential transcript stability of suboperonic members in several different bacteria.

3.5.4 *rimO-crhR* co-transcription and cold stress

The genes *rimO* and *crhR* are syntenic in many cyanobacteria (147), consistent with the idea that genomic context can indicate functional relatedness (267). It is therefore tempting to speculate that co-transcription of *rimO* and *crhR* may indicate that both proteins function in enhancing cellular fitness during cold stress. In support of this proposal, CrhR has been shown to co-precipitate with polysomes and RNA degradosome components (Chapter 2). Furthermore, DEAD-box RNA helicase association with cold adaptation is widespread in bacteria including the cold-induced *E. coli* helicases, CsdA and SrmB, that function in assembly of the large ribosomal subunit (109, 110), formation of a cold-adapted degradosome (178), and translation initiation (268).

3.5.5 Conclusion

In conclusion, we provide evidence that *rimO-crhR* is expressed as an operon whose transcript is rapidly processed by RNase E into monocistronic mRNAs with divergent half-lives. The process is auto-regulatory, as activity of the *slr0083*-encoded DEAD-box RNA helicase, CrhR, is associated with, but not absolutely required, for processing.

Further research is required to discern the role CrhR performs in the cleavage event and its potential to regulate additional operons in *Synechocystis*. As well, the function of the two stable by-products of *rimO-crhR* operon processing remains to be determined. RNA helicase catalysis of differential operon cistron expression is likely a more common mechanism for regulation of gene expression than previously anticipated.

Chapter 4: Regulation of *crhR* expression by fixed nitrogen availability and source

4.1 Summary

Cyanobacteria have a key role in the cycling and balance of bio-available carbon and nitrogen in aquatic ecosystems. In fulfilling this role, cyanobacteria must quickly respond to changes in the availability of carbon and nitrogen by regulating expression of gene products associated with transport and metabolism. Using an inactivation mutant of the stress-regulated RNA helicase of *Synechocystis* sp. PCC 6803, CrhR, evidence is presented that cyanobacteria deficient in helicase activity demonstrate altered growth rates and pigmentation in media containing various sources of fixed nitrogen. The expression of CrhR in media with fixed nitrogen, either urea or nitrate, is induced transiently after transfer to fresh media at both warm (30°C) and cold (20°C) temperatures. Conversely, when grown in nitrogen limited conditions, CrhR protein levels decrease rapidly in cold-stressed wild type cells. In contrast, CrhR protein levels do not decrease in a CrhR truncation mutant grown under nitrogen limited conditions. The data indicate that CrhR expression is regulated in response to the source of fixed nitrogen, with evidence of auto-regulatory pathways. The global nitrogen control factor, NtcA, mediates transcriptional repression of the *rimO-crhR* operon, as well as proteolysis of CrhR during nitrogen starvation. These results suggest a potential role for RNA helicase regulation of genes involved in nitrogen transport, metabolism and/or storage, or the coordination of nitrogen and carbon metabolism.

4.2 Introduction

As the primary producers in many ecosystems, cyanobacteria perform crucial roles in cycling nutrients on a worldwide scale, including carbon dioxide, oxygen, iron and nitrogen (269-272). Cyanobacteria are Gram-negative obligate photoautotrophs that obtain all their energy from light harvesting and carbon skeletons from Calvin-Benson-Bassham (CBB) cycle-based oxygenic photosynthetic carbon fixation (273). As such, survival of these free-living organisms is dependent on their ablity to sense and respond to the rapidly changing environmental conditions they continuously experience in their natural habitat. These responses are regulated at the genetic level, and cyanobacteria are known to rapidly alter gene expression in response to a variety of abiotic and biotic stresses (241, 274).

Obtaining fixed nitrogen is crucial for the survival of all organisms. Although some organisms can directly fix atmospheric nitrogen, including a variety of cyanobacteria, *Synechocystis* sp. PCC 6803 (hereafter *Synechocystis*) does not perform nitrogen fixation. Thus, *Synechocystis* must acquire and assimilate fixed nitrogen from its environment (275). Similar to other organisms, non-diazotrophic cyanobacteria such as *Synechocystis* express a number of genes which optimize nitrogen acquisition and assimilation, and can utilize a variety of fixed nitrogen sources for growth including ammonium, urea and nitrate/nitrite. Ammonium can be acquired by passive diffusion as ammonia or actively transported via one of three monocomponent permeases, *amt1, amt2* and *amt3* (276). Once transported, ammonium is rapidly assimilated, being incorporated into carbon skeletons primarily by sequential action of glutamine synthetase (GS) and glutamate synthetase (GOGAT) (277), but also via the glutamine dehydrogenase (GDH) pathway (278). Urea is actively transported via a high-affinity, ABC-type permease (*urt*) and hydrolyzed to ammonium and carbon dioxide by a constitutive urease (*ure*) (279). Urea also spontaneously decomposes into cyanate and ammonium. Although *Synechocystis* lacks a cyanate transporter and cannot grow on exogenous cyanate as the sole nitrogen source, if urea decomposition occurs inside the cell, the resulting cyanate can be further hydrolyzed to ammonium and carbon dioxide by the cyanase enzyme (280). Nitrate and nitrite are transported by an ABC-type bispecific transporter (*nrt*) (281), then reduced step-wise from nitrate to nitrite to ammonium by the ferredoxin-dependent nitrate reductase (*narB*) and nitrite reductase (*nirA*) (282-284). The reduction of nitrate and nitrite in cyanobacteria is dependent on photosynthesis as a source of reductant, as the reducing power for nitrate reduction comes from ferredoxins shared with the electron transport chain of photosynthesis (285). Cyanobacterial nitrogen uptake and assimilation pathways are summarized in Figure 4.1A.

Several regulatory networks that respond to nitrogen have also been characterized in cyanobacteria. The CRP-like global nitrogen regulator NtcA is a transcription factor that coordinates many genetic and physiological changes in response to nitrogen availability (286). NtcA affects expression of genes both positively and negatively by binding promoters containing the conserved NtcA-binding sequence $GTAN_8TAC$ (287). Regulation of NtcA activity is complex, being strongly enhanced by accumulation of

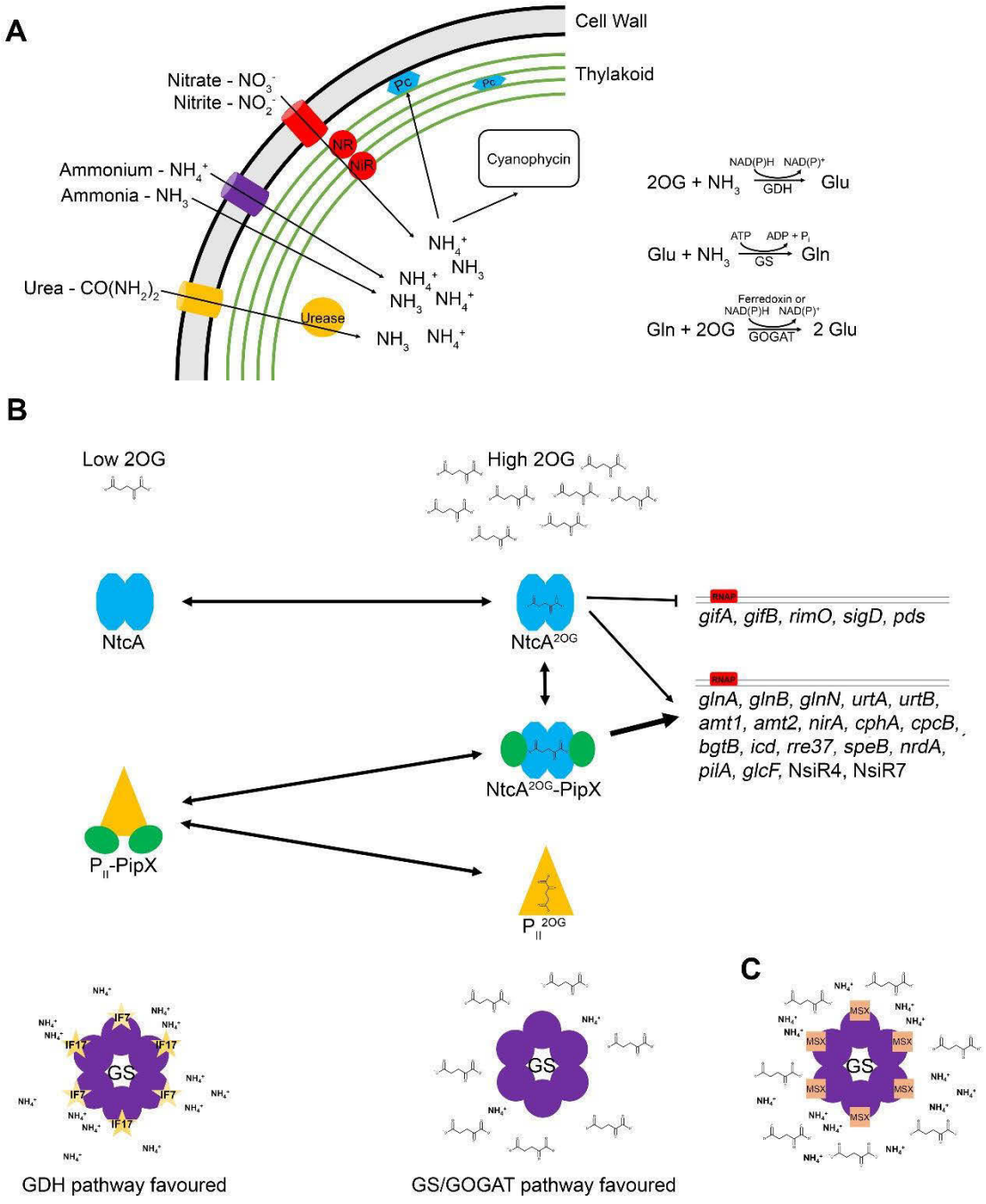
A
Cell Wall
Thylakoid
Nitrate - NO3-
Nitrite - NO2-
Ammonium - NH4+
Ammonia - NH3
Urea - CO(NH2)2
Pc
NR
NiR
Urease
Cyanophycin
NH4+
NH3
2OG + NH3 NAD(P)H NAD(P)+ GDH Glu
Glu + NH3 ATP ADP + Pi GS Gln
Gln + 2OG Ferredoxin or NAD(P)H NAD(P)+ GOGAT 2 Glu
B
Low 2OG
High 2OG
NtcA
NtcA2OG
RNAP
gifA, gifB, rimO, sigD, pds
glnA, glnB, glnN, urtA, urtB, amt1, amt2, nirA, cphA, cpcB, bgtB, icd, rre37, speB, nrdA, pilA, glcF, NsiR4, NsiR7
NtcA2OG-PipX
PII-PipX
PII2OG
C
GS
IF7
IF17
MSX
GDH pathway favoured
GS/GOGAT pathway favoured

Figure 4.1: Summary of nitrogen uptake, assimilation and regulation of nitrogen metabolism in cyanobacteria.

(A) An overview of uptake and assimilation pathways for three nitrogen sources in *Synechocystis*: ammonium, nitrate and urea. Within the cell, organic nitrogen can be stored as phycocyanin or in cyanophycin granules, or be assimilated into amino acids via the GDH or GS/GOGAT pathways. (B) Pathways for regulation of gene expression and nitrogen assimilation. During periods with plentiful intracellular ammonium, 2-oxoglutarate (2OG) does not accumulate, NtcA remains in an inactive state, and its co-activator, PipX, is sequestered by binding with P_{II}. GS activity is inhibited by binding of IF7 (*gifA*) and IF17 (*gifB*), resulting in the energetically favourable GDH pathway being preferred for ammonium assimilation. When intracellular ammonium levels are low, 2OG accumulates and binds to both P_{II} and NtcA, activating NtcA as a transcription factor. PipX preferentially binds the active $NtcA^{2OG}$ conformation, enhancing the effect of NtcA on its regulon. Negative regulation of *gifA* and *gifB* by NtcA, as well as proteolytic degradation of these proteins, allow for active GS, which has a higher affinity for ammonium than the GDH pathway. Examples of genes in the NtcA regulon are extracted from Giner-Lamia *et al.* (288) (C) GS activity is irreversibly inhibited by L-methionine sulfoximine (MSX) binding to the active site of GS, allowing for accumulation of 2OG and constitutive activation of the NtcA transcription factor regardless of the presence of ammonium or other fixed nitrogen.

2-oxoglutarate (2OG), the carbon skeleton required for the assimilation of nitrogen into amino acids (287, 289). Activity is further enhanced by binding of the P_{II}-interacting protein, PipX, to the NtcA-2OG complex (290). PipX is available to alternately bind to NtcA or be sequestered by the P_{II} protein, with the interaction dependent on 2OG availability (291, 292). The regulation of NtcA activity by PipX and 2OG is presented in Figure 4.1B. In conjunction, a second transcription factor, NtcB, is regulated by nitrite concentration, and specifically enhances expression of genes involved in the assimilation of nitrate/nitrite (293, 294). Additionally, non-coding RNAs, such as glutamine riboswitches and the sRNA NsiR4, contribute to the regulation of cyanobacterial nitrogen assimilation (263, 295). These regulatory networks allow for nitrogen-responsive changes to gene expression, cell physiology and metabolism.

In cyanobacteria, growth on different fixed nitrogen sources results in many genetic and physiological changes (288, 296-298). When ammonium is freely available and being incorporated into amino acids, most genes for nitrogen uptake and assimilation are expressed at a low basal level (299). An exception is the glutamine synthetase inhibitors IF7 (*gifA*) and IF17 (*gifB*), which are maximally expressed in ammonium (300), allowing for repression of nitrogen assimilation by inhibition of glutamine synthetase activity. A change in nitrogen source to nitrate causes an immediate increase in the expression of nitrogen uptake and assimilation genes, particularly the nitrate/nitrite transporter (*nrt*) and reductases (*narB* and *nirA*) (294, 301). When *Synechocystis* is stressed by depletion of fixed nitrogen, the early response (within 4 h) involves induction of genes for nitrogen uptake and assimilation (288, 302), ensuring the organism is capable of metabolizing nitrogen when it becomes available. In the interim, approximately 50% of the nitrogen storage molecule cyanophycin (multi-arginyl-L-polyaspartate) is consumed within 4 h, and complete depletion occurs by 12 h after nitrogen starvation (303). In addition, expression of genes involved in glycolysis, the pentose phosphate pathway and glycogen metabolism are induced through the activity of the sigma factor SigE, transcription of which is regulated by NtcA (298). This altered pattern of expression results in accumulation of glycogen, polyhydroxybutyrate and organic acids, reduction in nucleic acid abundance, and changes in relative abundance of amino acids during nitrogen starvation (304, 305). Physiologically, decreases in the

cellular N/C ratio, phycocyanin levels, oxygen evolution and growth rate relative to cells grown in nitrate-based medium become observable between 6 and 12 h of nitrogen starvation (302). Once degradation of the phycobiliproteins is complete, after about 2 days, degradation of chlorophyll *a* and carotenoids occurs (306); however, the cells retain the capacity to rapidly resume photosynthetic electron transfer for an extended period (302). Once *Synechocystis* cells are fully chlorotic with minimal photosynthetic activity, they can still resume vegetative growth in response to fixed nitrogen availability for at least 42 days (305). Thus, as fixed nitrogen is crucial for *Synechocystis* growth, genetic systems have evolved allowing rapid and specific responses to depletion of this vital resource. Cells undergo a linear program of stored nitrogen utilization, eventually leading to a quiescent state where they remain viable for extended periods. While the cellular changes in response to nitrogen availability described above are specific to the nitrogen stress response, many also relate to more general abiotic stress responses.

A regulatory gene associated with cellular response to abiotic stress in *Synechocystis* is the RNA helicase encoded by *crhR* (*slr0083*). RNA helicases are associated with regulation of RNA function and thus gene expression in all kingdoms of life through their ATP-dependent alteration of RNA and RNP structure (72, 307). Functionally, RNA helicases perform crucial roles in all aspects of RNA metabolism and are frequently associated with regulation of translation initiation, RNA decay and ribosome biogenesis (75). As the only DEAD-box RNA helicase encoded in the *Synechocystis* genome (41), it is likely that CrhR performs roles in multiple RNA metabolic pathways (73, 308). CrhR catalyzes both RNA duplex unwinding and annealing *in vitro* (153), a combination of functions conserved in only a few DEAD-box RNA helicases, and can thus potentially participate in regulation of RNA function using both activities.

Expression of CrhR was initially shown to be regulated by light-dark cycles through light-driven alteration of the redox poise of the photosynthetic electron transport chain (ETC) (41). Since then, *crhR* expression has been shown to also be regulated by salt stress (161), temperature shift (162, 164) and a range of abiotic stresses independent of temperature stress (163). Temperature regulation is extremely complex, occurring at several checkpoints, some of which are CrhR-dependent and thus auto-regulatory (164).

Down-regulation of CrhR abundance upon removal of the stress occurs through CrhR proteolysis (160). The auto-regulatory nature of *crhR* effects on its own expression was shown by the lack of regulation of transcript and protein half-lives in a partial genomic deletion mutant of *crhR*, $crhR_{TR}$ (104). The $crhR_{TR}$ mutant exhibits a diverse range of morphological and physiological abnormalities including defects in electron transport, abnormal thylakoid membrane and carboxysome structure, reduced oxygen evolution rates, and loss of cell surface texture, particularly at cold temperature (104). These defects are manifested in a severe cold sensitive growth phenotype, believed to primarily stem from a reduction in photosynthetic carbon fixation in the $crhR_{TR}$ strain at 20°C (104).

Here we examine *Synechocystis* growth and physiology in wild type and the $crhR_{TR}$ mutant strain, as well as the regulation of *crhR* expression at the transcript and protein level in response to the type and availability of fixed nitrogen. The results indicate that CrhR RNA helicase has a role in regulation of nitrogen uptake and assimilation, as the $crhR_{TR}$ mutant is sensitive to changes in the type of available fixed nitrogen, and CrhR protein is rapidly degraded during periods of nitrogen starvation. At the genetic level, the changes in *crhR* expression in the absence of fixed nitrogen are NtcA-regulated, with the glutamine synthetase-inhibitor MSX inducing degradation of CrhR in nitrate-based media. This expands the complement of abiotic stress responses mediated by CrhR to also include nitrogen stress.

4.3 Experimental procedures

4.3.1 Bacterial strains and growth conditions

Two strains of *Synechocystis* were used in this chapter, the wild type and $crhR_{TR}$ (Table 4.1), which has a spectinomycin cassette inserted between the *Pml*I site of *crhR* and the *Hpa*I site of *sll0080* (*argC*) resulting in truncation of *crhR*. This mutant expresses the truncated protein $CrhR_{TR}$, lacking the C-terminal extension and a portion of the helicase core (104). Both strains were maintained on BG-11 agar plates with a constant light irradiance of 50 μmol photons m^{-2} s^{-1}. Liquid cultures grown in 50 ml BG-11 medium at 30°C with shaking were used to inoculate 300 ml BG-11 cultures grown at 30°C with

Table 4.1: Bacterial strains, plasmids and oligonucleotides used in this chapter.

The T7 promoter is marked in bold for oligonucleotides.

Strain, plasmid or oligonucleotide	Relevant characteristic(s) or sequence*	Source, reference or application
***Synechocystis* strains**		
Wild type	glucose-tolerant strain	(41)
crhR$_{TR}$	*crhR*::spectinomycin cassette; C-terminal deletion of CrhR	(104)
Plasmids		
pProbeR	pBS with a 93 bp *Hinc*II-*Sac*II internal fragment of the *crhR* ORF	*crhR* (*slr0083*) riboprobe, (164)
Oligonucleotides		
DCsr20f	**TAATACGACTCACTATAGG**GGTGGTGCGATAACGTGG	*slr0082* riboprobe
DCsr20r	CGTTATTTCCGGTTGCC	*slr0082* riboprobe
gifAf	**TAATACGACTCACTATAGG**CTGCGGTCATAGGTTGTGC	*gifA (ssl1911)* riboprobe
gifAr	CTCTCATGATGCGCCACC	*gifA (ssl1911)* riboprobe
glnBf	**TAATACGACTCACTATAGG**CCGAATCCGTACCACCG	*glnB (ssl0707)* riboprobe
glnBr	GAGATTGTCGTCGACGAAGG	*glnB (ssl0707)* riboprobe
rnpBf	**TAATACGACTCACTATAGG**GGGCAGGAAAAAGACCAACC	*rnpB* riboprobe
rnpBr	TAACTGACCACTGAAAAGG	*rnpB* riboprobe
LAB2	GTAACCGGTACCAAAGACATTGTAACAGATTTACCAC	µMACS affinity purification
LAB8	Biotin-ACGGTGGATGTCCATATCCGCTG	µMACS affinity purification

continuous shaking and aeration with humidified air (105, 182). The media for the *crhR*$_{TR}$ mutant was supplemented with 50 μg ml^{-1} spectinomycin (Sigma) and 50 μg ml^{-1} streptomycin (Sigma) (104).

4.3.2 Experimental conditions

Liquid cultures were grown in 300 ml BG-11 until mid-to-late logarithmic phase, measured as an optical density (OD) of 0.4-0.6 at 750 nm. The cultures were then divided into two 150 ml cultures, with one kept at 30°C and the other placed at 20°C for 3 h to induce maximal expression of CrhR (164). Cultures were harvested by centrifugation (5 min, 5,000 ×*g*) at the respective growth temperature and washed with nitrogen-deplete medium (BG-11$_o$). The harvested cells were then suspended in 150 ml growth media supplemented with the indicated nitrogen source and grown with shaking and aeration at their respective temperatures. Transfer of the cells back to the normal nitrate-based growth medium (BG-11) or a second experimental growth medium was performed in the same manner.

Nitrogen-deplete medium (BG-11$_o$), was generated by replacing the 17.6 mM $NaNO_3$ and 6 μg ml^{-1} ferric ammonium citrate with 17.6 mM NaCl and 7 μg ml^{-1} ferric citrate. The other experimental growth media were prepared by adding filter-sterile urea or NH_4Cl to a final concentration of 2 mM in BG-11$_o$.

4.3.3 Protein analysis

Aliquots (15 ml) removed at the indicated times for protein extraction were harvested by centrifugation at the indicated growth temperature (7 min, 7,000 ×*g*) and frozen at -80°C until all related samples could be extracted simultaneously. Soluble protein was extracted by glass bead lysis, as described previously (182). Polypeptides (10 μg) were resolved by 10% SDS-PAGE, semi-dry transferred to Hybond ECL nitrocellulose membrane (0.45 μm, Amersham), probed with the indicated antibody and detected on X-ray film using the Amersham ECL Western Blotting Detection kit. Polyclonal antibodies against *Synechocystis* CrhR (1:5,000) and goat anti-rabbit IgG horseradish peroxidise complex (1:10,000, Sigma) were used.

4.3.4 Growth curves

Cultures grown in the indicated experimental media were sampled daily to measure the OD. Triplicate samples of 1 ml of each culture were removed from the culture, the OD_{750nm} measured in a Novaspec II spectrophotometer (Pharmacia) and plotted in Microsoft Excel. When chlorophyll *a* (Chl *a*) was used as a relative measure of culture growth, the pigment concentration of 1 ml of undiluted culture was determined as described below.

4.3.5 Pigment analysis

Cells were cultured in the indicated experimental media for 3 days for pigment analysis. Chl *a* was extracted by incubating a cell pellet harvested from 1 ml of culture diluted to OD_{750} = 0.5 in ice-cold 100 % methanol at -20°C overnight and concentration determined spectrophotometrically at 665 and 652 nm (309). The remaining cell pellet was washed with 1× PBS and lysed with 10 µg lysozyme overnight in a 37°C water bath (310) to release the phycobiliproteins. The phycocyanin and allophycocyanin concentrations were calculated from spectrophotometric absorption at 615 and 652 nm (311).

Whole-cell absorption spectra were obtained from cells cultured in the indicated growth media for 4 days. Using the wavescan program on an Ultrospec 3000 (Pharmacia), the absorbance of 1 ml of each culture was measured for wavelengths between 400 and 700 nm with an interval change of 1 nm. The absorbances for each culture were converted to % absorbance and normalized to the absorbance at 560 nm. Graphs of the absorption spectra in visible light for cells grown in each of the experimental media were generated in Microsoft Excel.

4.3.6 ROS/RNS analysis

Cells were cultured in the indicated growth media for 3 days at both 30°C and 20°C. A stock of the intracellular fluorescent dye to determine the general reactive oxygen species (ROS) content, 2',7'-dichlorodihydrofluorescein diacetate (H_2DCFDA, Molecular Probes), was prepared to 0.5 mM in DMSO immediately before use. Cultures were diluted to an OD_{750nm} of 0.5, and 1 ml of each culture was harvested by centrifugation. Cell pellets were washed, suspended in 1× PBS, and H_2DCFDA was added to 5 µM. Cell

samples were incubated with the dye for 30 min to allow for dye loading of the cells, harvested, washed and suspended in 1× PBS for an additional incubation of either 4 h (Figure 4.6 A) or overnight (Figure 4.6B). All steps were performed at the indicated growth temperature. A UV-transparent microtiter plate (Corning) was prepared with 200 µl of each treated sample, including controls for each condition prepared with 1× PBS buffer, and fluorescence was read in a SpectraMax M2 plate reader (Molecular Devices), with 10 scans per well, excitation 485 nm, emission 535 nm. Relative fluorescence for each sample was calculated by subtracting the control sample, lacking H_2DCFDA, from the H_2DCFDA-treated sample, then adjusting the scale of values such that the lowest value was set to 1.

4.3.7 Inhibitor treatments

Transcription and translation inhibitors were added to cultures following a 3 h cold induction at 20°C. Transcription was inhibited with rifampicin (400 µg ml-1, Sigma), which was added to the culture immediately following transfer to the nitrogen-depleted medium (BG-11_o). Treatments with chloramphenicol (Sigma, 250 µg ml^{-1}) and kanamycin sulfate (Sigma, 250 µg ml^{-1}) were performed by addition of the translation inhibitor to the culture following cold induction at 20°C for 2 h. The cultures were incubated for an additional 1 h at 20°C to allow inhibitor action. Cells were harvested by centrifugation, washed with BG-11_o and transferred to BG-11_o containing the translation inhibitor for the remainder of the experiment. The inhibitor stock solutions were 25 mg ml^{-1} rifampicin in methanol, 25 mg ml^{-1} chloramphenicol in ethanol and 50 mg ml^{-1} kanamycin sulfate in water.

The glutamine synthetase inhibitor L-methionine sulfoximine (MSX, Sigma) was used to simulate nitrogen starvation effects dependent on NtcA signaling (312), as depicted in Figure 4.1C. CrhR expression was induced by incubation at 20°C for 3 h in cultures growing in BG-11 medium. MSX was added to growth media at concentrations of 2 µM and 400 µM to simulate nitrogen starvation.

4.3.8 RNA analysis

Culture aliquots (50 ml) were combined with an equal volume of phenol stop solution (5% v/v phenol, 95% v/v ethanol) and harvested by centrifugation (10 min, 2,400 ×*g*). Cell pellets were washed with 50:100 TE and suspended in RNA breakage buffer (50:100 TE containing 0.5% v/v Triton X-100, 0.5% w/v Sarkosyl and 0.5% w/v SDS). Glass bead lysis was performed in the presence of 0.8× volume buffered phenol as described previously (182). The lysate was clarified by centrifugation (5 min, 13,000 ×*g*) and sequentially extracted with equal volumes of phenol, phenol:chloroform (1:1) and chloroform:isoamyl alcohol (24:1). The RNA was precipitated from the final aqueous layer by incubation with an equal volume of 4 M LiCl (16 h, -20°C) and subsequent centrifugation (30 min, 13,000 ×*g*, 4°C). RNA pellets were suspended in RNase-free water and stored at -80°C in 2.5× volume 100% v/v ethanol and 0.1× volume sodium acetate (3 M, pH 5.2).

Purified RNA (5 µg) was separated on 1.2% agarose formaldehyde-MOPS gels and transferred to Hybond-XL nylon membrane (Amersham) by diffusion blotting with 5× SSC overnight. The UV-crosslinked membranes were probed in formamide buffer as described previously (105, 149, 182) with ^{32}P-labelled anti-sense riboprobes against *glnB* (*ssl0707*, 126 nt), *gifA* (*ssl1911*, 154 nt), *rimO* (*slr0082*, 202 nt) or *rnpB* (133 nt) prepared by transcription with T7 RNA polymerase from PCR products generated using the indicated oligonucleotides (Table 4.1). The *crhR* (*slr0083*) riboprobe was produced by transcription with T3 RNA polymerase from *Hinc*II-digested pProbeR plasmid, consisting of pBS containing a 93 bp *Hinc*II-*Sac*II internal fragment of the *crhR* ORF (Figure 3.1) (164).

Images were generated by exposure of the radiolabelled blots to either autoradiography film (Amersham Hyperfilm MP) or a Storage Phosphor Screen (Molecular Dynamics) which was imaged in a Phosphorimager 445SI (Molecular Dynamics) at a resolution of 88 µm. Densitometry analysis and image output as .tif format of phosphorimages was completed using GelQuant.NET software provided by biochemlabsolutions.com. *crhR* abundance was normalized to the *rnpB* levels, when available, as described in Rosana *et al.* (164).

4.3.9 DNA affinity column purification and mass spectrometry

Proteins binding to the *rimO* promoter region were isolated by streptavidin DNA affinity column purification as described previously (165). The biotinylated target DNA was amplified by PCR with primers LAB2 and LAB8 (Table 4.1) from *Synechocystis* genomic DNA. Soluble protein was extracted from *Synechocystis* as described above. Soluble protein extract (6.8 mg), biotinylated target DNA (14 µg) and 50 µg poly(dI-dC) were combined in 1× EMSA buffer (10 mM Tris [pH 7.5], 50 mM NaCl, 1 mM EDTA, 5% glycerol, 1 mM DTT) and incubated for 2 h at 4°C with gentle agitation. An additional 15 minutes of incubation followed the addition of 100 µl µMACS Streptavadin Microbeads (Miltenyi Biotec). The mixture was applied to a µMACS column equilibrated with 1× EMSA buffer and held in a magnetic separator. Triplicate washes with increasing KCl concentration (0.1 M, 0.25 M and 1M) were performed. Following washing, the column was removed from the magnetic separator and eluted twice with 1 M KCl.

Eluted proteins were concentrated by TCA precipitation, then separated on a Mini-PROTEAN TGX 4-15% gradient SDS-polyacrylamide gel (Bio-Rad). Proteins were visualized by staining with Colloidal Coomassie (0.08% w/v Coomassie brilliant blue G250, 1.6% v/v orthophosphoric acid, 8% w/v ammonium sulfate, 20% v/v methanol). Mass spectrometry was performed at the Alberta Proteomics and Mass Spectrometry Facility (APM), University of Alberta. The excised lane was cut into 5 sections, destained twice in 100 mM ammonium bicarbonate/acetonitrile (50:50), reduced, and alkylated. Dehydrated samples were subjected to an overnight in-gel trypsin digestion (6 ng μl^{-1}) at room temperature. Peptides were extracted from the gel with 97% v/v water, 2% v/v acetonitrile, 1% v/v formic acid, followed by a second extraction with 48.5% v/v water, 51% v/v acetonitrile, 0.5% v/v formic acid. Fractions were resolved and ionized with nanoflow high-performance liquid chromatography (Easy-nLC II, ThermoScientific) coupled to an LTQ XL-Orbitrap hybrid mass spectrometer (ThermoScientific). A Pico-Frit fused silica capillary column (ProteoPepII; C18) with a 100 µM inner diameter (300 Å, 5 µm pore size) was used for Nanoflow chromatography and electrospray ionization. Results were processed using Proteome Discoverer 1.4 (ThermoScientific) and queried against the Uniprot *Synechocystis* database (SYNY3)

using SEQUEST (ThermoScientific). Search results were limited using a precursor mass tolerance of 10 ppm and a fragment mass tolerance of 0.8 Da.

4.4 Results

4.4.1 Nitrogen source affects growth and pigmentation

The growth rate of wild type *Synechocystis* and the *crhR*$_{TR}$ mutant strains were measured as growth curves using optical density of the culture at 750 nm (Figure 4.2). Typically, S*ynechocystis* is cultured at 30°C in a nitrate-based medium, (e.g. BG-11) which allows for optimal growth of wild type *Synechocystis*. In BG-11, both wild type and the *crhR* mutant strain grew optimally at 30°C. The growth of wild type was slightly reduced at 20°C, while *crhR*$_{TR}$ exhibited a significant cold-sensitive phenotype, consistent with previous observations (104). The two strains also grew optimally at 30°C, as expected, with 2 mM urea as the supplied nitrogen source; however, the cold-sensitive phenotypes of both the wild type and *crhR*$_{TR}$ strains were significantly less pronounced than in nitrate-based medium (Figure 4.2A and B). Culturing in medium with 2 mM ammonium chloride resulted in strong depression of *Synechocystis* growth, irrespective of temperature or *crhR* mutation (Figure 4.2C). Concentrations of ammonium chloride ranging from 1 mM to 5 mM all resulted in depression of *Synechocystis* growth (Figure 4.3). To minimize growth suppression and to ensure that chlorosis was not caused by nitrogen starvation over the timescale used, 2 mM ammonium chloride (hereafter 'ammonium') was used in these experiments. In nitrogen-free medium (BG-11o, Figure 4.2D), both wild type and *crhR*$_{TR}$ grew for a few days then halted, presumably upon depletion of stored nitrogen reserves. Temperature had a minimal effect on growth rate in nitrogen-deplete medium, indicating that nitrogen deprivation has a more immediate effect on growth rate than low temperature stress.

The combination of *crhR* mutation, temperature and nitrogen source also had a profound effect on light harvesting composition. In cyanobacteria, Chlorophyll *a* (Chl *a*) is present in the reaction centre of the photosystems and phycobiliproteins are organised into phycobilisomes, light harvesting antennae that transfer additional energy to Chl *a*. The only phycobiliproteins synthesized by *Synechocystis* are phycocyanin and

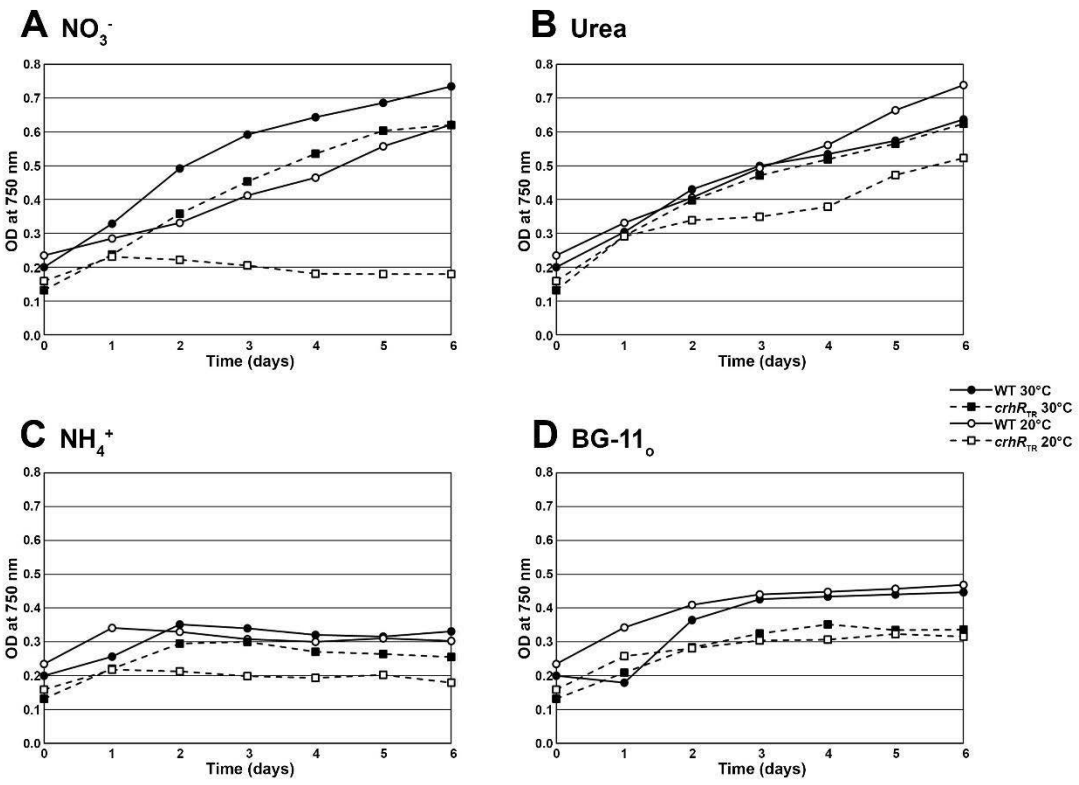

Figure 4.2: Effect of fixed nitrogen on the growth rate of *Synechocystis.*

Wild type (WT) *Synechocystis* and *crhR*$_{TR}$ were cultured at 30°C and 20°C in BG-11$_o$ medium with nitrogen supplied as (A) 17.6 mM sodium nitrate, (B) 2 mM urea, (C) 2 mM ammonium chloride, and (D) with no fixed nitrogen provided. Growth was measured every 24 h as OD at 750 nm. Data shown are averages of triplicate measurements from a representative experiment.

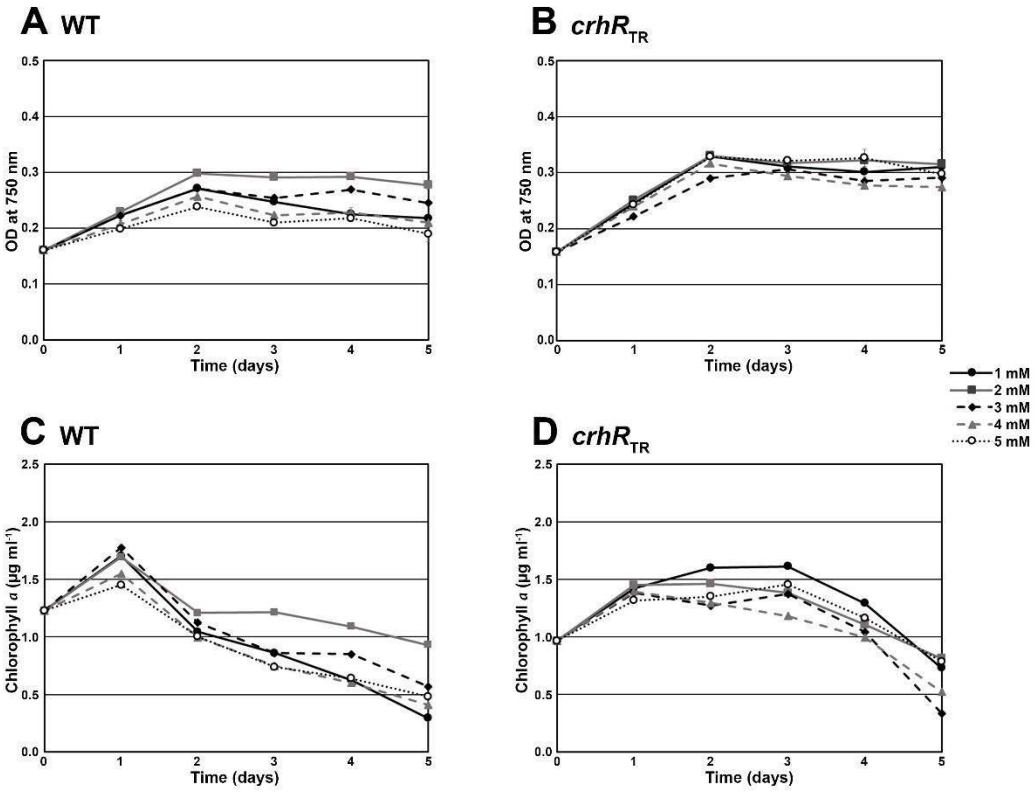

Figure 4.3: Concentration dependence of the effect of ammonium chloride on *Synechocystis* growth.

Cultures of wild type and *crhR*$_{TR}$ *Synechocystis* were prepared in BG-11$_o$ medium with the indicated concentrations of ammonium chloride and incubated at 30°C. (A-B) Growth was measured as OD at 750 nm and (C-D) Chl *a* concentration was used as a measure of culture health. Data shown are averages of triplicate measurements of a representative experiment.

allophycocyanin (313). Temperature and nitrogen source had relatively insignificant effects on Chl *a* levels in wild type cells (Figure 4.4A). The Chl *a* abundance in *crhR*$_{TR}$ mutant cells was normal in nitrate and urea at 30°C, but it was significantly reduced in ammonium and BG-11$_o$. At 20°C, Chl *a* was significantly but equally reduced in all nitrogen growth conditions in the *crhR*$_{TR}$ mutant (Figure 4.4A). The response of phycocyanin was more complicated. In general, the nitrogen sources nitrate, urea and ammonium, as well as temperature, had minimal effects on phycocyanin abundance in wild type cells, although a decrease in phycocyanin was observed in urea-based medium at 20°C (Figure 4.4B). BG-11$_o$ equally reduced wild type phycocyanin levels by ~50% at both growth temperatures in comparison to the other media. In the *crhR*$_{TR}$ mutant, temperature and nitrogen source both affected phycocyanin levels. Decreases were observed in nitrate and urea at 30°C, an effect that was enhanced at 20°C. Ammonium and BG-11$_o$ caused even further reductions in phycocyanin abundance at both temperatures. The relative allophycocyanin abundances (Figure 4.4B) for wild type at both temperatures and *crhR*$_{TR}$ at 30°C largely mirror those observed for phycocyanin; however, at 20°C, the *crhR* mutant did not exhibit the same reduction in allophycocyanin levels as observed for phycocyanin when grown in either urea-based or nitrogen-free media.

These effects on light harvesting abundance were reflected in whole cell absorbance scans of cultures grown in the various fixed nitrogen sources (Figure 4.5A-D). Overall, *crhR*$_{TR}$ cultures at 20°C have less pronounced absorbance peaks for phycocyanin (~630 nm), consistent with the reduced phycocyanin abundance observed with the extracted pigments (Figure 4.4B). Interestingly, lower peaks for Chl *a* (~440 nm) and carotenoids (~590 nm), in addition to phycocyanin, were observed for *crhR*$_{TR}$ in ammonium medium at 30°C. The visible responses to the different nitrogen sources also demonstrate the gross phenotypic changes in pigmentation, as shown in Figure 4.5E. Cultures grown in nitrate and urea maintained the predominantly green, Chl *a*-based colour typical of *Synechocystis* grown under our standard growth conditions, while cultures in BG-11$_o$ became increasingly yellow in appearance with time, consistent with chlorosis in the absence of available fixed nitrogen (314). Growth in ammonium as the sole nitrogen source resulted in a sequential colour change from green, to a pale blue

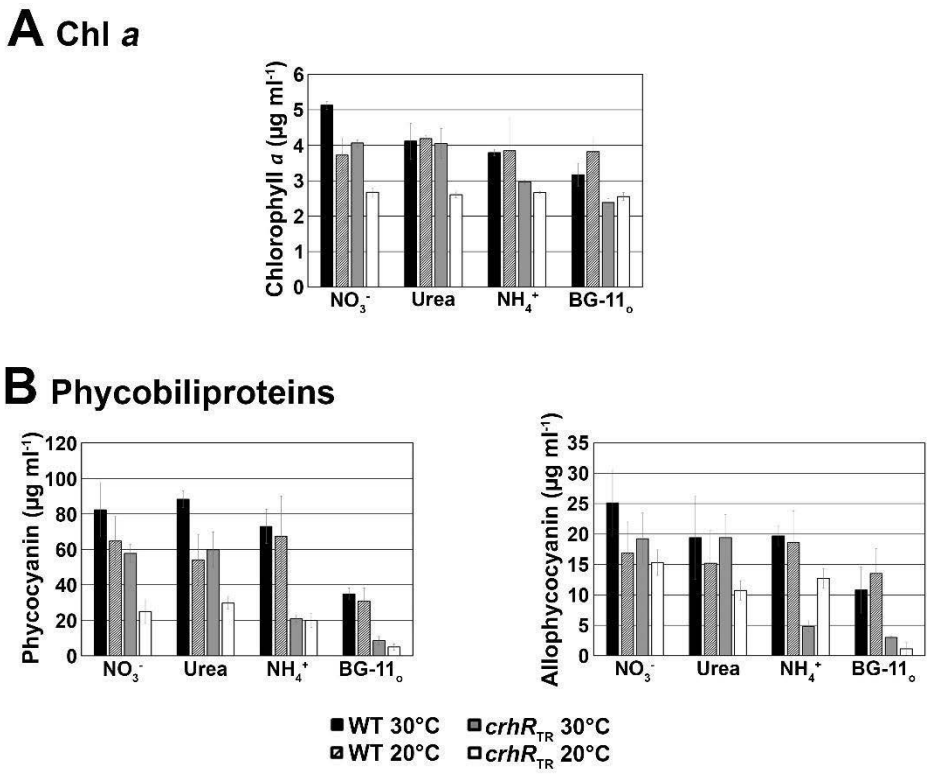

Figure 4.4: Effect of nitrogen source on *Synechocystis* pigmentation.

Wild type *Synechocystis* and *crhR*$_{TR}$ cells were cultured in BG-11$_o$ medium supplemented with 17.6 mM sodium nitrate, 2 mM urea, 2 mM ammonium chloride or no fixed nitrogen at 30°C and 20°C. Samples were harvested after 3 days for analysis. (A) Quantitation of extracted Chl *a* pigment normalized to an OD at 750 nm of 0.5 for each culture. (B) Quantitation of extracted phycobiliproteins from the same culture samples used in (A). Data shown are averages of triplicate measurements of a representative experiment.

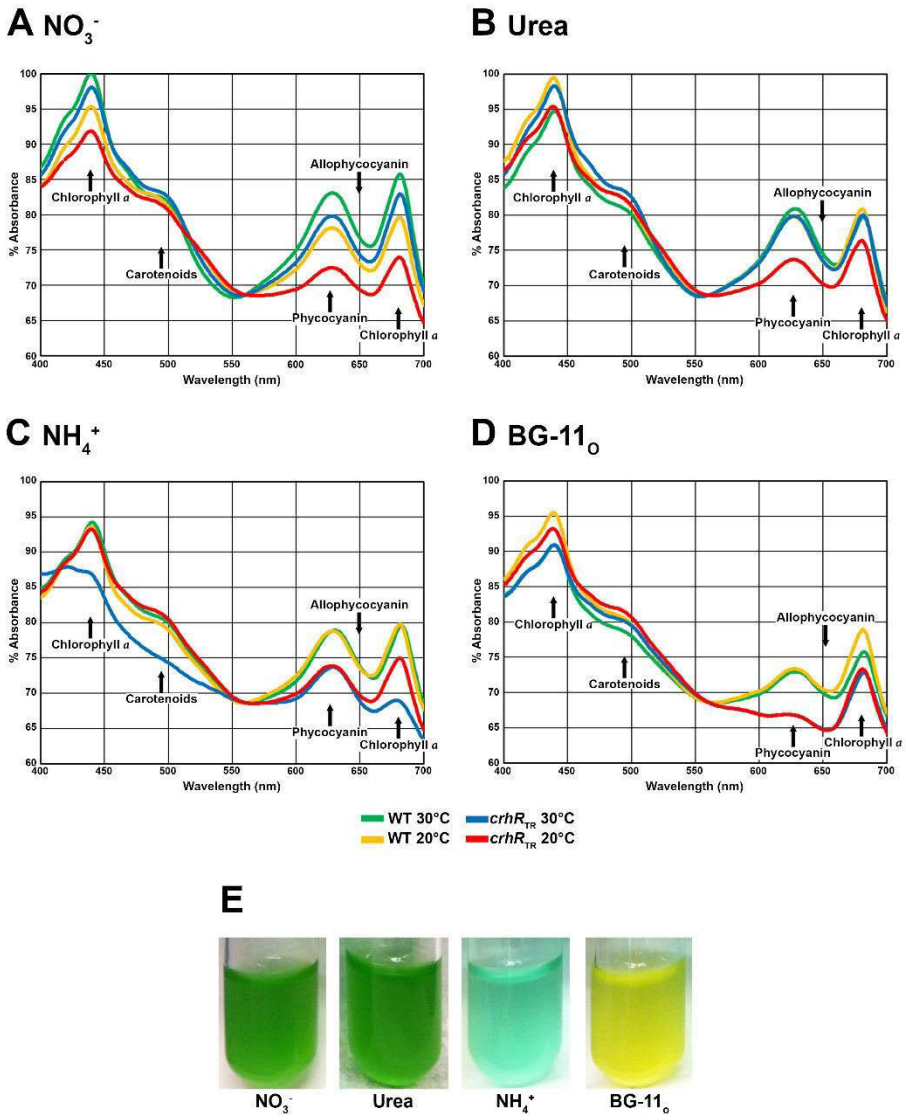

Figure 4.5: Effect of nitrogen source on the whole cell pigmentation of *Synechocystis*. Wild type *Synechocystis* and *crhR*$_{TR}$ cells were cultured in BG-11$_o$ medium supplemented with 17.6 mM sodium nitrate, 2 mM urea, 2 mM ammonium chloride or no fixed nitrogen at 30°C and 20°C. (A-D) Whole cell absorbance spectra normalized to the absorbance at 560 nm. Samples were analyzed after 3 days. The absorbance maximums for each pigment are indicated on the panels. (E) Photographs of wild type *Synechocystis* grown in the indicated nitrogen source at 20°C after 4 days. Data shown are averages of triplicate measurements of a representative experiment.

colour, to a silvery blue over several days, eventually losing all pigmentation (Figure 4.5E), consistent with the reductions in Chl *a* and phycocyanin observed in Figure 4.5C. Ammonium-grown cultures could not be rescued by return to a nitrate-based medium once the visible change in pigmentation occurred, the only condition observed to cause cell death in this study. Overall, ammonium and BG-11_o created the most dramatic effects on the viability and abundance of light harvesting pigments in *Synechocystis* at both 30°C and 20°C, with more pronounced effects in *crhR*$_{TR}$ mutant cells.

4.4.2 Nitrogen source effect on intracellular ROS abundance

To quantify the effect of nitrogen source on intracellular reactive oxygen species (ROS) in *Synechocystis*, the cell-permeable fluorescent ROS indicator, 2',7'-dichlorodihydrofluorescein diacetate (H_2DCFDA) was used. H_2DCFDA has previously been used with success in studies of ROS in other cyanobacteria (163, 315-317), and was used in *Synechocystis* with a variety of small refinements in the treatment conditions. Representative experiments with both short- and long-term incubations are shown.

When treated with H_2DCFDA, wild type and *crhR*$_{TR}$ cultures grown in nitrate-based medium exhibit higher fluorescent levels than cultures grown with urea, ammonium or no fixed nitrogen (Figure 4.6A), reflecting higher levels of ROS during growth in nitrate. When the incubation time after treatment is extended (Figure 4.6B), measured dye fluorescence at 30°C returns to the levels observed in the other media types, while the fluorescence at 20°C remains elevated, irrespective of strain. Interestingly, the fluorescence measured in wild type cultures at 20°C in urea or BG-11_o is higher with extended incubation relative to 30°C (Figure 4.6B). It is important to note that direct comparison between the fluorescence values from the two incubation times cannot be performed as H_2DCFDA is susceptible to photooxidation, and these experiments are performed, by necessity, in the light. Overall, these results indicate that cultures supplied with fresh nitrate, the nitrogen source in the standard growth medium BG-11, are under higher oxidative stress than cultures in the other nitrogen sources immediately after transfer. With extended incubation overnight, temperature becomes the major source of oxidative stress.

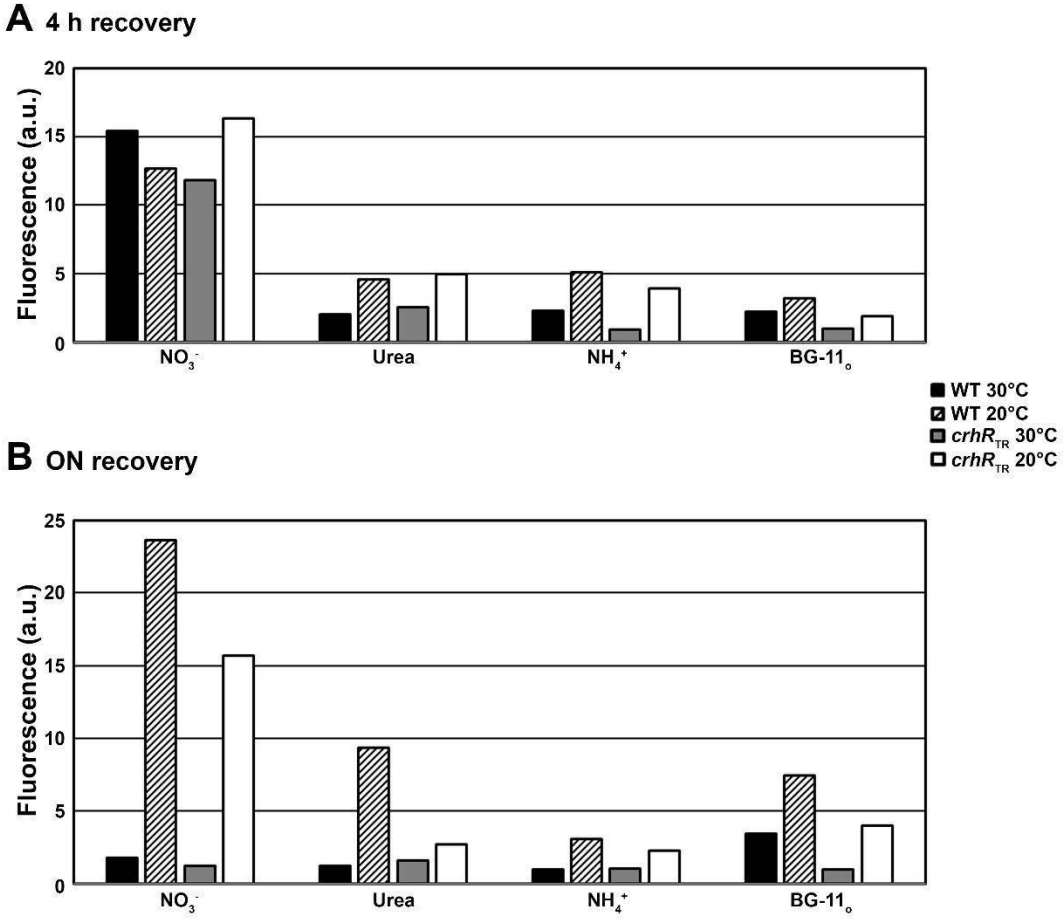

Figure 4.6: Effect of fixed nitrogen source on intracellular reactive oxygen species. Wild type *Synechocystis* and *crhR*$_{TR}$ were cultured in the indicated nitrogen media for 3 days. A sample of culture at an OD of 0.5 at 750 nm was treated with 5 µM H_2DCFDA in 1× PBS for 30 min. After treatment, cells were washed and suspended in 1× PBS, then incubated at the growth temperature for either 4 h (A) or overnight (B) in 1× PBS. Fluorescence was measured using an excitation wavelength of 485 nm and an emission wavelength of 535 nm.

4.4.3 Nitrogen source effect on CrhR abundance

The dramatic effects of *crhR* mutation and alteration of fixed nitrogen source on growth and light harvesting capability led to further investigation of the effects of changing the available nitrogen source on CrhR abundance. Overall, the most dramatic effects were observed when the cells were grown under conditions during which fixed nitrogen was being depleted or absent. Representative results of experiments are shown in Figures 4.7 through 4.11 and discussed below.

At 30°C, transfer from nitrate to ammonium or urea caused a gradual reduction in wild type CrhR levels that then recovered in response to transfer back to nitrate (Figure 4.7A and B). The changes were more pronounced in urea, with CrhR abundance decreasing more rapidly than observed in ammonium with a corresponding extended CrhR recovery time (Figure 4.7B), potentially associated with the rapid growth rate observed in urea (Figure 4.2B). A similar trend was observed at 20°C with ammonium; however, the rate of decrease in CrhR abundance was reduced at the lower temperature, presumably due to the induction of CrhR at low temperature (164). The change from nitrate to urea for wild type cells at 20°C resulted in an initial increase in CrhR levels, followed by a reduction to the initial cold-induced CrhR levels at 20°C by 24 h (Figure 4.7B). This increase in CrhR abundance appears to be enhanced compared to the maximum level of CrhR accumulation previously described in response to cold temperature (164). Further investigation of urea induction over a longer time course at 20°C indicated that CrhR abundance decreased back to the initial cold-induced levels within 10 h (Figure 4.7C). Transfer back to nitrate resulted in a similar pattern, with an initial increase in CrhR levels, followed by a reduction back to the initial cold-induced levels (Figure 4.7B).

The decrease in wild type CrhR levels in response to changes in nitrogen source at 30°C were not observed in *crhR*$_{TR}$ mutant cells, as transfer from nitrate to ammonium or urea and back to nitrate resulted in relatively mild changes in CrhR$_{TR}$ levels (Figure 4.8). The effects of changing nitrogen sources were more strongly observed at 20°C, where the shifts from nitrate to ammonium caused a gradual increase in CrhR$_{TR}$ abundance, which levelled off on return to nitrate-based medium (Figure 4.8A). Transfer from nitrate to urea resulted in a continuous increase in CrhR$_{TR}$ levels, a trend that continued in response

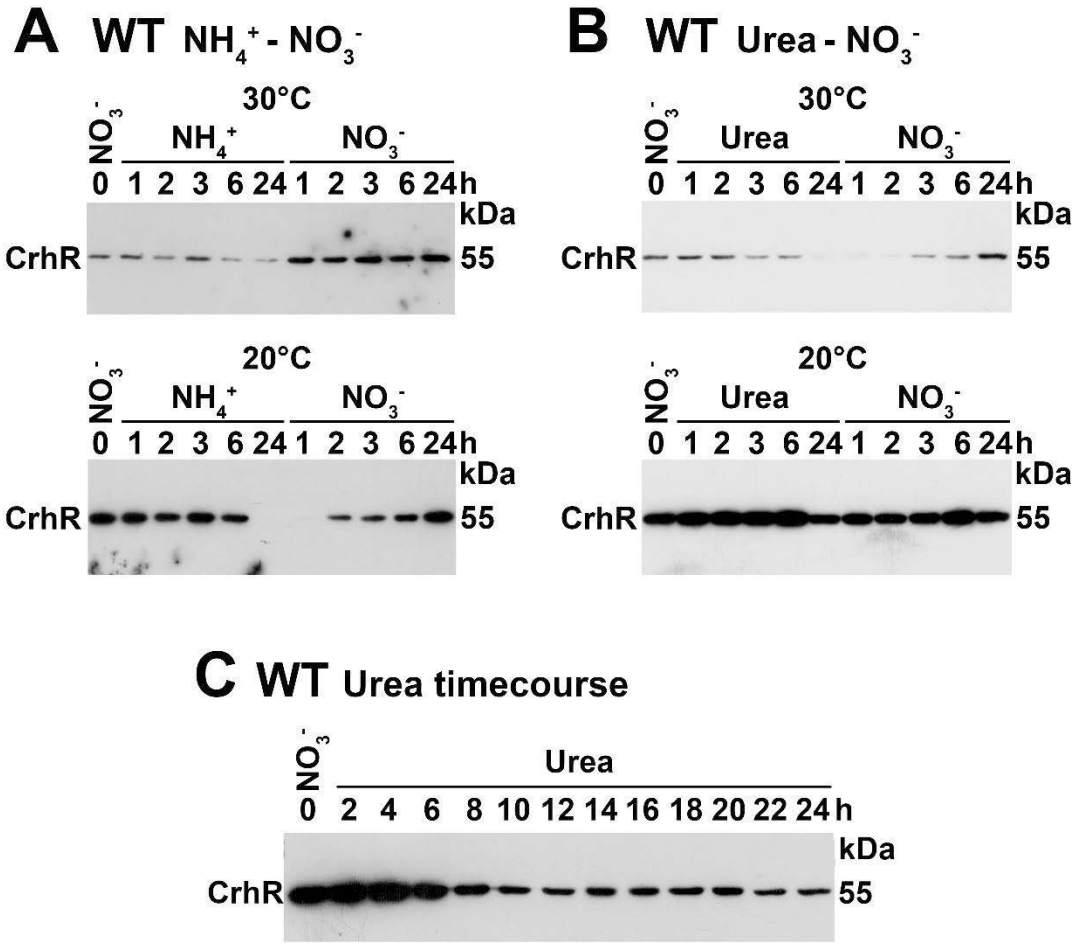

Figure 4.7: Changes in exogenous fixed nitrogen source affect CrhR expression. Cultures of wild type *Synechocystis* were cultured in nitrate medium to mid-log phase. (A-B) After a 3 h temperature induction for the 20°C treatments, cells were harvested by centrifugation and suspended in media containing either (A) 2 mM ammonium or (B) 2 mM urea for 24 h. The return to nitrate medium was performed using the same protocol. Cultures were incubated and harvested at the indicated temperature for the duration of the experiment. (C) After a 3 h temperature induction of CrhR levels at 20°C, cells were harvested and suspended in medium with 2 mM urea for 24 h at 20°C. Samples were collected every 2 h. CrhR protein was detected on Western blots containing 10 µg protein per lane with anti-CrhR antisera and ECL detection.

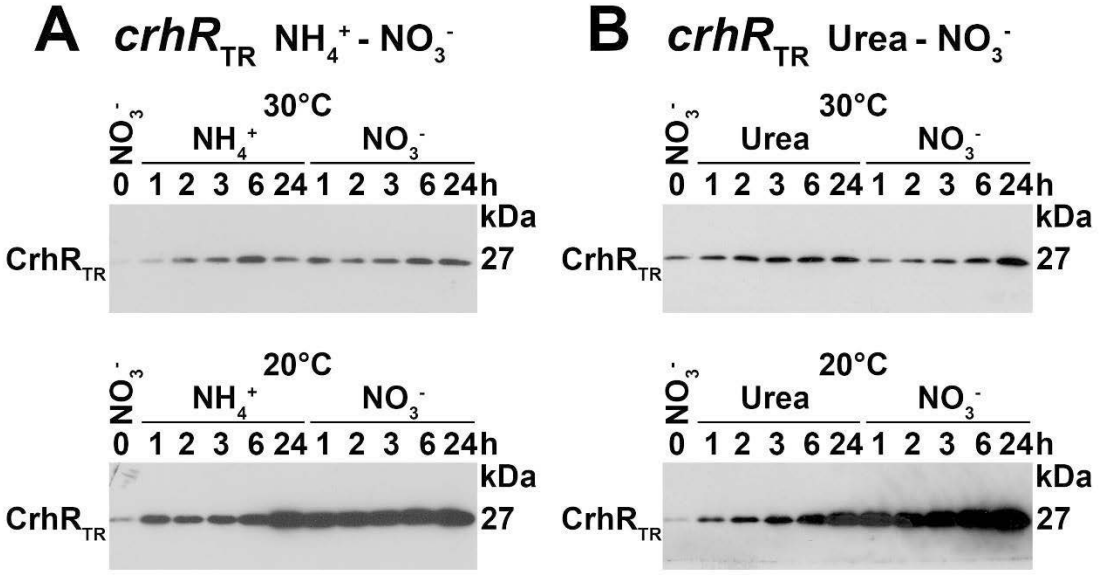

Figure 4.8: Changes in exogenous fixed nitrogen source affect CrhR$_{TR}$ expression. Cultures of *crhR*$_{TR}$ were grown in nitrate medium to mid-log phase. After a 3 h temperature induction for the 20°C treatment, cells were harvested by centrifugation and suspended in media containing either (A) 2 mM ammonium or (B) 2 mM urea for 24 h. The return to nitrate medium was performed using the same protocol. Cultures were incubated and harvested at the indicated temperature for the duration of the experiment. CrhR protein was detected on Western blots containing 10 µg protein per lane with anti-CrhR antisera and ECL detection.

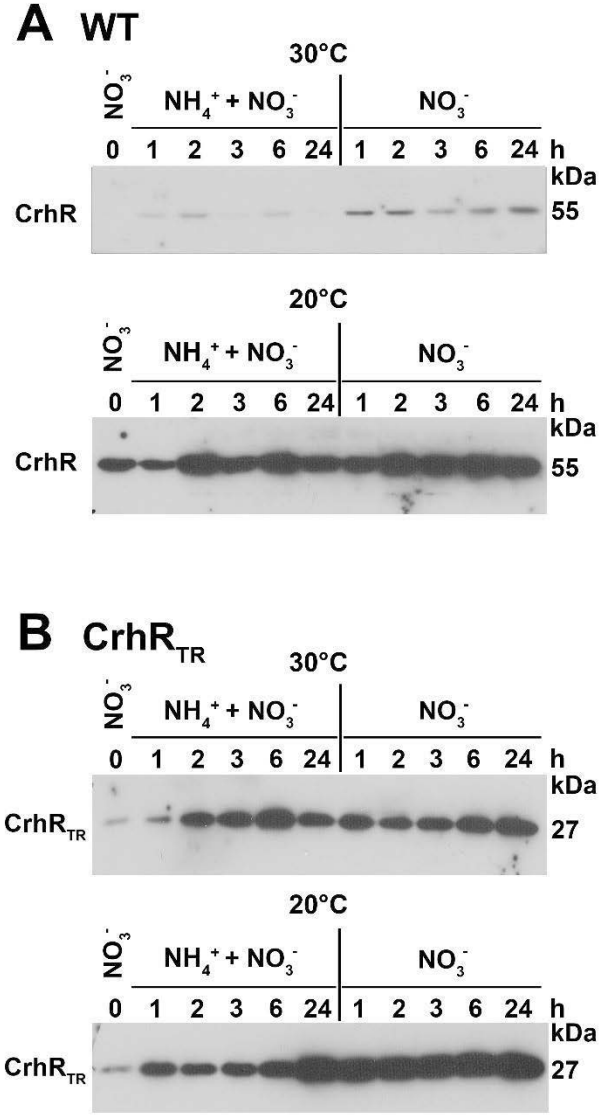

Figure 4.9: Effect of mixing nitrogen sources on CrhR abundance.

Cultures were grown in nitrate media at 30°C to mid-log phase. After an initial 3 h cold induction at 20°C for the low temperature cultures, cultures were harvested and suspended in medium with a combination of 17.6 mM sodium nitrate and 2 mM ammonium chloride for 24 h. The return to nitrate medium was performed using the same protocol. Cultures were incubated and samples were harvested at the incubated temperatures for the duration of the experiment. CrhR protein was detected by Western blotting with anti-CrhR antisera and ECL detection.

to transfer back to nitrate (Figure 4.8B). These results indicate that CrhR abundance is regulated in response to changes in the source of available fixed nitrogen in *Synechocystis*. In addition, based on the defects in CrhR regulation observed in the *crhR*$_{TR}$ mutant, nitrogen regulation of CrhR abundance likely involves an auto-regulatory mechanism, similar to temperature regulation of CrhR (164).

Ammonium-nitrate mixing experiments were performed to extend the nitrogen source analysis with the aim of investigating if one fixed nitrogen source was dominant in regulating CrhR abundance (Figure 4.9). Ammonium is known to be inhibitory to nitrate reduction in cyanobacteria, even at low concentration (277). The changes in CrhR abundance in wild type cells differed from those observed when treated solely with either nitrate or ammonium, with CrhR levels repeatedly increasing and decreasing over the 24 h experiment at both growth temperatures (Figure 4.9A). On return to nitrate, CrhR levels increased immediately, then stabilized at the steady-state temperature-dependent abundance previously determined for CrhR (164). In the *crhR*$_{TR}$ cultures, the response to mixed nitrate and ammonium was very similar to the changes in CrhR$_{TR}$ abundance in media with ammonium as the sole nitrogen source (Figure 4.9B). These results show that culturing in both nitrate and ammonium has an intermediate effect on CrhR abundance in wild type cells, while abundance of CrhR$_{TR}$ resembles that when cultured solely in ammonium.

4.4.4 CrhR abundance in response to nitrogen depletion

In contrast to the results obtained by transfer from nitrate to ammonium or urea shown in Figure 4.7, transfer of wild type *Synechocystis* from nitrate to BG-11$_o$ caused a dramatic and rapid decrease in CrhR abundance, an effect that was temperature independent (Figure 4.10A and B). CrhR levels were restored with transfer to media containing either nitrate or urea. Completely divergent from the results observed in wild type cells, transfer from nitrate to BG-11$_o$, did not affect CrhR$_{TR}$ levels which remained relatively constant at both 30 and 20°C (Figure 4.10C and D). Subsequent transfer back to nitrate did not affect CrhR$_{TR}$ abundance; however, it did increase marginally in response to transfer from BG-11$_o$ to urea (Figure 4.10D). The results suggest that the cellular response to nitrogen source and abundance is dramatically altered in the absence of functional CrhR activity,

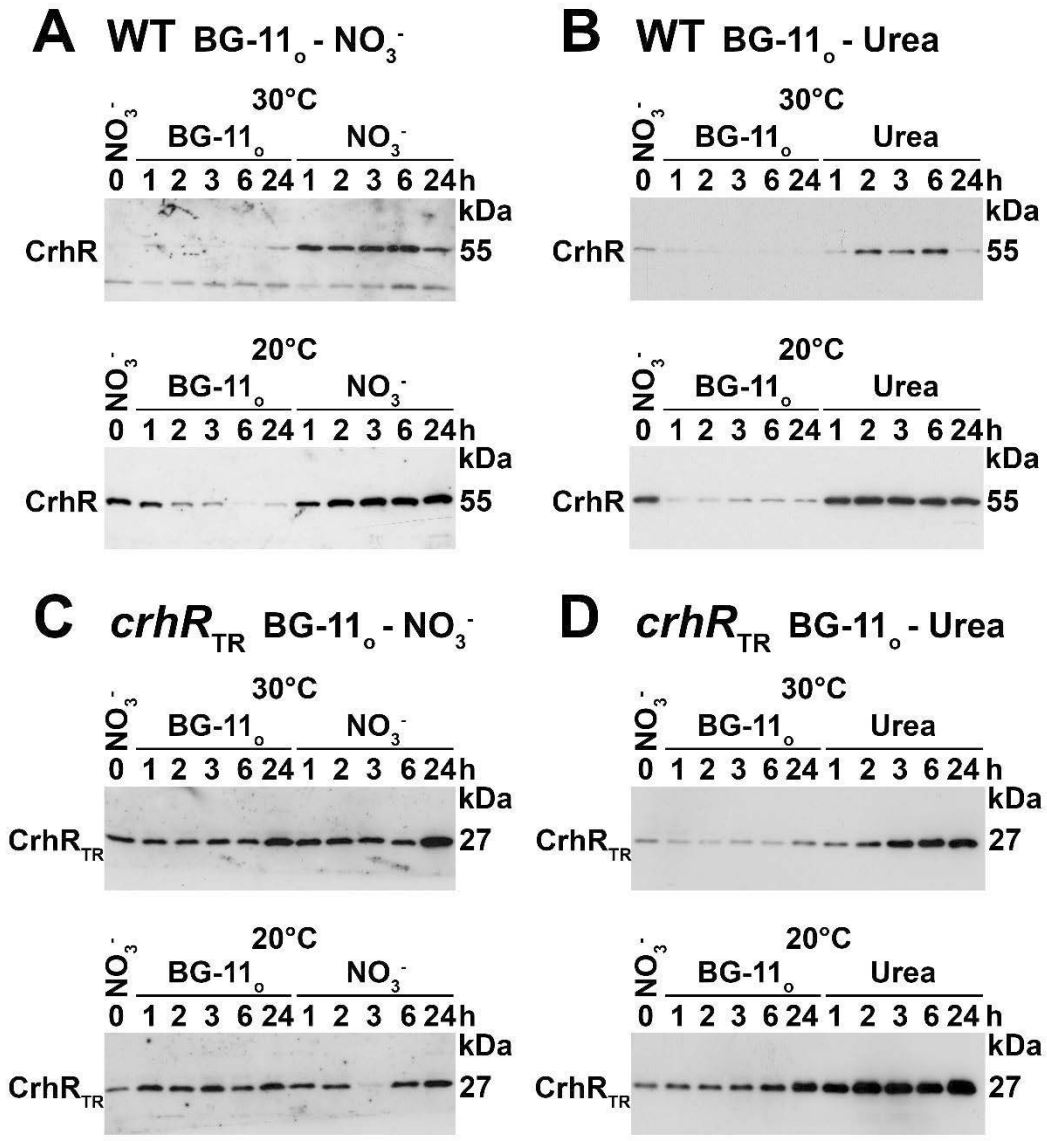

Figure 4.10: Nitrogen depletion induces nitrogen-dependent conditional proteolysis of CrhR.

Cultures of wild type *Synechocystis* and *crhR*$_{TR}$ were cultured in nitrate medium to mid-log phase. After a 3 h temperature induction of CrhR levels for the 20°C cultures, cells were harvested by centrifugation and suspended in the nitrogen-depleted medium (BG-11$_o$) for 24 h. The return to nitrate or urea media was performed using the same protocol. Cultures were maintained at the indicated temperature for the duration of the experiment. CrhR protein was detected on Western blots containing 10 µg of protein per lane with anti-CrhR antisera and ECL detection.

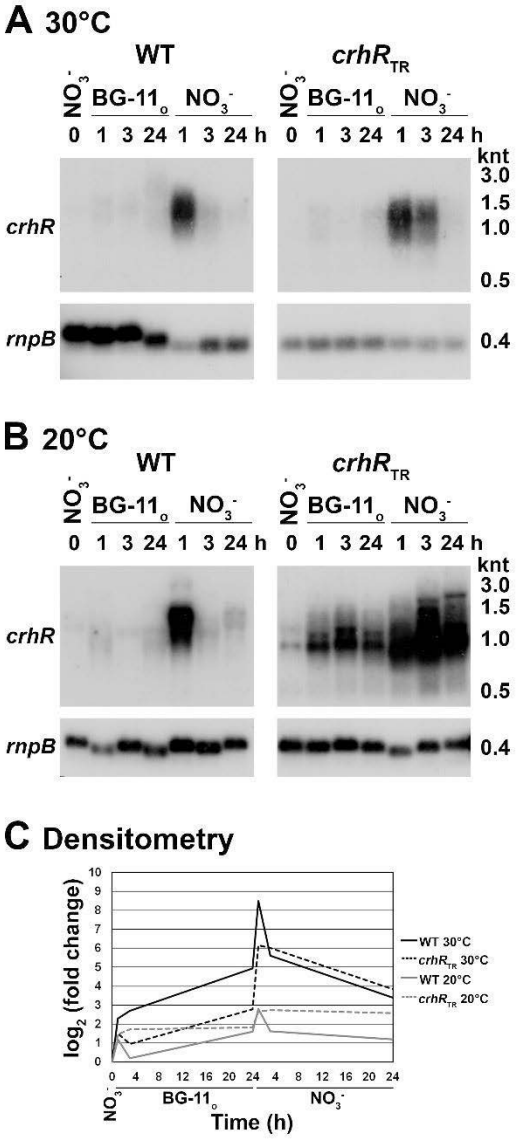

Figure 4.11: Northern blots of *crhR* abundance during nitrogen depletion.

Wild type and *crhR*$_{TR}$ were cultured to mid-log phase at 30°C in nitrate medium. After a 1 h incubation at the indicated temperatures, cells were harvested by centrifugation and suspended in BG-11$_o$ medium for 24 h. The return to nitrate medium was performed using the same protocol. Cultures were maintained at the indicated temperature for the duration of the experiment. Aliquots (5 µg) of total RNA were subjected to Northern blotting with ^{32}P-labelled antisense riboprobes against the *crhR* and *rnpB* transcripts and visualized by exposure to X-ray film. Signal intensities were determined using Gelquant.NET software and graphs of the relative fold change of *crhR* abundance were prepared after normalizing for RNA loading using *rnpB*.

an effect that is relatively temperature-independent. Again, this may indicate an auto-regulatory effect in the regulation of CrhR abundance in response to fixed nitrogen. Alternatively, the truncation of the $CrhR_{TR}$ protein may have removed a motif required for recognition by an adaptor or chaperone, inhibiting targeting of CrhR for proteolysis. Northern blotting was performed to determine if the BG-11_o-induced decrease in CrhR protein involved alteration of *crhR* transcript abundance or translation efficiency. As shown in Figure 4.11, *crhR* transcript abundance increased in BG-11_o at both 30°C and 20°C, in sharp contrast to the protein results. On return to nitrate-based media, a significant and rapid increase in *crhR* abundance was observed, consistent with the increase in CrhR protein. In wild type cultures, the transcript levels return to approximately basal levels within 3 h. In contrast, the decrease in $crhR_{TR}$ transcript abundance is delayed (30°C) or absent (20°C). From these results, it can be concluded that the changes in CrhR protein abundance in BG-11_o are not directly correlated with *crhR* transcript abundance. In addition, these results indicate that *crhR* transcript levels are transiently enhanced when fixed nitrogen becomes available following a period of nitrogen depletion, and that $crhR_{TR}$ cells are deficient in their ability to return *crhR* transcript abundance to the levels observed prior to nitrate treatment.

4.4.5 Nitrogen regulation: Requirement for *de novo* synthesis

Antibiotics were used to inhibit transcription and translation to determine if *de novo* RNA or protein synthesis was required for induction of CrhR depletion in response to transfer from nitrate to BG-11_o (Figure 4.12). The presence of translation inhibitors differentially affected the expected BG-11_o-induced degradation. As shown in Figure 4.12A and B, CrhR degradation did occur in the presence of kanamycin, although at a slower rate in comparison to Figure 4.10A, while chloramphenicol completely inhibited CrhR degradation. CrhR abundance also decreased in the presence of the transcription inhibitor rifampicin (Figure 4.12C), suggesting that *de novo* synthesis of RNAs coding for proteolytic proteins and/or chaperones is not required for the BG-11_o induction of CrhR degradation. The results indicate that a specific aspect of *de novo* protein synthesis, but not RNA synthesis, is required for BG-11_o-induced CrhR degradation. Specifically, the differential effect of the inhibitors on either translation initiation or elongation indicates

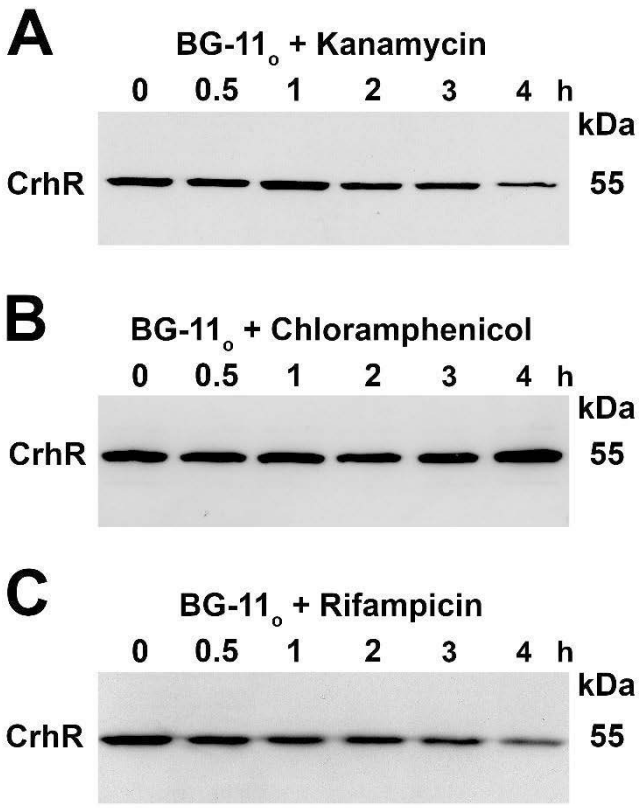

Figure 4.12: Nitrogen depletion-dependent CrhR proteolysis requires *de novo* protein synthesis.

Wild type *Synechocystis* were grown in nitrate-based medium at 30°C to mid-log phase. Expression of CrhR protein was induced at 20°C for 2 h, kanamycin or chloramphenicol were added and incubation continued for a further 1 h at 20°C. Cells were harvested and suspended in BG-11$_o$ medium containing (A) 250 µg ml^{-1} kanamycin, (B) 250 µg ml^{-1} chloramphenicol, or (C) 400 µg ml^{-1} rifampicin and samples were harvested at the indicated times.

that translation elongation is required for induction of CrhR degradation in response to nitrogen depletion. These results are consistent with the antibiotic inhibition of temperature-dependent proteolysis of CrhR previously reported (160), so it is surmised that the same mechanism for CrhR proteolysis is used in response to both temperature upshift and nitrogen depletion.

4.4.6 MSX inhibition of nitrogen assimilation affects CrhR expression

In order to investigate the signalling pathway for nitrogen-depleted degradation of CrhR, the glutamine synthetase inhibitor L-methionine-sulfoximine (MSX) was utilized to simulate nitrogen depletion in the presence of fixed nitrogen (318). MSX would therefore be expected to activate the global nitrogen transcription factor, NtcA, allowing analysis of the role of NtcA signalling in the pathways required for CrhR regulation. The nitrate and nitrite reductases of *Synechocystis* share reducing power with photosynthesis through ferredoxin (319), so MSX treatments were performed in the presence of nitrate to uncouple nitrogen metabolic signaling from redox signalling (312). The initial experiments were performed with 2 μM MSX, as Klotz *et al*. (312) had determined this was the optimal MSX dosage for another cyanobacterium, *Synechococcus elongatus*. Contrary to the findings in *S. elongatus*, bleaching was not observed in response to treatment with 2 μM MSX in *Synechocystis*, regardless of the supplied nitrogen source (Figure 4.13A-D). Bleaching was also not observed for concentrations of MSX ranging from 10 μM to 400 μM (Figure 4.13E), leading to the conclusion that induction of the NtcA regulon by MSX was not sufficient to induce bleaching in *Synechocystis*.

As bleaching could not be used as an indicator of successful inhibition of glutamine synthetase by MSX treatment, Northern blotting was performed to determine the effect on two canonical NtcA-regulated genes, *glnB* and *gifA*, encoding the P_{II} protein and the glutamine synthetase inactivating factor IF7, respectively. A previous study by Giner-Lamia, *et al*. (288) confirmed that *glnB* and *gifA* were regulated by NtcA in *Synechocystis*, reporting a significant upregulation of *glnB* and downregulation of *gifA* during nitrogen starvation. As expected, in nitrate-based medium, *glnB* abundance did not change significantly, while *gifA* transcript levels increased by 3.9-fold (Figure 4.14A). In cultures that were transferred to BG-11_o, pronounced changes in the abundance of *gifA*

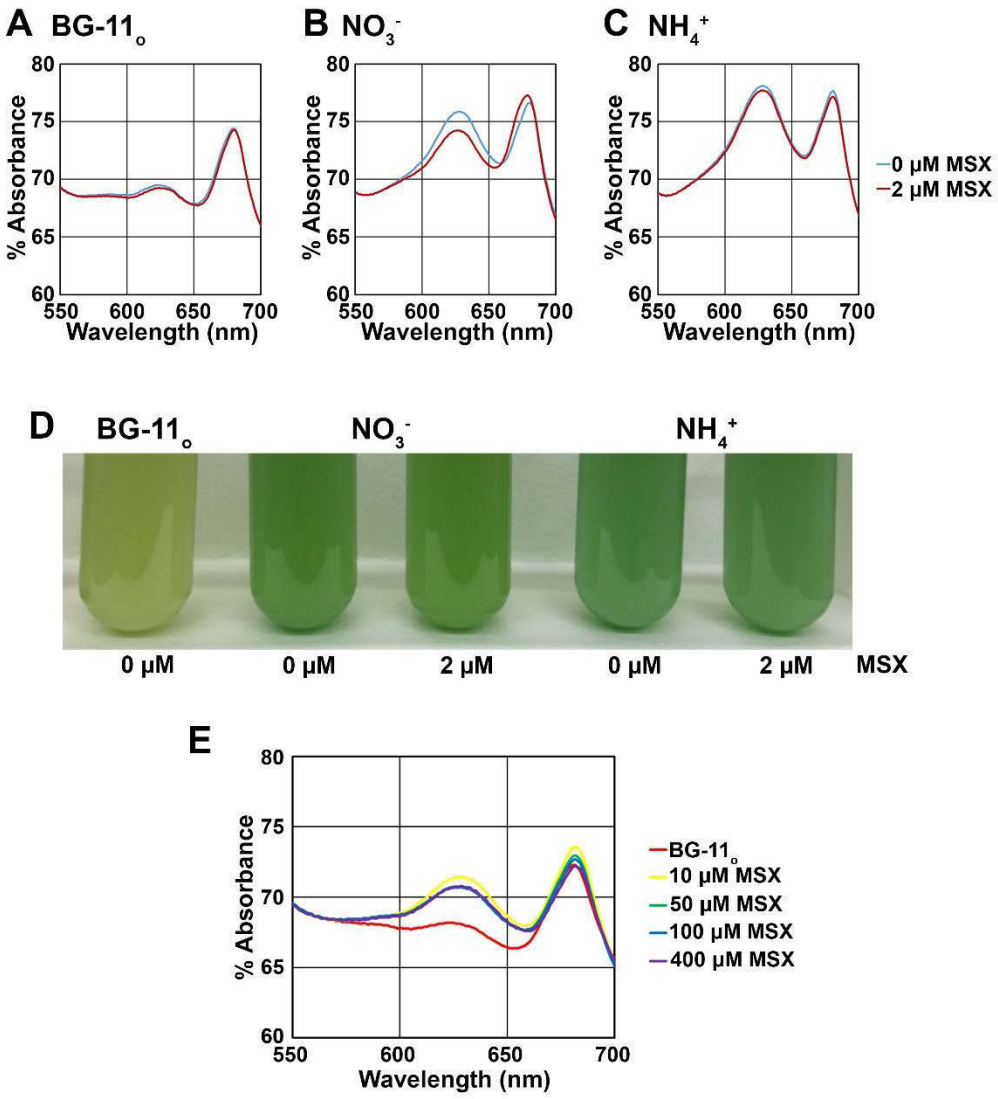

Figure 4.13: MSX treatment is not sufficient to induce chlorosis in *Synechocystis.* Whole cell absorbance spectra between 550 nm and 700 nm of *Synechocystis* with and without 2 µM MSX treatment in BG-11$_o$ (A), nitrate (B) and ammonium (C) media after 3 days. (D) Photographs of *Synechocystis* with 2 µM MSX treatment. (E) Whole cell absorbance spectra between 550 nm and 700 nm of *Synechocystis* grown in ammonium media with MSX concentrations ranging from 0 µM (BG-11$_o$) to 400 µM.

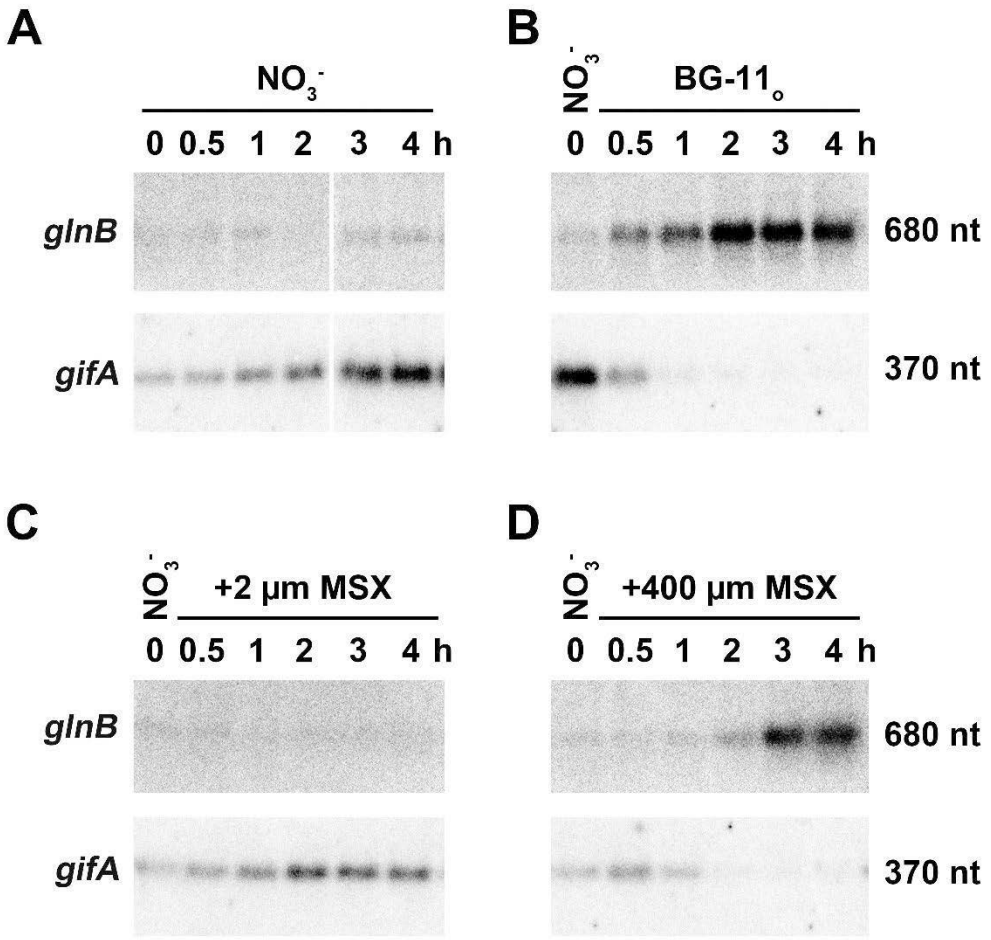

Figure 4.14: Response of canonical NtcA-regulated mRNAs *glnB* and *gifA* to MSX treatment.

Wild type *Synechocystis* was cultured to mid-log phase in nitrate-based (BG-11) media. Cells were untreated (A), harvested and suspended in BG-11_o (B), or subjected to MSX treatment at 2 µM (C) or 400 µM (D). Samples were collected at 20°C from cultures at the indicated timepoints for Northern analysis. Blots with 5 µg of total RNA per lane were probed with ^{32}P-labelled anti-sense riboprobes against RNAs encoding P_{II} (*glnB*) or IF7 (*gifA*), as indicated. Images were generated using a Phosphorimager 445SI.

and *glnB* transcripts were observed (Figure 4.14B). *glnB* transcript levels in nitrogen-depleted medium had a maximum 10.9-fold increase after 2 h, and after 4 h had decreased to only 7.9-fold above the 0 h levels (Figure 4.14B). The abundance of *gifA* decreased by 71.0-fold over 4 h in BG-11_o. These results were consistent with the observations of Giner-Lamia, *et al.* (288). Similar to the culture in nitrate, *glnB* transcript levels did not change in response to treatment with 2 μM MSX, and *gifA* increased (Figure 4.14C). The trends in *glnB* and *gifA* transcript levels for the culture treated with 400 μM MSX were more similar to BG-11_o, but with a slower rate of response, with a 10.7-fold increase in *glnB* and 4.4-fold decrease in *gifA* abundance after 4 h (Figure 4.14D). The results indicated that 400 μM MSX was sufficient to activate transcriptional regulation by NtcA in *Synechocystis* in response to perceived nitrogen starvation, albeit with slower kinetics. Thus, MSX treatment at 400 μM was utilized to further analyze the effects of NtcA-based regulation on *crhR* expression.

CrhR abundance in response to treatment with 400 μM MSX in nitrate-based medium was analysed by western blotting (Figure 4.15). After a 3 h incubation at 20°C to achieve maximal CrhR levels, the expected degradation of CrhR in response to nitrogen depletion in BG-11_o was observed in cells that were not treated with MSX (Figure 4.15A). Addition of MSX to 2 μM or 400 μM produced divergent results with respect to CrhR proteolysis at 20°C. MSX at low (2 μM) and high (400 μM) concentration either did not, or did, induce CrhR proteolysis, respectively (Figure 4.15B and C).

Unlike the rapid proteolysis of CrhR in cultures in nitrogen-depleted medium, CrhR levels decreased gradually with the 400 μM MSX treatment (Figure 4.15C). As expected, based on the lack of change in abundance of canonical NtcA-regulated genes in Figure 4.13, treatment with 2 μM MSX did not alter CrhR abundance (Figure 4.15B). As nitrate was supplied in the medium during MSX treatment, changes in redox electron flux between photosynthesis and nitrate reduction is likely not the trigger for CrhR proteolysis. Thus, the MSX results suggest that signalling downstream of glutamine synthetase (GS), most likely involving NtcA, is required for nitrogen depletion-dependent CrhR proteolysis.

It was also of interest to determine if MSX treatment was capable of affecting transcript abundance of *rimO* and *crhR*. Northern analysis indicated that the changes in

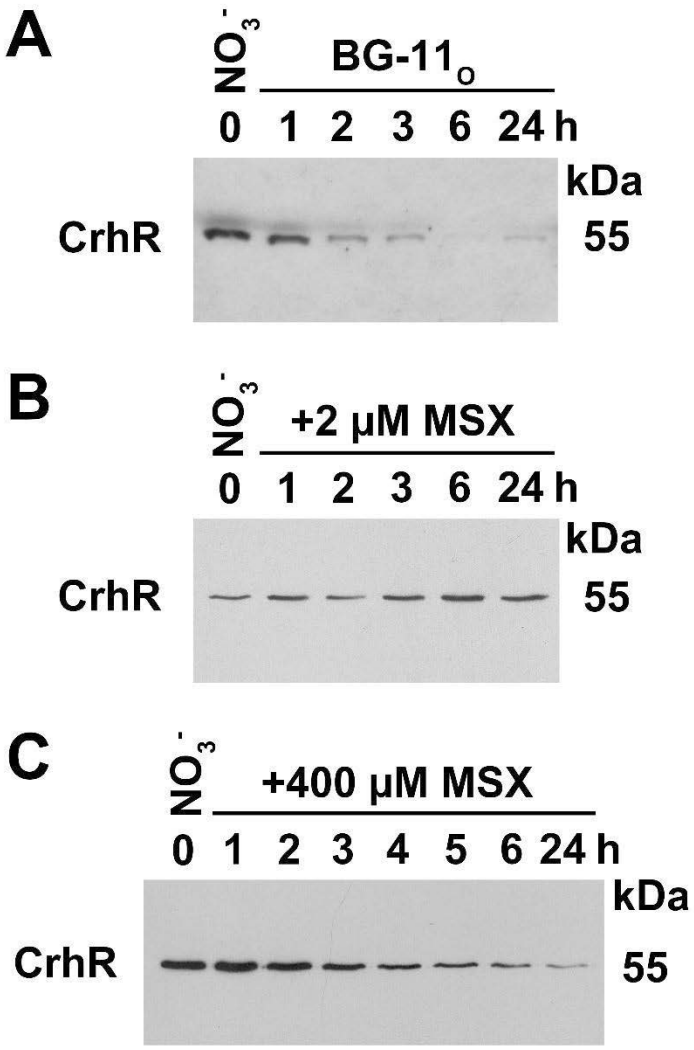

Figure 4.15: CrhR proteolysis can be induced with an inhibitor of glutamine synthetase, MSX.

Wild type *Synechocystis* was cultured to mid-log phase in nitrate-based (BG-11) medium. After a 3 h cold temperature induction of CrhR levels at 20°C, cultures were harvested and suspended in BG-11$_o$ (A) or treated with MSX at 2 µM (B) or 400 µM (C). Protein samples were collected at 20°C at the indicated timepoints and were analysed by Western blotting with anti-CrhR antisera and ECL detection.

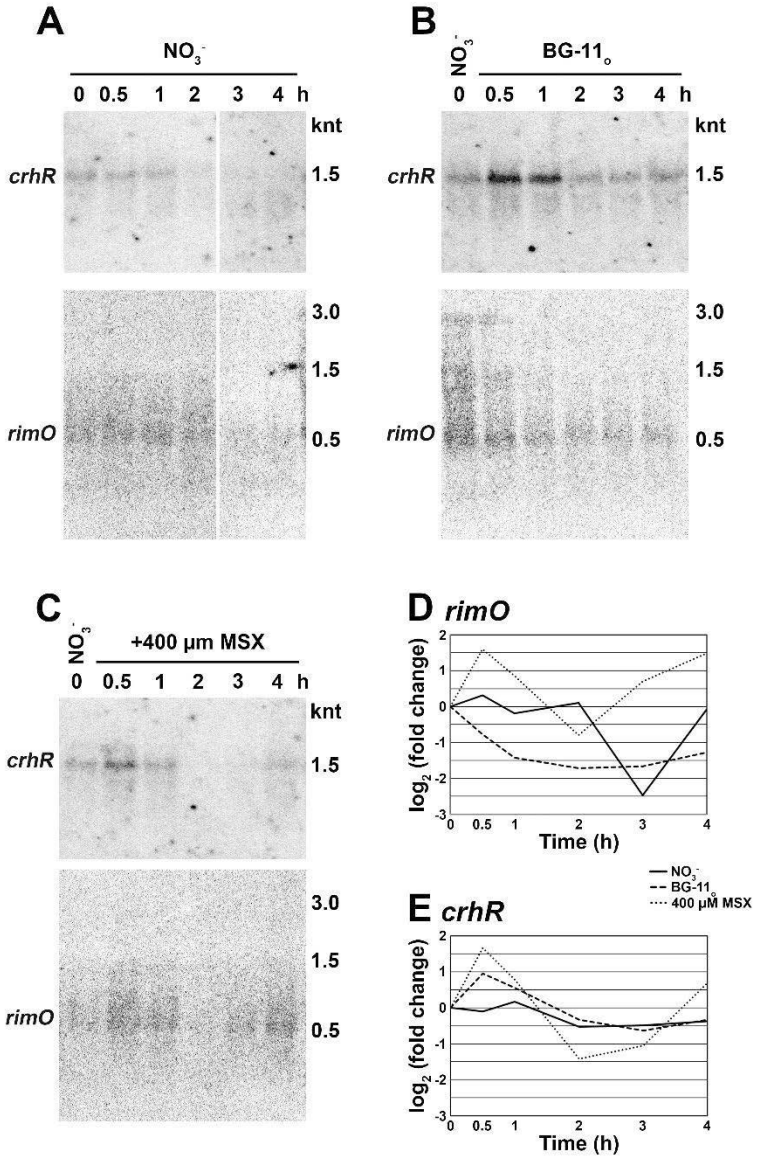

Figure 4.16: Northern analysis of the *rimO-crhR* operon in the presence of MSX. Wild type *Synechocystis* was cultured to mid-log phase in nitrate-based (BG-11) media. Cells were untreated (A), harvested and resuspended in BG-11$_o$ (B), or incubated in the presence of 400 µM MSX (C). Samples were harvested at 20°C at the indicated timepoints for Northern analysis. Blots with 5 µg of total RNA per lane were probed with ^{32}P-labelled anti-sense riboprobes against the transcripts *slr0082* (*rimO*) and *crhR*. Images were generated using a Phosphorimager 445SI. Densitometry graphs of the northern blots for *rimO* (D) and *crhR* (E) are also presented with quantitation for NO_3^-, BG-11$_o$, and 400 µM MSX.

rimO transcript abundance in response to BG-11_o or treatment with 400 µM MSX differed (Figure 4.16A-D). Since abundance of the *rimO* transcript increased in response to MSX treatment (Figure 4.16C), and thus the NtcA-based signalling cascade, it is likely that NtcA binding to the *rimO* promoter enhances transcription initiation for the *rimO-crhR* operon. BG-11_o treatment resulted in a decreased abundance of the *rimO* transcript (Figure 4.16B), indicating that while NtcA regulates the *rimO-crhR* operon, other factors also affect the abundance of *rimO* transcripts in response to changes in fixed nitrogen availability. Trends in the abundance of the *crhR* transcript were more consistent between the treatments (Figure 4.16A-C,E). Notably, the increase in *crhR* abundance in BG-11_o (Figure 4.16B), compared to the decrease observed for *rimO*, supports the differential regulation of the two cistrons as examined in more detail in Chapter 3.

4.4.7 NtcA interaction with the *rimO* promoter

CrhR is expressed from a dicistronic transcript consisting of *rimO* and *crhR* (Chapter 3). In an attempt to identify proteins regulating operon expression in response to nitrogen source, affinity chromatography was used to co-purify *Synechocystis* proteins interacting with the *rimO* promoter using a biotinylated DNA fragment corresponding to 333 bp upstream of the *rimO* transcription start site. After mass spectrometry, only one transcription factor, NtcA, was detected in the 21 identified proteins that eluted from the column (Table 4.2). Several enzymes involved in DNA replication and repair, subunits of the RNA polymerase and ribosome, and phycobiliproteins were also detected that do not immediately appear to have a plausible role in CrhR expression. Bioinformatics analysis of the *rimO* promoter identified two putative NtcA binding sites having similarity to the NtcA consensus sequence of $GTAN_8TAC$ (287) centered at -52.5 bp ($GTAN_8CAC$, genomic position 2885980-2885993) and -16 bp ($GTAN_7TAC$, genomic position 2886017-2886029) (Figure 4.17). In support of our observation, Giner-Lamia, *et al.* (288) subsequently identified *rimO* as a putative member of the NtcA regulon using ChIP-seq. In these experiments, *rimO* transcript abundance was also observed to decrease during nitrogen starvation, consistent with the observations here.

Table 4.2: Mass spectrometry analysis of proteins co-purified with the *rimO* promoter.

Locus tag	Gene code	Description	PSM #	Gene ontology	Uniprot accession #
slr2058	topA	DNA topoisomerase	216	DNA topological change	P73810
slr0707	polA	DNA polymerase I	214	DNA replication	Q55971
sll0766	radC	DNA repair protein RadC	79	DNA repair	P52601
sll1423	ntcA	Global nitrogen regulator	55	Transcription	P33779
sll1577	cpcB	C-phycocyanin beta chain	52	Photosynthesis	Q54714
slr1689	mutM	Formamidopyrimidine-DNA glycosylase	30	DNA repair	P74290
sll0416	groL2	60 kDa chaperonin 2	17	Protein folding	P22034
sll1580	cpcC1	Phycobilisome 32.1 kDa linker polypeptide, phycocyanin-associated, rod 1	17	Photosynthesis	P73203
slr2076	groL1	60 kDa chaperonin 1	16	Protein folding	Q05972
slr1844	uvrA	UvrABC system protein A	15	DNA repair	P73412
sll1579	cpcC2	Phycobilisome 32.1 kDa linker polypeptide, phycocyanin-associated, rod 2	14	Photosynthesis	P73204
sll1804	rpsC	30S ribosomal protein S3	13	Translation	P73314
sll1578	cpcA	C-phycocyanin, alpha chain	11	Photosynthesis	Q54715
sll0947	hpf	Ribosome hibernation promotion factor	5	Translation	P74518
slr1265	rpoC1	DNA-directed RNA polymerase subunit gamma	4	Transcription	P74177
slr0164	clpR	Putative ATP-dependent Clp protease proteolytic subunit-like	4	Protein degradation	P74466
slr1986	apcB	Allophycocyanin, beta chain	4	Photosynthesis	Q01952
slr0009	cbbL	Ribulose biphosphate carboxylase large chain	3	Photorespiration	P54205
sll1945	dxs	1-deoxy-D-xylulose-5-phosphate synthase	2	Terpenoid biosynthesis	P73067
slr2067	apcA	Allophycocyanin, alpha chain	2	Photosynthesis	Q01951
slr0335	apcE	Phycobiliprotein ApcE	2	Photosynthesis	Q55544

Figure 4.17: Putative NtcA binding sites in the *rimO* promoter.

The sequence of the 333 bp biotinylated-DNA fragment used in the DNA affinity purifications is displayed. Base numbering corresponds to the *Synechocystis* genome (34). The transcription start site for the *rimO-crhR* operon is located immediately after the end of the sequence, at genomic position 2886039. The putative -10 promoter element is underlined. Two putative binding sites for NtcA, similar to the cyanobacterial consensus sequence, GTAN$_8$TAC (287), are highlighted in blue (2885980-2885993; GTAN$_8$CAC) and green (2886017-2886029; GTAN$_7$TAC).

4.5 Discussion

In this chapter, it is shown that the *Synechocystis* DEAD-box RNA helicase, CrhR, is required for normal cellular responses to changes in the availability and source of fixed nitrogen. Changes in nitrogen source produce differing effects in physiological markers, including growth rate and photosynthetic pigmentation, between wild type *Synechocystis* and the *crhR*$_{TR}$ strain. In addition, expression of CrhR is regulated by both the availability and type of fixed nitrogen, with transient enhancement of CrhR abundance observed following changes in the nitrogen compound available to the organism, while depletion of fixed nitrogen resulted in proteolytic degradation of CrhR. Evidence supporting a role for the global nitrogen regulator NtcA in mediating transcriptional regulation of *crhR* in response to nitrogen at sites upstream of the *rimO-crhR* operon is also presented. These results indicate a putative role for CrhR RNA helicase in mediating genetic responses in nitrogen uptake and assimilation pathways in *Synechocystis*, expanding the complement of abiotic stress responses that include CrhR.

The lack of growth and reduction in pigmentation observed with ammonium-based media was contrary to observations from other groups who routinely culture wild type *Synechocystis* at 10-15 mM ammonium concentrations (296, 320-322). A study specifically examining ammonium toxicity in *Synechocystis* found no effects on photosynthetic activity at 10 mM ammonium chloride (322), whereas here, growth and pigmentation effects were observed with concentrations as low as 1 mM. As was discussed in Chapter 1, there is heterogeneity at the genomic level in the sub-strains of *Synechocystis* maintained in research facilities (39, 40), with resulting differences in sub-strain phenotypes and stress responses (323). As the severe ammonium-sensitive phenotype exhibited is specific to the sub-strain of *Synechocystis* that has been maintained at the University of Alberta for over 20 years (41), it has likely been acquired during that time. Genome sequencing of the wild type *Synechocystis* sub-strain used in this study and comparison to the other characterized *Synechocystis* sub-strains may identify a lab-acquired mutation that is causing the ammonium-sensitive phenotype observed. Similar growth defects in ammonium have previously been observed in *Synechocystis* deficient in ammonium uptake (320), or turnover in PSII subunits that are susceptible to photodamage (322, 324). Based on the absence of chlorosis, as observed

with nitrogen deprivation, ammonium uptake is still able to occur in the ammonium-grown *Synechocystis*, intimating that the cause of the ammonium sensitive phenotype observed is likely related to the PSII repair cycle. The D1 protein, part of the reaction centre of PSII, is highly sensitive to irreversible photooxidative damage, an effect that is increased by ammonium (322). Proteolytic degradation of photodamaged D1 protein by the FtsH2 protease allows for its replacement in the reaction centre with *de novo* D1 (322) and continued photoautotrophic growth. Deficiencies in either proteolysis or *de novo* synthesis of D1 protein would result in loss of photosynthetic capacity and accumulating damage in PSII, consistent with the impaired growth and pale blue pigmentation observed. Alternatively, as accumulation of ammonium in the cell may affect intracellular pH, the acquired mutation(s) in this strain may be in pathways that maintain pH homeostasis in the cell.

CrhR expression in ammonium was also likely affected by ammonium toxicity, particularly at 20°C, where CrhR abundance was initially similar to urea and nitrate, then suddenly was undetectable. Depletion of CrhR could be an unintended consequence of the ammonium toxicity, or it could reflect a larger shift in the metabolism and energetics of the organism as it responds to the accumulating effects of ammonium toxicity. The maintenance of elevated CrhR abundance in media containing combined nitrate and ammonium at 20°C was insightful. If the decrease in CrhR abundance was due to normal nitrogen signalling, rather than an ammonium toxicity response, this would be unexpected, as ammonium repression of gene expression through NtcA is classically considered the basis of nitrogen-based regulation of gene expression in cyanobacteria (275, 325). This indicates that growth in nitrate is able to rescue effects of the ammonium-sensitivity on CrhR gene expression; however, it must occur via a mechanism that bypasses the global nitrogen control of ammonium repression.

As severe morphological and physiological defects have been previously reported for *crhR*$_{TR}$ during low temperature stress when grown in the nitrate-based BG-11 medium (104), restoration of the growth rate of the *crhR*$_{TR}$ strain at low temperature to near wild type levels by growth in media containing 2 mM urea was unexpected. Currently, the cause of the severe low temperature phenotype of *crhR*$_{TR}$ is posited to be due to deficiencies in photosynthetic carbon fixation resulting from reduced electron flow

through the photosynthetic electron transport chain (104). Similarly, Sireesha *et al*. (158) also attributed the phenotypic effects of *crhR* mutation to an inability to acclimate the photosynthetic pathways to low temperature stress, particularly with energy distribution between the photosystems and photosystem stoichiometry. Low-temperature induced nitrogen limitation in nitrate-based media was previously observed in another cyanobacterium, *Synechococcus* sp. PCC 7002, at 15°C, resulting in chlorosis and supressed growth, phenotypes that were not observed with low-temperature growth in urea (326). Unlike nitrate reduction, urea hydrolysis does not require reducing power from ferredoxin (283); thus, the reduction in the cold-sensitive phenotype observed in urea may indicate that nitrogen deprivation, due to lower rates of nitrate reduction, contributes to the severity of growth impairment and chlorotic pigmentation changes when *crhR*$_{TR}$ is grown in nitrate.

The sensing and signal transduction pathway that regulates CrhR expression in response to nitrogen source or availability is of particular interest. Linking the regulation of carbon and nitrogen metabolism is essential in a photosynthetic organism, such as cyanobacteria, to ensure that the utilization of energy from photosynthesis is balanced between carbon and nitrogen acquisition. Regulation of the related regulatory proteins NtcA, P_{II}, PipX and NAGK is one of the best examples of this, as their activity is modulated by the balance between 2-oxoglutarate, a measure of carbon availability, and ammonium, a measure of nitrogen availability (327). Further tuning of these regulators by altering the phosphorylation of P_{II} occurs in response to photosynthetic electron transport in *Synechocystis* (328, 329), ensuring a balance between the reductant required for carbon fixation and nitrogen assimilation. Redox regulation of CrhR expression in response to a range of abiotic stresses occurs though a convergent sensing pathway dependent on the redox poise of the quinones located at either the Q_B site of PSII or the plastoquinone pool (163). The increased overall abundance of CrhR observed at low temperature in both urea and nitrate, in comparison to CrhR abundance at 30°C, can be attributed to the sensing of decreased temperature due to its effects on the redox state of the plastoquinone pool. The signal regulating the decrease in CrhR abundance in ammonium or urea in comparison to nitrate-based media observed by 24 hours could also be the redox status of the plastoquinone pool, as the electron transport chains and

energetics of photosynthesis, nitrogen metabolism and respiration are highly interconnected in cyanobacteria (319). Electron transport chain inhibitors, DCMU and DBMIB, have been utilized previously to verify if stresses are sensed through plastoquinone (163, 330); however, they are not well suited to use with nitrogen stress, as treatment with DCMU or DBMIB artificially oxidizes the downstream electron transport chain, including ferredoxin. This slows or halts carbon fixation, nitrate reduction and nitrogen assimilation via the GS/GOGAT pathway, simultaneously affecting regulation of NtcA and its regulon.

The glutamine synthetase inhibitor L-methionine-sulfoximine (MSX) was used to simulate nitrogen starvation in the presence of nitrate to allow for decoupling of nitrogen metabolic and redox signals (312). Growth of cyanobacteria, including *Synechocystis*, under conditions of nitrogen deprivation stress results in chlorosis, a quiescence mechanism that visually manifests as a yellowing of the cells due to the degradation of the phycobiliproteins (306, 314). Both the wild type and *crhR*$_{TR}$ strains exhibited a plateau in growth, and depletion of phycobiliproteins in BG-11$_o$ medium, consistent with chlorosis. Unexpectedly, following treatment with MSX, regardless of concentration of MSX or nitrogen source in the media, visible degradation of the phycobiliproteins was not observed. This was not consistent with the observations of Klotz *et al*. (312), who were able to induce bleaching of *Synechococcus elongatus* PCC 7942 with concentrations as low as 2 μM MSX. Degradation of phycobiliproteins during chlorosis, the cause of the bleaching phenotype, is mediated by the Clp-protease adaptor protein NblA (331, 332). Expression of NblA is regulated by metabolic signals (333), the redox status of the electron transport chain (312) and a network of proteins, including response regulators (327, 333-335), ensuring degradation of phycobiliproteins is responsive to environmental stresses. Characterization of the majority of the proteins and conditions that regulate NblA expression has been conducted in *Synechococcus elongatus* and *Nostoc* sp. PCC 7120, with minimal investigation in *Synechocystis*. Interestingly, *Synechocystis* encodes a dicistronic operon with two gene copies of NblA which form a functional heterodimer (336, 337), in contrast to the homodimeric functional units of other cyanobacteria. A difference in regulatory organization may also accompany the altered gene structure in

Synechocystis, rendering inhibition of glutamine synthetase insufficient to initiate degradation of phycobiliproteins.

In the absence of bleaching as a visual measure of glutamine synthetase inhibition, transcript abundance of two NtcA-regulated genes, *glnB*, encoding a PII signal transduction protein (288), and *gifA*, encoding a glutamine synthetase inactivating factor (300) was used to identify a concentration of MSX that successfully mimicked nitrogen starvation. Unlike *Synechococcus elongatus* (312), 2 μM MSX was insufficient to induce gene expression changes in *Synechocystis* similar to those observed during nitrogen depletion. We also tested MS at 400 μM, a concentration in the same order of magnitude as previous experiments using MSX treatment with *Synechocystis* (338, 339). At 400 μM, the expected NtcA-dependent changes in *gifA* and *glnB* transcript abundance were induced. Treatment with 400 μM MSX was sufficient to induce CrhR proteolysis in the presence of nitrate-based medium, indicating that the regulatory signal for CrhR proteolysis during nitrogen depletion is the accumulation of 2-oxoglutarate in the absence of ammonium, with NtcA regulating an aspect of the proteolytic mechanism, likely expression of an adaptor or chaperone.

The identification of the transcription factor NtcA binding the promoter for the *rimO-crhR* operon expands the complement of transcription factors that affect expression of *crhR*. This adds NtcA regulation of the dicistronic operon promoter upstream of *rimO* as a mechanism of transcriptional regulation, in addition to the already characterized repression of the promoter immediately upstream of *crhR* by a redox-regulated LexA ortholog (165). In *Synechocystis*, expression of NtcA is driven from two promoters, one constitutive and one regulated in response to both nitrogen and the redox status of the electron transport chain, sensed through the reduction of the thiol residues on the NtcA protein (340). Thus, *ntcA* expression bears similarities to that of *crhR*, which is also dependent on light illumination and responsive to changes in the redox status of the photosynthetic electron transport chain. As *crhR* expression is enhanced under reducing conditions (341), the same conditions in which the NtcA protein is active, NtcA would be expected to act as a transcriptional activator of the *rimO-crhR* operon; however, the only condition in which NtcA has thus far been observed to bind strongly to the *rimO* promoter, nitrogen deprivation, resulted in decreased expression of *rimO* (288). Timing

differences in the experiments may explain some of this discrepancy, as, at least in response to temperature stress, accumulation of the *rimO* transcript is very short-lived, lasting less than an hour, (Chapter 3), while the transcriptome in Giner-Lamia *et al.* (288) was generated after four hours of nitrogen starvation. It is also possible that a second signal regulates transcription from the *rimO-crhR* operon promoter during nitrogen starvation, as the *rimO* transcript accumulation observed with MSX treatment, simulating nitrogen starvation, unexpectedly increased after 4 hours, while the abundance observed in nitrogen-deplete medium decreased, consistent with Giner-Lamia *et al*. (288). This observation implies that while NtcA may act as a repressor of the *rimO-crhR* operon transcript, other transcriptional regulators also likely modulate expression of the discistronic operon in response to nitrogen signalling.

Regulation of CrhR expression in response to changes in the source of fixed nitrogen is complex, seemingly involving multiple regulators acting at various stages of expression. This is consistent with CrhR expression at low temperature, where expression is regulated at transcriptional, post-transcriptional and even post-translational levels by a complex network of regulators (164). During low temperature expression, CrhR expression was auto-regulatory, with some, but not all of these regulatory checkpoints CrhR-dependent (164). At 20°C, CrhR had previously been observed to accumulate to a maximal level in both wild type and *crhR*$_{TR}$; however, upon transfer from the nitrate-based BG-11 growth medium to a urea-based medium, CrhR continued to accumulate. In wild type *Synechocystis*, this increased accumulation of CrhR protein was transient, but in *crhR*$_{TR,}$ the truncated protein continued to accumulate, even after return to the nitrate-based medium. This indicates that some of the additional levels of regulation observed for CrhR expression during nitrogen stress are auto-regulatory. It is of interest to note that many of the auto-regulatory checkpoints in CrhR expression involve decreasing CrhR protein levels from an elevated state. Perhaps CrhR auto-regulation occurs when abundance of CrhR is sufficient to exceed that required for its function, allowing free and active CrhR to interact with regulatory pathways that decrease CrhR expression including the induction of proteolysis. Alternatively, a protein motif required for targeting of excess CrhR protein for degradation may be absent in CrhR$_{TR}$, allowing it to accumulate in excess.

Regulation of CrhR expression in response to nitrogen stress may provide some insights into the function of CrhR in *Synechocystis.* Similar to CrhR, expression of many bacterial DEAD-box RNA helicases are regulated by temperature and/or salt (102-106, 161, 342). An increased requirement for the helicase protein during these abiotic stresses has been explained in the context of the increased stability of nucleic acid secondary structure at lower temperatures and increased salt concentrations (74). Unlike those other DEAD-box proteins, CrhR is regulated in response to an increased complement of stresses, many of which are sensed through the redox poise of the photosynthetic electron transport chain (163), which does not have a direct link to increased RNA stability. Nitrogen has now been shown to be another stress that affects CrhR expression but does not directly affect RNA stability. During nitrogen deprivation, CrhR is rapidly degraded, even at lower temperature, when RNA secondary structures are more stable and the activity of an RNA helicase is presumed to be important. Proteolysis of CrhR occurs in the early stages of chlorosis, when the cell is still upregulating genes for transport and assimilation of nitrogen, prior to degradation of the phycobiliproteins and other preparations for senescence (302). This is significant, as it indicates CrhR is not required in expression of the nitrogen transport and assimilation pathways while cells are scavenging for available nitrogen, nor is it required during cellular preparations for senescence. Rather, CrhR is only expressed when nitrogen is freely available and cellular metabolism is proceeding normally. Considered together with the common sensing of other stresses that regulate CrhR through the photosynthetic electron transport chain (163), the trends of CrhR expression in nitrogen may indicate that CrhR expression in nitrogen is also linked to the redox poise of the electron transport chain. CrhR accumulates when conditions near the plastoquinone pool are reducing (163). There is careful coordination of the availability of reductants with metabolic processes and stress in cyanobacteria, particularly to avoid accumulation of excess reducing power within the electron transport chain (319). Even in the early stages of chlorosis, reductants, a source of energy for the cell, are conserved where possible. Down-regulation of CrhR under this condition, and upregulation when reductants are plentiful may indicate that CrhR regulates the expression of proteins, such as electron sinks, to help remove excess electrons from the electron transport chain. Consistent with this proposal, *crhR* mutation

has been shown to reduce abundance of transcripts for subunits for ATP synthase and NADH dehydrogenase, as well as flavoproteins (147). This may link redox regulation of CrhR expression with nitrogen stresses, as the reduction of nitrite and nitrate has been shown to be an electron sink for the photosynthetic electron transport chain (312).

In this chapter, CrhR expression was shown to be sensitive to changes in the source and availability of fixed nitrogen. In particular, nitrogen depletion induced rapid proteolysis of CrhR. Regulation of CrhR expression during nitrogen stresses was shown to be related to both global nitrogen control, through NtcA, as well as the redox status of the photosynthetic electron chain, with some of these regulatory checkpoints CrhR-dependent. As regulation of CrhR expression is also known to be responsive to salt (161), temperature (104), heavy metals (163) and light (41), a model of CrhR RNA helicase as a modulator of RNA secondary structures in response to an increasing variety of stresses is emerging.

Chapter 5: Distribution of DEAD-box RNA helicases in cyanobacteria

5.1 Summary

DEAD-box RNA helicases have roles in many RNA processes, modulating RNA structures and mediating interactions between functional protein complexes and RNA. In cyanobacteria, DEAD-box RNA helicase proteins form three distinct clades. Two of these clades, the CsdA-like and RhlE-like helicases, cluster with the homologous proteins from *E. coli*. The third clade, the CrhR-like helicases, is unique to cyanobacteria and characterized by a conserved sequence motif in the C-terminal extension of the helicase. Distribution of the CrhR-like helicases throughout cyanobacterial diversity and conservation of the *rimO-crhR* operon suggest that the CrhR-like helicases evolved early in the cyanobacterial lineage. Functions for the CrhR-like, CsdA-like, and RhlE-like helicases in expression and maintenance of photosynthetic systems, ribosome biogenesis, and coordination of CrhR/CsdA function, respectively, are proposed.

5.2 Introduction

Regulation of the expression of gene products occurs at many levels. At the post-transcriptional level, modulation of RNA structure can regulate gene expression by altering RNA stability or translation efficiency. In many cases, these RNA structural changes require interactions with proteins, such as chaperones (343, 344) or helicases (77, 231, 345). RNA helicases function in all aspects of RNA metabolism, regulating a diverse range of cellular processes by unwinding and, more rarely, annealing RNA duplexes, performing local strand separation, and by mediating RNA-protein interactions (64, 72, 231, 346). Generally, RNA helicases share a conserved structure, with two RecA-like functional domains containing a series of conserved sequence motifs that participate in RNA binding, and ATP binding and hydrolysis (see Figure 1.4) (76, 78, 82). The largest family of RNA helicases, the DEAD-box proteins, have 12 highly conserved sequence motifs (72), conferring a biochemical activity of ATP-dependent local RNA strand separation (86). Some DEAD-box proteins can also displace proteins from RNA or clamp to RNA and serve as a nucleation site for the recruitment of other proteins to form functional complexes (72, 87, 346). In eukaryotes, DEAD-box helicases are essential for survival, as they are intimately involved in almost all cellular processes, including translation, splicing and RNA degradation (72). Prokaryotic DEAD-box

proteins are also involved in ribosome biogenesis, translation and RNA processing and degradation; however, their function is generally only required under non-optimal conditions (75).

Classification of prokaryotic DEAD-box helicases is often based on the RNA processes the protein participates in (67, 182), but phylogenetic methods have also started to be used (75, 107). Based on conserved sequence domains, Lopez-Ramirez *et al.* (107) classified bacterial DEAD-box proteins into three major groups: proteins that contain a DbpA RNA binding domain (including CsdA and DbpA from *E. coli*, and DeaD/YxiN from *B. subtilis*), proteins lacking the DbpA domain (including SrmB and RhlB from *E. coli*, and CshA, CshB and YfmL from *B. subtilis*), and RhlE-like proteins. These classifications, based on sequence and structure, generally relate well to the cellular functions of the DEAD-box protein. For example, the DbpA RNA binding domain facilitates recognition and binding of hairpin 92 of the 23S rRNA precursor by a DEAD-box RNA helicase (114, 118, 347). All of the well-characterized DEAD-box proteins containing this domain, DbpA, CsdA, and YxiN, participate in maturation of the 50S ribosomal subunit, and specifically the 23S rRNA precursor (109, 113, 119). These phylogenetic classifications aid in deducing putative functions of DEAD-box helicases from protein sequences as they are annotated in newly sequenced genomes.

The quantity and diversity of sequenced cyanobacterial genomes available in publicly accessible databases has increased substantially since these phylogenetic studies of bacterial DEAD-box proteins (75, 107). Cyanobacteria have metabolic and lifestyle differences to other bacteria as they are the only prokaryotes that perform oxygenic photosynthesis. It was therefore of interest to explore how DEAD-box proteins in this divergent group of organisms relate to those found in other bacteria.

Four DEAD-box RNA helicases have been experimentally identified in cyanobacteria to date: CrhA from *Anabaena variabilis* UTCC 387 (148), CrhB and CrhC from *Nostoc* sp. PCC 7120 (105), and CrhR from *Synechocystis* sp. PCC 6803 (41), with two examples, CrhA and CrhB, receiving only limited study. CrhC is a cold-induced protein (105) that interacts with ribosomes and localizes to the cytoplasmic face of the plasma membrane near the cell poles (152). Expression of CrhR is regulated in response to the redox poise of the plastoquinone pool of the photosynthetic electron transport chain

(41, 163). In Chapter 2, CrhR was shown to cosediment with polysomes and RNA degradosome components and localize to the thylakoid membrane. Consistent with localization to the thylakoid membrane, *crhR* mutation results in disruption to photosynthesis, particularly at low temperatures (104, 158). As the cyanobacterial DEAD-box proteins, and in particular CrhR, demonstrate localizations unique to cyanobacteria, further study of these proteins across the diversity of cyanobacteria is warranted.

In this chapter, it was demonstrated that cyanobacterial DEAD-box proteins form three major groups, two with homology to the *E. coli* DEAD-box proteins CsdA and RhlE, and a third unique to cyanobacteria, the CrhR-like helicases. The CrhR-like proteins are found throughout cyanobacteria diversity and share a conserved sequence domain in the C-terminal extension that identifies them as a separate clade within the DEAD-box RNA helicase family. In addition, synteny of the dicistronic *rimO-crhR* operon is well conserved, suggesting early acquisition of CrhR-like proteins in the cyanobacterial lineage. CsdA-like helicases, which occur only in *Synechococcales*, have a DbpA RNA binding motif in the C-terminus and may have been acquired following a loss of the CrhR-like helicase in the ancestral lineage. Strains with RhlE-like helicases also encode at least one other DEAD-box protein in the genome. Based on similarities to characterized homologs, functions for CsdA, CrhR and RhlE in ribosome biogenesis, expression and maintenance of photosynthetic systems, and coordination of CsdA/CrhR function, respectively, are proposed.

5.3 Methods

5.3.1 Sequence data

Predicted and known amino acid sequences of cyanobacterial DEAD-box RNA helicases were obtained from the NCBI non-redundant (nr) protein database. The helicase core domain (amino acids F9-R338) of the sole DEAD-box RNA helicase in *Synechocystis* sp. PCC 6803, CrhR, was retrieved from NCBI (accession WP_010873784.1) for use as the query sequence. A BLASTp search, restricted to cyanobacteria (taxid: 1117), yielded 461 unique DEAD-box RNA helicase sequences. These sequences were curated for full-

length sequences that contained the 12 conserved motifs of the DEAD-box helicase protein family (see Figure 1.4), resulting in a total of 362 sequences from 280 strains of cyanobacteria. The sequences of the five DEAD-box proteins from *Escherichia coli* were also retrieved from NCBI to verify correct branching.

5.3.2 Sequence alignments and phylogenetic analysis

The helicase sequences were collected in MEGA7 v7.0.21 (348), where multiple sequence alignments of the protein sequences were generated using the integrated MUSCLE algorithm (349) with default parameters. This alignment was exported in FASTA format and converted to relaxed Phylip format using NCLconverter v2.1 (350), accessed via the CIPRES science gateway (351).

The maximum likelihood tree was created using RAxML-HPC Blackbox v8.2.10 (352), accessed via CIPRES (351) using default settings, with the exception of the amino acid substitution matrix, which was set to LG (353). Rapid bootstrapping ran for 252 replicates before auto-termination with MRE-based bootstrapping criteria (354). The output tree was visualized in iTOL v4.3.2 (355). Taxa colours correspond to the cyanobacterial order.

The Euler diagram representing the distribution of the helicase families across cyanobacterial strains was created as a three-set Euler diagram in EulerAPE v.3.0 (356), consisting of CrhR-like, CsdA-like and RhlE-like helicases. The fourth set, for the unclassified helicases, was added with approximate scaling in Adobe Illustrator to visually demonstrate the intersection of the unclassified helicases with the CrhR-like and RhlE-like proteins.

5.3.3 Gene context analysis

Genes surrounding each DEAD-box protein in the respective cyanobacterial genome were identified using the NCBI Genome Viewer. Related genes were identified from annotations of conserved motifs.

5.3.4 C-terminal motif identification

Alignments of the C-terminal domains for sequences from each helicase subfamily were generated in MUSCLE (349). Alignments of a selection of sequences from the subfamily were used for visualization of the alignments. Alignments including all sequences in the subfamily were used to generate sequence logos in WebLogo3 (357).

5.3.5 Pfam domain identification

Protein sequences were searched against the Pfam database (358) using the EMBL-EBI web portal with an E-value cut-off of 1.0.

5.3.6 *rpoC* neighbour-joining tree

rpoC2 gene sequences were identified by searching the genome sequences with the RpoC2 protein of *Synechocystis* sp. PCC 6803 (BA000022.2: 853497-857450). *rpoC2* sequences were used instead of 16S rDNA as the genome for *Phormidesmis preistleyi* ANA is incomplete, and lacks sequences for the 16S rDNA and several core conserved genes often used in concatenated gene trees. *rpoC2* nucleotide sequences were aligned by MUSCLE (349) with default parameters. A neighbour-joining tree was generated in Jalview v.2.11 using a BLOSUM62 scoring matrix (359).

5.4 Results

5.4.1 Cyanobacterial DEAD-box RNA helicases form 3 distinct clades

The amino acid sequence of the *Synechocystis* sp. PCC 6803 DEAD-box protein, CrhR, was used to generate a query sequence that included all 12 of the conserved sequence motifs characteristic of DEAD-box RNA helicases. The query sequence (F9-R338) was utilized as it contained amino acids corresponding to the RNA helicase core, which is highly conserved in all DEAD-box RNA helicases (72) This sequence included the 12 conserved sequence motifs characteristic of DEAD-box proteins, containing all amino acids between the conserved phenylalanine upstream of the Q motif (80) and the final arginine of motif VI (360) (see Figure 1.4). The NCBI non-redundant (nr) protein database was searched with this query, returning 461 unique cyanobacterial records,

which were further curated to remove sequences from other superfamily 1 and 2 helicase families, as well as incomplete sequences. The resulting 362 cyanobacterial DEAD-box protein sequences (Table 5.1) were aligned, and the phylogenetic relationships were identified by construction of an unrooted maximum likelihood tree using RAxML (352).

The majority of the cyanobacterial DEAD-box RNA helicase proteins cluster into three clades, each having a bootstrap value ≥95% (Figure 5.1). Two of the *E. coli* helicase sequences, RhlE and CsdA, fall within these groups, while the remaining three, DbpA, RhlB and SrmB, do not group with the cyanobacterial helicase sequences. These three clades are labelled CsdA-like and RhlE-like, corresponding to the *E. coli* helicases that cluster with them, and CrhR-like, for the most characterized protein sequence in the group, CrhR, from *Synechocystis* sp. PCC 6803 (41). Of the 362 cyanobacterial DEAD-box proteins in this analysis, 185 fall within the CrhR-like helicases, 92 in CsdA-like, and 71 in RhlE-like (Figure 5.1A). 14 of the cyanobacterial helicase proteins do not cluster with any of these three protein groups.

Examining the distribution of helicases belonging to the three groups demonstrates that 199 cyanobacterial strains contain a single type of DEAD-box protein, 67 strains contain two types, and 4 strains contain three types (Figure 5.1A). Of the strains encoding ungrouped DEAD-box proteins, three strains also encode either a CrhR-like or RhlE-like protein, while the remaining seven encode solely DEAD-box proteins that do not cluster with the three protein subfamilies defined in this study. It is important to note that the methodology of this study does not allow for enumeration of the rare examples of cyanobacterial strains that do not encode DEAD-box RNA helicases, such as the model organism *Synechococcus elongatus*, of which there are several genome sequences available (361). DEAD-box proteins were also not identified in the proposed basal-branching order *Gloeomargaritales*, which only has one sequenced representative genome (362). Based on the currently available sequence data, it can be concluded each cyanobacterium can encode between zero and three different DEAD-box proteins, with a strong tendency for helicase-specific clustering within related cyanobacterial lineages.

Table 5.1: DEAD-box RNA helicase proteins encoded in cyanobacterial genomes. The list of sequence identifiers obtained by the search of the NCBI non-redundant sequences database using the helicase core domain (F9-R338) of the DEAD-box protein CrhR from *Synechocystis* sp. PCC 6803. The order, species, strain and accession number for each protein is indicated, as well as the corresponding group (CrhR, CsdA or RhlE) within the DEAD-box protein family.

Order	Species	Strain	Accession Number	Group
Chroococcales				
	Aphanothece halophytica	PCC 7418	WP_015227798.1	CrhR
	Candidatus Atelocyanobacterium thalassa isolate	ALOHA	WP_012954034.1	CrhR
	Candidatus Atelocyanobacterium thalassa isolate	SIO64986	KFF41262.1	CrhR
	Chroogloeocystis siderophila	5.2 s.c.1	WP_073551513.1	CrhR
	Crocosphaera watsonii	WH 8501	WP_007303466.1	CrhR
	Cyanobacterium aponinum	PCC 10605	WP_015219980.1	CrhR
	Cyanobacterium sp.	IPPAS B-1200	WP_069789285.1	CrhR
	Cyanobacterium stanieri	PCC 7202	AFZ47545.1	CrhR
	Geminocystis herdmanii	PCC 6308	WP_017294180.1	CrhR
	Geminocystis sp.	NIES-3708	WP_066348995.1	CrhR
	Geminocystis sp.	NIES-3709	WP_066117391.1	CrhR
	Gloeocapsa sp.	PCC 7428	WP_015190184.1	CrhR
	Gloeocapsa sp.	PCC 73106	WP_006530822.1	CrhR
	Microcystis aeruginosa	KW	WP_079208639.1	CrhR
	Microcystis aeruginosa	NIES-44	WP_045361726.1	CrhR
	Microcystis aeruginosa	NIES-88	WP_061432786.1	CrhR
	Microcystis aeruginosa	NIES-98	WP_069474107.1	CrhR
	Microcystis aeruginosa	NIES-843	WP_012265913.1	CrhR
	Microcystis aeruginosa	NIES-2481	WP_066030023.1	CrhR
	Microcystis aeruginosa	NIES-2549	WP_046662813.1	CrhR
	Microcystis aeruginosa	PCC 7005	WP_024970412.1	CrhR
	Microcystis aeruginosa	PCC 7806	WP_002741230.1	CrhR
	Microcystis aeruginosa	PCC 9432	WP_002733094.1	CrhR
	Microcystis aeruginosa	PCC 9443	WP_002769059.1	CrhR
	Microcystis aeruginosa	PCC 9701	WP_004268339.1	CrhR
	Microcystis aeruginosa	PCC 9717	WP_002763242.1	CrhR
	Microcystis aeruginosa	PCC 9806	WP_002781592.1	CrhR
	Microcystis aeruginosa	SPC777	WP_016516037.1	CrhR
	Microcystis panniformis	FACHB-1757	WP_052277776.1	CrhR
	Microcystis sp.	T1-4	WP_008198520.1	CrhR
	Rubidibacter lacunae	KORDI 51-2	WP_022606644.1	CrhR
Chroococcidiopsidales				
	Chroococcidiopsis thermalis	PCC 7203	WP_015155494.1	CrhR
Gloeobacterales				
	Gloeobacter kilaueensis	JS1	WP_023172363.1	No group
	Gloeobacter violaceus	PCC 7421 (a)	WP_011142503.1	No group
	Gloeobacter violaceus	PCC 7421 (b)	WP_011142321.1	No group

Order	Species	Strain	Accession Number	Group
Nostocales				
	Anabaena cylindrica	PCC 7122	WP_015216841.1	CrhR
	Anabaena cylindrica	PCC 7122	WP_015217396.1	RhlE
	Anabaena sp.	90	WP_015081159.1	CrhR
	Anabaena sp.	90	WP_015079554.1	RhlE
	Anabaena sp.	AL09	OBQ05623.1	CrhR
	Anabaena sp.	AL09	OBQ03207.1	RhlE
	Anabaena sp.	ATCC 33047	WP_066377041.1	CrhR
	Anabaena sp.	CRKS33	OBQ40729.1	CrhR
	Anabaena sp.	CRKS33	OBQ32742.1	RhlE
	Anabaena sp.	LE011-02	OBQ04690.1	CrhR
	Anabaena sp.	LE011-02	OBQ05997.1	RhlE
	Anabaena sp.	PCC 7108	WP_016953324.1	CrhR
	Anabaena sp.	PCC 7108	WP_016951584.1	RhlE
	Anabaena sp.	WA102	WP_053540454.1	CrhR
	Anabaena sp.	WA102	WP_053539369.1	RhlE
	Anabaena sp.	WA113	OBQ22342.1	CrhR
	Anabaena sp.	WA113	OBQ18746.1	RhlE
	Anabaena variabilis	ATCC 29413	ABA20266.1	CrhR
	Anabaena variabilis	ATCC 29413	ABA21574.1	RhlE
	Aphanizomenon flos-aquae	2012/KM1/D3	WP_039204634.1	CrhR
	Aphanizomenon flos-aquae	2012/KM1/D3	WP_039200299.1	RhlE
	Aphanizomenon flos-aquae	LD13	OBQ18590.1	CrhR
	Aphanizomenon flos-aquae	LD13	OBQ22990.1	RhlE
	Aphanizomenon flos-aquae	NIES-81	WP_027404570.1	CrhR
	Aphanizomenon flos-aquae	NIES-81	WP_027401622.1	RhlE
	Calothrix sp.	336/3	WP_035153586.1	CrhR
	Calothrix sp.	HK-06	WP_073618868.1	CrhR
	Calothrix sp.	HK-06	WP_073622274.1	RhlE
	Calothrix sp.	PCC 6303	WP_015200162.1	CrhR
	Calothrix sp.	PCC 6303	WP_015195959.1	RhlE
	Calothrix sp.	PCC 7103	WP_019489262.1	CrhR
	Calothrix sp.	PCC 7103	WP_035173265.1	RhlE
	Calothrix sp.	PCC 7507	WP_015131393.1	CrhR
	Calothrix sp.	PCC 7507	WP_015132072.1	RhlE
	Chlorogloeopsis fritschii	PCC 6912	WP_016873588.1	CrhR
	Chlorogloeopsis sp.	PCC 7702	WP_017322836.1	CrhR
	Chrysosporum ovalisporum	UAM-MAO	CEJ43554.1	CrhR
	Cylindrospermopsis raciborskii	CS-505	WP_006276327.1	CrhR
	Cylindrospermopsis raciborskii	MVCC14	WP_071250936.1	CrhR
	Cylindrospermopsis sp.	CR12	WP_057176886.1	CrhR
	Cylindrospermum stagnale	PCC 7417	WP_015206929.1	CrhR
	Cylindrospermum stagnale	PCC 7417	WP_015209745.1	RhlE
	Dolichospermum circinale	AWQC131C	WP_028090653.1	CrhR
	Dolichospermum circinale	AWQC131C	WP_028091112.1	RhlE
	Dolichospermum circinale	AWQC310F	WP_028084471.1	CrhR
	Dolichospermum circinale	AWQC310F	WP_028084089.1	RhlE
	Fischerella major	NIES-592	WP_073555827.1	CrhR
	Fischerella muscicola	PCC 73103	WP_016860456.1	CrhR
	Fischerella muscicola	PCC 7414	WP_026085820.1	CrhR
	Fischerella sp.	JSC-11	WP_009453863.1	CrhR
	Fischerella sp.	NIES-3754	WP_062246540.1	CrhR

Order	Species	Strain	Accession Number	Group
Nostocales				
	Fischerella sp.	PCC 9339	WP_017311292.1	CrhR
	Fischerella sp.	PCC 9605	WP_026731393.1	CrhR
	Fortiea contorta	PCC 7126	WP_017654089.1	CrhR
	Hapalosiphon sp.	MRB220	WP_026721223.1	CrhR
	Hassallia byssoidea	VB512170	KIF28888.1	CrhR
	Hassallia byssoidea	VB512170 (a)	KIF30245.1	No group
	Hassallia byssoidea	VB512170 (b)	KIF31317.1	No group
	Mastigocladopsis repens	PCC 10914	WP_017315850.1	CrhR
	Mastigocoleus testarum	BC008	WP_027842873.1	CrhR
	Nodularia spumigena	CCY9414	WP_006195458.1	CrhR
	Nodularia spumigena	CCY9414	WP_006195497.1	RhlE
	Nodularia spumigena	CENA596	WP_063873820.1	CrhR
	Nostoc azollae	0708	WP_013190002.1	CrhR
	Nostoc azollae	0708	ADI63752.1	RhlE
	Nostoc calcicola	FACHB-389	WP_073642635.1	CrhR
	Nostoc piscinale	CENA21	WP_062295266.1	CrhR
	Nostoc punctiforme	PCC 73102	WP_012410842.1	CrhR
	Nostoc punctiforme	PCC 73102	WP_012409963.1	RhlE
	Nostoc sp.	KVJ20	WP_069069063.1	CrhR
	Nostoc sp.	KVJ20	WP_069072171.1	RhlE
	Nostoc sp.	MBR 210	OCQ99908.1	CrhR
	Nostoc sp.	NIES-3756	WP_067773294.1	CrhR
	Nostoc sp.	NIES-3756	WP_067768693.1	RhlE
	Nostoc sp.	PCC 7107	WP_015111687.1	CrhR
	Nostoc sp.	PCC 7107	AFY45650.1	RhlE
	Nostoc sp.	PCC 7120	WP_010995395.1	CrhR
	Nostoc sp.	PCC 7120	WP_010998849.1	RhlE
	Nostoc sp.	PCC 7524	WP_015138780.1	CrhR
	Raphidiopsis brookii	D9	WP_009343384.1	CrhR
	Richelia intracellularis	HH01	WP_008231885.1	CrhR
	Richelia intracellularis	RC01	CDN14942.1	CrhR
	Rivularia sp.	PCC 7116	WP_015121796.1	CrhR
	Scytonema hofmanni	UTEX B 1581	WP_029631515.1	RhlE
	Scytonema hofmanni	UTEX B 1581	WP_029633835.1	CrhR
	Scytonema hofmannii	PCC 7110	WP_017746800.1	CrhR
	Scytonema sp.	HK-05	WP_073628368.1	CrhR
	Scytonema tolypothrichoides	VB-61278	WP_048871842.1	CrhR
	Tolypothrix bouteillei	VB521301	WP_038078122.1	CrhR
	Tolypothrix campylonemoides	VB511288	WP_071838559.1	No group
	Tolypothrix campylonemoides	VB511288	WP_041035416.1	CrhR
	Tolypothrix sp.	PCC 7601	WP_045867700.1	CrhR
	Trichormus sp.	NMC-1	WP_071190055.1	CrhR
	Trichormus sp.	NMC-1	WP_071190771.1	RhlE
Oscillatoriales				
	Arthrospira maxima	CS-328	WP_006670629.1	CrhR
	Arthrospira platensis	C1	WP_035760177.1	CrhR
	Arthrospira platensis	NIES-39	WP_043468916.1	CrhR
	Arthrospira platensis	Paraca	WP_006617243.1	CrhR
	Coleofasciculus chthonoplastes	PCC 7420	WP_006102098.1	CrhR
	Crinalium epipsammum	PCC 9333	WP_015205239.1	CrhR

Order	Species	Strain	Accession Number	Group
Oscillatoriales				
	Cyanothece sp.	ATCC 51142	WP_009543508.1	CrhR
	Cyanothece sp.	CCY0110	WP_008276945.1	CrhR
	Cyanothece sp.	PCC 7425	WP_012629831.1	CrhR
	Cyanothece sp.	PCC 7822	WP_013323350.1	CrhR
	Cyanothece sp.	PCC 8801	WP_015785253.1	CrhR
	Desertifilum sp.	IPPAS B-1220	WP_069967535.1	CrhR
	filamentous cyanobacterium	ESFC-1	WP_018396245.1	CrhR
	Geitlerinema sp.	PCC 7105	WP_017661231.1	No group
	Geitlerinema sp.	PCC 7407	WP_015173091.1	CrhR
	Geitlerinema sp.	PCC 9228	WP_071517408.1	CrhR
	Limnoraphis robusta	CS-951	WP_046278382.1	CrhR
	Lyngbya aestuarii	BL J	WP_023065801.1	CrhR
	Lyngbya confervoides	BDU141951	WP_044150923.1	RhlE
	Lyngbya confervoides	BDU141951	WP_063776105.1	No group
	Lyngbya sp.	PCC 8106	WP_039896992.1	CrhR
	Microcoleus sp.	PCC 7113	WP_015182542.1	RhlE
	Microcoleus sp.	PCC 7113	WP_015184396.1	CrhR
	Microcoleus vaginatus	FGP-2	WP_006633595.1	CrhR
	Moorea bouillonii	PNG5-198	WP_075900005.1	CrhR
	Moorea producens	3L	WP_008177600.1	CrhR
	Moorea producens	JHB	WP_071104591.1	CrhR
	Moorea producens	PAL-8-15-08-1	WP_070393209.1	CrhR
	Oscillatoria acuminata	PCC 6304	WP_015146953.1	CrhR
	Oscillatoria nigro-viridis	PCC 7112	WP_015177386.1	CrhR
	Oscillatoria sp.	PCC 10802	WP_017715337.1	CrhR
	Oscillatoria sp.	PCC 6506	WP_007354567.1	CrhR
	Oscillatoriales cyanobacterium	CG2_30_40_61	OIP73250.1	CrhR
	Oscillatoriales cyanobacterium	CG2_30_44_21	OIP71395.1	CrhR
	Oscillatoriales cyanobacterium	CG2_30_44_21	OIP71446.1	RhlE
	Oscillatoriales cyanobacterium	JSC-12	WP_009557052.1	CrhR
	Oscillatoriales cyanobacterium	MTP1	WP_058883613.1	CrhR
	Oscillatoriales cyanobacterium	USR001	OCR00684.1	CrhR
	Phormidium ambiguum	IAM M-71	WP_073595642.1	RhlE
	Phormidium ambiguum	IAM M-71	WP_073595739.1	CrhR
	Phormidium sp.	OSCR	KPQ34456.1	No group
	Phormidium tenue	NIES-30	WP_073610295.1	RhlE
	Phormidium tenue	NIES-30	WP_073607089.1	CrhR
	Planktothricoides sp.	SR001	WP_054466936.1	CrhR
	Planktothrix agardhii	NIVA-CYA 126/8	WP_042151026.1	CrhR
	Planktothrix agardhii	PCC 7805	CUM60384.1	CrhR
	Planktothrix paucivesiculata	PCC 9631	CUR15004.1	CrhR
	Planktothrix rubescens	7821	WP_026787128.1	CrhR
	Planktothrix serta	PCC 8927	CUR16751.1	CrhR
	Planktothrix sp.	PCC 11201	WP_079680322.1	CrhR
	Planktothrix tepida	PCC 9214	WP_072718935.1	CrhR
	Roseofilum reptotaenium	AO1-A	OJJ22692.1	CrhR
	Trichodesmium erythraeum	IMS101	ABG52788.1	CrhR

Order	Species	Strain	Accession Number	Group
Pleurocapsales				
	Hydrococcus rivularis	NIES-593	WP_073598826.1	CrhR
	Myxosarcina sp.	GI1	WP_036485380.1	CrhR
	Pleurocapsa sp.	PCC 7319	WP_019508420.1	CrhR
	Pleurocapsa sp.	PCC 7327	WP_015145756.1	CrhR
	Stanieria cyanosphaera	PCC 7437	WP_015194510.1	CrhR
	Stanieria sp.	NIES-3757	BAU65148.1	CrhR
	Xenococcus sp.	PCC 7305	WP_006508547.1	CrhR
Spirulinales				
	Spirulina major	PCC 6313	WP_072621974.1	CrhR
	Spirulina subsalsa	PCC 9445	WP_017305715.1	CrhR
Synechococcales				
	Acaryochloris marina	MBIC11017	WP_012162240.1	CrhR
	Acaryochloris marina	MBIC11017	WP_012160835.1	CsdA
	Acaryochloris sp.	CCMEE 5410	WP_010476696.1	CrhR
	Acaryochloris sp.	CCMEE 5410	WP_010469002.1	CsdA
	Aphanocapsa montana	BDHKU210001 (a)	KIF26984.1	No group
	Aphanocapsa montana	BDHKU210001 (b)	KIF27867.1	No group
	Candidatus Synechococcus spongiarum		WP_074457638.1	CsdA
	Candidatus Synechococcus spongiarum	142	KKZ10452.1	CsdA
	Candidatus Synechococcus spongiarum	LMB bulk15M	OOV28380.1	CsdA
	Candidatus Synechococcus spongiarum	SH4	WP_025782217.1	CsdA
	Candidatus Synechococcus spongiarum	SP3	KKZ12789.1	CsdA
	Chamaesiphon minutus	PCC 6605	AFY93922.1	CrhR
	Cyanobium gracile	PCC 6307	AFY27888.1	RhlE
	Cyanobium gracile	PCC 6307	WP_015108547.1	CsdA
	Cyanobium sp.	CACIAM 14	KEF42712.1	RhlE
	Cyanobium sp.	CACIAM 14	KEF42202.1	CsdA
	Cyanobium sp.	NIES-981	SBO41936.1	RhlE
	Cyanobium sp.	NIES-981	SBO42872.1	CsdA
	Cyanobium sp.	PCC 7001	WP_006910544.1	RhlE
	Cyanobium sp.	PCC 7001	EDY39500.1	CsdA
	Dactylococcopsis salina	PCC 8305	WP_015230714.1	CrhR
	Leptolyngbya boryana	IAM M-101	WP_036045359.1	CrhR
	Leptolyngbya sp.	'hensonii'	WP_075596736.1	CrhR
	Leptolyngbya sp.	'hensonii'	WP_075601042.1	RhlE
	Leptolyngbya sp.	Heron Island J	WP_023075084.1	RhlE
	Leptolyngbya sp.	Heron Island J	WP_023073685.1	CrhR
	Leptolyngbya sp.	Heron Island J	WP_036052321.1	CsdA
	Leptolyngbya sp.	JSC-1	WP_036003541.1	CrhR
	Leptolyngbya sp.	KIOST-1	WP_035986653.1	RhlE
	Leptolyngbya sp.	KIOST-1	WP_035986580.1	CrhR
	Leptolyngbya sp.	NIES-2104	WP_058994620.1	CrhR
	Leptolyngbya sp.	NIES-3755	WP_068384456.1	CrhR
	Leptolyngbya sp.	O-77	BAU42382.1	CrhR
	Leptolyngbya sp.	O-77	BAU44142.1	RhlE
	Leptolyngbya sp.	PCC 6406	WP_008312463.1	RhlE
	Leptolyngbya sp.	PCC 7375	WP_006514332.1	RhlE
	Leptolyngbya sp.	PCC 7375	WP_006515861.1	CrhR
	Leptolyngbya sp.	PCC 7375	WP_006517045.1	CsdA

Order	Species	Strain	Accession Number	Group
Synechococcales				
	Leptolyngbya sp.	PCC 7376	WP_015132458.1	RhlE
	Leptolyngbya sp.	PCC 7376	WP_015135334.1	CrhR
	Leptolyngbya valderiana	BDU 20041 (a)	OAB57648.1	No group
	Leptolyngbya valderiana	BDU 20041 (b)	WP_063718621.1	No group
	Limnothrix rosea	IAM M-220	WP_075890464.1	RhlE
	Limnothrix rosea	IAM M-220	WP_075892628.1	CrhR
	Limnothrix sp.	CACIAM 69d	OKY70165.1	CrhR
	Limnothrix sp.	P13C2	OCQ91779.1	CrhR
	Neosynechococcus sphagnicola	sy1	WP_052128427.1	RhlE
	Neosynechococcus sphagnicola	sy1	WP_052128892.1	CrhR
	Nodosilinea nodulosa	PCC 7104	WP_017300039.1	RhlE
	Nodosilinea nodulosa	PCC 7104	WP_017300013.1	CrhR
	Phormidesmis priestleyi	Ana	KPQ37420.1	RhlE
	Phormidesmis priestleyi	Ana	KPQ34081.1	CrhR
	Phormidesmis priestleyi	Ana	KPQ31693.1	CsdA
	Phormidesmis priestleyi	BC1401	WP_068814569.1	CrhR
	Phormidesmis priestleyi	ULC007	WP_073069542.1	CrhR
	Phormidesmis priestleyi	ULC007	WP_073074629.1	RhlE
	Prochlorococcus marinus	AS9601	WP_011818638.1	CsdA
	Prochlorococcus marinus	GP2	WP_032524576.1	CsdA
	Prochlorococcus marinus	MIT 1312	KZR62459.1	CsdA
	Prochlorococcus marinus	MIT 1313	KZR69712.1	CsdA
	Prochlorococcus marinus	MIT 1320	KZR74671.1	CsdA
	Prochlorococcus marinus	MIT 1323	KZR76670.1	CsdA
	Prochlorococcus marinus	MIT 1342	KZR84025.1	CsdA
	Prochlorococcus marinus	MIT 9107	WP_032514218.1	CsdA
	Prochlorococcus marinus	MIT 9201	WP_032522590.1	CsdA
	Prochlorococcus marinus	MIT 9202	WP_002807683.1	CsdA
	Prochlorococcus marinus	MIT 9211	WP_012195637.1	CsdA
	Prochlorococcus marinus	MIT 9215	WP_012007924.1	CsdA
	Prochlorococcus marinus	MIT 9301	WP_011863159.1	CsdA
	Prochlorococcus marinus	MIT 9302	WP_032527473.1	CsdA
	Prochlorococcus marinus	MIT 9303	ABM77716.1	CsdA
	Prochlorococcus marinus	MIT 9312	WP_011376662.1	CsdA
	Prochlorococcus marinus	MIT 9313	CAE21258.1	CsdA
	Prochlorococcus marinus	MIT 9314	WP_032515082.1	CsdA
	Prochlorococcus marinus	MIT 9321	WP_032516671.1	CsdA
	Prochlorococcus marinus	MIT 9322	WP_032518542.1	CsdA
	Prochlorococcus marinus	MIT 9515	WP_011820499.1	CsdA
	Prochlorococcus marinus	NATL1A	WP_011824061.1	CsdA
	Prochlorococcus marinus	NATL2A	WP_011294736.1	CsdA
	Prochlorococcus marinus	PAC1	WP_036906556.1	CsdA
	Prochlorococcus marinus	SB	WP_032519145.1	CsdA
	Prochlorococcus marinus	SCGC AAA795-F05	WP_075508085.1	CsdA
	Prochlorococcus marinus	SCGC AAA795-I15	WP_075448480.1	CsdA
	Prochlorococcus marinus	SCGC AAA795-J16	WP_075487375.1	CsdA
	Prochlorococcus marinus	SCGC AAA795-M23	WP_075438860.1	CsdA
	Prochlorococcus marinus subsp. marinus	CCMP1375	WP_011125246.1	CsdA
	Prochlorococcus marinus subsp. pastoris	CCMP1986	WP_011132734.1	CsdA
	Prochlorococcus sp.	HOT208_60m_805A16	WP_079293733.1	CsdA
	Prochlorococcus sp.	HOT208_60m_808G21	WP_079292895.1	CsdA

Order	Species	Strain	Accession Number	Group
Synechococcales				
	Prochlorococcus sp.	HOT208_60m_808M21	WP_079339458.1	CsdA
	Prochlorococcus sp.	HOT208_60m_810B23	WP_079300013.1	CsdA
	Prochlorococcus sp.	HOT208_60m_813B04	WP_079331862.1	CsdA
	Prochlorococcus sp.	HOT208_60m_813E23	WP_079334503.1	CsdA
	Prochlorococcus sp.	HOT208_60m_813G15	WP_079322771.1	CsdA
	Prochlorococcus sp.	HOT208_60m_813I02	WP_079330881.1	CsdA
	Prochlorococcus sp.	HOT208_60m_813O14	WP_079317072.1	CsdA
	Prochlorococcus sp.	HOT212_60m_824E10	WP_079342754.1	CsdA
	Prochlorococcus sp.	MIT 0601	KGG12263.1	CsdA
	Prochlorococcus sp.	MIT 0602	WP_036917918.1	CsdA
	Prochlorococcus sp.	MIT 0604	WP_042850581.1	CsdA
	Prochlorococcus sp.	MIT 0701	KGG25182.1	CsdA
	Prochlorococcus sp.	MIT 0801	WP_038653462.1	CsdA
	Prochlorococcus sp.	MIT 1303	KZR65207.1	CsdA
	Prochlorococcus sp.	MIT 1306	KZR62829.1	CsdA
	Prochlorococcus sp.	RS50	WP_077142451.1	CsdA
	Prochlorococcus sp.	SS52	WP_036974731.1	CsdA
	Pseudanabaena biceps	PCC 7429	WP_009629066.1	CrhR
	Pseudanabaena biceps	PCC 7429	WP_009629206.1	RhlE
	Pseudanabaena sp.	PCC 6802	WP_019503121.1	CrhR
	Pseudanabaena sp.	PCC 7367	WP_015166541.1	CrhR
	Pseudanabaena sp.	Roaring Creek	WP_055074499.1	CrhR
	Pseudanabaena sp.	Roaring Creek	WP_055074844.1	RhlE
	Synechococcus sp.	BL107	WP_050749884.1	RhlE
	Synechococcus sp.	BL107	WP_009789521.1	CsdA
	Synechococcus sp.	CB0101	WP_050778783.1	RhlE
	Synechococcus sp.	CB0101	WP_043716891.1	CsdA
	Synechococcus sp.	CB0205	WP_029626348.1	RhlE
	Synechococcus sp.	CB0205	WP_029626387.1	CsdA
	Synechococcus sp.	CC9311	WP_011619228.1	RhlE
	Synechococcus sp.	CC9311	WP_011618985.1	CsdA
	Synechococcus sp.	CC9605	ABB35397.1	CsdA
	Synechococcus sp.	CC9616	WP_028951803.1	CsdA
	Synechococcus sp.	CC9902	WP_011360193.1	CsdA
	Synechococcus sp.	CC9902	WP_071818395.1	RhlE
	Synechococcus sp.	KORDI-49	WP_043691566.1	CsdA
	Synechococcus sp.	KORDI-52	WP_038557033.1	CsdA
	Synechococcus sp.	KORDI-100	AII43180.1	CsdA
	Synechococcus sp.	MIT S9504	KZR88066.1	RhlE
	Synechococcus sp.	MIT S9504	WP_067325214.1	CsdA
	Synechococcus sp.	MIT S9508	WP_067097210.1	RhlE
	Synechococcus sp.	MIT S9508	WP_067096793.1	CsdA
	Synechococcus sp.	MIT S9509	WP_066905108.1	CsdA
	Synechococcus sp.	NIES-970	BAW96345.1	RhlE
	Synechococcus sp.	NIES-970	BAW95895.1	CrhR
	Synechococcus sp.	NKBG15041c	WP_024544561.1	RhlE
	Synechococcus sp.	NKBG15041c	WP_024544991.1	CrhR
	Synechococcus sp.	PCC 7002	WP_012306248.1	CrhR
	Synechococcus sp.	PCC 7003	WP_065713301.1	CrhR
	Synechococcus sp.	PCC 7335	WP_038016552.1	RhlE
	Synechococcus sp.	PCC 7335	WP_006457592.1	CrhR

Order	Species	Strain	Accession Number	Group
Synechococcales				
	Synechococcus sp.	PCC 7335	WP_006457666.1	CsdA
	Synechococcus sp.	PCC 7336	WP_017325424.1	CsdA
	Synechococcus sp.	PCC 7502	WP_015169589.1	CrhR
	Synechococcus sp.	RCC307	WP_011935977.1	CsdA
	Synechococcus sp.	RS9916	WP_007097992.1	RhlE
	Synechococcus sp.	RS9916	WP_038023305.1	CsdA
	Synechococcus sp.	RS9917	WP_050752552.1	RhlE
	Synechococcus sp.	RS9917	WP_007100168.1	CsdA
	Synechococcus sp.	SynAce01	WP_071800114.1	RhlE
	Synechococcus sp.	SynAce01	WP_071799904.1	CsdA
	Synechococcus sp.	Tous	OON11948.1	CsdA
	Synechococcus sp.	Tous	OON11565.1	RhlE
	Synechococcus sp.	WH 5701	WP_050751433.1	CsdA
	Synechococcus sp.	WH 5701	WP_006170577.1	RhlE
	Synechococcus sp.	WH 7803	WP_050815880.1	RhlE
	Synechococcus sp.	WH 7803	WP_011933414.1	CsdA
	Synechococcus sp.	WH 7805	EAR18874.1	RhlE
	Synechococcus sp.	WH 7805	WP_006041683.1	CsdA
	Synechococcus sp.	WH 8016	WP_038013123.1	RhlE
	Synechococcus sp.	WH 8016	WP_006852341.1	CsdA
	Synechococcus sp.	WH 8020	WP_048348119.1	RhlE
	Synechococcus sp.	WH 8020	WP_048346274.1	CsdA
	Synechococcus sp.	WH 8102	WP_011127785.1	CsdA
	Synechococcus sp.	WH 8103	WP_049691925.1	CsdA
	Synechococcus sp.	WH 8109	AHF63353.1	CsdA
	Synechocystis sp.	PCC 6714	AIE75077.1	CrhR
	Synechocystis sp.	PCC 6803	BAA10556.1	CrhR
	Synechocystis sp.	PCC 7509	WP_009633465.1	RhlE
	Synechocystis sp.	PCC 7509	WP_009631343.1	CrhR
Unclassified				
	Cyanobacteria bacterium	13_1_20CM_4_61_6	OLE96526.1	No group
	cyanobacterium endosymbiont of *Epithemia turgida*		WP_044107193.1	CrhR
Enterobacterales				
	Escherichia coli	K-12	WP_001295553.1	CsdA
	Escherichia coli	K-12	WP_000123737.1	DbpA
	Escherichia coli	K-12	WP_000047499.1	RhlB
	Escherichia coli	K-12	WP_000007101.1	RhlE
	Escherichia coli	K-12	WP_000219193.1	SrmB

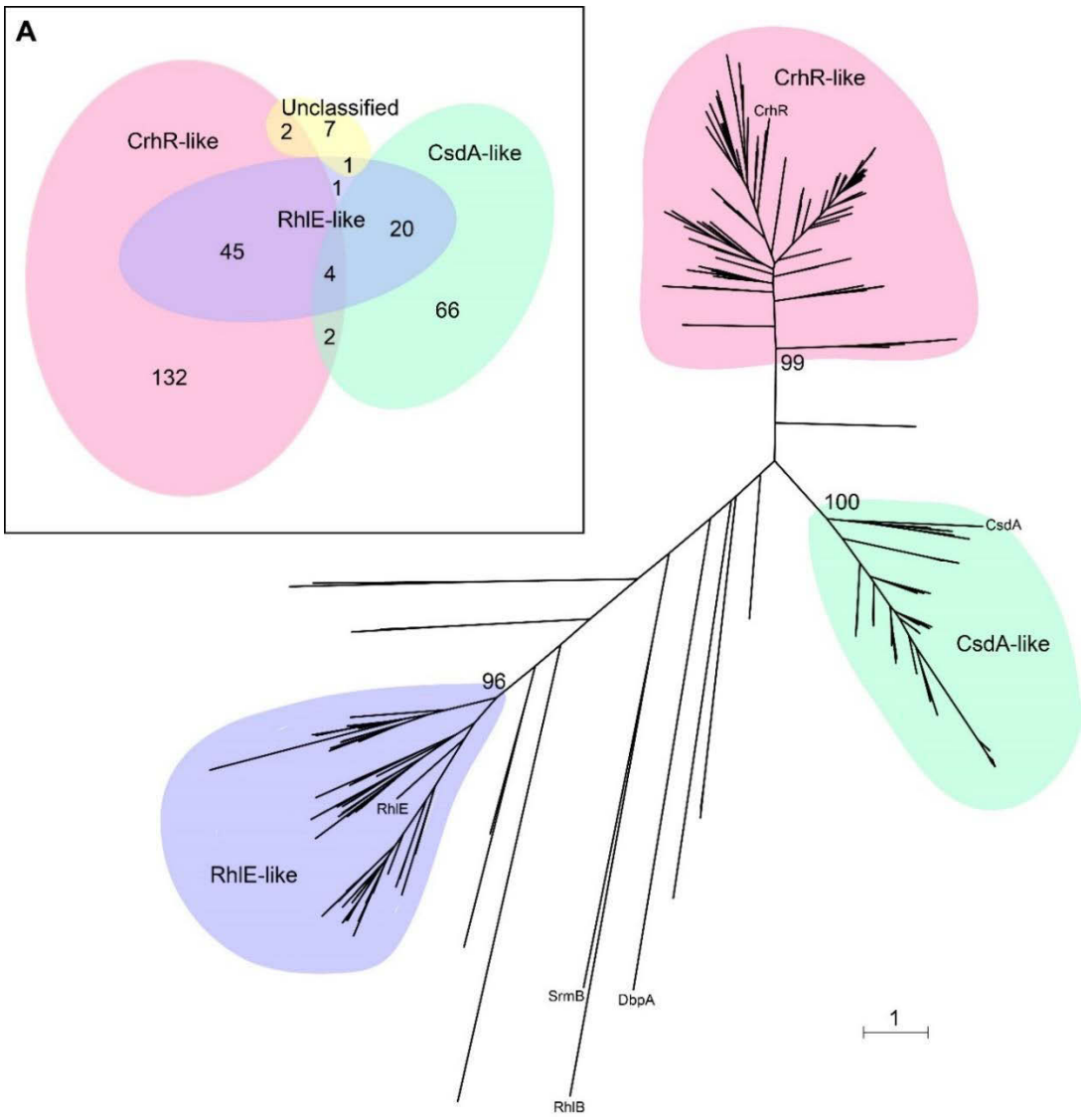

Figure 5.1: Cyanobacterial DEAD-box proteins cluster into three clades.[19]

The maximum likelihood tree shows the 362 cyanobacterial DEAD-box proteins form three major groups with bootstrap values ≥95%, corresponding to CsdA-like and RhlE-like proteins, and a clade unique to cyanobacteria, CrhR-like proteins, named for the sole DEAD-box RNA helicase encoded in the genome of *Synechocystis* sp. PCC 6803. Bootstrap values at the root of each clade, as well as the positions of the 5 DEAD-box proteins of *Escherichia coli* and CrhR from *Synechocystis* sp. PCC 6803, are indicated. The distribution of the DEAD-box protein clades identified in the 280 cyanobacterial strains used in the analysis is represented by the Euler diagram shown in inset panel (A).

[19] This analysis was inspired by a preliminary phylogenetic analysis by J. Georg and W.R. Hess (166) that included 72 cyanobacterial DEAD-box RNA helicases.

5.4.2 CrhR-like proteins are conserved across cyanobacterial diversity

The maximum-likelihood tree of the cyanobacterial DEAD-box RNA helicases was also visualized with the species, strain and order of the cyanobacteria encoding each protein indicated (Figure 5.2). CrhR-like proteins occur in every order of cyanobacteria that encode DEAD-box proteins except *Gloeobacteriales* (Figure 5.2), the oldest branching extant group of cyanobacteria (363). This genera represents a unique branch of cyanobacteria that lack thylakoid membranes, with photosynthesis occurring in the cytoplasmic membrane (9). While *Gloeobacter violacius* PCC 7421 and *Gloeobacter kilaueensis* JS1 still encode DEAD-box proteins, only one of the *Gloeobacter* proteins clusters weakly with any of the three cyanobacterial DEAD-box helicase subfamilies defined in this chapter. Conservation of the CrhR-like helicases throughout the diversity of cyanobacteria that evolved following branching from the *Gloeobacterales* and *Gloeomargaritales*, and absence of these proteins from organisms other than cyanobacteria, indicates that it is likely that the ancestral CrhR-like protein arose early in the radiation of the cyanobacterial crown group.

Conservation of the CrhR-like helicases in cyanobacteria can also be examined by looking at the gene neighbourhood of the helicase. In *Synechocystis* sp. PCC 6803, *crhR* is expressed from a dicistronic operon with the gene for the ribosomal protein S12 methylthiotransferase *rimO* (Chapter 3). Of the 185 cyanobacterial strains that encode CrhR-like helicases in this study, only 19 (10.3%) do not preserve the synteny of the *rimO-crhR* operon from *Synechocystis* (Figure 5.3). Many strains of cyanobacteria conserve additional genes in the genetic neighborhood of *crhR* (Figure 5.3), with 62.7% of strains encoding a vitamin K epoxide reductase (*VKOR*) and photosystem I stabilizing protein (*btpA*) upstream of the *rimO-crhR* operon. Of those, 57.7% also encode a diguanylate cyclase (*wspR*), L-aspartate oxidase (*nadB*) and photosystem II complex extrinsic protein (*psbU*) further upstream. These proteins have roles in photosynthesis, membrane protein stability, protein folding and cellular energetics. The strong conservation of the *rimO-crhR* gene pair, as well as upstream genes in many strains, supports an early acquisition of the CrhR-like proteins in cyanobacteria. Maintenance of the *rimO-crhR* operon structure throughout cyanobacterial diversity also intimates that

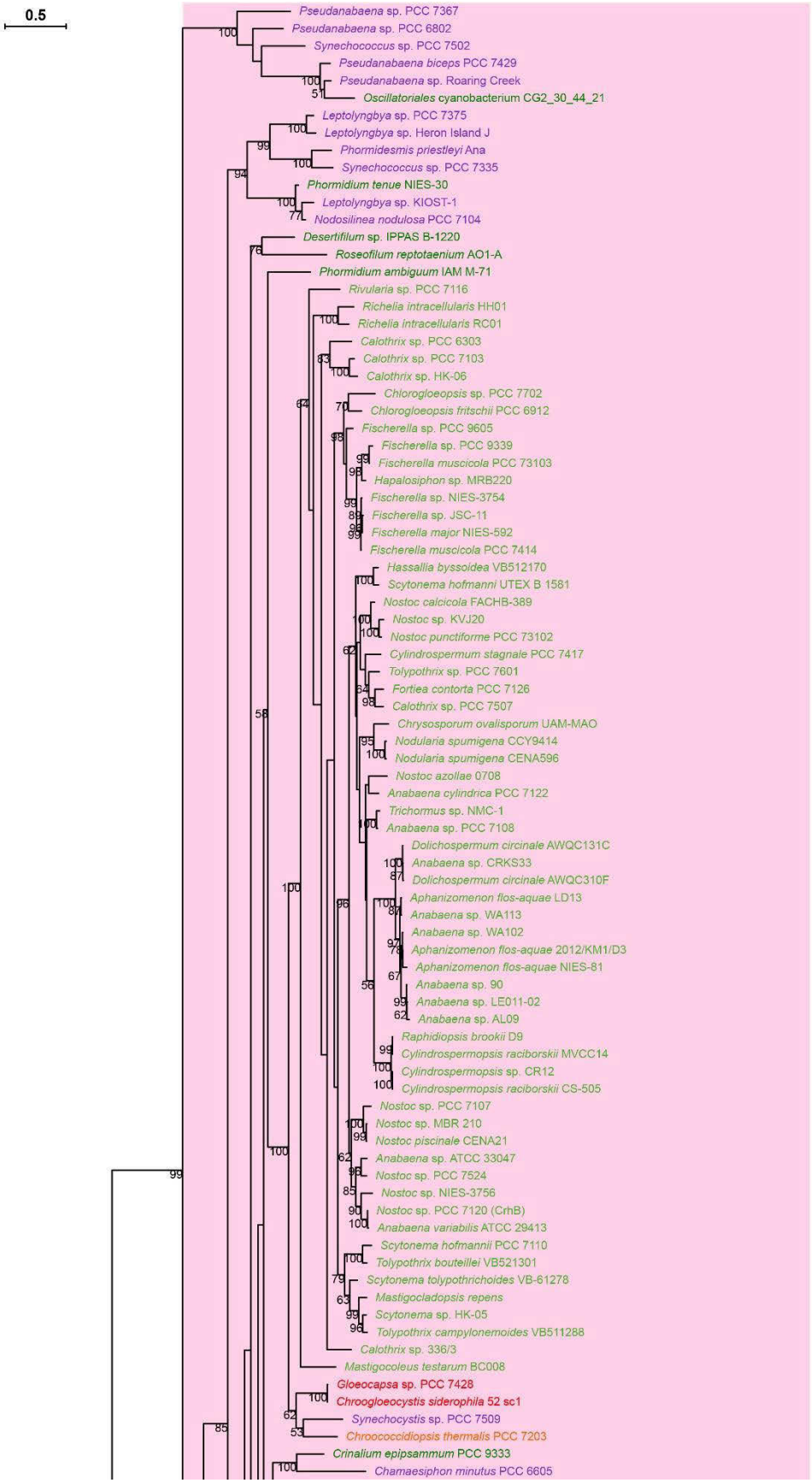
0.5
Pseudanabaena sp. PCC 7367
Pseudanabaena sp. PCC 6802
Synechococcus sp. PCC 7502
Pseudanabaena biceps PCC 7429
Pseudanabaena sp. Roaring Creek
Oscillatoriales cyanobacterium CG2_30_44_21
Leptolyngbya sp. PCC 7375
Leptolyngbya sp. Heron Island J
Phormidesmis priestleyi Ana
Synechococcus sp. PCC 7335
Phormidium tenue NIES-30
Leptolyngbya sp. KIOST-1
Nodosilinea nodulosa PCC 7104
Desertifilum sp. IPPAS B-1220
Roseofilum reptotaenium AO1-A
Phormidium ambiguum IAM M-71
Rivularia sp. PCC 7116
Richelia intracellularis HH01
Richelia intracellularis RC01
Calothrix sp. PCC 6303
Calothrix sp. PCC 7103
Calothrix sp. HK-06
Chlorogloeopsis sp. PCC 7702
Chlorogloeopsis fritschii PCC 6912
Fischerella sp. PCC 9605
Fischerella sp. PCC 9339
Fischerella muscicola PCC 73103
Hapalosiphon sp. MRB220
Fischerella sp. NIES-3754
Fischerella sp. JSC-11
Fischerella major NIES-592
Fischerella muscicola PCC 7414
Hassallia byssoidea VB512170
Scytonema hofmanni UTEX B 1581
Nostoc calcicola FACHB-389
Nostoc sp. KVJ20
Nostoc punctiforme PCC 73102
Cylindrospermum stagnale PCC 7417
Tolypothrix sp. PCC 7601
Fortiea contorta PCC 7126
Calothrix sp. PCC 7507
Chrysosporum ovalisporum UAM-MAO
Nodularia spumigena CCY9414
Nodularia spumigena CENA596
Nostoc azollae 0708
Anabaena cylindrica PCC 7122
Trichormus sp. NMC-1
Anabaena sp. PCC 7108
Dolichospermum circinale AWQC131C
Anabaena sp. CRKS33
Dolichospermum circinale AWQC310F
Aphanizomenon flos-aquae LD13
Anabaena sp. WA113
Anabaena sp. WA102
Aphanizomenon flos-aquae 2012/KM1/D3
Aphanizomenon flos-aquae NIES-81
Anabaena sp. 90
Anabaena sp. LE011-02
Anabaena sp. AL09
Raphidiopsis brookii D9
Cylindrospermopsis raciborskii MVCC14
Cylindrospermopsis sp. CR12
Cylindrospermopsis raciborskii CS-505
Nostoc sp. PCC 7107
Nostoc sp. MBR 210
Nostoc piscinale CENA21
Anabaena sp. ATCC 33047
Nostoc sp. PCC 7524
Nostoc sp. NIES-3756
Nostoc sp. PCC 7120 (CrhB)
Anabaena variabilis ATCC 29413
Scytonema hofmannii PCC 7110
Tolypothrix bouteillei VB521301
Scytonema tolypothrichoides VB-61278
Mastigocladopsis repens
Scytonema sp. HK-05
Tolypothrix campylonemoides VB511288
Calothrix sp. 336/3
Mastigocoleus testarum BC008
Gloeocapsa sp. PCC 7428
Chroogloeocystis siderophila 52 sc1
Synechocystis sp. PCC 7509
Chroococcidiopsis thermalis PCC 7203
Crinalium epipsammum PCC 9333
Chamaesiphon minutus PCC 6605

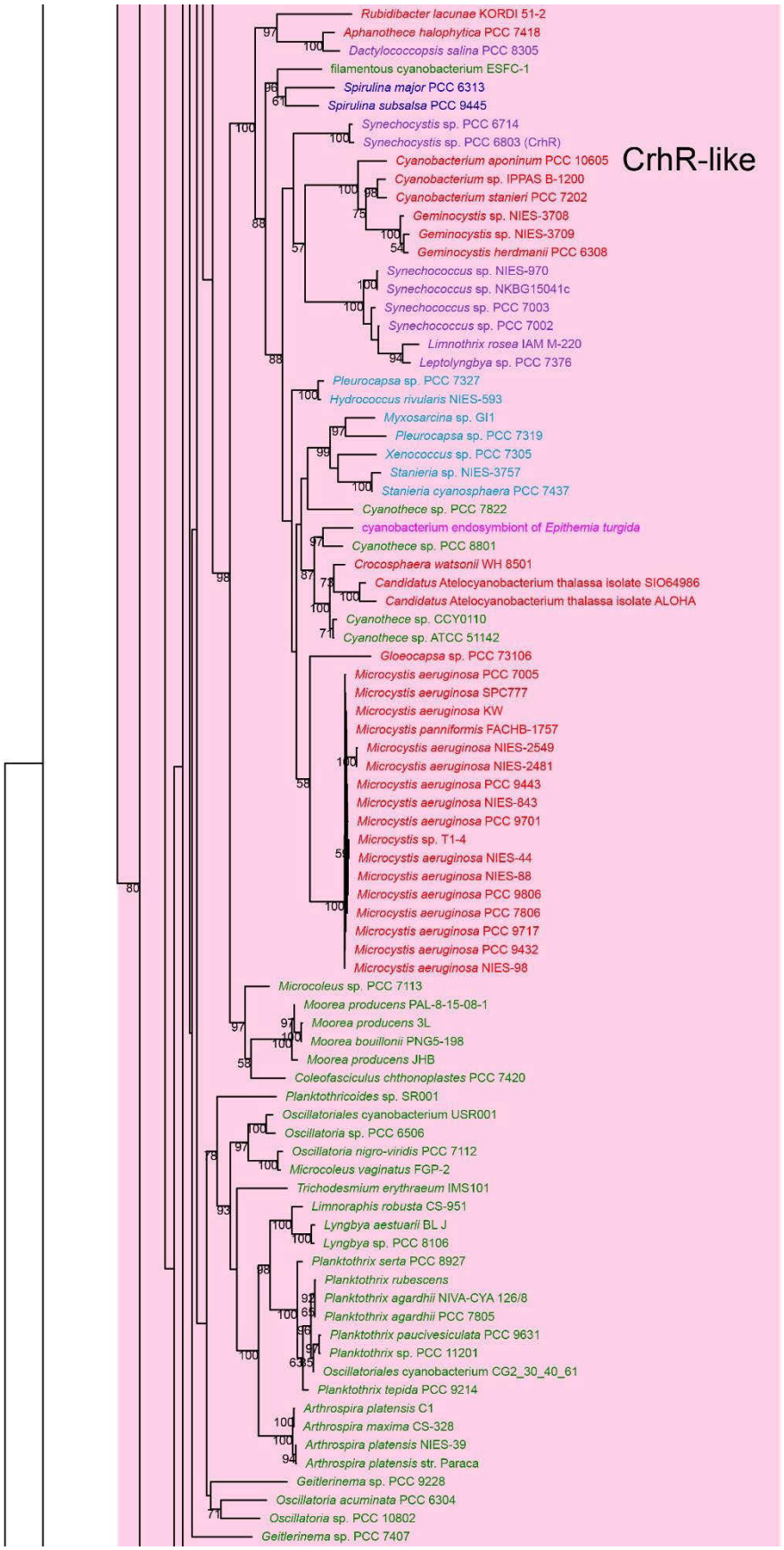
CrhR-like
Rubidibacter lacunae KORDI 51-2
Aphanothece halophytica PCC 7418
Dactylococcopsis salina PCC 8305
filamentous cyanobacterium ESFC-1
Spirulina major PCC 6313
Spirulina subsalsa PCC 9445
Synechocystis sp. PCC 6714
Synechocystis sp. PCC 6803 (CrhR)
Cyanobacterium aponinum PCC 10605
Cyanobacterium sp. IPPAS B-1200
Cyanobacterium stanieri PCC 7202
Geminocystis sp. NIES-3708
Geminocystis sp. NIES-3709
Geminocystis herdmanii PCC 6308
Synechococcus sp. NIES-970
Synechococcus sp. NKBG15041c
Synechococcus sp. PCC 7003
Synechococcus sp. PCC 7002
Limnothrix rosea IAM M-220
Leptolyngbya sp. PCC 7376
Pleurocapsa sp. PCC 7327
Hydrococcus rivularis NIES-593
Myxosarcina sp. GI1
Pleurocapsa sp. PCC 7319
Xenococcus sp. PCC 7305
Stanieria sp. NIES-3757
Stanieria cyanosphaera PCC 7437
Cyanothece sp. PCC 7822
cyanobacterium endosymbiont of Epithemia turgida
Cyanothece sp. PCC 8801
Crocosphaera watsonii WH 8501
Candidatus Atelocyanobacterium thalassa isolate SIO64986
Candidatus Atelocyanobacterium thalassa isolate ALOHA
Cyanothece sp. CCY0110
Cyanothece sp. ATCC 51142
Gloeocapsa sp. PCC 73106
Microcystis aeruginosa PCC 7005
Microcystis aeruginosa SPC777
Microcystis aeruginosa KW
Microcystis panniformis FACHB-1757
Microcystis aeruginosa NIES-2549
Microcystis aeruginosa NIES-2481
Microcystis aeruginosa PCC 9443
Microcystis aeruginosa NIES-843
Microcystis aeruginosa PCC 9701
Microcystis sp. T1-4
Microcystis aeruginosa NIES-44
Microcystis aeruginosa NIES-88
Microcystis aeruginosa PCC 9806
Microcystis aeruginosa PCC 7806
Microcystis aeruginosa PCC 9717
Microcystis aeruginosa PCC 9432
Microcystis aeruginosa NIES-98
Microcoleus sp. PCC 7113
Moorea producens PAL-8-15-08-1
Moorea producens 3L
Moorea bouillonii PNG5-198
Moorea producens JHB
Coleofasciculus chthonoplastes PCC 7420
Planktothricoides sp. SR001
Oscillatoriales cyanobacterium USR001
Oscillatoria sp. PCC 6506
Oscillatoria nigro-viridis PCC 7112
Microcoleus vaginatus FGP-2
Trichodesmium erythraeum IMS101
Limnoraphis robusta CS-951
Lyngbya aestuarii BL J
Lyngbya sp. PCC 8106
Planktothrix serta PCC 8927
Planktothrix rubescens
Planktothrix agardhii NIVA-CYA 126/8
Planktothrix agardhii PCC 7805
Planktothrix paucivesiculata PCC 9631
Planktothrix sp. PCC 11201
Oscillatoriales cyanobacterium CG2_30_40_61
Planktothrix tepida PCC 9214
Arthrospira platensis C1
Arthrospira maxima CS-328
Arthrospira platensis NIES-39
Arthrospira platensis str. Paraca
Geitlerinema sp. PCC 9228
Oscillatoria acuminata PCC 6304
Oscillatoria sp. PCC 10802
Geitlerinema sp. PCC 7407

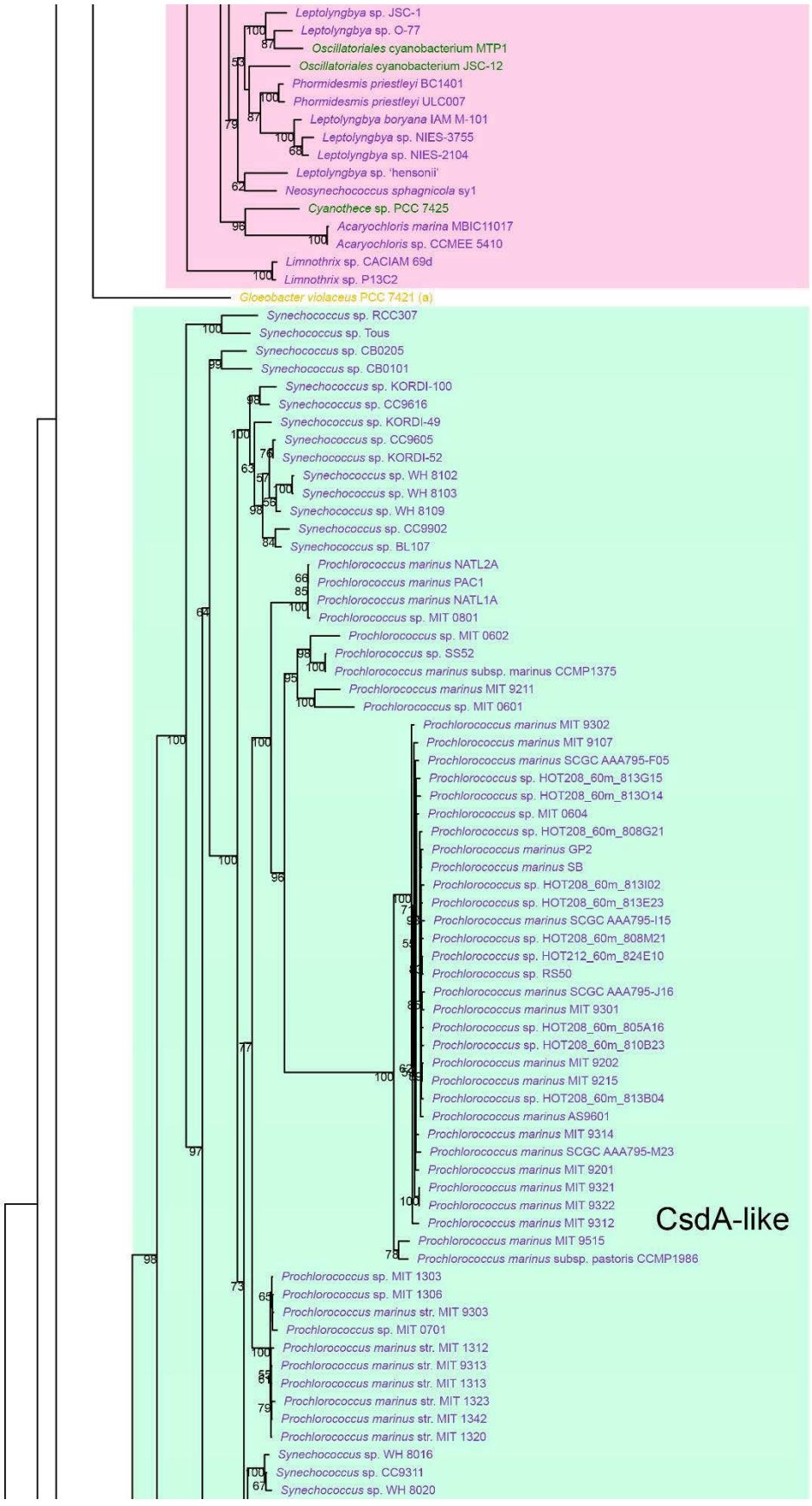
Leptolyngbya sp. JSC-1
Leptolyngbya sp. O-77
Oscillatoriales cyanobacterium MTP1
Oscillatoriales cyanobacterium JSC-12
Phormidesmis priestleyi BC1401
Phormidesmis priestleyi ULC007
Leptolyngbya boryana IAM M-101
Leptolyngbya sp. NIES-3755
Leptolyngbya sp. NIES-2104
Leptolyngbya sp. 'hensonii'
Neosynechococcus sphagnicola sy1
Cyanothece sp. PCC 7425
Acaryochloris marina MBIC11017
Acaryochloris sp. CCMEE 5410
Limnothrix sp. CACIAM 69d
Limnothrix sp. P13C2
Gloeobacter violaceus PCC 7421 (a)
Synechococcus sp. RCC307
Synechococcus sp. Tous
Synechococcus sp. CB0205
Synechococcus sp. CB0101
Synechococcus sp. KORDI-100
Synechococcus sp. CC9616
Synechococcus sp. KORDI-49
Synechococcus sp. CC9605
Synechococcus sp. KORDI-52
Synechococcus sp. WH 8102
Synechococcus sp. WH 8103
Synechococcus sp. WH 8109
Synechococcus sp. CC9902
Synechococcus sp. BL107
Prochlorococcus marinus NATL2A
Prochlorococcus marinus PAC1
Prochlorococcus marinus NATL1A
Prochlorococcus sp. MIT 0801
Prochlorococcus sp. MIT 0602
Prochlorococcus sp. SS52
Prochlorococcus marinus subsp. marinus CCMP1375
Prochlorococcus marinus MIT 9211
Prochlorococcus sp. MIT 0601
Prochlorococcus marinus MIT 9302
Prochlorococcus marinus MIT 9107
Prochlorococcus marinus SCGC AAA795-F05
Prochlorococcus sp. HOT208_60m_813G15
Prochlorococcus sp. HOT208_60m_813O14
Prochlorococcus sp. MIT 0604
Prochlorococcus sp. HOT208_60m_808G21
Prochlorococcus marinus GP2
Prochlorococcus marinus SB
Prochlorococcus sp. HOT208_60m_813I02
Prochlorococcus sp. HOT208_60m_813E23
Prochlorococcus marinus SCGC AAA795-I15
Prochlorococcus sp. HOT208_60m_808M21
Prochlorococcus sp. HOT212_60m_824E10
Prochlorococcus sp. RS50
Prochlorococcus marinus SCGC AAA795-J16
Prochlorococcus marinus MIT 9301
Prochlorococcus sp. HOT208_60m_805A16
Prochlorococcus sp. HOT208_60m_810B23
Prochlorococcus marinus MIT 9202
Prochlorococcus marinus MIT 9215
Prochlorococcus sp. HOT208_60m_813B04
Prochlorococcus marinus AS9601
Prochlorococcus marinus MIT 9314
Prochlorococcus marinus SCGC AAA795-M23
Prochlorococcus marinus MIT 9201
Prochlorococcus marinus MIT 9321
Prochlorococcus marinus MIT 9322
Prochlorococcus marinus MIT 9312
CsdA-like
Prochlorococcus marinus MIT 9515
Prochlorococcus marinus subsp. pastoris CCMP1986
Prochlorococcus sp. MIT 1303
Prochlorococcus sp. MIT 1306
Prochlorococcus marinus str. MIT 9303
Prochlorococcus sp. MIT 0701
Prochlorococcus marinus str. MIT 1312
Prochlorococcus marinus str. MIT 9313
Prochlorococcus marinus str. MIT 1313
Prochlorococcus marinus str. MIT 1323
Prochlorococcus marinus str. MIT 1342
Prochlorococcus marinus str. MIT 1320
Synechococcus sp. WH 8016
Synechococcus sp. CC9311
Synechococcus sp. WH 8020

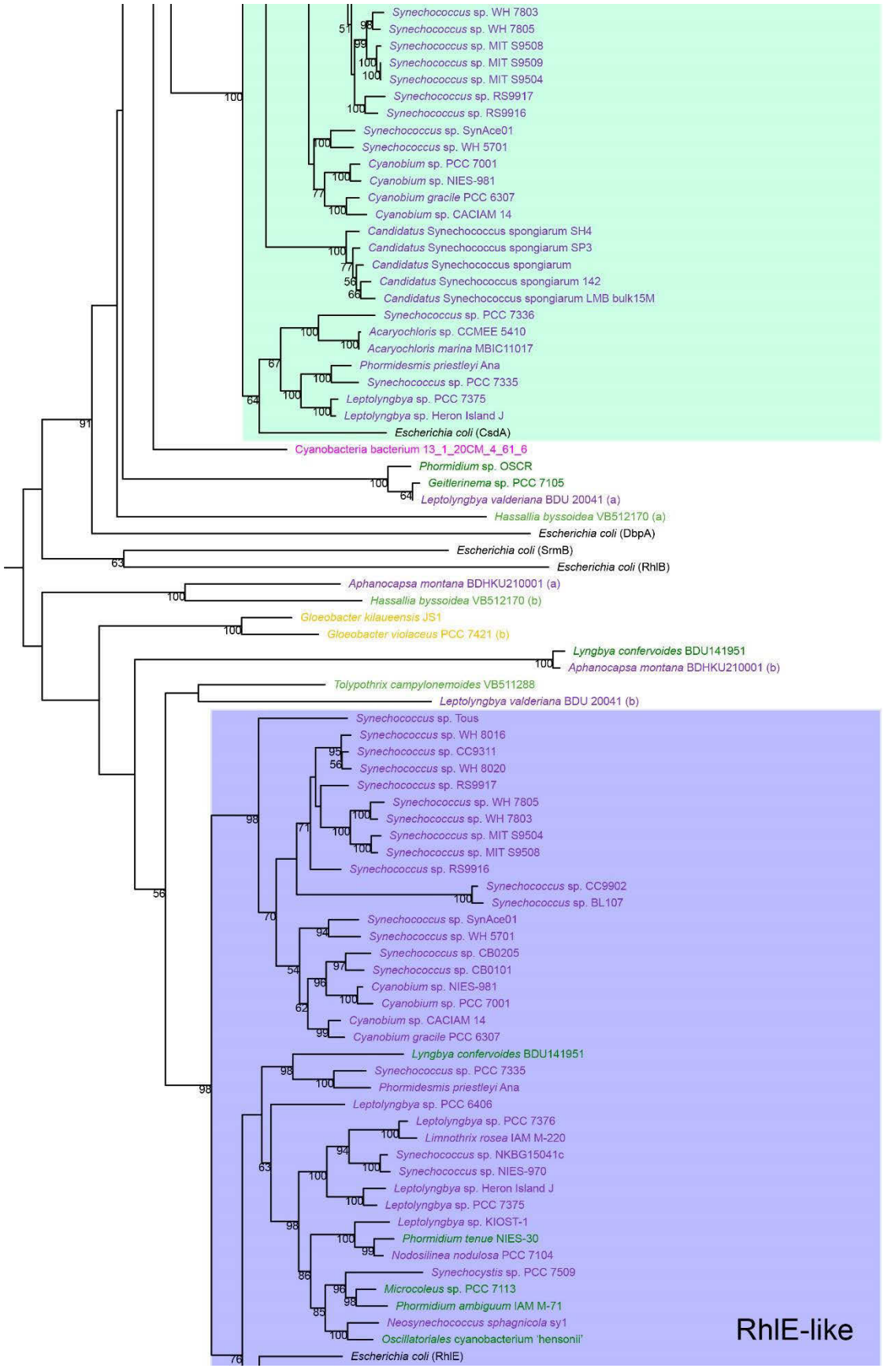
Synechococcus sp. WH 7803
Synechococcus sp. WH 7805
Synechococcus sp. MIT S9508
Synechococcus sp. MIT S9509
Synechococcus sp. MIT S9504
Synechococcus sp. RS9917
Synechococcus sp. RS9916
Synechococcus sp. SynAce01
Synechococcus sp. WH 5701
Cyanobium sp. PCC 7001
Cyanobium sp. NIES-981
Cyanobium gracile PCC 6307
Cyanobium sp. CACIAM 14
Candidatus Synechococcus spongiarum SH4
Candidatus Synechococcus spongiarum SP3
Candidatus Synechococcus spongiarum
Candidatus Synechococcus spongiarum 142
Candidatus Synechococcus spongiarum LMB bulk15M
Synechococcus sp. PCC 7336
Acaryochloris sp. CCMEE 5410
Acaryochloris marina MBIC11017
Phormidesmis priestleyi Ana
Synechococcus sp. PCC 7335
Leptolyngbya sp. PCC 7375
Leptolyngbya sp. Heron Island J
Escherichia coli (CsdA)
Cyanobacteria bacterium 13_1_20CM_4_61_6
Phormidium sp. OSCR
Geitlerinema sp. PCC 7105
Leptolyngbya valderiana BDU 20041 (a)
Hassallia byssoidea VB512170 (a)
Escherichia coli (DbpA)
Escherichia coli (SrmB)
Escherichia coli (RhlB)
Aphanocapsa montana BDHKU210001 (a)
Hassallia byssoidea VB512170 (b)
Gloeobacter kilaueensis JS1
Gloeobacter violaceus PCC 7421 (b)
Lyngbya confervoides BDU141951
Aphanocapsa montana BDHKU210001 (b)
Tolypothrix campylonemoides VB511288
Leptolyngbya valderiana BDU 20041 (b)
Synechococcus sp. Tous
Synechococcus sp. WH 8016
Synechococcus sp. CC9311
Synechococcus sp. WH 8020
Synechococcus sp. RS9917
Synechococcus sp. WH 7805
Synechococcus sp. WH 7803
Synechococcus sp. MIT S9504
Synechococcus sp. MIT S9508
Synechococcus sp. RS9916
Synechococcus sp. CC9902
Synechococcus sp. BL107
Synechococcus sp. SynAce01
Synechococcus sp. WH 5701
Synechococcus sp. CB0205
Synechococcus sp. CB0101
Cyanobium sp. NIES-981
Cyanobium sp. PCC 7001
Cyanobium sp. CACIAM 14
Cyanobium gracile PCC 6307
Lyngbya confervoides BDU141951
Synechococcus sp. PCC 7335
Phormidesmis priestleyi Ana
Leptolyngbya sp. PCC 6406
Leptolyngbya sp. PCC 7376
Limnothrix rosea IAM M-220
Synechococcus sp. NKBG15041c
Synechococcus sp. NIES-970
Leptolyngbya sp. Heron Island J
Leptolyngbya sp. PCC 7375
Leptolyngbya sp. KIOST-1
Phormidium tenue NIES-30
Nodosilinea nodulosa PCC 7104
Synechocystis sp. PCC 7509
Microcoleus sp. PCC 7113
Phormidium ambiguum IAM M-71
Neosynechococcus sphagnicola sy1
Oscillatoriales cyanobacterium 'hensonii'
Escherichia coli (RhlE)
RhlE-like

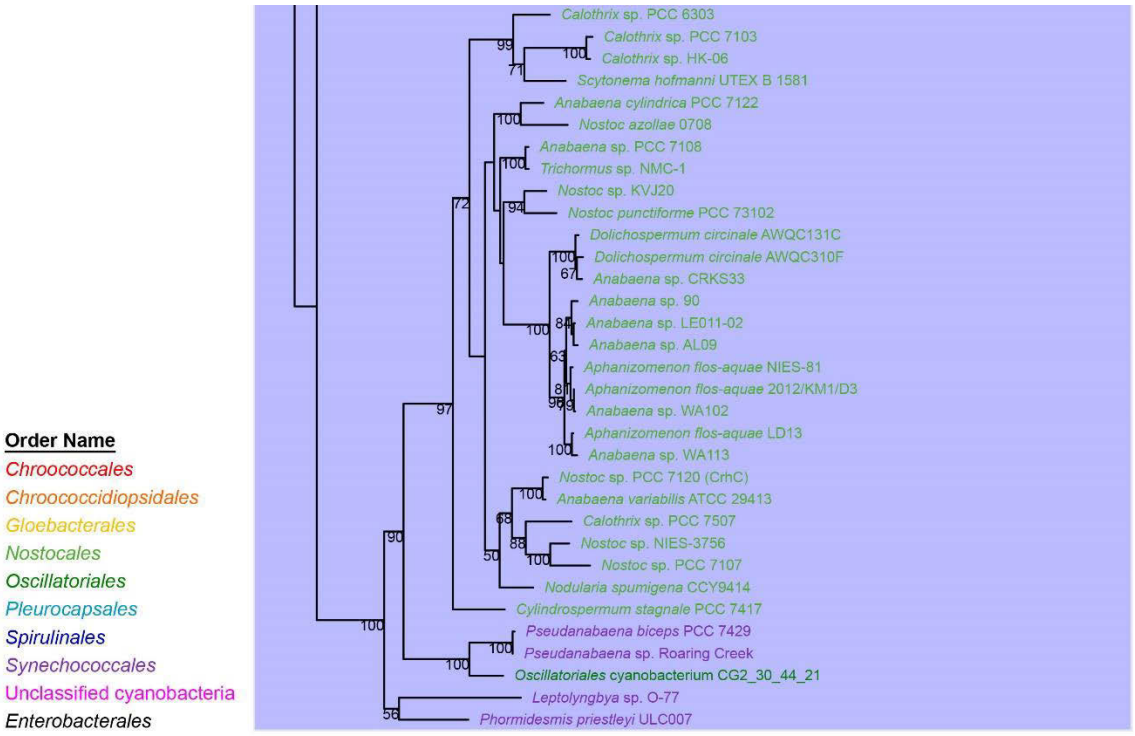

Figure 5.2: Maximum likelihood tree of cyanobacterial DEAD-box RNA helicase proteins.

The mid-point rooted maximum likelihood tree shows three major clades, corresponding to CrhR-like, CsdA-like and RhlE-like proteins. The DEAD-box proteins of *E. coli* (CsdA, DbpA, RhlB, RhlE and SrmB) are included to verify classification of the cyanobacterial proteins. The branches are scaled to show evolutionary distance with bootstrap values ≥ 50% shown at the nodes. The strain names are coloured to denote the common taxonomic orders.

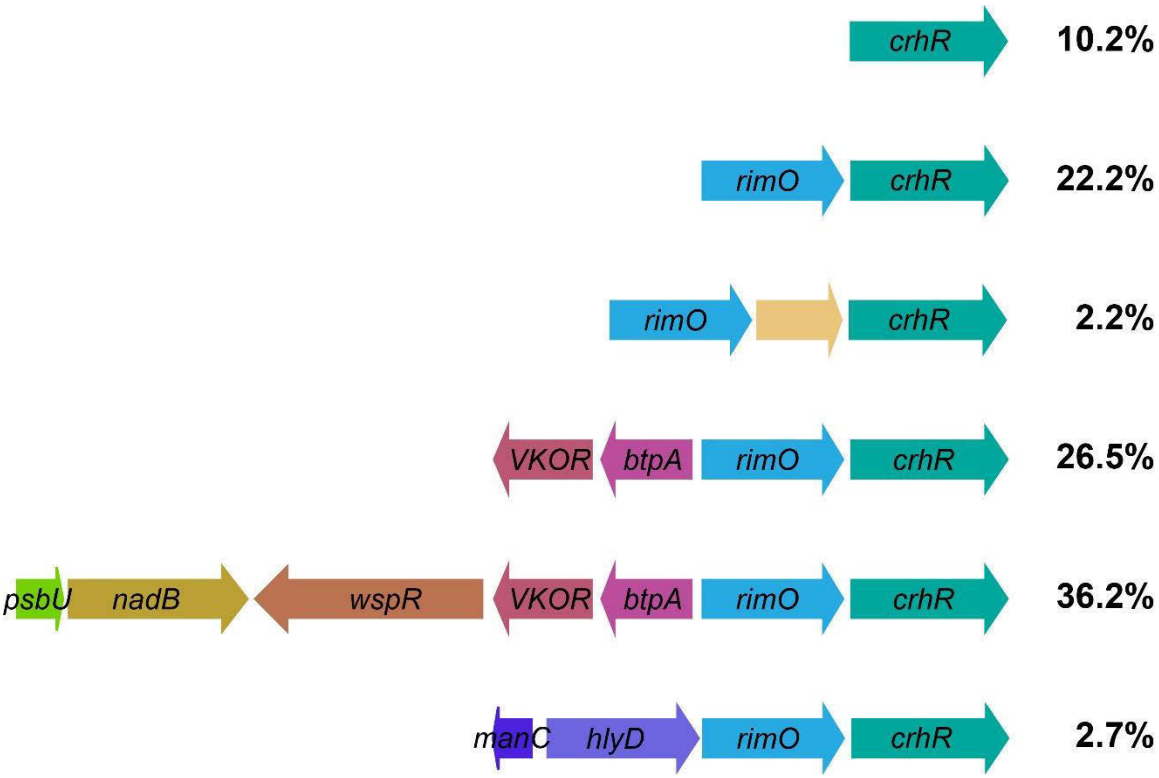

Figure 5.3: Conserved gene sequence surrounding CrhR-like DEAD box RNA helicases.

Gene synteny surrounding the DEAD-box RNA helicase in strains containing CrhR-like proteins. Percentages represent the relative proportion of cyanobacterial strains in this analysis possessing the indicated gene sequence surrounding CrhR. Functionally related genes have similar colours. The cutoff to be considered as a separate example of conserved gene context was conservation in 2% of the strains.

the functions of the RimO and CrhR proteins are likely related, as products of highly conserved gene pairs are typically functionally related and often physically interact (364).

5.4.3 A conserved sequence motif in the C-terminus of CrhR-like proteins characterizes the CrhR-like clade

The C-terminal extension in CrhR-like helicases extends 150-200 amino acids past the conserved helicase motif VI (HRIGR, see Figure 1.4). Within the C-terminal extension, a conserved sequence motif of 50 amino acids can be found in all CrhR-like helicases (Figure 5.4). This sequence motif is unique to cyanobacterial DEAD-box RNA helicases, with no other sequences containing this motif identified by either a search of the Pfam protein families database (358) or a search of the NCBI protein database by BLAST. The DEAD-box protein from *Gloeobacter violaceus* PCC 7421 (WP_011142503.1), the nearest branching protein to the CrhR-like group of DEAD-box proteins, also does not have the conserved CrhR sequence motif in its C-terminus; however, it does have shorter regions of sequence conservation with the CrhR-like proteins in the C-terminal extension (Figure 5.5). This was unexpected, as, other than proteins containing the DbpA RNA binding domain, sequence conservation in the C-terminal extension of DEAD-box RNA helicases is generally minimal (107). It is therefore likely that both the CrhR-like helicases and the DEAD-box protein from *Gloeobacter violaceus* PCC 7421 share a common ancestral protein, with evolution of the CrhR-specific C-terminal motif occurring after the divergence of *Gloeobacter* sp.

5.4.4 CsdA-like proteins are found in primarily unicellular strains of the order *Synechococcales*

Proteins of the CsdA-like subfamily are solely encoded in the order *Synechococcales*, primarily in unicellular strains, excepting three filamentous *Synechococcales* strains, *Leptolyngbya* sp. Heron Island J, *Leptolyngbya* sp. PCC 7375 and *Phormidesmis preistleyi* Ana. These three filamentous strains, as well as the unicellular *Synechococcus* sp. PCC 7335, are the only strains that encode DEAD-box proteins from all three subfamilies and will be discussed below. Other than the four strains encoding proteins from all three groups, CsdA-like proteins are only found in species of *Acarychloris,*

A

```
Cyanothece sp. ATCC 51142 ACB53784.1                          326 YIHRIGRTGRAGKTGTAISLVEPIDRRMVRQIEKRLRQKLETCKLPSRSQ 375
Cyanothece sp. CCY0110 WP_008276945.1                         326 YIHRIGRTGRAGKTGTAISLIEPIDRRMVRQIEKRLRQKLETCKLPSRSQ 375
Cyanothece sp. PCC 8801 ACK68200.1                            326 YIHRIGRTGRAGKTGTAISLVEPIDRRMIKQIERKLRQQLEICQIPSRSQ 375
Cyanothece sp. PCC 7822 WP_013323350.1                        326 YIHRIGRTGRAGKTGTAISLIEPIDRRMLRQIEHRVGHRLDVSQLPDRSL 375
Microcystis aeruginosa NIES-843 BAG02718.1                    326 YIHRIGRTGRAGKTGTAISLVEPIDRRLLRQIEQRLRQRLESSPIPSRTE 375
Synechococcus sp. PCC 7002 AAG43442.1                         326 YIHRIGRTGRAGKTGTAIALVEPSDRRLLRQIERRVKQSLKVSTIPSRTE 375
Synechocystis sp. PCC 6803 AGF52848.1                         329 YIHRIGRTGRAGKTGKAIALVEPIDRRLLRSIENRLKQQIEVCTIPNRSQ 378
Acaryochloris marina MBIC11017 WP_012162240.1                 326 YVHRIGRTGRAGNEGTAISLVHALDRWKLHEIEKHIRQEIPTLPTPTRSA 375
Cyanothece sp. PCC 7425 WP_012629831.1                        326 YVHRIGRTGRAGKTGIAVSLFQPLERHKLGQIERHIRQKLTVQDAPNRTQ 375
Synechococcus sp. PCC 7335 WP_006457592.1                     326 YVHRIGRTGRAGKEGRAVSIVMTLEKYKLSRIEKRFKKSVEYCKIPTQAQ 375
Arthrospira platensis NIES-39 BAI88967.1                      346 YVHRIGRTGRAGREGKAITLIQPIDRRKLRNIERHLRQTLSIQSIPKRAE 395
Lyngbya sp. PCC 8106 WP_039896992.1                           326 YVHRIGRTGRAGREGKAITLLQPMDRRKLRMIERHLRHNFTTLTIPKRSQ 375
Trichodesmium erythraeum IMS101 WP_044137765.1                333 YVHRIGRTGRAGREGTAISLIHPVDKRKLRLIERHLRQRLNTRSIPKRSQ 382
Coleofasciculus chthonoplastes PCC 7420 WP_006102098.1        326 YIHRIGRTGRAGKTGTAISLIQPFERRKLHQIERKVRQNLQVSRIPTRSQ 375
Anabaena variabilis ATCC 29413 WP_011317513.1                 326 YVHRIGRTGRAGKEGTAITLVQPFERRKQQIFERHVRQNWQLLSIPTRAQ 375
Nostoc sp. PCC 7120 WP_010995395.1                            326 YVHRIGRTGRAGKEGTAITLVQPFERRKQQIFERHVRQNWQLLSIPTRAQ 375
Nostoc punctiforme PCC 73102 WP_012410842.1                   326 YVHRIGRTGRAGKEGTAISLVQPFERRKQQTFERHNRQSWQLLSIPTRAQ 375
Nostoc azollae 0708 WP_013190002.1                            326 YVHRIGRTGRAGKEGTAISLVQPFERRKQQAFERHNRQNWQVLTIPTRAQ 375
Raphidiopsis brookii D9 WP_009343384.1                        327 YVHRIGRTGRAGKEGTAISLVQPFERRKQQAFERHNRQNWQVLSIPTRAQ 376
Cylindrospermopsis raciborskii CS-505 WP_006276327.1          327 YVHRIGRTGRAGKEGTAISLVQPFERRKQQAFERHNRQNWQVLSIPTRAQ 376

Cyanothece sp. ATCC 51142 ACB53784.1                          376 VEAKRLEKLQNEIKESLAGERMASFLPLVRELSDEYDPQAIAAAALQMIY 425
Cyanothece sp. CCY0110 WP_008276945.1                         376 VEAKRLEKLQNQIKESLAGERMASFLPLVRELSDEYDPQAIAAAALQMIY 425
Cyanothece sp. PCC 8801 ACK68200.1                            376 VESKRLEKLQRQIQESLAGERMASFLPIVRELSAEYDPQAIAAAALQMVY 425
Cyanothece sp. PCC 7822 WP_013323350.1                        376 VEAKRLSKLQTQVKETLAGERMASFLPLVRELSAEYDPLAIAAAALQMVY 425
Microcystis aeruginosa NIES-843 BAG02718.1                    376 VEAKRLAKLQNQLKEALSGERMASFLPLVRDLSEEYDPQAIAAAALQMIY 425
Synechococcus sp. PCC 7002 AAG43442.1                         376 VEAQRVTRLETQVREALAGERMASFLPIVKRLGDEYDPQAIAAAVLQMMY 425
Synechocystis sp. PCC 6803 AGF52848.1                         379 VEAKRIEKLQEQLKEALTGERMASFLPLVRELSDEYDAQAIAAAALQMIY 428
Acaryochloris marina MBIC11017 WP_012162240.1                 376 IEGRRLEKLTEELHSILTGERLASFLPTVSQLGEDYDTQTIAAAALQMAF 425
Cyanothece sp. PCC 7425 WP_012629831.1                        376 IAARRLERMKDQVRSALMGERMASFLPIVSQLSEEYDVQAIAAAALQLAF 425
Synechococcus sp. PCC 7335 WP_006457592.1                     376 IAARHLEKLQARVREAVTSERVASFLPIVSQLSEEYDIRTIAAAALQMAY 425
Arthrospira platensis NIES-39 BAI88967.1                      396 IEARYIDRLKDRVRDALAGERMASFLPIVSQLSEEYDPHAIAAAALQLAY 445
Lyngbya sp. PCC 8106 WP_039896992.1                           376 IEARYIERLKDKVLEALTGERMASFLPIVAQLGEEYEPHAIAAAALQMAY 425
Trichodesmium erythraeum IMS101 WP_044137765.1                383 IEARQLQKLQDKVRSALSGERMASFLPLISQLGKEYDPHAIAAAALQIAY 432
Coleofasciculus chthonoplastes PCC 7420 WP_006102098.1        376 IEARRLEKLQDELREALTGERMASFLPIVRELSEEYDPHAIAAAALQMVY 425
Anabaena variabilis ATCC 29413 WP_011317513.1                 376 IEARHILKLQEQVREALAGERLASFLPIVSELIEKYDAQAIAAAALQIAY 425
Nostoc sp. PCC 7120 WP_010995395.1                            376 IEARHILKLQEQVREALAGERLASFLPIVSELIEKYDAQAIAAAALQIAY 425
Nostoc punctiforme PCC 73102 WP_012410842.1                   376 IEARHILKLQEQVREALTGERLASFLPIVSELIEEYDAQAIAAAALQIAY 425
Nostoc azollae 0708 WP_013190002.1                            376 IEARHIKKLQEQVAEALTGERLASFLPIISELIEKYDAQAIAAAALQIAY 425
Raphidiopsis brookii D9 WP_009343384.1                        377 IEAKHIQKLKEQVSEALAGERLASFLPIISELTEKYDAQAIAAAALQLAY 426
Cylindrospermopsis raciborskii CS-505 WP_006276327.1          377 IEAKHIQKLKEQVSEALAGERLASFLPIISELTEKYDAQAIAAAALQLAY 426

Cyanothece sp. ATCC 51142 ACB53784.1                          426 DQDCP-DWMKTDWEVPES----TVPK--PVI-KRKGKY------NSNHSK 461
Cyanothece sp. CCY0110 WP_008276945.1                         426 DQDCP-DWMKTDWEVPES----TVPK--PII-KRKGKY---------NSNK 459
Cyanothece sp. PCC 8801 ACK68200.1                            426 DQDCP-NWMKTDWEVPEA----SVPK--PVI-KRKPSP------NNNGGK 461
Cyanothece sp. PCC 7822 WP_013323350.1                        426 DQDCP-NWMKTDWEVPKE----TAPK--PML-KQQRRY----------N 456
Microcystis aeruginosa NIES-843 BAG02718.1                    426 DQNCP-QWMKTDWEVPAA----TSSK--PVI-NKTPRS--------GGSK 459
Synechococcus sp. PCC 7002 AAG43442.1                         426 DNNSP-EWLNEDWEVPEV----NTKT--GLP-KPTKKG----GRSGRRSN 463
Synechocystis sp. PCC 6803 AGF52848.1                         429 DQSCP-HWMKSDWEVPEV----DFNK--PVL-RRGRNA--GGGQNKSGGG 468
Acaryochloris marina MBIC11017 WP_012162240.1                 426 DRYPAITANLDDWSSKNKNGGRSSRKAKPVL-NKRRS-------------- 461
Cyanothece sp. PCC 7425 WP_012629831.1                        426 DQNRP----------LPEV------PE--PAL-PVEPVL------------ 445
Synechococcus sp. PCC 7335 WP_006457592.1                     426 DQARP-THLRNEDHSDRK----PTPK--PKLLPSRRQSKEA---------- 459
Arthrospira platensis NIES-39 BAI88967.1                      446 DQTRPASIGRDDYEDDDD---AVSNK--PKL-IKRRRP------------ 477
Lyngbya sp. PCC 8106 WP_039896992.1                           426 DQTRP-NWEETDYPHEEE--VKSIPK--PKL-TKKRRS------------ 457
Trichodesmium erythraeum IMS101 WP_044137765.1                433 DETRP-AWMGLDYSQEEDEPMYETPK--PRL------------------ 460
Coleofasciculus chthonoplastes PCC 7420 WP_006102098.1        426 DHTQP-ELAAIEVDNKVE-------R--PKL-VKRRNN---------- 452
Anabaena variabilis ATCC 29413 WP_011317513.1                 426 DQTRP-AWLSTDAEIPEE--VASTPK--PKLGGKRREF---------SGD 461
Nostoc sp. PCC 7120 WP_010995395.1                            426 DQTRP-AWLSTDAEIPEE--VASTPK--PKLGGKRREF---------SGD 461
Nostoc punctiforme PCC 73102 WP_012410842.1                   426 DQTRP-AWLSSDVEIPQE--ESSAPK--PRL-GKRRES---------SSD 460
Nostoc azollae 0708 WP_013190002.1                            426 DQTRP-DWLQSGVDIPQE---EPSPK--PKL-NKHRDSGEYPRSGGGERE 468
Raphidiopsis brookii D9 WP_009343384.1                        427 DQTRP-AWLQNGVDIPVE---EPTPK--PKI-NKRRES------GDGNGV 463
Cylindrospermopsis raciborskii CS-505 WP_006276327.1          427 DQTRP-AWLQNGVDIPVE---EPTPK--PKI-NKRRES------SDGNGA 463

Cyanothece sp. ATCC 51142 ACB53784.1                          462 HNGNSNR--------GNRKIVTHQQSR---------------------- 480
Cyanothece sp. CCY0110 WP_008276945.1                         460 HNSNSNR--------GNRKIVSHQPGR---------------------- 478
Cyanothece sp. PCC 8801 ACK68200.1                            462 YNRRSQAPQRSGG--SDRKVVTHNHN---------------------- 485
Cyanothece sp. PCC 7822 WP_013323350.1                        457 KSGKPSKFEKSGRH-GDRKPVIQNQSR---------------------- 482
Microcystis aeruginosa NIES-843 BAG02718.1                    460 YPSKSNNRPS-----LDKKIVFQER---------------------- 479
Synechococcus sp. PCC 7002 AAG43442.1                         464 YKGSGGGYKGDRS--RGRRSYSSNHS---------------------- 487
Synechocystis sp. PCC 6803 AGF52848.1                         469 YQGKPGKPRRSS---GGRRSAYSDRQQ---------------------- 492
Acaryochloris marina MBIC11017 WP_012162240.1                 462 ----------------SNRSEISAST---------------------- 471
Cyanothece sp. PCC 7425 WP_012629831.1                        446 ----------------KQQRFNQKPVSR---------------------- 457
Synechococcus sp. PCC 7335 WP_006457592.1                     460 ----------------DVQKAAVEEGVR---------------------- 471
Arthrospira platensis NIES-39 BAI88967.1                      478 ------------------ASVSNNS---------------------- 484
Lyngbya sp. PCC 8106 WP_039896992.1                           458 ----------------RDSEPQNKSSVGSGN---------------- 472
Trichodesmium erythraeum IMS101 WP_044137765.1                461 ----------------KKQLPK---------------------- 466
Coleofasciculus chthonoplastes PCC 7420 WP_006102098.1        453 ----------------KSKESVTHNRSR---------------------- 464
Anabaena variabilis ATCC 29413 WP_011317513.1                 462 RGRSNWNKSDNNNSDDERRGTPKPKLRTSRRETSATPSNPKLGSPAARES 511
Nostoc sp. PCC 7120 WP_010995395.1                            462 RGRSNWNKSDNNNSDDERRGTPKPKLRTGRRETSATPSNPKLGSPAARES 511
Nostoc punctiforme PCC 73102 WP_012410842.1                   461 RPRSAWKSDSNNG--EERHSSPKPKLR-TSGHESSASPSKKIGSPTARES 507
Nostoc azollae 0708 WP_013190002.1                            469 RSRSSWSKSDNGG--DEGRGTPKPRLRTTTQRESSVTPSQKLGSHRE--- 513
Raphidiopsis brookii D9 WP_009343384.1                        464 GRGRSWSKSDYG---DESKPTPKPKLR---RREPSVSPSN---------- 497
Cylindrospermopsis raciborskii CS-505 WP_006276327.1          464 GRSRSWSKSDYG---DDSRPTPKPKLR---RREPSVSPSN---------- 497
```

B

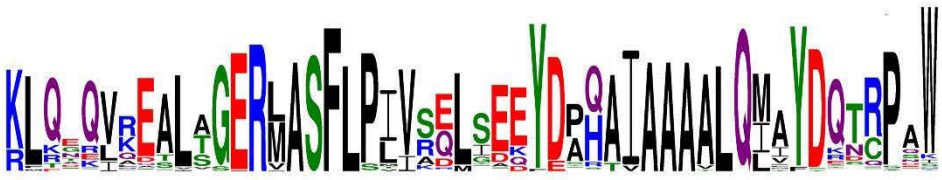

Figure 5.4: The C-terminal extension of CrhR-like helicases contains a unique, highly conserved sequence motif.

(A)Alignment of the C-terminal extensions of selected CrhR-like DEAD box proteins generated by MUSCLE. The unique conserved sequence motif is marked with a grey background on the alignment. (B) Sequence logo of the conserved CrhR-specific sequence motif. The sequence logo was generated from an alignment of all 185 CrhR-like DEAD-box RNA helicase sequences.

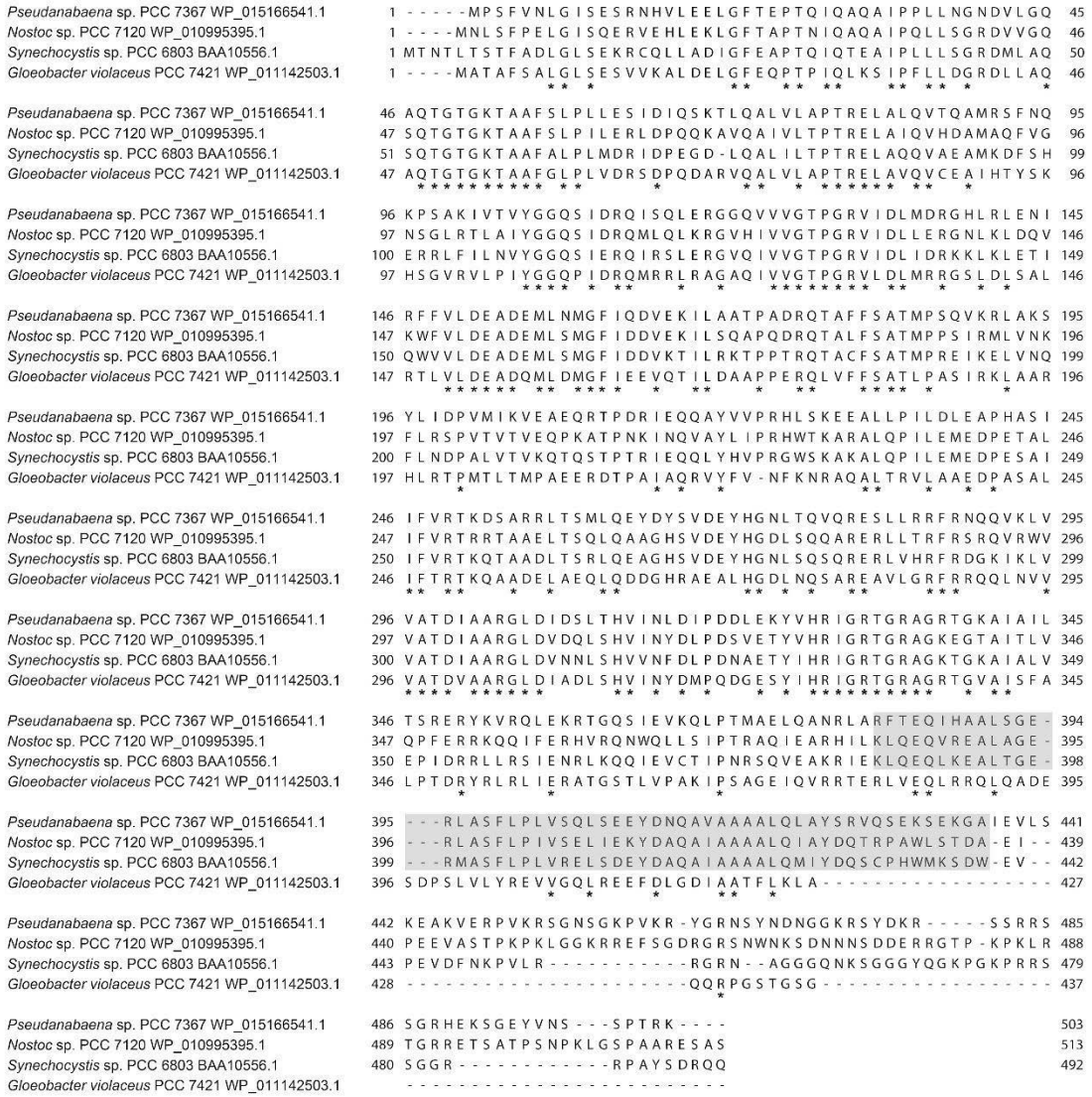

Figure 5.5: *Gloeobacter violaceus* PCC 7421 DEAD box helicase lacks the CrhR-specific domain.

Muscle alignment was performed using selected representatives of the CrhR-like helicase clade against the CrhR-related protein from *Gloeobacter violaceus* PCC 7421. Note the divergence of the *G. violaceus* helicase in the C-terminal domain, where the conserved sequence motif which defines the cyanobacterial CrhR clade is highlighted in grey.

Cyanobium, *Prochlocococcus* and *Synechococcus*. The strains from the *Cyanobium, Prochlorococcus* and *Synechococcus* genera that encode CsdA are monophyletic, based on both 16S rRNA (363) and concatenated gene (365) phylogenies. The most closely related species of cyanobacteria to these strains is *Synechococcus elongatus* (365), which does not encode a DEAD-box protein in its genome.

Co-occurrence of CrhR-like and CsdA-like proteins, excepting the four strains that encode all three subfamilies, is restricted to the genera *Acharychloris* (Figure 5.2). Cyanobacteria belonging to *Acharychloris*, like *Gloeocapsa*, have divergent photosynthetic pathways, as they are capable of photosynthesis using the far-red spectrum, with chlorophyll *d* as the primary photosynthetic pigment and an altered complement of phycobiliproteins that do not form phycobilisomes at the surface of the thylakoid membrane (366). As *Acharychloris* sp. and the four strains that encode all three subfamilies are more distantly related to the other *Cyanobium, Prochlorococcus* and *Synechococcus* strains that encode CsdA (365), it is possible that CsdA-like proteins were acquired separately by the different cyanobacterial lineages.

5.4.5 CsdA-like proteins contain a DbpA RNA binding domain in the C-terminal extension

As the *E. coli* DEAD-box RNA helicase CsdA, which has a DbpA RNA binding motif in its C-terminal extension, clustered within the cyanobacterial CsdA-like clade, the C-terminal extension of helicases in this chapter were also examined for a DbpA RNA binding motif. The C-terminal extension of the CsdA-like DEAD-box RNA helicases extends 200-235 amino acids past the final motif of the helicase core region, the HRIGR motif VI (see Figure 1.4). In CsdA-like cyanobacterial helicases, the C-terminal extension contains a DbpA RNA binding motif (Figure 5.6). Two other cyanobacterial helicases also contain a DbpA RNA binding motif in their C-terminus: proteins from an unclassified cyanobacteria bacterium strain 13_1_20CM_4_61_6 (OLE96526.1) and *Hassallia byssoidea* VB512170 (KIF31317.1). These strains cluster near the CsdA-like proteins and *E. coli* DbpA, respectively, with low bootstrapping support, suggesting a more distant relation within the same larger group of DbpA-containing DEAD-box proteins.

A

B

```
Synechococcus sp. Tous OON11948.1                    1 HRIGRTGRAGREGDAILFLSPRERRLLYGLERAVGCAIEPMEVPSDAEIN  50
Synechococcus sp. CB0205 WP_029626387.1              1 HRIGRTGRAGRTGNAILFVTPRERRFITGLERAVGRPIEPMEIPTNASIN  50
Synechococcus sp. KORDI-100 AII43180.1               1 HRIGRTGRAGRTGEAVLFVSPRERRFISNLERATGQPIEPMEIPGNAAIN  50
Synechococcus sp. WH 8102 WP_011127785.1             1 HRIGRTGRAGRTGEAVLFVTPRERRFINNLERATGQPIEAMEVPGNSAIN  50
Prochlorococcus marinus NATL1A WP_011824061.1        1 HRIGRTGRAGRNGEAILFVNPRERSFLSNLERAVGQPIEKMDIPDNDLIN  50
Prochlorococcus marinus subsp. marinus CCMP1375 WP_011125246.1  1 HRIGRTGRAGRSGEAILFISPRERSYLNNLERAVGQSIERMEIPNNESIN  50
Prochlorococcus marinus SB WP_032519145.1            1 HRIGRTGRAGRSGEAILFVNQREKHFLRNLENSTRTKIEEINIPSNKIIN  50
Prochlorococcus marinus subsp. pastoris CCMP1986 WP_011132734.1  1 HRIGRTGRAGRSGEAILFVNQREKHFLRNLENSTRNKIEEIEIPNNKIIN  50
Prochlorococcus marinus MIT 9313 CAE21258.1          1 HRIGRTGRAGRSGEAILFVNPRERRFVGGFERAVGQPIEPMDIPNNAAIN  50
Synechococcus sp. WH 8016 WP_006852341.1             1 HRIGRTGRAGRSGEAILFITPRERRFVGNLERAVGQAIEPMDIPSNAEIN  50
Synechococcus sp. WH 7805 WP_006041683.1             1 HRIGRTGRAGRTGEAILFVTPRERRFVGNLERAVNQSIEPMDIPSNAEIN  50
Synechococcus sp. RS9917 WP_007100168.1              1 HRIGRTGRAGRSGEAILFVTPRERRFVNNLERATGQPIEPMQIPSNAEIN  50
Synechococcus sp. WH 5701 WP_050751433.1             1 HRIGRTGRAGRQGDAILFLTPRERRFLGGLERAVGKAITPMEVPTNADIN  50
Cyanobium sp. PCC 7001 EDY39500.1                    1 HRIGRTGRAGRSGEAILFLTPRERRFLGGLERAAGKPIEPMEVPSNATIN  50
Candidatus Synechococcus spongiarum SP3 KKZ12789.1   1 HRIGRTGRAGRQGRALLLATPRERRLVQAIERANGGQLEMMELPDADTVN  50
Acaryochloris marina MBIC11017 WP_012160835.1        1 HRIGRTGRAGRQGDAILFVSSREKRMLRSIEQATRQPIQPMQIPSHADIA  50
Synechococcus sp. PCC 7335 WP_006457666.1            1 HRIGRTGRAGREGEAILFVTPREKRLLSSIERSTRQRIERMEMPSTEVVN  50

Synechococcus sp. Tous OON11948.1                   51 QQRLDQLQEKLTCLLT---EPVASERQQEVALMAEIIQRLSRETEATPEQ  97
Synechococcus sp. CB0205 WP_029626387.1             51 QSRLDRLRERLSETVKGLNSEETSNLSEQQALLSEIIKRVGQESEVAPEQ 100
Synechococcus sp. KORDI-100 AII43180.1              51 QGRLDRLRLRLSEAAR---NGR--PSEEETALLKELIQRIGTELEMTPDQ  95
Synechococcus sp. WH 8102 WP_011127785.1            51 QGRLDRLHKRLSEAAH---NER--SYEEEAALLKELLQRIGTELELSPEQ  95
Prochlorococcus marinus NATL1A WP_011824061.1       51 NNRIKKLQAKLIKAAS---TER--DNPEEANILEELIKNVEKELDIDPKD  95
Prochlorococcus marinus subsp. marinus CCMP1375 WP_011125246.1  51 NHRIQKIKRDLLTTAS---QKR--KDQEETNLIKEVINEIESELEITPKE  95
Prochlorococcus marinus SB WP_032519145.1           51 EKRMEKLIDNVNESSL---AKD--ENEENKALIIDVLDNLKEKYSMDDSN  95
Prochlorococcus marinus subsp. pastoris CCMP1986 WP_011132734.1  51 EKRMGKLITNLNESSL---DQE--NNEEKKALMIDILDTLREKHSMEDSN  95
Prochlorococcus marinus MIT 9313 CAE21258.1         51 QSRLDRLRQRLTTAAK---TER--DNSEETALLQELIQRVVQELSLSPEQ  95
Synechococcus sp. WH 8016 WP_006852341.1            51 QSRLDRLRTRLSAEAT---SED--KPEEETALLQELIQRVAQELEVEPGQ  95
Synechococcus sp. WH 7805 WP_006041683.1            51 QSRLDRLRNRLSEAAV---CEA----DDETPLLQELIQRVAQEHELSADQ  93
Synechococcus sp. RS9917 WP_007100168.1             51 QARLDNLRQKLTAVAT---GDGAERQADEGPLLQELLQRVAQEHSLSMEQ  97
Synechococcus sp. WH 5701 WP_050751433.1            51 QSRLDRLRERVTALVG---TPR--SDEQELALLSEILQRVGSEISATPEQ  95
Cyanobium sp. PCC 7001 EDY39500.1                   51 QNRLDRLRQRLTNALH---KSA--VSPEEQALLSEIVQRVAQEQTCTPEQ  95
Candidatus Synechococcus spongiarum SP3 KKZ12789.1  51 QRRRQRFKERILAALD----------GTDVPVFEQLVQELSAEKGLPVEH  90
Acaryochloris marina MBIC11017 WP_012160835.1       51 DRRIVQFKQVITDTIE----------DQDLDFFEDLISNYQQEQDLSLRE  90
Synechococcus sp. PCC 7335 WP_006457666.1           51 DQRIERFKQKITNALA----------QEDSAFFTQILEQYEQEHDVPAIE  90

Synechococcus sp. Tous OON11948.1                   98 LALAALRLSQGDQPLLVV-PQVQNS--VTRMGRNERPERGERRG------ 138
Synechococcus sp. CB0205 WP_029626387.1            101 LALAALQMAVGDQPLLVH-DDENWIRQQPQSRDGRRNDRFGDRDRGPRNA 149
Synechococcus sp. KORDI-100 AII43180.1              96 LALAALGLAIGPAPLLCQ-GDEEWI--QQAMAGGLRRRERGERGDRDRRR 142
Synechococcus sp. WH 8102 WP_011127785.1            96 LAYAALSMAIGPDPLLRQKGDDEWI--HNNQRRD-RDRDRDRGGERRERR 142
Prochlorococcus marinus NATL1A WP_011824061.1       96 LTLAALNLAVGFNALLEN-GNEDWI--RQSAQRNTRNDRRDNNKFKQRRR 142
Prochlorococcus marinus subsp. marinus CCMP1375 WP_011125246.1  96 IALAAINLSIGESPLLIN-TDESWI--NQAERFRKSNDRRDNRG------ 136
Prochlorococcus marinus SB WP_032519145.1           96 IAMAAINLVIGNKSFFVN-EDDSWINKQNNTDRNRSNRNSNNRMRNSNRR 144
Prochlorococcus marinus subsp. pastoris CCMP1986 WP_011132734.1  96 IAMAAINLAIGNKSFFIN-EDESWLYRQNNSDRNRSNRNGNNRMRNTNRR 144
Prochlorococcus marinus MIT 9313 CAE21258.1         96 LALAALEFAVGPGPILVQ-ADEGWL--QQSTQRNRRNDRHESRG------ 136
Synechococcus sp. WH 8016 WP_006852341.1            96 LTLAAMRLAVGEGPLLVQ-GDESWL--KAPMRNDRRDDRRGDRGGH---- 138
Synechococcus sp. WH 7805 WP_006041683.1            94 LALAALRLVVGDQPLLVS-GDESWL--QAPVRTERRDDRRGDRG------ 134
Synechococcus sp. RS9917 WP_007100168.1             98 LALAALTLAVGDQPLLVQ-GDESWL--QNANRGRTREDRLGSRGGDRGDR 144
Synechococcus sp. WH 5701 WP_050751433.1            96 LALAALQLAVGDRPLLVQ-GAETWR--QPTPSRE-RQRSGDDDRRGDRRS 141
Cyanobium sp. PCC 7001 EDY39500.1                   96 LALAALELSLGGKPLLLH-GNDDFT--QVRSQGPNRRDGRESRDGRDFGN 142
Candidatus Synechococcus spongiarum SP3 KKZ12789.1  91 IAAALAQLVQGAKPFACS-AEEPLL----------------------- 114
Acaryochloris marina MBIC11017 WP_012160835.1       91 IAASLAYLVQKDKPLVPP----------------KEDLSSDPGHAVQTS 123
Synechococcus sp. PCC 7335 WP_006457666.1           91 IAGALAKLLQGDEPLLLE----------------EKTKPKRRDGGS------ 120

Synechococcus sp. Tous OON11948.1                  139 ------PGGRGSDSPESHMERFRVEVGWRDRIKPGHIVGAIANETGLDGK 182
Synechococcus sp. CB0205 WP_029626387.1            150 PGARR-GPREQSGPPEDHMDRFRIEVGWRDRIKPGNIVGAIANESGLNGR 198
Synechococcus sp. KORDI-100 AII43180.1             143 SDR-------PSRPPEDHMQRYRVEVGHRDRVKPGNLVGAIAGETGLQGR 185
Synechococcus sp. WH 8102 WP_011127785.1           143 SDR-------PARAPEENMQRYRVEVGHRDRVKPGNLVGAIAGETGLQGR 185
Prochlorococcus marinus NATL1A WP_011824061.1      143 GDF-------DNNRLEDEMDRFRVEVGHRDRVKPGNLVGAIANEAGLKGR 185
Prochlorococcus marinus subsp. marinus CCMP1375 WP_011125246.1  137 RSRR--RNDLDIGTTEKDKERFRVDVGHRDRVKPGNIVGAIANESGLNGR 184
Prochlorococcus marinus SB WP_032519145.1          145 NNYQ-----------NDSFETYKFNFGKFDGVRVANIISSICNSTNINGR 183
Prochlorococcus marinus subsp. pastoris CCMP1986 WP_011132734.1  145 NNYQ-----------NDSFETYKFNFGKMDRVRVANIISSICTSTNINGR 183
Prochlorococcus marinus MIT 9313 CAE21258.1        137 GSGR--RPERSSRPPEDHMERFRVEVGHRDRVKPGNLVGAIANESGLEGR 184
Synechococcus sp. WH 8016 WP_006852341.1           139 ERGR--RPERASRPPEDDMERFRVEVGHRDRVKPGNLVGAIANESGLEGR 186
Synechococcus sp. WH 7805 WP_006041683.1           135 RDRR--RPERDARPPEDNMTRYRVEVGHRDRVKPGNLVGAIANESGLQGR 182
Synechococcus sp. RS9917 WP_007100168.1            145 GDRR--RQERPSRPPEDNMERFRVEVGHRDRVKPGNLVGAIANESGLQGR 192
Synechococcus sp. WH 5701 WP_050751433.1           142 PSRTGGSRLDASTPPDADMERFRIEVGWQDRVKPGNIVGAIANEAGLNGR 191
Cyanobium sp. PCC 7001 EDY39500.1                  143 REPRRGRSERPVGAPEPDMERFRVELGWRDRIKPGNLVGAIANETGLQGR 192
Candidatus Synechococcus spongiarum SP3 KKZ12789.1 115 ----PLKPRRQSRPLAAHMERYRIEVGWKHRVKPGNIVGALANQAGIRGQ 160
Acaryochloris marina MBIC11017 WP_012160835.1       124 N-----WAADLGKPSHQQMQLFRIEVGRQHEVKPKNIVGAIANEVNLAPR 168
Synechococcus sp. PCC 7335 WP_006457666.1           121 ----------GAATHSVGMERFRVEVGKNHRVKPGHIVGAIANETGLANK 160

Synechococcus sp. Tous OON11948.1                  183 KIGRINIFDDHSTIDLPKGMPPELMRTLSQVKVMQKELQITRLAVG---- 228
Synechococcus sp. CB0205 WP_029626387.1            199 SIGRIQIFDSHSLVDLPKGMPEDVFHNLKRLKVLNRELQISRVQG----- 243
Synechococcus sp. KORDI-100 AII43180.1             186 MIGRIQIFDNHSLVDLPKGMPEDVFNNLRRLRVMNRELQISQAS------ 229
Synechococcus sp. WH 8102 WP_011127785.1           186 AIGRIQIFDNHSFVDLPKGMPEDVFNSLRRLRVMNRELQITQAS------ 229
Prochlorococcus marinus NATL1A WP_011824061.1      186 SIGRIRIFENYSLVDLPKQMPDKVFQALKKVKVMNRELQINRAD------ 229
Prochlorococcus marinus subsp. marinus CCMP1375 WP_011125246.1  185 MIGRIQIFESYSLVDLPKGMPTKIFQSLKRVKVMNKELNINRYT------ 228
Prochlorococcus marinus SB WP_032519145.1          184 SIGKIQIFNDYSLVDLPRDLHRETKNKLKKIKVRN---------------- 218
Prochlorococcus marinus subsp. pastoris CCMP1986 WP_011132734.1  184 LIGKIQIFNEYSLVDLPRDLHGEVKNKLKNLRIRN---------------- 218
Prochlorococcus marinus MIT 9313 CAE21258.1        185 MIGRIQIFESHSLVDLPKGMPEDVFKDLKRLKVMNRELHIQRAS------ 228
Synechococcus sp. WH 8016 WP_006852341.1           187 MIGRIQIFETHSLVDLPKGMPENVFNSLRRLKVMNRELQIRQDS------ 230
Synechococcus sp. WH 7805 WP_006041683.1           183 MIGRIQIFESHSLVDLPKGMPDDVFDSLQRLKVLNRELQITKAS------ 226
Synechococcus sp. RS9917 WP_007100168.1            193 MIGRIQIFESHTLVDLPKGMPQDVFQSLKHLKVMNRELQIRPFT------ 236
Synechococcus sp. WH 5701 WP_050751433.1           192 SIGRIQIFDTHSTVDLPSGMPEDVFNALRRLRVMNKELQITRHNS----- 236
Cyanobium sp. PCC 7001 EDY39500.1                  193 AIGRIQIFDTHSIIDLPKGMPEDIFQGLRNLRVLNKPLQISRFRG----- 237
Candidatus Synechococcus spongiarum SP3 KKZ12789.1 161 SIGRIHIFDEHSTVDLPKDLPEDLFATLRTMRVVSKPLRIRKLEASMV-- 208
Acaryochloris marina MBIC11017 WP_012160835.1       169 YIGQIKLFDTFSTVYLPECMPKPVFQHLKQVRVRGQKLNISLCTKEERSR 218
Synechococcus sp. PCC 7335 WP_006457666.1           161 YIGRISVYDDYSTVDLPVGIPKETFELLRGVKVLDHPMNITSLGKTRDEG 210

Synechococcus sp. Tous OON11948.1                      - - - - - - - - - - - - - - - - - - - - - - - - - - - - - - - - - - - -
Synechococcus sp. CB0205 WP_029626387.1                - - - - - - - - - - - - - - - - - - - - - - - - - - - - - - - - - - - -
Synechococcus sp. KORDI-100 AII43180.1                 - - - - - - - - - - - - - - - - - - - - - - - - - - - - - - - - - - - -
Synechococcus sp. WH 8102 WP_011127785.1               - - - - - - - - - - - - - - - - - - - - - - - - - - - - - - - - - - - -
Prochlorococcus marinus NATL1A WP_011824061.1          - - - - - - - - - - - - - - - - - - - - - - - - - - - - - - - - - - - -
Prochlorococcus marinus subsp. marinus CCMP1375 WP_011125246.1  - - - - - - - - - - - - - - - - - - - - - - - - - - - - - - - - - - - -
Prochlorococcus marinus SB WP_032519145.1              - - - - - - - - - - - - - - - - - - - - - - - - - - - - - - - - - - - -
Prochlorococcus marinus subsp. pastoris CCMP1986 WP_011132734.1  - - - - - - - - - - - - - - - - - - - - - - - - - - - - - - - - - - - -
Prochlorococcus marinus MIT 9313 CAE21258.1            - - - - - - - - - - - - - - - - - - - - - - - - - - - - - - - - - - - -
Synechococcus sp. WH 8016 WP_006852341.1               - - - - - - - - - - - - - - - - - - - - - - - - - - - - - - - - - - - -
Synechococcus sp. WH 7805 WP_006041683.1               - - - - - - - - - - - - - - - - - - - - - - - - - - - - - - - - - - - -
Synechococcus sp. RS9917 WP_007100168.1                - - - - - - - - - - - - - - - - - - - - - - - - - - - - - - - - - - - -
Synechococcus sp. WH 5701 WP_050751433.1               - - - - - - - - - - - - - - - - - - - - - - - - - - - - - - - - - - - -
Cyanobium sp. PCC 7001 EDY39500.1                      - - - - - - - - - - - - - - - - - - - - - - - - - - - - - - - - - - - -
Candidatus Synechococcus spongiarum SP3 KKZ12789.1     - - - - - - - - - - - - - - - - - - - - - - - - - - - - - - - - - - - -
Acaryochloris marina MBIC11017 WP_012160835.1      219 KHSGKSSHKGRHKKHSHRKAKAGKR-----                          243
Synechococcus sp. PCC 7335 WP_006457666.1          211 NWREGKPKRRRNTRSGPPFKKKRRKDKATV                          240
```

Figure 5.6: The C-terminal extension of the CsdA-like helicases contains a DpbA RNA binding domain.

(A) A schematic showing the Pfam domains present in the CsdA-like helicases: the DEAD/DEAH box helicase domain (DEAD, PF00270), the helicase conserved C-terminal domain (Helicase_C, PF00271), and the DbpA RNA binding domain (DbpA, PF03880). (B) Alignments generated with MUSCLE of the C-terminal extensions of selected CsdA-like helicases. The conserved DbpA RNA binding domain is marked with a grey background. Note that this domain is not present in members of the CrhR-like clade.

5.4.6 RhlE-like helicases co-occur with another DEAD-box protein

RhlE-like proteins essentially only occur in strains of cyanobacteria with at least one other DEAD-box protein (Figure 5.7). *Leptolyngbya* sp. PCC 6406 is the only cyanobacteria in this chapter that encodes an RhlE-like helicase as its only identified DEAD-box protein (Table 5.1); however, as the genome sequence of this organism is a high-quality draft sequence, it is possible that an additional DEAD-box RNA helicase is encoded in the remaining gapped regions. Genomes that encode both CsdA-like and RhlE-like proteins are restricted to unicellular cyanobacteria of the genera *Cyanobium* and *Synechococcus*. Similarly, co-occurrence of CrhR-like and RhlE-like proteins is found in filamentous cyanobacteria of the orders *Nostocales*, *Oscillatoriales* and *Synechococcales*. The three exceptions are the unicellular strains *Synechocystis* sp. PCC 7509, *Synechococcus* sp. NIES-970 and *Synechococcus* sp. NKBG15041c, which encode both a CrhR-like and RhlE-like helicase. Polyphyly has long been a known issue in the genera *Synechococcus* (367), and *Synechocystis* (368), so I suggest that these strains are likely misclassified. The RhlE-like proteins cluster into two major related groups that, apart from the four strains that encode all three types of cyanobacterial DEAD-box proteins, correlate with the co-occurrence of CsdA- or CrhR-like helicases (Figure 5.7). This suggests that RhlE-like helicases were acquired at least twice in cyanobacterial lineages, once in the lineage with CsdA-like helicases and at least once in strains with CrhR-like proteins.

The RhlE like proteins have a short C-terminal extension of approximately 75-100 amino acids that lacks sequence conservation (Figure 5.8). It was also noted from the alignments that all RhlE-like proteins from *Nostocales* had a substitution of phenylalanine for the serine in the conserved motif III (84), resulting in a sequence change from SAT→FAT.

5.4.7 Proteins from all three helicase clades are only encoded in four related strains of cyanobacteria

The only cyanobacterial strains that encode a CrhR-like, CsdA-like and RhlE-like helicase within the same genome are *Leptolyngbya* sp. PCC 7375*, Leptolyngbya* sp.

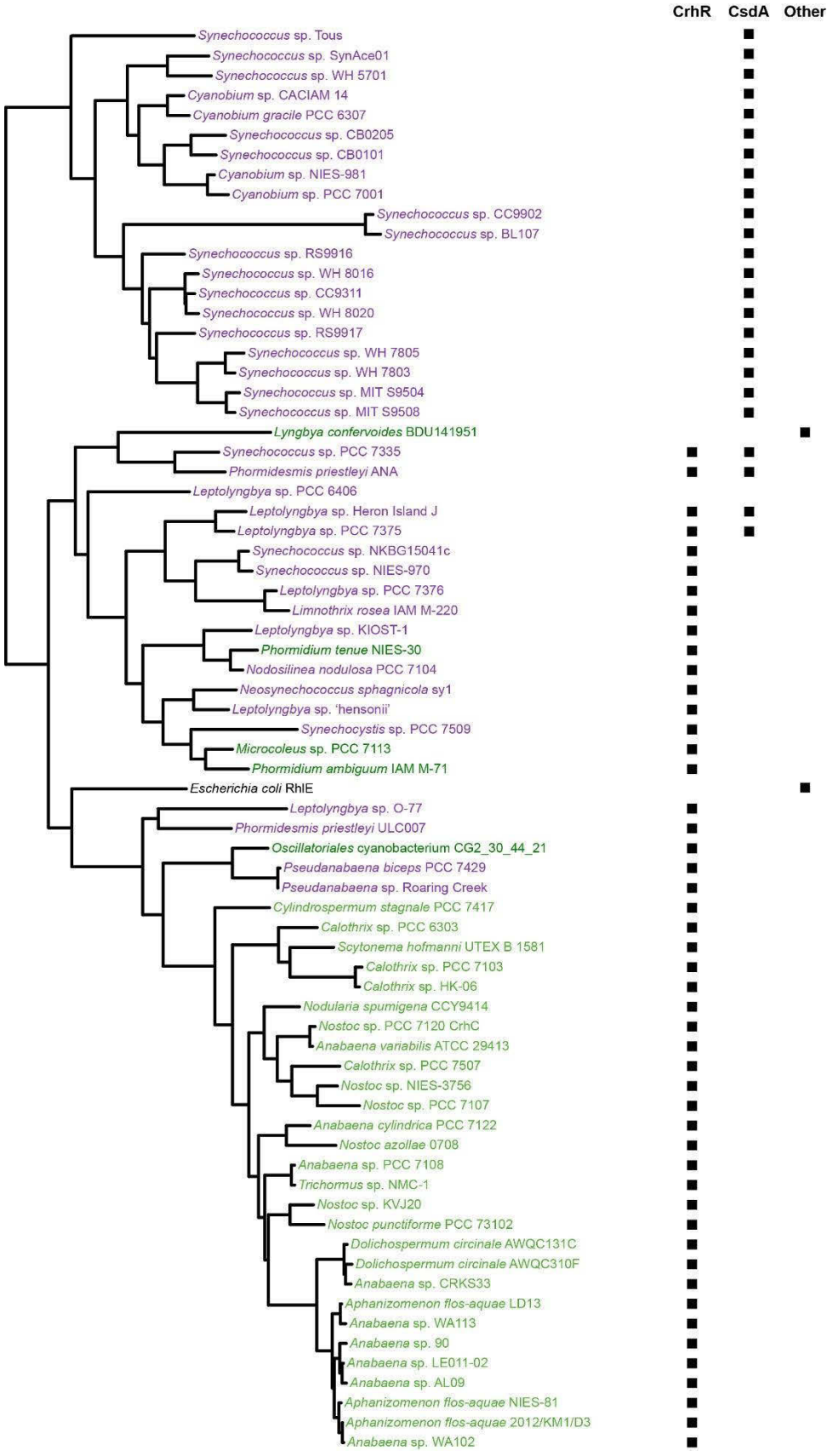
CrhR
CsdA
Other
Synechococcus sp. Tous
Synechococcus sp. SynAce01
Synechococcus sp. WH 5701
Cyanobium sp. CACIAM 14
Cyanobium gracile PCC 6307
Synechococcus sp. CB0205
Synechococcus sp. CB0101
Cyanobium sp. NIES-981
Cyanobium sp. PCC 7001
Synechococcus sp. CC9902
Synechococcus sp. BL107
Synechococcus sp. RS9916
Synechococcus sp. WH 8016
Synechococcus sp. CC9311
Synechococcus sp. WH 8020
Synechococcus sp. RS9917
Synechococcus sp. WH 7805
Synechococcus sp. WH 7803
Synechococcus sp. MIT S9504
Synechococcus sp. MIT S9508
Lyngbya confervoides BDU141951
Synechococcus sp. PCC 7335
Phormidesmis priestleyi ANA
Leptolyngbya sp. PCC 6406
Leptolyngbya sp. Heron Island J
Leptolyngbya sp. PCC 7375
Synechococcus sp. NKBG15041c
Synechococcus sp. NIES-970
Leptolyngbya sp. PCC 7376
Limnothrix rosea IAM M-220
Leptolyngbya sp. KIOST-1
Phormidium tenue NIES-30
Nodosilinea nodulosa PCC 7104
Neosynechococcus sphagnicola sy1
Leptolyngbya sp. 'hensonii'
Synechocystis sp. PCC 7509
Microcoleus sp. PCC 7113
Phormidium ambiguum IAM M-71
Escherichia coli RhlE
Leptolyngbya sp. O-77
Phormidesmis priestleyi ULC007
Oscillatoriales cyanobacterium CG2_30_44_21
Pseudanabaena biceps PCC 7429
Pseudanabaena sp. Roaring Creek
Cylindrospermum stagnale PCC 7417
Calothrix sp. PCC 6303
Scytonema hofmanni UTEX B 1581
Calothrix sp. PCC 7103
Calothrix sp. HK-06
Nodularia spumigena CCY9414
Nostoc sp. PCC 7120 CrhC
Anabaena variabilis ATCC 29413
Calothrix sp. PCC 7507
Nostoc sp. NIES-3756
Nostoc sp. PCC 7107
Anabaena cylindrica PCC 7122
Nostoc azollae 0708
Anabaena sp. PCC 7108
Trichormus sp. NMC-1
Nostoc sp. KVJ20
Nostoc punctiforme PCC 73102
Dolichospermum circinale AWQC131C
Dolichospermum circinale AWQC310F
Anabaena sp. CRKS33
Aphanizomenon flos-aquae LD13
Anabaena sp. WA113
Anabaena sp. 90
Anabaena sp. LE011-02
Anabaena sp. AL09
Aphanizomenon flos-aquae NIES-81
Aphanizomenon flos-aquae 2012/KM1/D3
Anabaena sp. WA102

Figure 5.7: Co-occurrence of RhlE-like helicases with CsdA- and CrhR- like proteins.

The RhlE-like maximum likelihood helicase tree was extracted from Figure 5.2. Annotations indicate whether the second DEAD-box protein in each strain is from the CrhR-like or CsdA-like groups. Essentially, RhlE is only found in conjunction with either CrhR or CsdA. Taxa colours indicate the cyanobacterial taxonomic order: purple-*Synechococcales*, light green-*Nostocales*, dark green-*Oscillatoriales*. The position of *E. coli* RhlE is provided to verify the classification.

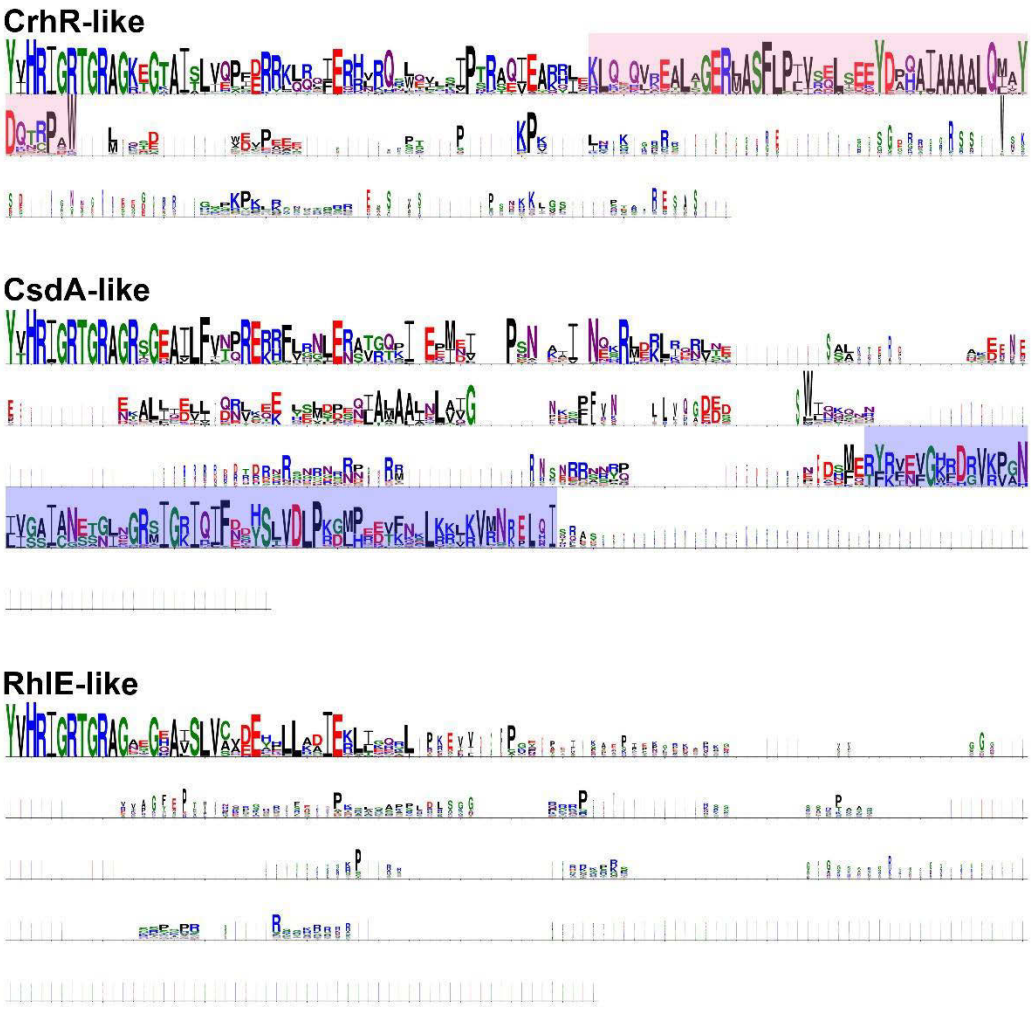

Figure 5.8: Conservation in the C-terminal extension of cyanobacterial DEAD-box proteins.

Comparisons of the conservation in the C-terminal extensions of the three clades of cyanobacterial DEAD-box RNA helicases are shown using sequence logos, with the size of the amino acid indicating its conservation. The CrhR-specific sequence motif is indicated in pink and the DbpA RNA binding domain is marked in blue. Sequence logos were generated in WebLogo3 from alignments of all cyanobacterial DEAD-box proteins in each clade.

Heron Island J, *Phormidesmis priestleyi* ANA, and *Synechococcus* sp. PCC 7335 (Figure 5.2). Although these four strains are annotated as members of three separate genera, 16S rDNA, *rpoC* and/or concatenated gene phylogenies indicate they are more closely related than another closely related strain, *Leptolyngbya* sp. PCC 6406 (365, 369, 370). As all four of these strains have not been included in the same phylogenetic analysis to date, an *rpoC* gene tree was constructed (Figure 5.9) to confirm that the strains were closely related. As expected, *Leptolyngbya* sp. PCC 7375*, Leptolyngbya* sp. Heron Island J, *Phormidesmis priestleyi* ANA, and *Synechococcus* sp. PCC 7335 clustered together, with the closely related *Leptolyngbya* sp. PCC 6406 and *Nodosilinea nodulosa* PCC 7104 forming the outgroups (Figure 5.9). This confirms that, despite the differences in current taxonomy and cellular morphology, the four strains of cyanobacteria that encode examples of all three groups of cyanobacterial DEAD-box proteins are closely related.

5.5 Discussion

Cyanobacteria are unique among prokaryotes, as they are the only bacteria that perform oxygenic photosynthesis. In this chapter, it was shown that the complement of DEAD-box RNA helicases encoded by cyanobacteria is also unique, as proteins with homology to the helicases of *E. coli*, the CsdA-like and RhlE-like protein groups, are only encoded within the genomes of select cyanobacterial taxa. In contrast, the DEAD-box RNA helicase group that can be found across cyanobacterial diversity, the CrhR-like proteins, is unique to all organisms. The C-terminal extension domain of the DEAD-box RNA helicase was found to be a defining characteristic of this unique clade.

The CsdA-like helicases have a DbpA RNA binding domain near the C-terminal end of the protein, similar to the canonical family member CsdA in *E. coli* (107). The presence of the DbpA RNA binding domain, which assists DbpA in binding specifically to hairpin 92 of the 23S rRNA (347, 371) may indicate that the cyanobacterial CsdA-like helicases have a role in ribosome biogenesis, and more specifically maturation of the 23S rRNA precursor, similar to DbpA (113, 115). The domain may also provide more general RNA chaperone properties for the helicase, as some proteins with a DbpA RNA binding domain, including CsdA, do not bind to the 23S rRNA at hairpin 92 (106). As these proteins have significant homology with CsdA, the cyanobacterial CsdA-like proteins

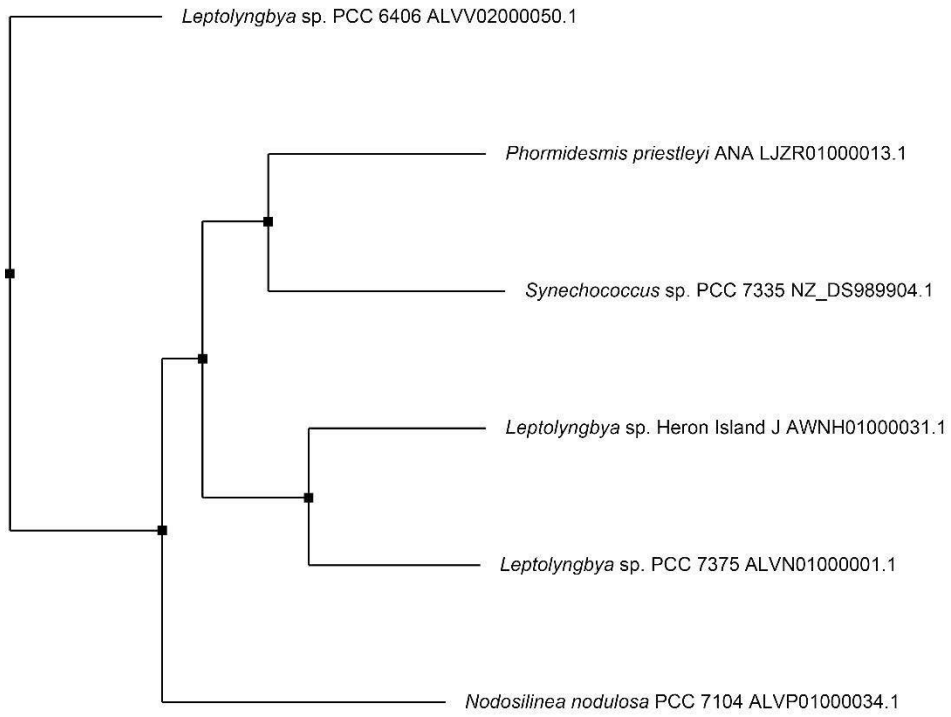

Figure 5.9: *rpoC2* neighbour-joining tree of cyanobacteria that encode CrhR-, CsdA- and RhlE-like helicases.

Nucleotide sequences for the RNA polymerase beta' subunit, *rpoC2*, were aligned by MUSCLE and used to construct a neighbour-joining tree showing that the four cyanobacterial strains that encode DEAD-box proteins from all three clades of cyanobacterial DEAD-box proteins are closely related.

may constitute a multifunctional helicase that can function in ribosome biogenesis, translation initiation and RNA degradation (106, 109, 113, 123, 124, 178).

A sequence motif of approximately 50 amino acids that is unique to the CrhR-like group of cyanobacterial DEAD-box RNA helicases is located within the C-terminal extension of the CrhR-like proteins. This sequence motif does not occur as a module in other proteins; however, CrhR-like proteins containing this motif are widely distributed among cyanobacteria. Thus, it is likely that the CrhR-specific domain arose as a specialization of a DEAD-box protein in the ancestral cyanobacterial lineage. This suggests that CrhR-like helicases have a particular function that is unique to cyanobacteria. As CrhR-like helicases are often the sole DEAD-box protein in a cyanobacterial genome, it is likely that they function in multiple RNA processes. We propose that the unique function of CrhR-like helicases likely relates to oxygenic photosynthesis, a metabolic process that is only performed by cyanobacteria in the prokaryotic world. This conjecture is supported by the co-precipitation of CrhR from *Synechocystis* with polysomes and RNA degradosome components (Chapter 2) and the altered expression of ~10% of the *Synechocystis* transcriptome, consisting of both mRNA and ncRNAs, in a *crhR* truncation mutant (147). Physiologically, and consistent with the altered expression profiles, CrhR mutation results in significant disruption to photosynthesis, with cells exhibiting reduced pigment abundance, oxygen evolution rates and carbon dioxide fixation rates (104). These physiological changes can also be associated with the regulation of crhR expression by a range of abiotic stresses (41, 160, 163, 164), including nitrogen stress (Chapter 4). Taken together, these effects are consistent with CrhR RNA helicase localization to the thylakoid membrane space (Chapter 2), the site of light harvesting and ATP and NADPH formation in *Synechocystis*. We therefore propose that CrhR-like RNA helicases perform a unique function, coordinating expression of genes required to maintain oxygenic photosynthesis in response to abiotic stresses in cyanobacteria.

Support for this proposed function of the CrhR-like helicases may also be found in the conserved gene synteny surrounding the CrhR-like proteins. The *rimO-crhR* operon of *Synechocystis* is conserved in 89.8% of strains with CrhR-like helicases. Over 60% of strains also have further conservation of synteny, with conserved genes relating to

photosynthesis, energy transfer from the electron transport chain and membrane protein stability. In particular, the activities of many of these proteins could protect the photosynthetic electron transport chain from oxidative damage if an excess of reductant was to accumulate. For example, PsbU stabilizes the oxygen-evolving complex of PSII and protects it from inactivation in response to stress, such as heat (372). The vitamin K epoxide reductase (VKOR) and L-aspartate oxidase (*nadB*) act as electron sinks, as they both can use quinones from the electron transport chain as the source of energy for their biochemical activity (373, 374). Expression of these proteins may be regulated under similar conditions as CrhR, which is induced in response to increasing reduction of the photosynthetic electron transport chain (163).

The RhlE-like helicases in cyanobacteria lack a conserved C-terminal domain. Interestingly, DEAD-box proteins from this group are essentially only encoded in genomes with at least one other DEAD-box helicase. This is consistent with the distribution of RhlE-like proteins generally in prokaryotes, with only a limited number of genomes encoding solely an RhlE-like DEAD-box helicase (107). This also supports conservation of the proposed function of the RhlE helicase in *E. coli* as a helicase that functions cooperatively with other DEAD-box proteins during ribosome biogenesis (111).

Distribution of these three groups of DEAD-box RNA helicases in cyanobacteria suggest DEAD-box proteins were acquired independently by cyanobacteria several times. The CrhR-like proteins, with functional links to photosynthesis, are widely distributed throughout cyanobacterial diversity and contain a sequence domain unique to the CrhR-like group of DEAD-box RNA helicases. This suggests that the precursor of CrhR-like DEAD-box helicases arose early in cyanobacterial evolution, allowing it to be present in the majority of cyanobacterial orders. A common ancestor of the *Synechococcus* and *Prochlorococcus* genera likely lost the CrhR-like helicase. Early branching *Synechococcus* and *Prochlorococcus* phyla, based on 16S rRNA (363), contain CrhR-like helicases; however, CrhR-like proteins are absent from *Synechococcus elongatus* PCC 7942 and the strains with CsdA-like helicases. It is possible that the CsdA-like helicases were acquired by horizontal gene transfer in this lineage that lacked a CrhR-like helicase and were maintained as they conferred an advantage to cyanobacteria lacking DEAD-box

RNA helicases. Acquisition of RhlE-like helicases in cyanobacteria was likely also by horizontal gene transfer, possibly several events, as they are generally only found in proteobacteria (107).

In summary, DEAD-box RNA helicases encoded in cyanobacterial genomes can generally be classified into three protein groups on the basis of conserved sequences in the C-terminal extension of the helicase. Two of these groups, the CsdA-like and RhlE-like helicases, have significant similarity to the *E. coli* proteins of the same name. The third group, the CrhR-like helicases, are unique to cyanobacteria and are characterized by a sequence motif in the C-terminal extension of the protein that is only found in CrhR-like helicases. Based on prior characterization of the namesake protein, CrhR, it is likely that CrhR-like proteins are multifunctional helicases, with a role related to maintenance of photosynthesis and the integrity of the thylakoid membrane.

Chapter 6: Conclusions

DEAD box RNA helicases are ubiquitous enzymes that interact with and remodel cellular RNAs participating in major RNA processes, such as ribosome biogenesis, translation and RNA degradation (73, 75, 176). In prokaryotes, some of these enzymes are strictly specialized to a perform a unique function, such as DbpA of *E. coli*, which recognizes and binds to hairpin 92 of the 23S rRNA precursor (114) to assist maturation of the large ribosomal subunit. Other DEAD-box proteins appear to function more as a generalist in the cell. An example would be CsdA in *E. coli*, which performs roles in a variety of RNA metabolic processes. These include roles in the maturation of the large ribosomal subunit, particularly at low temperature, by processing the 5' terminus of the 23S rRNA (109), translation initiation (106, 123, 124) and as a member of the RNA degradosome, possibly creating a cold-adapted degradosome (178). Cyanobacterial genomes typically encode only a few DEAD-box proteins, for example one in *Synechocystis* (41) and two in *Nostoc* (105). Since cyanobacteria encode a limited complement of DEAD-box RNA helicases, understanding the functional role(s) they fulfill in the cell and the diversity and distribution of DEAD-box proteins throughout cyanobacteria was of interest.

Two cyanobacterial DEAD-box RNA helicases have been characterized experimentally: CrhC from *Nostoc* and CrhR from *Synechocystis*. Expression of *crhC* is regulated in response to temperature- and light-derived metabolic capacity, with expression induced specifically by low temperature in the light (105, 149). CrhC exhibits limited dsRNA unwinding (151) and thus potentially functions primarily as an RNA chaperone, clamping the RNA to maintain correct secondary structure and acting as a scaffold for recruitment of other proteins (72). CrhC protein co-localizes with ribosomes to the cytoplasmic face of the plasma membrane, with a bias to the cell poles (152). It has also been shown that inactivation of a close homolog of CrhC, *crhA*, in *Anabaena variabilis* results in truncation of the *Anabaena* filaments (148). Together, these results suggest that CrhC primarily functions at the cell poles to promote translation and co-translocation of proteins across the cytoplasmic membrane in *Nostoc* and *Anabaena*, contributing to maintenance of the organism's filamentous morphology (148, 152).

Cyanobacterial RNA helicase redox (CrhR), the focus of this thesis, is the sole DEAD-box RNA helicase encoded in the *Synechocystis* genome. *In vitro*, CrhR exhibits the classic biochemical activities of a DEAD-box RNA helicase (72): it possesses ATP-

dependent RNA binding and RNA-dependent ATPase activities (153); however, CrhR is also capable of annealing complementary RNA strands and possibly performing strand exchange (153), biochemical activities that are relatively rare in DEAD-box proteins (154-156). While CrhR has been shown to perform this diverse range of biochemical activities *in vitro*, how this biochemical potential relates to the physiological function of the protein is unknown.

Mutational and expression studies involving *crhR* provide some suggestions as to the physiological role CrhR performs in *Synechocystis*. *crhR* expression is regulated in response to a variety of abiotic stresses, including temperature, salt, light and heavy metal stress (41, 104, 161, 163). Induction of *crhR* expression during these stresses is regulated in response to their effect on the redox poise of the photosynthetic electron transport chain in *Synechocystis* (163). *crhR* expression is also regulated through alteration of transcript stability (164) by processing and degradation, as well as proteolysis (160), processes that are CrhR-dependent and thus auto-regulatory. Truncation of *crhR* produces a range of physiological effects, resulting in a severe cold sensitive phenotype exemplified by a reduced growth rate and pigmentation, changes to the cell ultrastructure including disordered thylakoid membranes, and decreased photosynthetic capacity (104). Taken together, these results indicate that CrhR likely functions in pathways that allow the cell to adapt its photosynthetic apparatus to abiotic stresses, although the mechanisms by which CrhR functions in those pathways are unknown. Thus, the aim of this thesis was to use CrhR as a model helicase in cyanobacteria to further explore the physiological function of cyanobacterial DEAD-box RNA helicases. The major conclusions of the thesis, summarized below, are also presented in Figure 6.1.

In Chapter 2, evidence was presented for co-localization of CrhR with *Synechocystis* polysome complexes and RNA degradation proteins. Co-precipitation of CrhR with polysomes was RNA-dependent and required stalling of the polysome complexes with a translation inhibitor, such as chloramphenicol, indicating association of CrhR with polysome complexes occurs via binding of either a ribosomal RNA or the mRNA template during translation. Association of CrhR with actively translating polysome complexes, rather than ribosomal subunits, was unexpected as most well characterized DEAD-box proteins from *E. coli* and *B. subtilis* have documented roles in

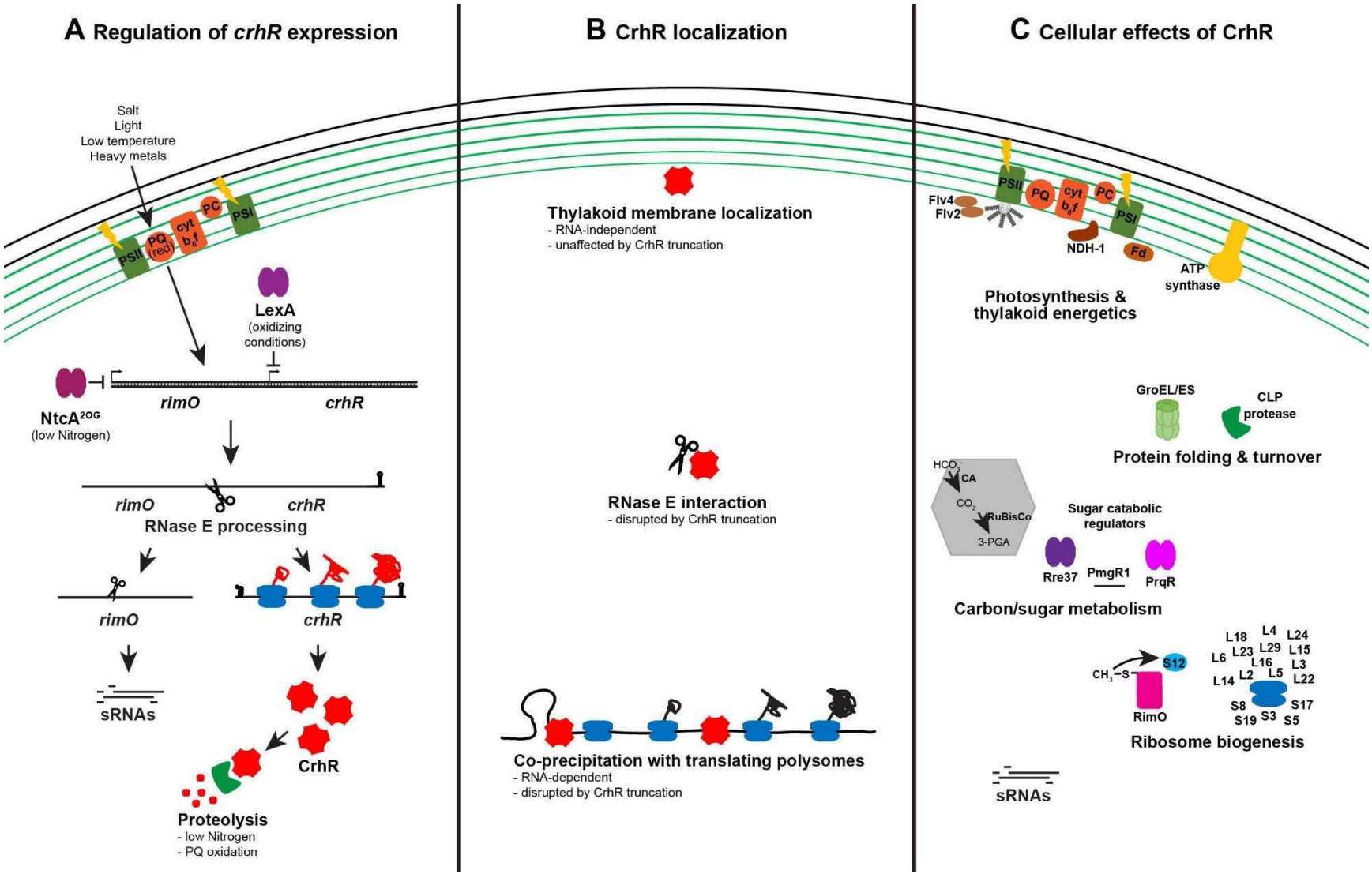
A Regulation of crhR expression
Salt
Light
Low temperature
Heavy metals
PSII
PQ (red)
cyt b6f
PC
PSI
LexA
(oxidizing conditions)
NtcA2OG
(low Nitrogen)
rimO
crhR
RNase E processing
rimO
crhR
rimO
crhR
sRNAs
CrhR
Proteolysis
- low Nitrogen
- PQ oxidation
B CrhR localization
Thylakoid membrane localization
- RNA-independent
- unaffected by CrhR truncation
RNase E interaction
- disrupted by CrhR truncation
Co-precipitation with translating polysomes
- RNA-dependent
- disrupted by CrhR truncation
C Cellular effects of CrhR
Flv4
Flv2
PSII
PQ
cyt b6f
PC
PSI
NDH-1
Fd
ATP synthase
Photosynthesis & thylakoid energetics
GroEL/ES
CLP protease
Protein folding & turnover
HCO3-
CA
CO2
RuBisCo
3-PGA
Sugar catabolic regulators
Rre37
PmgR1
PrqR
Carbon/sugar metabolism
CH3-S
S12
RimO
L18
L4
L24
L6
L23
L29
L15
L16
L3
L14
L2
L5
L22
S8
S17
S19
S3
S5
Ribosome biogenesis
sRNAs

Figure 6.1: CrhR in a *Synechocystis* cell: linking stress-responsive expression through to functions in cellular adaptation.
Summary model of the role of CrhR in *Synechocystis* from (A) regulation of *crhR* expression to (B) insights into CrhR function from protein localization though (C) the cellular effects of CrhR mutation. (A) Effects of nitrogen on *crhR* expression (Chapter 4) and processing of the *rimO-crhR* operon by RNase E (Chapter 3) are combined with prior studies (41, 163-165) to develop a comprehensive model for the regulation of *crhR* expression during stresses that affect the photosynthetic electron transport chain and/or nutrient availability. (B) Localization of CrhR to the thylakoid membrane (Chapter 2), as well as association with translating polysomes (Chapter 2) and RNase E (Chapter 3) suggest roles for CrhR in the processes of translation and RNA processing/degradation, particularly of thylakoid membrane-associated proteins. (C) The physiology (104, 158), and transcript and protein expression (147, 159, 375) of *crhR* mutants support a role for CrhR in mediating the expression of genes for maintenance of photosynthesis and electron transfer in the thylakoid membrane.
CA: carbonic anhydrase, cyt b_6f: cytochrome b_6f, Fd: ferredoxin, Flv2/Flv4: flavodiiron proteins, NDH-1: NADH dehydrogenase, PC: plastocyanin, PQ: plastoquinone, PSI: photosystem I, PSII: photosystem II.

ribosome maturation (109, 110, 116, 119, 176). CrhR is expressed from a conserved discistronic operon, *rimO-crhR*, with the ribosomal protein S12 methylthiotransferase, and could be predicted to also function in ribosomal modification; however, CrhR was found to only associate with polysome complexes, rather than 30S, 50S or 70S ribosome subunits. While this does not preclude a role in ribosome biogenesis, particularly as expression of the *sll1799-ssl3441* ribosomal protein operon is affected by CrhR truncation (147), the interaction of CrhR with polysome complexes specifically suggests a function for CrhR in translation.

Functions in protein translation are frequently proposed for prokaryotic DEAD-box RNA helicases, where helicase activity would be beneficial in resolving inhibitory secondary structures in the mRNA, allowing for enhanced translation especially under specific growth stresses (73, 376). Circumstantial evidence exists that CsdA in *E. coli* and *P. aeruginosa* may enhance translation initiation of select proteins, likely by resolving inhibitory structures in the 5' UTR (123-125). While CrhR and homologous cyanobacterial helicases were shown to form a unique protein clade distinct from any of the *E. coli* DEAD-box RNA helicases (Chapter 5), the *E. coli* helicase with the highest homology to CrhR was CsdA. This may suggest that CrhR helicases have some functional similarity to CsdA, most likely involving translation; however, the mechanism by which CsdA and CrhR participate in translation appears to differ based on the divergence of the conserved sequence motifs in the C-terminal extensions of the proteins.

RNA degradosome components were also co-precipitated with polysome complexes (Chapter 2). CrhR was not identified as part of the *Synechocystis* minimal degradosome in a prior study (192); however, the experiments were performed under conditions where CrhR is known to be minimally expressed (164). In Chapter 3, it was shown that the dicistronic *rimO-crhR* transcript is rapidly processed into two monocistronic transcripts of differing fates at low temperature, destabilizing the upstream *rimO* and stabilizing the downstream *crhR* transcript (Chapter 3). Processing of the *rimO-crhR* transcript occurs at a site possessing both conserved secondary structure and an RNase E cleavage consensus sequence (250, 256) that is cleaved *in vitro* by recombinant RNase E. While CrhR is not required for the processing event, unprocessed dicistronic transcripts gradually accumulate in the *crhR* truncation mutant, suggesting CrhR auto-

regulates processing of its own transcript. Thus, while it is not known if CrhR interacts directly with the degradosome complex in *Synechocystis*, it does affect the activity of RNase E, a component of the minimal degradosome (192). CrhR may function as an RNA clamp, generating and/or maintaining the ssRNA structure required for RNase E cleavage, thereby accelerating the processing event. Considering CrhR is the sole DEAD-box protein encoded in *Synechocystis*, it is possible that CrhR, like other bacterial RNA helicases (144, 176-178), performs multiple, divergent roles *in vivo*. One *E. coli* helicase, RhlB, has been suggested to have a simultaneous role in translating polysomes and RNA degradation, mediating interactions between the 50S ribosomal subunit in polysome complexes and the scaffolding domain of RNase E (144). Similar roles have been suggested for *H. pylori* RhpA and *S. aureus* CshA helicases, which also co-localize with both ribosome and degradosome proteins (120, 143). These examples of helicases from other eubacteria that associate with both ribosomes and RNA degradosomes support roles for CrhR in both translation and RNA processing/degradation.

Depending on the substrates of CrhR, a function for CrhR RNA helicase activity in translation and possibly RNA processing and degradation could allow CrhR activity to affect expression of many genes in *Synechocystis*. Indeed, microarray and proteomic studies (147, 159, 375) show that mutation of *crhR*, whether by truncation (147) or inactivation (159, 375), has profound effects on gene expression in *Synechocystis*. Altered trends in expression were demonstrated for approximately 10% of annotated mRNAs and ncRNAs (147) and at least 55 proteins (375) relating to diverse functional categories. A few of the differentially regulated proteins, the phycobiliprotein subunits and PsbO, a photosystem II component (375), and transcripts, encoding subunits of ATP synthase and NADH dehydrogenase and flavodiiron proteins (147), have functions in photosynthesis and energy metabolism. Transcripts and proteins with protein degradation and chaperone activities were also affected by *crhR* mutation (147, 159, 375). In particular, many of these gene products function to protect the photosynthetic proteins from oxidative damage, either by acting as electron sinks for excess reductant or assisting in turnover of damaged proteins. A function for CrhR in the translation, maturation and possibly degradation of these transcripts would provide a possible mechanism for the deleterious effects of *crhR* mutation on photosynthesis.

Interaction of CrhR with the photosynthetic thylakoid membrane is not limited to the effects of CrhR on expression of its components, as CrhR localizes to the thylakoid membrane region in *Synechocystis* (Chapter 2). Interestingly, although localization of CrhR to the thylakoid membrane is dependent on protein-protein interactions, the specialized CrhR-specific sequence domain conserved in the C-terminus of CrhR-like helicases in cyanobacteria is not required for this interaction, as a truncation mutant of *crhR,* $CrhR_{TR}$, localizes properly to the thylakoid membrane (Chapter 2). Compartmentalization of CrhR to the thylakoid membrane may allow the cyanobacterium to enhance the rapidity and specificity with which it can adapt the photosynthetic apparatus to abiotic stresses. For example, the photosystem II reaction centre protein D1 is differentially expressed depending on light quantity and quality (377). In the dark, translation of this protein is pre-initiated, then elongation is paused at a conserved site (187, 378). Following exposure to light, the D1 mRNA-bound polysome is targeted to the thylakoid membrane where translation continues (187). The mechanisms regulating this translational arrest process are not known. If an RNA duplex or interaction with the nascent polypeptide chain were blocking translation elongation, the helicase activity of thylakoid membrane-localized CrhR could assist in the resumption of translation elongation by resolving the inhibitory interaction. It is important to note that CrhR localization to the thylakoid membrane space is RNA-independent, while its association with polysomes is RNA-dependent. Thus, although CrhR compartmentalization to the thylakoid membrane space is likely to enhance its effects on expression of proteins that are embedded in or interact with the thylakoid membrane, that localization occurs independently of CrhR association with polysome complexes.

Induction of *crhR* expression in response to diverse abiotic stresses is regulated by the redox poise of the quinones at Q_B or the plastoquinone pool in the photosynthetic electron transport chain (163). In Chapter 4, an additional stress, nitrogen availability, was identified that affects *crhR* expression. CrhR protein is expressed when exogenous fixed nitrogen is available; however, under nitrogen-deplete conditions, CrhR protein is rapidly degraded and expression of *crhR* from the *rimO-crhR* promoter is repressed by the global nitrogen regulator NtcA. This suggests the activity of CrhR is required under conditions when fixed nitrogen is freely available, but is deleterious to the organism

during nitrogen starvation, even prior to the visible effects of chlorosis. As genes for nitrogen transport and assimilation are up-regulated during early stages of the chlorotic response, when CrhR is absent, it is unlikely that CrhR regulates these genes. Nitrogen stress also relates to the redox poise of photosynthesis, as the energetics of nitrogen assimilation are linked to reducing equivalents provided from the photosynthetic electron transport chain (283, 319) and some nitrogen responsive genes are also regulated in response to the redox poise of the electron transport chain (312, 328, 329, 338). Thus, we propose that the role of CrhR during nitrogen stress, like other abiotic stresses, is to maintain the efficiency of photosynthesis and electron transfer in the thylakoid membrane.

The conservation of CrhR-like proteins across the diversity of cyanobacterial lineages suggests that DEAD-box RNA helicases from the CrhR-like clade likely perform an important, conserved function in photosynthetic cyanobacteria. Based on the evidence presented in this thesis, a role for CrhR in regulating translation, particularly of substrate RNAs related to the maintenance of photosynthesis and electron transfer in the thylakoid membrane space, is proposed. Although it does not aid in thylakoid membrane localization, the unique C-terminal sequence motif characteristic of the CrhR-like proteins may function to mediate interaction with the polysomes, either by binding the ribosomal RNAs and/or proteins or, more likely, by interacting with its complement of substrate RNAs. The results presented here indicate that the conserved CrhR-specific sequence motif, identifying a unique clade within DEAD-box RNA helicases, may also be a component required for the auto-regulation of CrhR abundance, most likely mediating interactions with other regulators that act on *crhR* transcript and protein. Other cyanobacterial DEAD-box proteins group into two clades, the CsdA-like and RhlE-like helicases, with homology to the respective proteins in *E. coli*. Helicases from these two clades are restricted to select cyanobacterial lineages, reflecting later acquisition of the genes in comparison to CrhR-like helicases and a function that is likely less specialized to cyanobacteria.

Overall, the results reported in this thesis provide unique insights into the regulation of CrhR expression by RNA processing and nitrogen metabolism, as well as auto-regulation of CrhR expression. From CrhR localization and expression,

understanding of the physiological role of this helicase has also increased. These findings contribute to our understanding of CrhR as a redox-regulated RNA helicase, and indicate that CrhR functions in the cellular processes of translation and RNA processing/degradation, primarily mediating expression of genes related to the maintenance of photosynthesis and electron transfer in the thylakoid membrane. This connects expression of CrhR with its cellular effect, providing a paradigm in which a shift in redox poise of the photosynthetic electron transport chain to become more reducing induces expression of *crhR*, which then adjusts expression of electron sinks, protein chaperones and proteases to protect the photosynthetic membranes from oxidative damage. This protective regulatory mechanism may be conserved across cyanobacteria, as DEAD-box RNA helicases homologous to CrhR are found in various cyanobacterial lineages.

References

1. Schirrmeister, B. E., M. Gugger, and P. C. J. Donoghue. 2015. Cyanobacteria and the great oxidation event: evidence from genes and fossils. Palaeontology 58:769-785.

2. Stanier, R. Y., and C. B. van Niel. 1962. The concept of a bacterium. Arch Mikrobiol 42:17-35.

3. Jürgens, U. J., and J. Weckesser. 1985. The fine structure and chemical composition of the cell wall and sheath layers of cyanobacteria. Ann Inst Pasteur/Microbiol 136:41-44.

4. Stanier, R. Y., W. R. Sistrom, T. A. Hansen, B. A. Whitton, R. W. Castenholz, N. Pfennig, V. N. Gorlenko, E. N. Kondratieva, K. E. Eimhjellen, R. Whittenbury, R. L. Gherna, and H. G. Trüper. 1978. Proposal to place the nomenclature of the cyanobacteria (blue-green algae) under the rules of the international code of nomenclature of bacteria. Int J Syst Evol Microbiol 28:335-336.

5. Oren, A., and S. Ventura. 2017. The current status of cyanobacterial nomenclature under the "prokaryotic" and the "botanical" code. Antonie van Leeuwenhoek 110:1257-1269.

6. Turner, S., T. C. Huang, and S. M. Chaw. 2001. Molecular phylogeny of nitrogen-fixing unicellular cyanobacteria. Bot Bull Acad Sin 42:181-186.

7. Gugger, M. F., and L. Hoffmann. 2004. Polyphyly of true branching cyanobacteria (Stigonematales). Int J Syst Evol Microbiol 54:349-357.

8. Urbach, E., D. L. Robertson, and S. W. Chisholm. 1992. Multiple evolutionary origins of prochlorophytes within the cyanobacterial radiation. Nature 355:267-270.

9. Rippka, R., J. Waterbury, and G. Cohen-Bazire. 1974. A cyanobacterium which lacks thylakoids. Arch Microbiol 100:419-436.

10. Mitsui, A., S. Kumazawa, A. Takahashi, H. Ikemoto, S. Cao, and T. Arai. 1986. Strategy by which nitrogen fixing unicellular cyanobacteria grow photoautotrophically. Nature 323:720-722.

11. Di Rienzi, S. C., I. Sharon, K. C. Wrighton, O. Koren, L. A. Hug, B. C. Thomas, J. K. Goodrich, J. T. Bell, T. D. Spector, J. F. Banfield, and R. E. Ley. 2013. The human gut and groundwater harbor non-photosynthetic bacteria belonging to a new candidate phylum sibling to Cyanobacteria. eLife 2:e01102.

12. Ley, R. E., F. Bäckhed, P. Turnbaugh, C. A. Lozupone, R. D. Knight, and J. I. Gordon. 2005. Obesity alters gut microbial ecology. Proc Natl Acad Sci USA 102:11070-11075.

13. Soo, R. M., C. T. Skennerton, Y. Sekiguchi, M. Imelfort, S. J. Paech, P. G. Dennis, J. A. Steen, D. H. Parks, G. W. Tyson, and P. Hugenholtz. 2014. An expanded genomic representation of the phylum Cyanobacteria. Genome Biol Evol 6:1031-1045.

14. Shih, P. M., J. Hemp, L. M. Ward, N. J. Matzke, and W. W. Fischer. 2017. Crown group Oxyphotobacteria postdate the rise of oxygen. Geobiology 15:19-29.

15. Soo, R. M., J. Hemp, D. H. Parks, W. W. Fischer, and P. Hugenholtz. 2017. On the origins of oxygenic photosynthesis and aerobic respiration in Cyanobacteria. Science 355:1436-1440.

16. Iturriaga, R., and B. G. Mitchell. 1986. Chroococcoid cyanobacteria: a significant component in the food web dynamics of the open ocean. Mar Ecol Prog Ser 28:291-297.

17. Stockner, J. G., and N. J. Antia. 1986. Algal picoplankton from marine and freshwater ecosystems: a multidisciplinary perspective. Can J Fish Aquat Sci 43:2472-2503.

18. Hoffmann, L. 1989. Algae of terrestrial habitats. Bot Rev 55:77-105.

19. Honegger, R. 1991. Functional aspects of the lichen symbiosis. Annu Rev Plant Physiol Plant Mol Biol 42:553-578.

20. Büdel, B., T. Dulic, T. Darienko, N. Rybalka, and T. Friedl. 2016. Cyanobacteria and algae of biological soil crusts, p. 55-80. *In* B. Weber, B. Büdel, and J. Belnap (eds.), Biological soil crusts; an organizing principle in drylands. Springer, Cham.

21. Gibbs, M. 1967. Photosynthesis. Annu Rev Biochem 36:757-784.

22. Margulis, L. 1971. The origin of plant and animal cells. Am Sci 59:230-235.

23. Martin, W., T. Rujan, E. Richly, A. Hansen, S. Cornelsen, T. Lins, D. Leister, B. Stoebe, M. Hasegawa, and D. Penny. 2002. Evolutionary analysis of *Arabidopsis*, cyanobacterial, and chloroplast genomes reveals plastid phylogeny and thousands of cyanobacterial genes in the nucleus. Proc Natl Acad Sci USA 99:12246-12251.

24. Huisman, J., G. A. Codd, H. W. Paerl, B. W. Ibelings, J. M. H. Verspagen, and P. M. Visser. 2018. Cyanobacterial blooms. Nat Rev Microbiol 16:471-483.

25. Paerl, H. W., and T. G. Otten. 2013. Harmful cyanobacterial blooms: causes, consequences, and controls. Microb Ecol 65:995-1010.

26. Pipal, M., J. Priebojova, T. Koci, L. Blahova, M. Smutna, and K. Hilscherova. 2020. Field cyanobacterial blooms producing retinoid compounds cause teratogenicity in zebrafish embryos. Chemosphere 241:125061.

27. Rabalais, N. N., R. J. Díaz, L. A. Levin, R. E. Turner, D. Gilbert, and J. Zhang. 2010. Dynamics and distribution of natural and human-caused hypoxia. Biogeosciences 7:585-619.

28. Nozzi, N. E., J. W. K. Oliver, and S. Atsumi. 2013. Cyanobacteria as a platform for biofuel production. Front Bioeng Biotechnol 1:7.

29. Troschl, C., K. Meixner, and B. Drosg. 2017. Cyanobacterial PHA production - review of recent advances and a summary of three years' working experience running a pilot plant. Bioengineering 4:26.

30. Brand, L. A., and G. W. Owttrim. 2017. Cyanobacterial biofactories: combining evolved and synthetic genetic regulatory mechanisms to yield carbon-neutral bioproducts. J Postdoctoral Res 5:19-24.

31. Rosgaard, L., A. J. de Porcellinis, J. H. Jacobsen, N. Frigaard, and Y. Sakuragi. 2012. Bioengineering of carbon fixation, biofuels, and biochemicals in cyanobacteria and plants. J Biotechnol 162:134-147.

32. Stanier, R. Y., R. Kunisawa, M. Mandel, and G. Cohen-Bazire. 1971. Purification and properties of unicellular blue-green algae (order *Chroococcales*). Bacteriol Rev 35:171-205.

33. Rippka, R., J. Deruelles, J. B. Waterbury, M. Herdman, and R. Y. Stanier. 1979. Generic assignments, strain histories and properties of pure cultures of cyanobacteria. Microbiology 111:1-61.

34. Kaneko, T., S. Sato, H. Kotani, A. Tanaka, E. Asamizu, Y. Nakamura, N. Miyajima, M. Hirosawa, M. Sugiura, S. Sasamoto, T. Kimura, T. Hosouchi, A. Matsuno, A. Muraki, N. Nakazaki, K. Naruo, S. Okumura, S. Shimpo, C. Takeuchi, T. Wada, A. Watanabe, M. Yamada, M. Yasuda, and S. Tabata. 1996. Sequence analysis of the genome of the unicellular cyanobacterium *Synechocystis* sp. strain PCC6803. II. sequence determination of the entire genome and assignment of potential protein-coding regions. DNA Res 3:109-136.

35. Kaneko, T., Y. Nakamura, S. Sasamoto, A. Watanabe, M. Kohara, M. Matsumoto, S. Shimpo, M. Yamada, and S. Tabata. 2003. Structural analysis of four large plasmids harboring in a unicellular cyanobacterium, *Synechocystis* sp. PCC 6803. DNA Res 10:221-228.

36. Yang, X., and B. A. McFadden. 1993. A small plasmid, pCA2.4, from the cyanobacterium *Synechocystis* sp. strain PCC 6803 encodes a rep protein and replicates by a rolling circle mechanism. J Bacteriol 175:3981-3991.

37. Yang, X., and B. A. McFadden. 1994. The complete DNA sequence and replication analysis of the plasmid pCB2.4 from the cyanobacterium *Synechocystis* PCC 6803. Plasmid 31:131-137.

38. Xu, W., and B. A. McFadden. 1997. Sequence analysis of plasmid pCC5.2 from cyanobacterium *Synechocystis* PCC 6803 that replicates by a rolling circle mechanism. Plasmid 37:95.

39. Trautmann, D., B. Voss, A. Wilde, S. Al-Babili, and W. R. Hess. 2012. Microevolution in cyanobacteria: re-sequencing a motile substrain of *Synechocystis* sp. PCC 6803. DNA Res 19:435-448.

40. Kanesaki, Y., Y. Shiwa, N. Tajima, M. Suzuki, S. Watanabe, N. Sato, M. Ikeuchi, and H. Yoshikawa. 2012. Identification of substrain-specific mutations by massively parallel whole-genome resequencing of *Synechocystis* sp. PCC 6803. DNA Res 19:67-79.

41. Kujat, S. L., and G. W. Owttrim. 2000. Redox-regulated RNA helicase expression. Plant Physiol 124:703-714.

42. Nakamura, Y., T. Kaneko, M. Hirosawa, N. Miyajima, and S. Tabata. 1998. CyanoBase, a www database containing the complete nucleotide sequence of the genome of *Synechocystis* sp. strain PCC6803. Nucleic Acids Res 26:63-67.

43. Fujisawa, T., R. Narikawa, S. Maeda, S. Watanabe, Y. Kanesaki, K. Kobayashi, J. Nomata, M. Hanaoka, M. Watanabe, S. Ehira, E. Suzuki, K. Awai, and Y. Nakamura. 2017. CyanoBase: a large-scale update on its 20th anniversary. Nucleic Acids Res 45:D551-D554.

44. Ikeuchi, M., and S. Tabata. 2001. *Synechocystis* sp. PCC 6803 - a useful tool in the study of the genetics of cyanobacteria. Photosynth Res 70:73-83.

45. Grigorieva, G., and S. Shestakov. 1982. Transformation in the cyanobacterium *Synechocystis* sp. 6803. FEMS Microbiol Lett 13:367-370.

46. Williams, J. G. K. 1988. Construction of specific mutations in photosystem II photosynthetic reaction center by genetic engineering methods in *Synechocystis* 6803. Methods Enzymol 167:766-778.

47. Griese, M., C. Lange, and J. Soppa. 2011. Ploidy in cyanobacteria. FEMS Microbiol Lett 323:124-131.

48. Zerulla, K., K. Ludt, and J. Soppa. 2016. The ploidy level of *Synechocystis* sp. PCC 6803 is highly variable and is influenced by growth phase and by chemical and physical external parameters. Microbiology 162:730-739.

49. Marraccini, P., S. Bulteau, C. Cassier-Chauvat, P. Mermet-Bouvier, and F. Chauvat. 1993. A conjugative plasmid vector for promotor analysis in several cyanobacteria of the genera *Synechococcus* and *Synechocystis*. Plant Mol Biol 23:905-909.

50. Camsund, D., T. Heidorn, and P. Lindblad. 2014. Design and analysis of LacI-repressed promoters and DNA-looping in a cyanobacterium. J Biol Eng 8:4.

51. Schneider, G. J., and R. Haselkorn. 1988. RNA polymerase subunit homology among cyanobacteria, other eubacteria and archaebacteria. J Bacteriol 170:4136-4140.

52. Heidorn, T., D. Camsund, H. H. Huang, P. Lindberg, P. Oliveira, K. Stensjö, and P. Lindblad. 2011. Synthetic biology in cyanobacteria: engineering and analyzing novel functions. Methods Enzymol 497:539-579.

53. Viola, S., T. Rühle, and D. Leister. 2014. A single vector-based strategy for marker-less gene replacement in *Synechocystis* sp. PCC 6803. Microb Cell Fact 13:4.

54. Xiao, Y., S. Wang, S. Rommelfanger, A. Balassy, C. Barba-Ostria, P. Gu, J. M. Galazka, and F. Zhang. 2018. Developing a Cas9-based tool to engineer native plasmids in *Synechocystis* sp. PCC 6803. Biotechnol Bioeng 115:2305-2314.

55. Yao, L., I. Cengic, J. Anfelt, and E. P. Hudson. 2016. Multiple gene repression in cyanobacteria using CRISPRi. ACS Synth Biol 5:207-212.

56. Vasudevan, R., G. A. R. Gale, A. A. Schiavon, A. Puzorjov, J. Malin, M. D. Gillespie, K. Vavitsas, V. Zulkower, B. Wang, C. J. Howe, D. J. Lea-Smith, and A. J. McCormick. 2019. CyanoGate: a modular cloning suite for engineering cyanobacteria based on the plant MoClo syntax. Plant Physiol 180:39-55.

57. Gorbalenya, A. E., and E. V. Koonin. 1993. Helicases: amino acid sequence comparisons and structure-function relationships. Curr Opin Struct Biol 3:419-429.

58. Singleton, M. R., M. S. Dillingham, and D. B. Wigley. 2007. Structure and mechanism of helicases and nucleic acid translocases. Ann Rev Biochem 76:23-50.

59. Fairman-Williams, M. E., U. P. Guenther, and E. Jankowsky. 2010. SF1 and SF2 helicases: family matters. Curr Opin Struct Biol 20:313-324.

60. Leeds, N. B., E. C. Small, S. L. Hiley, T. R. Hughes, and J. P. Staley. 2006. The splicing factor Prp43p, a DEAH box ATPase, functions in ribosome biogenesis. Mol Cell Biol 26:513-522.

61. Koo, J. T., J. Choe, and S. L. Moseley. 2004. HrpA, a DEAH-box RNA helicase, is involved in mRNA processing of a fimbrial operon in *Escherichia coli*. Mol Microbiol 52:1813-1826.

62. Martin, R., A. U. Straub, C. Doebele, and M. T. Bohnsack. 2012. DExD/H-box RNA helicases in ribosome biogenesis. RNA Biol 9:4-18.

63. Martin, A., S. Schneider, and B. Schwer. 2002. Prp43 is an essential RNA-dependent ATPase required for release of lariat-intron from the spliceosome. J Biol Chem 277:17743-17750.

64. Tanner, N. K., and P. Linder. 2001. DExD/H box RNA helicases: from generic motors to specific dissociation functions. Mol Cell 8:251-262.

65. Weir, J. R., F. Bonneau, J. Hentschel, and E. Conti. 2010. Structural analysis reveals the characteristic features of Mtr4, a DExH helicase involved in nuclear RNA processing and surveillance. Proc Natl Acad Sci USA 107:12139-12144.

66. Byrd, A. K., and K. D. Raney. 2012. Superfamily 2 helicases. Front Biosci 17:2070-2088.

67. Khemici, V., and P. Linder. 2016. RNA helicases in bacteria. Curr Opin Microbiol 30:58-66.

68. Loo, Y. M., and M. Gale Jr. 2011. Immune signaling by RIG-I-like receptors. Immunity 34:680-692.

69. Kwong, A. D., J. L. Kim, and C. Lin. 2000. Structure and function of hepatitis C virus NS3 helicase. Curr Top Microbiol 242:171-197.

70. Gwack, Y., D. W. Kim, J. H. Han, and J. Choe. 1996. Characterization of RNA binding activity and RNA helicase activity of the hepatitis C virus NS3 protein. Biochem Biophys Res Comm 225:654-659.

71. Shuman, S. 1993. Vaccinia virus RNA helicase. Directionality and substrate specificity. J Biol Chem 268:11798-11802.

72. Linder, P., and E. Jankowsky. 2011. From unwinding to clamping — the DEAD box RNA helicase family. Nat Rev Mol Cell Biol 12:505-516.

73. Owttrim, G. W. 2012. RNA helicases: Diverse roles in prokaryotic response to abiotic stress. RNA Biol 10:96-110.

74. Owttrim, G. W. 2006. RNA helicases and abiotic stress. Nucleic Acids Res 34:3220-3230.

75. Redder, P., S. Hausmann, V. Khemici, H. Yasrebi, and P. Linder. 2015. Bacterial versatility requires DEAD-box RNA helicases. FEMS Microbiol Rev 39:392-412.

76. Schmid, S. R., and P. Linder. 1992. D-E-A-D protein family of putative RNA helicases. Mol Microbiol 6:283-291.

77. Linder, P., and Fuller-Pace, F. 2015. Happy birthday: 25 years of DEAD-box proteins. Methods Mol Biol 1259:17-33.

78. Walker, J. E., M. Saraste, M. J. Runswick, and N. J. Gay. 1982. Distantly related sequences in the alpha- and beta-subunits of ATP synthase, myosin, kinases and other ATP-requiring enzymes and a common nucleotide binding fold. EMBO J 1:945-651.

79. Tanner, N. K., O. Cordin, J. Banroques, M. Doère, and P. Linder. 2003. The Q Motif: A newly identified motif in DEAD box helicases may regulate ATP binding and hydrolysis. Mol Cell 11:127-138.

80. Cordin, O., N. K. Tanner, M. Doère, P. Linder, and J. Banroques. 2004. The newly discovered Q motif of DEAD-box RNA helicases regulates RNA-binding and helicase activity. EMBO J 23:2478-2487.

81. Sengoku, T., O. Nureki, A. Nakamura, S. Kobayashi, and S. Yokoyama. 2006. Structural basis for RNA unwinding by the DEAD-box protein *Drosophila* Vasa. Cell 125:287-300.

82. Schütz, P., T. Karlberg, S. van den Berg, R. Collins, L. Lehtiö, M. Högbom, L. Holmberg-Schiavone, W. Tempel, H. W. Park, M. Hammarström, M. Moche, A. G.

Thorsell, and H. Schüler. 2010. Comparative structural analysis of human DEAD-box RNA helicases. PLoS ONE 5:e12791.

83. Rogers Jr, G. W., W. F. Lima, and W. C. Merrick. 2001. Further characterization of the helicase activity of eIF4A. Substrate specificity. J Biol Chem 276:12598-12608.

84. Banroques, J., M. Doère, M. Dreyfus, P. Linder, and N. K. Tanner. 2010. Motif III in superfamily 2 "helicases" helps convert the binding energy of ATP into a high-affinity RNA binding site in the yeast DEAD-box protein Ded1. J Mol Biol 396:949.

85. Liu, F., A. Putnam, and E. Jankowsky. 2008. ATP hydrolysis is required for DEAD-box protein recycling but not for duplex unwinding. Proc Natl Acad Sci USA 105:20209-20214.

86. Yang, Q., and E. Jankowsky. 2006. The DEAD-box protein Ded1 unwinds RNA duplexes by a mode distinct from translocating helicases. Nat Struct Mol Biol 13:981-986.

87. Liu, F., A. Putnam, and E. Jankowsky. 2014. DEAD-box helicases form nucleotide-dependent, long-lived complexes with RNA. Biochemistry 53:423-433.

88. Seal, S. N., A. Schmidt, and A. Marcus. 1983. Eukaryotic initiation factor 4A is the component that interacts with ATP in protein chain initiation. Proc Natl Acad Sci USA 80:6562-6565.

89. Lawson, T. G., K. A. Lee, M. M. Maimone, R. D. Abramson, T. E. Dever, W. C. Merrick, and R. E. Thach. 1989. Dissociation of double-stranded polynucleotide helical structures by eukaryotic initiation factors, as revealed by a novel assay. Biochemistry 28:4729-4734.

90. Rozen, F., I. Edery, K. Meerovitch, T. E. Dever, W. C. Merrick, and N. Sonenberg. 1990. Bidirectional RNA helicase activity of eucaryotic translation initiation factors 4A and 4F. Mol Cell Biol 10:1134-1144.

91. Svitkin, Y. V., A. Pause, A. Haghighat, S. Pyronnet, G. Witherell, G. J. Belsham, and N. Sonenberg. 2001. The requirement for eukaryotic initiation factor 4A (elF4A) in translation is in direct proportion to the degree of mRNA 5' secondary structure. RNA 7:382-394.

92. Pestova, T. V., and V. G. Kolupaeva. 2002. The roles of individual eukaryotic translation initiation factors in ribosomal scanning and initiation codon selection. Genes Dev 16:2906-2922.

93. Cordin, O., and J. D. Beggs. 2012. RNA helicases in splicing. RNA Biol 10:83-95.

94. Halls, C., S. Mohr, M. Del Campo, Q. Yang, E. Jankowsky, and A. M. Lambowitz. 2007. Involvement of DEAD-box proteins in group I and group II intron splicing. Biochemical characterization of Mss116p, ATP hydrolysis-dependent and -independent mechanisms, and general RNA chaperone activity. J Mol Biol 365:835-855.

95. Potratz, J. P., M. Del Campo, R. Z. Wolf, A. M. Lambowitz, and R. Russell. 2011. ATP-dependent roles of the DEAD-box protein Mss116p in group II intron splicing *in vitro* and *in vivo*. J Mol Biol 411:661-679.

96. Huang, H. R., C. E. Rowe, S. Mohr, Y. Jiang, A. M. Lambowitz, and P. S. Perlman. 2005. The splicing of yeast mitochondrial group I and group II introns requires a DEAD-box protein with RNA chaperone function. Proc Natl Acad Sci USA 102:163-168.

97. Del Campo, M., S. Mohr, Y. Jiang, H. Jia, E. Jankowsky, and A. M. Lambowitz. 2009. Unwinding by local strand separation is critical for the function of DEAD-box proteins as RNA chaperones. J Mol Biol 389:674-693.

98. Stepien, P. P., S. P. Margossian, D. Landsman, and R. A. Butow. 1992. The yeast nuclear gene *suv3* affecting mitochondrial post-transcriptional processes encodes a putative ATP-dependent RNA helicase. Proc Natl Acad Sci USA 89:6813-6817.

99. Margossian, S. P., H. Li, H. P. Zassenhaus, and R. A. Butow. 1996. The DExH box protein Suv3p is a component of a yeast mitochondrial 3'-to-5' exoribonuclease that suppresses group I intron toxicity. Cell 84:199-209.

100. Dziembowski, A., M. Malewicz, M. Minczuk, P. Golik, A. Dmochowska, and P. P. Stepien. 1998. The yeast nuclear gene DSS1, which codes for a putative RNase II, is necessary for the function of the mitochondrial degradosome in processing and turnover of RNA. Mol Gen Genet 260:108-114.

101. Guo, X. E., C. F. Chen, D. D. H. Wang, A. S. Modrek, V. H. Phan, W. H. Lee, and P. L. Chen. 2011. Uncoupling the roles of the SUV3 helicase in maintenance of mitochondrial genome stability and RNA degradation. J Biol Chem 286:38783-38794.

102. Jagessar, K. L., and C. Jain. 2010. Functional and molecular analysis of *Escherichia coli* strains lacking multiple DEAD-box helicases. RNA 16:1386-1392.

103. Cartier, G., F. Lorieux, F. Allemand, M. Dreyfus, and T. Bizebard. 2010. Cold adaptation in DEAD-box proteins. Biochemistry 49:2636-2646.

104. Rosana, A. R. R., M. Ventakesh, D. Chamot, L. M. Patterson-Fortin, O. Tarassova, G. S. Espie, and G. W. Owttrim. 2012. Inactivation of a low temperature-induced RNA helicase in *Synechocystis* sp. PCC 6803: physiological and morphological consequences. Plant Cell Physiol 53:646-658.

105. Chamot, D., W. C. Magee, E. Yu, and G. W. Owttrim. 1999. A cold shock-induced cyanobacterial RNA helicase. J Bacteriol 181:1728.

106. Jones, P. G., M. Mitta, Y. Kim, W. Jiang, and M. Inouye. 1996. Cold shock induces a major ribosomal-associated protein that unwinds double-stranded RNA in *Escherichia coli*. Proc Natl Acad Sci USA 93:76-80.

107. López-Ramírez, V., L. D. Alcaraz, G. Moreno-Hagelsieb, and G. Olmedo-Álvarez. 2011. Phylogenetic distribution and evolutionary history of bacterial DEAD-box proteins. J Mol Evol 72:413-431.

108. Chandran, V., L. Poljak, N. F. Vanzo, A. Leroy, R. N. Miguel, J. Fernandez-Recio, J. Parkinson, C. Burns, A. J. Carpousis, and B. F. Luisi. 2007. Recognition and cooperation between the ATP-dependent RNA helicase RhlB and ribonuclease RNase E. J Mol Biol 367:113-132.

109. Charollais, J., M. Dreyfus, and I. Iost. 2004. CsdA, a cold-shock RNA helicase from *Escherichia coli,* is involved in the biogenesis of 50S ribosomal subunit. Nucleic Acids Res 32:2751-2759.

110. Charollais, J., D. Pflieger, J. Vinh, M. Dreyfus, and I. Iost. 2003. The DEAD-box RNA helicase SrmB is involved in the assembly of 50S ribosomal subunits in *Escherichia coli*. Mol Microbiol 48:1253-1265.

111. Jain, C. 2008. The *E. coli* RhlE RNA helicase regulates the function of related RNA helicases during ribosome assembly. RNA 14:381-389.

112. Böddeker, N., K. Stade, and F. Franceschi. 1997. Characterization of DbpA, an *Escherichia coli* DEAD box protein with ATP independent RNA unwinding activity. Nucleic Acids Res 25:537-545.

113. Peil, L., K. Virumäe, and J. Remme. 2008. Ribosome assembly in *Escherichia coli* strains lacking the RNA helicase DeaD/CsdA or DbpA. FEBS J 275:3772-3782.

114. Nicol, S. M., and F. V. Fuller-Pace. 1995. The "DEAD box" protein DbpA interacts specifically with the peptidyltransferase center in 23S rRNA. Proc Natl Acad Sci USA 92:11681-11685.

115. Sharpe Elles, L. M., M. T. Sykes, J. R. Williamson, and O. C. Uhlenbeck. 2009. A dominant negative mutant of the *E. coli* RNA helicase DbpA blocks assembly of the 50S ribosomal subunit. Nucleic Acids Res 37:6503-6514.

116. Iost, I., and C. Jain. 2019. A DEAD-box protein regulates ribosome assembly through control of ribosomal protein synthesis. Nucleic Acids Res 47:8193-8206.

117. Netterling, S., K. Vaitkevicius, S. Nord, and J. Johansson. 2012. A *Listeria monocytogenes* RNA helicase essential for growth and ribosomal maturation at low temperatures uses its C terminus for appropriate interaction with the ribosome. J Bacteriol 194:4377-4385.

118. Kossen, K., and O. C. Uhlenbeck. 1999. Cloning and biochemical characterization of *Bacillus subtilis* YxiN, a DEAD protein specifically activated by 23S rRNA: delineation of a novel sub-family of bacterial DEAD proteins. Nucleic Acids Res 27:3811-3820.

119. Lehnik-Habrink, M., L. Rempeters, A. T. Kovács, C. Wrede, C. Baierlein, H. Krebber, O. P. Kuipers, and J. Stülke. 2013. DEAD-Box RNA helicases in *Bacillus subtilis* have multiple functions and act independently from each other. J Bacteriol 195:534-544.

120. Giraud, C., S. Hausmann, S. Lemeille, J. Prados, P. Redder, and P. Linder. 2015. The C-terminal region of the RNA helicase CshA is required for the interaction with the degradosome and turnover of bulk RNA in the opportunistic pathogen *Staphylococcus aureus*. RNA Biol 12:658-674.

121. Takyar, S., R. P. Hickerson, and H. F. Noller. 2005. mRNA helicase activity of the ribosome. Cell 120:49-58.

122. Qu, X., J. D. Wen, L. Lancaster, H. F. Noller, C. Bustamante, and I. Tinoco Jr. 2011. The ribosome uses two active mechanisms to unwind mRNA during translation. Nature 475:118-121.

123. Butland, G., N. J. Krogan, J. Xu, W. H. Yang, H. Aoki, J. S. Li, N. Krogan, J. Menendez, G. Cagney, G. C. Kiani, M. G. Jessulat, N. Datta, I. Ivanov, M. G. Abouhaidar, A. Emili, J. Greenblatt, M. C. Ganoza, and A. Golshani. 2007.

Investigating the *in vivo* activity of the DeaD protein using protein-protein interactions and the translational activity of structured chloramphenicol acetyltransferase mRNAs. J Cell Biochem 100:642-652.

124. Vakulskas, C. A., A. Pannuri, D. Cortés-Selva, T. R. Zere, B. M. Ahmer, P. Babitzke, and T. Romeo. 2014. Global effects of the DEAD-box RNA helicase DeaD (CsdA) on gene expression over a broad range of temperatures. Mol Microbiol 92:945-958.

125. Intile, P. J., G. J. Balzer, M. C. Wolfgang, and T. L. Yahr. 2015. The RNA helicase DeaD stimulates ExsA translation to promote expression of *Pseudomonas aeruginosa* type III secretion system. J Bacteriol 197:2664-2674.

126. Iost, I., and M. Dreyfus. 1994. mRNAs can be stabilized by DEAD-box proteins. Nature 372:193-196.

127. Py, B., C. F. Higgins, H. M. Krisch, and A. J. Carpousis. 1996. A DEAD-box RNA helicase in the *Escherichia coli* RNA degradosome. Nature 381:169-172.

128. Coburn, G. A., X. Miao, D. J. Briant, and G. A. Mackie. 1999. Reconstitution of a minimal RNA degradosome demonstrates functional coordination between a 3' exonuclease and a DEAD-box RNA helicase. Genes Dev 13:2594-2603.

129. Morita, T., H. Kawamoto, T. Mizota, T. Inada, and H. Aiba. 2004. Enolase in the RNA degradosome plays a crucial role in the rapid decay of glucose transporter mRNA in response to phosphosugar stress in *Escherichia coli*. Mol Microbiol 54:1063-1075.

130. Taraseviciene, L., G. R. Björk, and B. E. Uhlin. 1995. Evidence for an RNA binding region in the *Escherichia coli* processing endoribonuclease RNase E. J Biol Chem 270:26391-26398.

131. McDowall, K. J., and S. N. Cohen. 1996. The N-terminal domain of the *rne* gene product has RNase E activity and is non-overlapping with the arginine-rich RNA-binding site. J Mol Biol 255:349-355.

132. Vanzo, N. F., Y. S. Li, B. Py, E. Blum, C. F. Higgins, L. C. Raynal, H. M. Krisch, and A. J. Carpousis. 1998. Ribonuclease E organizes the protein interactions in the *Escherichia coli* RNA degradosome. Genes Dev 12:2770-2781.

133. Callaghan, A. J., J. P. Aurikko, L. L. Ilag, J. G. Grossmann, V. Chandran, K. Kühnel, L. Poljak, A. J. Carpousis, C. V. Robinson, M. F. Symmons, and B. F. Luisi. 2004. Studies of the RNA degradosome-organizing domain of the *Escherichia coli* ribonuclease RNase E. J Mol Biol 340:965-979.

134. Worrall, J. A. R., M. Górna, N. T. Crump, L. G. Phillips, A. C. Tuck, A. J. Price, V. N. Bavro, and B. F. Luisi. 2008. Reconstitution and analysis of the multienzyme *Escherichia coli* RNA degradosome. J Mol Biol 382:870-883.

135. Misra, T. K., and D. Apirion. 1979. RNase E, an RNA processing enzyme from *Escherichia coli*. J Biol Chem 254:11154-11159.

136. McLaren, R. S., S. F. Newbury, G. S. Dance, H. C. Causton, and C. F. Higgins. 1991. mRNA degradation by processive 3'-5' exoribonucleases *in vitro* and the implications for prokaryotic mRNA decay *in vivo*. J Mol Biol 221:81-95.

137. Lin, P. H., and S. Lin-Chao. 2005. RhlB helicase rather than enolase is the beta-subunit of the *Escherichia coli* polynucleotide phosphorylase (PNPase)-exoribonucleolytic complex. Proc Natl Acad Sci USA 102:16590-16595.

138. Aït-Bara, S., and A. J. Carpousis. 2010. Characterization of the RNA degradosomes of *Pseudoalteromonas haloplanktis*: conservation of the RNase E-RhlB interaction in the gammaproteobacteria. J Bacteriol 192:5413-5423.

139. Hardwick, S. W., V. S. Y. Chan, R. W. Broadhurst, and B. F. Luisi. 2011. An RNA degradosome assembly in *Caulobacter crescentus*. Nucleic Acids Res 39:1449-1459.

140. Aguirre, A. A., A. M. Vicente, S. W. Hardwick, D. M. Alvelos, R. R. Mazzon, B. F. Luisi, and M. V. Marques. 2017. Association of the cold shock DEAD-box RNA helicase RhlE to the RNA degradosome in *Caulobacter crescentus*. J Bacteriol 199:135.

141. Jäger, S., O. Fuhrmann, C. Heck, M. Hebermehl, E. Schiltz, R. Rauhut, and G. Klug. 2001. An mRNA degrading complex in *Rhodobacter capsulatus*. Nucleic Acids Res 29:4581-4588.

142. Lehnik-Habrink, M., H. Pförtner, L. Rempeters, N. Pietack, C. Herzberg, and J. Stülke. 2010. The RNA degradosome in *Bacillus subtilis*: identification of CshA as the major RNA helicase in the multiprotein complex. Mol Microbiol 77:958-971.

143. Redko, Y., S. Aubert, A. Stachowicz, P. Lenormand, A. Namane, F. Darfeuille, M. Thibonnier, and H. De Reuse. 2013. A minimal bacterial RNase J-based degradosome is associated with translating ribosomes. Nucleic Acids Res 41:288-301.

144. Tsai, Y. C., D. Du, L. Domínguez-Malfavón, D. Dimastrogiovanni, J. Cross, A. J. Callaghan, J. García-Mena, and B. F. Luisi. 2012. Recognition of the 70S ribosome and polysome by the RNA degradosome in *Escherichia coli*. Nucleic Acids Res 40:10417-10431.

145. Ikeda, Y., M. Yagi, T. Morita, and H. Aiba. 2011. Hfq binding at RhlB-recognition region of RNase E is crucial for the rapid degradation of target mRNAs mediated by sRNAs in *Escherichia coli*. Mol Microbiol 79:419-432.

146. Resch, A., B. Većerek, K. Palavra, and U. Bläsi. 2010. Requirement of the CsdA DEAD-box helicase for low temperature riboregulation of *rpoS* mRNA. RNA Biol 7:796-802.

147. Georg, J., A. R. R. Rosana, D. Chamot, A. Migur, W. R. Hess, and G. W. Owttrim. 2019. Inactivation of the RNA helicase CrhR impacts a specific subset of the

transcriptome in the cyanobacterium *Synechocystis* sp. PCC 6803. RNA Biol 16:1205-1214.

148. Magee, W. C. 1997. Characterization of a cyanobacterial RNA helicase gene. MSc Thesis, University of Alberta, Edmonton, Alberta.

149. Chamot, D., and G. W. Owttrim. 2000. Regulation of cold shock-induced RNA helicase gene expression in the cyanobacterium *Anabaena* sp. strain PCC 7120. J Bacteriol 182:1251-1256.

150. Brown, J. M. 2005. 5′ UTR RNA secondary structure of a cold-induced RNA helicase functions as a thermosensor. MSc Thesis, University of Alberta, Edmonton, Alberta.

151. Yu, E., and G. W. Owttrim. 2000. Characterization of the cold stress-induced cyanobacterial DEAD-box protein CrhC as an RNA helicase. Nucleic Acids Res 28:3926-3934.

152. El-Fahmawi, B., and G. W. Owttrim. 2003. Polar-biased localization of the cold stress-induced RNA helicase CrhC, in the cyanobacterium *Anabaena* sp. strain PCC 7120. Mol Microbiol 50:1439-1448.

153. Chamot, D., K. R. Colvin, S. L. Kujat-Choy, and G. W. Owttrim. 2005. RNA structural rearrangement via unwinding and annealing by the cyanobacterial RNA helicase, CrhR. J Biol Chem 280:2036-2044.

154. Rössler, O. G., A. Straka, and H. Stahl. 2001. Rearrangement of structured RNA via branch migration structures catalysed by the highly related DEAD-box proteins p68 and p72. Nucleic Acids Res 29:2088-2096.

155. Yang, Q., and E. Jankowsky. 2005. ATP- and ADP-dependent modulation of RNA unwinding and strand annealing activities by the DEAD-box protein DED1. Biochemistry 44:13591-13601.

156. Stampfl, S., M. Doetsch, M. Beich-Frandsen, and R. Schroeder. 2013. Characterization of the kinetics of RNA annealing and strand displacement activities of the *E. coli* DEAD-box helicase CsdA. RNA Biol 10:149-156.

157. Skeik, R. M. 2012. Dimerization of the DEAD-box RNA helicase redox, CrhR. MSc Thesis, University of Alberta, Edmonton, Alberta.

158. Sireesha, K., B. Radharani, P. S. Krishna, N. Sreedhar, R. Subramanyam, P. Mohanty, and J. S. S. Prakash. 2012. RNA helicase, CrhR is indispensable for the energy redistribution and the regulation of photosystem stoichiometry at low temperature in *Synechocystis* sp PCC 6803. Biochim Biophys Acta 1817:1525-1536.

159. Prakash, J. S. S., P. S. Krishna, K. Sirisha, Y. Kanesaki, I. Suzuki, S. Shivaji, and N. Murata. 2010. An RNA helicase, CrhR, regulates the low-temperature-inducible expression of heat-shock genes *groES*, *groEL*1 and *groEL*2 in *Synechocystis* sp. PCC 6803. Microbiology 156:442-451.

160. Tarassova, O. S., D. Chamot, and G. W. Owttrim. 2014. Conditional, temperature-induced proteolytic regulation of cyanobacterial RNA helicase expression. J Bacteriol 196:1560-1568.

161. Vinnemeier, J., and M. Hagemann. 1999. Identification of salt-regulated genes in the genome of the cyanobacterium *Synechocystis* sp. strain PCC 6803 by subtractive RNA hybridization. Arch Microbiol 172:377-386.

162. Suzuki, I., Y. Kanesaki, K. Mikami, M. Kanehisa, and N. Murata. 2001. Cold-regulated genes under control of the cold sensor Hik33 in *Synechocystis*. Mol Microbiol 40:235-244.

163. Ritter, S. P. A., A. C. Lewis, S. L. Vincent, L. L. Lo, A. P. A. Cunha, D. Chamot, I. Ensminger, G. S. Espie, and G. W. Owttrim. 2020. Evidence for convergent sensing of multiple abiotic stresses in cyanobacteria. Biochim Biophys Acta 1864:129462.

164. Rosana, A. R. R., D. Chamot, and G. W. Owttrim. 2012. Autoregulation of RNA helicase expression in response to temperature stress in *Synechocystis* sp. PCC 6803. PLoS One 7:e48683.

165. Patterson-Fortin, L. M., K. R. Colvin, and G. W. Owttrim. 2006. A LexA-related protein regulates redox-sensitive expression of the cyanobacterial RNA helicase, *crhR*. Nucleic Acids Res 34:3446-3454.

166. Georg, J. 2010. A hidden layer of genetic information - regulatory non-protein-coding RNAs in *Synechocystis* PCC6803. PhD Thesis, Universitat Freiburg im Breisgau, Freiburg, Germany.

167. Komeili, A., Z. Li, D. K. Newman, and G. J. Jensen. 2006. Magnetosomes are cell membrane invaginations organized by the actin-like protein MamK. Science 311:242-245.

168. Kerfeld, C. A., M. R. Sawaya, S. Tanaka, C. V. Nguyen, M. Phillips, M. Beeby, and T. O. Yeates. 2005. Protein structures forming the shell of primitive bacterial organelles. Science 309:936-938.

169. Campos, M., and C. Jacobs-Wagner. 2013. Cellular organization of the transfer of genetic information. Curr Opin Microbiol 16:171-176.

170. Khemici, V., I. Toesca, L. Poljak, N. F. Vanzo, and A. J. Carpousis. 2004. The RNase E of *Escherichia coli* has at least two binding sites for DEAD-box RNA helicases: functional replacement of RhlB by RhlE. Mol Microbiol 54:1422-1430.

171. Lehnik-Habrink, M., J. Newman, F. M. Rothe, A. S. Solovyova, C. Rodrigues, C. Herzberg, F. M. Commichau, R. J. Lewis, and J. Stülke. 2011. RNase Y in *Bacillus subtilis*: a natively disordered protein that is the functional equivalent of RNase E from *Escherichia coli*. J Bacteriol 193:5431-5441.

172. Mingam, A., C. Toffano-Nioche, V. Brunaud, N. Boudet, M. Kreis, and A. Lecharny. 2004. DEAD-box RNA helicases in *Arabidopsis thaliana*: establishing a

link between quantitative expression, gene structure and evolution of a family of genes. Plant Biotechnol J 2:401-415.

173. Kalman, M., H. Murphy, and M. Cashel. 1991. rhlB, a new *Escherichia coli* K-12 gene with an RNA helicase-like protein sequence motif, one of at least five such possible genes in a prokaryote. New Biol 3:886-895.

174. Liou, G. G., W. N. Jane, S. N. Cohen, N. S. Lin, and S. Lin-Chao. 2001. RNA degradosomes exist *in vivo* in *Escherichia coli* as multicomponent complexes associated with the cytoplasmic membrane via the N-terminal region of ribonuclease E. Proc Natl Acad Sci USA 98:63-68.

175. Bäreclev, C., K. Vaitkevicius, S. Netterling, and J. Johansson. 2014. DExD-box RNA-helicases in *Listeria monocytogenes* are important for growth, ribosomal maturation, rRNA processing and virulence factor expression. RNA Biol 11:1457-1466.

176. Iost, I., T. Bizebard, and M. Dreyfus. 2013. Functions of DEAD-box proteins in bacteria: current knowledge and pending questions. Biochim Biophys Acta 1829:866-877.

177. Pandiani, F., J. Brillard, I. Bornard, C. Michaud, S. Chamot, C. Nguyen-the, and V. Broussolle. 2010. Differential involvement of the five RNA helicases in adaptation of *Bacillus cereus* ATCC 14579 to low growth temperatures. Appl Environ Microbiol 76:6692-6697.

178. Prud'homme-Généreux, A., R. K. Beran, I. Iost, C. S. Ramey, G. A. Mackie, and R. W. Simons. 2004. Physical and functional interactions among RNase E, polynucleotide phosphorylase and the cold-shock protein, CsdA: evidence for a 'cold shock degradosome'. Mol Microbiol 54:1409-1421.

179. Strahl, H., C. Turlan, S. Khalid, P. J. Bond, J. M. Kebalo, P. Peyron, L. Poljak, M. Bouvier, L. Hamoen, B. F. Luisi, and A. J. Carpousis. 2015. Membrane recognition and dynamics of the RNA degradosome. PLoS Genet 11:e1004961.

180. Bayas, C. A., J. Wang, M. K. Lee, J. M. Schrader, L. Shapiro, and W. E. Moerner. 2018. Spatial organization and dynamics of RNase E and ribosomes in *Caulobacter crescentus*. Proc Natl Acad Sci USA 115:E3712-E3721.

181. Hunger, K., C. L. Beckering, F. Wiegeshoff, P. L. Graumann, and M. A. Marahiel. 2006. Cold-induced putative DEAD box RNA helicases CshA and CshB are essential for cold adaptation and interact with cold shock protein B in *Bacillus subtilis*. J Bacteriol 188:240-248.

182. Owttrim, G. W. 2012. RNA helicases in cyanobacteria: biochemical and molecular approaches. Methods Enzymol 511:385-403.

183. Elhai, J., A. Vepritskiy, A. M. Muro-Pastor, E. Flores, and C. P. Wolk. 1997. Reduction of conjugal transfer efficiency by three restriction activities of *Anabaena* sp. strain PCC 7120. J Bacteriol 179:1998-2005.

184. Thomas, C. M., and C. A. Smith. 1987. Incompatibility group P plasmids: genetics, evolution and use in genetic manipulation. Ann Rev Microbiol 41:77-101.

185. Jiang, Y., and M. K. Deyholos. 2009. Functional characterization of *Arabidopsis* NaCl-inducible WRKY25 and WRKY33 transcription factors in abiotic stresses. Plant Mol Biol 69:91-105.

186. Qi, Q., M. Hao, W. Ng, S. C. Slater, S. R. Baszis, J. D. Weiss, and H. E. Valentin. 2005. Application of the *Synechococcus* nirA promoter to establish an inducible expression system for engineering the *Synechocystis* tocopherol pathway. Appl Environ Microbiol 71:5678-5684.

187. Tyystjärvi, T., M. Herranen, and E. M. Aro. 2001. Regulation of translation elongation in cyanobacteria: Membrane targeting of the ribosome nascent-chain complexes controls the synthesis of D1 protein. Mol Microbiol 40:476-484.

188. Murata, N., and T. Omata. 1988. Isolation of cyanobacterial plasma membranes. Methods Enzymol 167:245-251.

189. Huang, F., I. Parmryd, F. Nilsson, A. L. Persson, H. B. Pakrasi, B. Andersson, and B. Norling. 2002. Proteomics of *Synechocystis* sp. strain PCC 6803: identification of plasma membrane proteins. Mol Cell Proteomics 1:956-966.

190. Weiner, M. P., and G. L. Costa. 1994. Rapid PCR site-directed mutagenesis. Genome Res 4:131.

191. Rosana, A. R. R. 2013. Autoregulation of RNA helicase operon expression. MSc Thesis, University of Alberta, Edmonton, Alberta.

192. Zhang, J. Y., X. M. Deng, F. P. Li, L. Wang, Q. Y. Huang, C. C. Zhang, and W. L. Chen. 2014. RNase E forms a complex with polynucleotide phosphorylase in cyanobacteria via a cyanobacterial-specific nonapeptide in the noncatalytic region. RNA 20:568.

193. Senissar, M., A. Le Saux, N. Belgareh-Touzé, C. Adam, J. Banroques, and N. K. Tanner. 2014. The DEAD-box helicase Ded1 from yeast is an mRNP cap-associated protein that shuttles between the cytoplasm and nucleus. Nucleic Acids Res 42:10005-10022.

194. van de Meene, A. M. L., M. F. Hohmann-Marriott, W. F. J. Vermaas, and R. W. Roberson. 2006. The three-dimensional structure of the cyanobacterium *Synechocystis* sp. PCC 6803. Arch Microbiol 184:259-270.

195. Norling, B., E. Zak, B. Andersson, and H. Pakrasi. 1998. 2D-isolation of pure plasma and thylakoid membranes from the cyanobacterium *Synechocystis* sp. PCC 6803. FEBS Lett 436:189-192.

196. Huang, F., E. Hedman, C. Funk, T. Kieselbach, W. P. Schröder, and B. Norling. 2004. Isolation of outer membrane of *Synechocystis* sp. PCC 6803 and its proteomic characterization. Mol Cell Proteomics 3:586.

197. Srivastava, R., T. Pisareva, and B. Norling. 2005. Proteomic studies of the thylakoid membrane of *Synechocystis* sp. PCC 6803. Proteomics 5:4905.

198. Simon, W. J., J. J. Hall, I. Suzuki, N. Murata, and A. R. Slabas. 2002. Proteomic study of the soluble proteins from the unicellular cyanobacterium *Synechocystis* sp. PCC6803 using automated matrix-assisted laser desorption/ionization-time of flight peptide mass fingerprinting. Proteomics 2:1735-1742.

199. Georg, J., D. Dienst, N. Schürgers, T. Wallner, D. Kopp, D. Stazic, E. Kuchmina, S. Klähn, H. Lokstein, W. R. Hess, and A. Wilde. 2014. The small regulatory RNA SyR1/PsrR1 controls photosynthetic functions in cyanobacteria. Plant Cell 26:3661-3679.

200. Tyystjärvi, T., S. Sirpiö, and E. M. Aro. 2004. Post-transcriptional regulation of the psbA gene family in the cyanobacterium *Synechococcus* sp. PCC 7942. FEBS Lett 576:211-215.

201. Koonin, E. V., Y. I. Wolf, and L. Aravind. 2001. Prediction of the archaeal exosome and its connections with the proteasome and the translation and transcription machineries by a comparative-genomic approach. Genome Res 11:240-252.

202. Hu, W., T. J. Sweet, S. Chamnongpol, K. E. Baker, and J. Coller. 2009. Cotranslational mRNA decay in *Saccharomyces cerevisiae*. Nature 461:225-229.

203. Fiorini, F., F. Bonneau, and H. Le Hir. 2012. Biochemical characterization of the RNA helicase UPF1 involved in nonsense-mediated mRNA decay. Methods Enzymol 511:255.

204. Sweet, T., C. Kovalak, and J. Coller. 2012. The DEAD-box protein Dhh1 promotes decapping by slowing ribosome movement. PLoS Biol 10:e1001342.

205. Bergholz, P. W., C. Bakermans, and J. M. Tiedje. 2009. *Psychrobacter articus* 273-4 uses resource efficiency and molecular motion adaptations for subzero temperature growth. J Bacteriol 191:13862-13867.

206. Schureck, M. A., J. A. Dunkle, T. Maehigashi, S. J. Miles, and C. M. Dunham. 2016. Defining the mRNA recognition signature of a bacterial toxin protein. Proc Natl Acad Sci USA 112:13862-13867.

207. Prévost, K., G. Desnoyers, J. F. Jacques, F. Lavoie, and E. Massé. 2011. Small RNA-induced mRNA degradation achieved through both translation block and activated cleavage. Genes Dev 25:385.

208. Bøggild, A., M. Overgaard, P. Valentin-Hansen, and D. E. Brodersen. 2009. Cyanobacteria contain a structural homologue of the Hfq protein with altered RNA-binding properties. FEBS J 276:3904-3915.

209. Price, M. N., A. P. Arkin, and E. J. Alm. 2006. The life-cycle of operons. PLoS Genet 2:e96.

210. Memon, D., A. K. Singh, H. B. Pakrasi, and P. P. Wangikar. 2013. A global analysis of adaptive evolution of operons in cyanobacteria. Antonie Van Leeuwenhoek 103:331-346.

211. Jacob, F., and J. Monod. 1961. Genetic regulatory mechanisms in the synthesis of proteins. J Mol Biol 3:318-356.

212. Conlon, E. M., B. L. Postier, B. A. Methé, K. P. Nevin, and D. R. Lovley. 2012. A bayesian model for pooling gene expression studies that incorporates co-regulation information. PLoS One 7:e52137.

213. Nickel, M., G. Homuth, C. Böhnisch, U. Mäder, and T. Schweder. 2004. Cold induction of the *Bacillus subtilis bkd* operon is mediated by increased mRNA stability. Mol Genet Genomics 272:98-107.

214. Gulati, A., and S. Mahadevan. 2001. The *Escherichia coli* antiterminator protein BglG stabilizes the 5' region of the *bgl* mRNA. J Biosci 26:193-203.

215. Smolke, C. D., T. A. Carrier, and J. D. Keasling. 2000. Coordinated, differential expression of two genes through directed mRNA cleavage and stabilization by secondary structures. Appl Environ Microbiol 66:5399-5405.

216. Papenfort, K., Y. Sun, M. Miyakoshi, C. Vanderpool, and J. Vogel. 2013. Small RNA-mediated activation of sugar phosphatase mRNA regulates glucose homeostasis. Cell 153:426-437.

217. Wang, X., S. C. Ji, H. J. Jeon, Y. Lee, and H. M. Lim. 2015. Two-level inhibition of *galK* expression by Spot 42: Degradation of mRNA mK2 and enhanced transcription termination before the *galK* gene. Proc Natl Acad Sci USA 112:7581-7586.

218. Jäger, S., A. Jäger, and G. Klug. 2004. CIRCE is not involved in heat-dependent transcription of *groESL* but in stabilization of the mRNA 5′-end in *Rhodobacter capsulatus*. Nucleic Acids Res 32:386-396.

219. Mossey, P., and A. Das. 2013. Expression of *Agrobacterium tumefaciens* octopine Ti-plasmid *virB8* gene is regulated by translational coupling. Plasmid 69:72-80.

220. Heidrich, N., A. Chinali, U. Gerth, and S. Brantl. 2006. The small untranslated RNA SR1 from the *Bacillus subtilis* genome is involved in the regulation of arginine catabolism. Mol Microbiol 62:520-536.

221. Even, S., O. Pellegrini, L. Zig, V. Labas, J. Vinh, D. Bréchemmier-Baey, and H. Putzer. 2005. Ribonucleases J1 and J2: two novel endoribonucleases in *B. subtilis* with functional homology to *E. coli* RNase E. Nucleic Acids Res 33:2141-2152.

222. Mohanty, B. K., and S. R. Kushner. 2009. Processing of the *Escherichia coli leuX* tRNA transcript, encoding tRNA Leu5, requires either the 3′→5′ exoribonuclease polynucleotide phosphorylase or RNase P to remove the Rho-independent transcription terminator. Nucleic Acids Res 38:597-607.

223. Arraiano, C. M., J. M. Andrade, S. Domingues, I. B. Guinote, M. Malecki, R. G. Matos, R. N. Moreira, V. Pobre, F. P. Reis, M. Saramago, I. J. Silva, and S. C. Viegas. 2010. The critical role of RNA processing and degradation in the control of gene expression. FEMS Microbiol Rev 34:883-923.

224. Dar, D., and R. Sorek. 2018. Extensive reshaping of bacterial operons by programmed mRNA decay. PLoS Genet 14:e1007354.

225. Conway, T., J. P. Creecy, S. M. Maddox, J. E. Grissom, T. L. Conkle, T. M. Shadid, J. Teramoto, P. San Miguel, T. Shimada, A. Ishihama, H. Mori, and B. L. Wanner. 2014. Unprecedented high-resolution view of bacterial operon architecture revealed by RNA sequencing. mBio 5:1442.

226. Gao, H., Z. K. Yang, L. Wu, D. K. Thompson, and J. Zhou. 2006. Global transcriptome analysis of the cold shock response of *Shewanella oneidensis* MR-1 and mutational analysis of its classical cold shock proteins. J Bacteriol 188:4560-4569.

227. Gaubig, L. C., T. Waldminghaus, and F. Narberhaus. 2011. Multiple layers of control govern expression of the *Escherichia coli ibpAB* heat-shock operon. Microbiology 157:66-76.

228. Lee, S. J., A. Xie, W. Jiang, J. P. Etchegaray, P. G. Jones, and M. Inouye. 2006. Family of the major cold-shock protein, CspA (CS7.4), of *Escherichia coli*, whose members show a high sequence similarity with the eukaryotic Y-box binding proteins. Mol Microbiol 11:833-839.

229. Rocak, S., and P. Linder. 2004. DEAD-box proteins: the driving forces behind RNA metabolism. Nat Rev Mol Cell Biol 5:232-241.

230. Linder, P., and G. W. Owttrim. 2009. Plant RNA helicases: linking aberrant and silencing RNA. Trends Plant Sci 14:344-352.

231. Jankowsky, E. 2011. RNA helicases at work: binding and rearranging. Trends Biochem Sci 36:19-29.

232. Sato, N. 1995. A family of cold-regulated RNA-binding protein genes in the cyanobacterium *Anabaena variabilis* M3. Nucleic Acids Res 23:2161-2167.

233. Sinetova, M. A., and D. A. Los. 2016. New insights in cyanobacterial cold stress responses: Genes, sensors and molecular triggers. Biochim Biophys Acta 1860:2391-2403.

234. Mikami, K., Y. Kanesaki, I. Suzuki, and N. Murata. 2002. The histidine kinase Hik33 perceives osmotic stress and cold stress in *Synechocystis* sp. PCC 6803. Mol Microbiol 46:905-915.

235. Suzuki, I., D. A. Los, Y. Kanesaki, K. Mikami, and N. Murata. 2000. The pathway for perception and transduction of low-temperature signals in *Synechocystis*. EMBO J 19:1327-1334.

236. Imamura, S., and M. Asayama. 2009. Sigma factors for cyanobacterial transcription. Gene Regul Syst Bio 3:65-87.

237. Ungerer, J. L., B. S. Pratte, and T. Thiel. 2010. RNA processing of nitrogenase transcripts in the cyanobacterium *Anabaena variabilis*. J Bacteriol 192:3311-3320.

238. Pratte, B. S., R. Sheridan, J. A. James, and T. Thiel. 2013. Regulation of V-nitrogenase genes in *Anabaena variabilis* by RNA processing and by dual repressors. Mol Microbiol 88:413-424.

239. Pratte, B. S., and T. Thiel. 2014. Regulation of nitrogenase gene expression by transcript stability in the cyanobacterium *Anabana variabilis*. J Bacteriol 196:3609-3621.

240. Pratte, B. S., J. L. Ungerer, and T. Thiel. 2015. Role of RNA secondary structure and processing in stability of the *nifH1* transcript in the cyanobacterium *Anabaena variabilis*. J Bacteriol 197:1408-1422.

241. Kopf, M., S. Klähn, I. Scholz, J. K. F. Matthiessen, W. R. Hess, and B. Voß. 2014. Comparative analysis of the primary transcriptome of *Synechocystis* sp. PCC 6803. DNA Res 21:527-539.

242. Schneider, C. A., W. S. Rasband, and K. W. Eliceiri. 2012. NIH Image to ImageJ: 25 years of image analysis. Nat Methods 9:671-675.

243. Weisburg, W. G., S. M. Barns, D. A. Pelletier, and D. J. Lane. 1991. 16S ribosomal DNA amplification for phylogenetic study. J Bacteriol 173:697-703.

244. Ausubel, F. M., R. Brent, R. E. Kingston, D. D. Moore, J. G. Seidman, J. A. Smith and K. Struhl (eds.). 1995. Current Protocols in Molecular Biology. John Wiley & Sons, Inc., U.S.A.

245. Polidoros, A. N., K. Pasentsis, and A. S. Tsaftaris. 2006. Rolling circle amplification-RACE: a method for simultaneous isolation of 5' and 3' cDNA ends from amplified cDNA templates. Biotechniques 41:35-42.

246. Wright, P. R., J. Georg, M. Mann, D. A. Sorescu, A. S. Richter, S. Lott, R. Kleinkauf, W. R. Hess, and R. Backofen. 2014. CopraRNA and IntaRNA: predicting small RNA targets, networks and interaction domains. Nucleic Acids Res 42:119.

247. Huang, D. W., B. T. Sherman, and R. A. Lempicki. 2009. Systematic and integrative analysis of large gene lists using DAVID bioinformatics resources. Nat Protoc 4:44-57.

248. Lorenz, R., S. H. Bernhart, C. Höner zu Siederdissen, H. Tafer, C. Flamm, P. F. Stadler, and I. L. Hofacker. 2011. ViennaRNA package 2.0. Algorithms Mol Biol 6:26.

249. Darty, K., A. Denise, and Y. Ponty. 2009. VARNA: interactive drawing and editing of the RNA secondary structure. Bioinformatics 25:1974-1975.

250. Behler, J., K. Sharma, V. Reimann, A. Wilde, H. Urlaub, and W. R. Hess. 2018. The host-encoded RNase E endonuclease as the crRNA maturation enzyme in a CRISPR–Cas subtype III-Bv system. Nat Microbiol 3:367-377.

251. Anton, B. P., L. Saleh, J. S. Benner, E. A. Raleigh, S. Kasif, and R. J. Roberts. 2008. RimO, a MiaB-like enzyme, methylthiolates the universally conserved Asp88 residue of ribosomal protein S12 in *Escherichia coli*. Proc Nat Acad Sci USA 105:1826-1831.

252. Pierrel, F., T. Douki, M. Fontecave, and M. Atta. 2004. MiaB protein is a bifunctional radical-S-adenosylmethionine enzyme involved in thiolation and methylation of tRNA. J Biol Chem 279:47555-47563.

253. Mitschke, J., J. Georg, I. Scholz, C. M. Sharma, D. Dienst, J. Bantscheff, B. Voß, C. Steglich, A. Wilde, J. Vogel, and W. R. Hess. 2011. An experimentally anchored map of transcriptional start sites in the model cyanobacterium *Synechocystis* sp. PCC6803. Proc Natl Acad Sci USA 108:2124-2129.

254. Huang, D. W., B. T. Sherman, and R.A Lempicki. 2009. Bioinformatics enrichment tools: paths toward the comprehensive functional analysis of large gene lists. Nucleic Acids Res 37:1-13.

255. Kujat Choy, S. L. 2001. A redox-regulated RNA helicase gene. PhD Thesis, University of Alberta, Edmonton, Alberta.

256. Chao, Y., L. Li, D. Girodat, K. U. Förstner, N. Said, C. Corcoran, M. Śmiga, K. Papenfort, R. Reinhardt, H. J. Wieden, B. F. Luisi, and J. Vogel. 2017. In vivo cleavage map illuminates the central role of RNase E in coding and non-coding RNA pathways. Mol Cell 65:39-51.

257. Horie, Y., Y. Ito, M. Ono, N. Moriwaki, H. Kato, Y. Hamakubo, T. Amano, M. Wachi, M. Shirai, and M. Asayama. 2007. Dark-induced mRNA instability involves RNase E/G-type endoribonuclease cleavage at the AU-box and SD sequences in cyanobacteria. Mol Genet Genomics 278:331-346.

258. Migur, A. 2020. Multitasking DEAD-box RNA helicase CrhR from *Synechocystis* sp. PCC 6803. PhD Thesis, Universitat Freiburg im Breisgau, Freiburg, Germany.

259. Laing, E., V. Mersinias, C. P. Smith, and S. J. Hubbard. 2006. Analysis of gene expression in operons of *Streptomyces coelicolor*. Genome Biol 7:R46.

260. Lim, H. N., Y. Lee, and R. Hussein. 2011. Fundamental relationship between operon organization and gene expression. Proc Natl Acad Sci USA 108:10626-10631.

261. Cam, K., G. Rome, H. M. Krisch, and J. P. Bouché. 1996. RNase E processing of essential cell division genes mRNA in *Escherichia coli*. Nucleic Acids Res 24:3065-3070.

262. Cameron, J. C., G. C. Gordon, and B. F. Pfleger. 2015. Genetic and genomic analysis of RNases in model cyanobacteria. Photosynth Res 126:171-183.

263. Klähn, S., C. Schaal, J. Georg, D. Baumgartner, G. Knippen, M. Hagemann, A. M. Muro-Pastor, and W. R. Hess. 2015. The sRNA NsiR4 is involved in nitrogen assimilation control in cyanobacteria by targeting glutamine synthetase inactivating factor IF7. Proc Natl Acad Sci USA 112:E6243-E6252.

264. Pei, G., T. Sun, S. Chen, L. Chen, and W. Zhang. 2017. Systematic and functional identification of small non-coding RNAs associated with exogenous biofuel stress in cyanobacterium *Synechocystis* sp. PCC 6803. Biotechnol Biofuels 10:57.

265. Chao, Y., K. Papenfort, R. Reinhardt, C. M. Sharma, and J. Vogel. 2012. An atlas of Hfq-bound transcripts reveals 3' UTRs as a genomic reservoir of regulatory small RNAs. EMBO J 31:4005-4019.

266. Dar, D., and R. Sorek. 2018. Bacterial noncoding RNAs excised from within protein-coding transcripts. mBio 9:1730.

267. Huynen, M., B. Snel, W. Lathe III, and P. Bork. 2000. Predicting protein function by genomic context: quantitative evaluation and qualitative inferences. Genome Res 10:1204-1210.

268. Lu, J., H. Aoki, and M. C. Ganoza. 1999. Molecular characterization of a prokaryotic translation factor homologous to the eukaryotic initiation factor eIF4A. Int J Biochem Cell Biol 31:215-229.

269. Carpenter, E. J., and K. Romans. 1991. Major role of the cyanobacterium *Trichodesmium* in nutrient cycling in the North Atlantic Ocean. Science 254:1356-1358.

270. Jardillier, L., M. V. Zubkov, J. Pearman, and D. J. Scanlan. 2010. Significant CO_2 fixation by small prymnesiophytes in the subtropical and tropical northeast Atlantic Ocean. ISME J 4:1180-1192.

271. Sohm, J. A., E. A. Webb, and D. G. Capone. 2011. Emerging patterns of marine nitrogen fixation. Nat Rev Microbiol 9:499-508.

272. Tortell, P. D., M. T. Maldonado, J. Granger, and N. M. Price. 1999. Marine bacteria and biogeochemical cycling of iron in the oceans. FEMS Microbiol Ecol 29:1-11.

273. Pelroy, R. A., and J. A. Bassham. 1972. Photosynthetic and dark carbon metabolism in unicellular blue-green algae. Arch Mikrobiol 86:25-38.

274. Qian, H., S. Yu, Z. Sun, X. Xie, W. Liu, and Z. Fu. 2010. Effects of copper sulfate, hydrogen peroxide and N-phenyl-2-naphthylamine on oxidative stress and the expression of genes involved photosynthesis and microcystin disposition in *Microcystis aeruginosa*. Aquat Toxicol 99:405-412.

275. Herrero, A., A. M. Muro-Pastor, and E. Flores. 2001. Nitrogen control in cyanobacteria. J Bacteriol 183:411-425.

276. Montesinos, M. L., A. M. Muro-Pastor, A. Herrero, and E. Flores. 1998. Ammonium/methylammonium permeases of a cyanobacterium: identification and analysis of three nitrogen-regulated *amt* genes in *Synechocystis* sp. PCC 6803 J Biol Chem 273:31463-31470.

277. Flores, E., M. G. Guerrero, and M. Losada. 1980. Short-term ammonium inhibition of nitrate utilization by *Anacystis nidulans* and other cyanobacteria. Arch Microbiol 128:137-144.

278. Reyes, J. C., and F. J. Florencio. 1993. A new type of glutamine synthetase in cyanobacteria: the protein encoded by the *glnN* gene supports nitrogen assimilation in *Synechocystis* sp. strain PCC 6803. J Bacteriol 176:1260-1267.

279. Valladares, A., M. L. Montesinos, A. Herrero, and E. Flores. 2002. An ABC-type, high-affinity urea permease identified in cyanobacteria. Mol Microbiol 43:703-715.

280. Espie, G. S., F. Jalali, T. Tong, N. J. Zacal, and A. K. C. So. 2007. Involvement of the *cynABDS* operon and the CO_2-concentrating mechanism in the light-dependent transport and metabolism of cyanate by cyanobacteria. J Bacteriol 189:1013-1024.

281. Cai, Y., and C. P. Wolk. 1997. Nitrogen deprivation of *Anabaena* sp. strain PCC 7120 elicits rapid activation of a gene cluster that is essential for uptake and utilization of nitrate. J Bacteriol 179:258-266.

282. Hattori, A., and I. Uesugi. 1968. Purification and properties of nitrite reductase from the blue-green alga *Anabaena cylindrica*. Plant Cell Physiol 9:689-699.

283. Manzano, C., P. Candau, C. Gomez-Moreno, A. M. Relimpio, and M. Losada. 1976. Ferredoxin-dependent photosynthetic reduction of nitrate and nitrite by particles of *Anacystis nidulans*. Mol Cell Biochem 10:161-169.

284. Rubio, L. M., E. Flores, and A. Herrero. 2002. Purification, cofactor analysis, and site-directed mutagenesis of *Synechococcus* ferredoxin-nitrate reductase. Photosynth Res 72:13-26.

285. Flores, E., M. G. Guerrero, and M. Losada. 1983. Photosynthetic nature of nitrate uptake and reduction in the cyanobacterium *Anacystis nidulans*. Biochim Biophys Acta 722:408-416.

286. Vega-Palas, M. A., F. Madueño, A. Herrero, and E. Flores. 1990. Identification and cloning of a regulatory gene for nitrogen assimilation in the cyanobacterium *Synechococcus* sp. strain PCC 7942. J Bacteriol 172:643-647.

287. Luque, I., E. Flores, and A. Herrero. 1994. Molecular mechanism for the operation of nitrogen control in cyanobacteria. EMBO J 13:2862-2869.

288. Giner-Lamia, J., R. Robles-Rengel, M. A. Hernández-Prieto, M. I. Muro-Pastor, F. J. Florencio, and M. E. Futschik. 2017. Identification of the direct regulon of NtcA during early acclimation to nitrogen starvation in the cyanobacterium *Synechocystis* sp. PCC 6803. Nucleic Acids Res 45:11800-11820.

289. Zhao, M. S., Y. L. Jiang, Y. X. He, Y. F. Chen, Y. B. Teng, Y. Chen, C. C. Zhang, and C. Z. Zhou. 2010. Structural basis for the allosteric control of the global transcription factor NtcA by the nitrogen starvation signal 2-oxoglutarate. Proc Natl Acad Sci USA 107:12487-12492.

290. Camargo, S., A. Valladares, K. Forchhammer, and A. Herrero. 2014. Effects of PipX on NtcA-dependent promoters and characterization of the *cox3* promoter region in the heterocyst-forming cyanobacterium *Anabaena* sp. PCC 7120. FEBS Lett 588:1787-1794.

291. Llácer, J. L., J. Espinosa, M. A. Castells, A. Contreras, K. Forchhammer, and V. Rubio. 2010. Structural basis for the regulation of NtcA-dependent transcription by proteins PipX and PII. Proc Natl Acad Sci USA 107:15397-15402.

292. Lüddecke, J., and K. Forchhammer. 2015. Energy sensing versus 2-oxoglutarate dependent ATPase switch in the control of *Synechococcus* PII interaction with its targets NAGK and PipX. PLoS One 10:e0137114.

293. Ohashi, Y., W. Shi, N. Takatani, M. Aichi, S. Maeda, S. Watanabe, H. Yoshikawa, and T. Omata. 2011. Regulation of nitrate assimilation in cyanobacteria. J Exp Bot 62:1411-1424.

294. Kikuchi, H., M. Aichi, I. Suzuki, and T. Omato. 1996. Positive regulation by nitrite of the nitrate assimilation operon in the cyanobacteria *Synechococcus* sp. strain PCC 7942 and *Plectonema boryanum*. J Bacteriol 178:5822-5825.

295. Klähn, S., P. Bolay, P. Wright R., R. Atilho M., K. Brewer I., M. Hagemann, R. Breaker R., and W. Hess R. 2018. A glutamine riboswitch is a key element for the regulation of glutamine synthetase in cyanobacteria. Nucleic Acids Res 46:10082-10094.

296. Kolodny, N. H., D. Bauer, K. Bryce, K. Klucevsek, A. Lane, L. Medeiros, W. Mercer, S. Moin, D. Park, J. Petersen, J. Wright, C. Yuen, A. J. Wolfson, and M. M. Allen. 2006. Effect of nitrogen source on cyanophycin synthesis in *Synechocystis* sp. strain PCC 6308. J Bacteriol 188:934-940.

297. Herrero, A., A. M. Muro-Pastor, A. Valladares, and E. Flores. 2004. Cellular differentiation and the NtcA transcription factor in filamentous cyanobacteria. FEMS Microbiol Rev 28:469-487.

298. Osanai, T., S. Imamura, M. Asayama, M. Shirai, I. Suzuki, N. Murata, and K. Tanaka. 2006. Nitrogen induction of sugar catabolic gene expression in *Synechocystis* sp. PCC 6803. DNA Res 13:185-195.

299. Flores, E., A. M. Muro-Pastor, and A. Herrero. 1999. Cyanobacterial nitrogen assimilation genes and NtcA-dependent control of gene expression, p. 463-478. *In*

G. A. Peschek, W. Löffelhardt, and G. Schmetterer (eds.), The Phototrophic Prokaryotes. Springer, Boston, MA.

300. García-Domínguez, M., J. C. Reyes, and F. J. Florencio. 2002. NtcA represses transcription of *gifA* and *gifB*, genes that encode inhibitors of glutamine synthetase type I from *Synechocystis* sp. PCC 6803. Mol Microbiol 35:1192-1201.

301. Suzuki, I., H. Kikuchi, S. Nakanishi, Y. Fujita, T. Sugiyama, and T. Omata. 1995. A novel nitrate reductase gene from the cyanobacterium *Plectonema boryanum*. J Bacteriol 177:6137-6143.

302. Krasikov, V., E. Aguirre von Wobeser, H. L. Dekker, J. Huisman, and H. C. P. Matthijs. 2012. Time-series resolution of gradual nitrogen starvation and its impact on photosynthesis in the cyanobacterium *Synechocystis* PCC 6803. Physiol Plantarum 145:426-439.

303. Liu, D., and C. Yang. 2014. The nitrogen-regulated response regulator NrrA controls cyanophycin synthesis and glycogen catabolism in the cyanobacterium *Synechocystis* sp. PCC 6803. J Biol Chem 289:2055-2071.

304. Osanai, T., A. Oikawa, T. Shirai, A. Kuwahara, H. Iijima, K. Tanaka, M. Ikeuchi, A. Kondo, K. Saito, and M. Y. Hirai. 2014. Capillary electrophoresis–mass spectrometry reveals the distribution of carbon metabolites during nitrogen starvation in *Synechocystis* sp. PCC 6803. Environ Microbiol 16:512-524.

305. Klotz, A., J. Georg, L. Bučinská, S. Watanabe, V. Reimann, W. Januszewski, R. Sobotka, D. Jendrossek, W. Hess, and K. Forchhammer. 2016. Awakening of a dormant cyanobacterium from nitrogen chlorosis reveals a genetically determined program. Curr Biol 26:2862-2872.

306. Görl, M., J. Sauer, T. Baier, and K. Forchhammer. 1998. Nitrogen-starvation-induced chlorosis in *Synechococcus* PCC 7942: adaptation to long-term survival. Microbiology 144:2449-2458.

307. Bourgeois, C. F., F. Mortreux, and D. Auboeuf. 2016. The multiple functions of RNA helicases as drivers and regulators of gene expression. Nat Rev Mol Cell Biol 17:426-438.

308. Rosana, A. R. R., D. S. Whitford, R. P. Fahlman, and G. W. Owttrim. 2016. Cyanobacterial RNA helicase, CrhR, localizes to the thylakoid membrane region and co-sediments with degradosome and polysome complexes in *Synechocystis* sp. PCC 6803. J Bacteriol 198:2089-2099.

309. Porra, R. J., W. A. Thompson, and P. E. Kriedemann. 1989. Determination of accurate extinction coefficients and simultaneous equations for assaying chlorophylls *a* and *b* extracted with four different solvents: verification of the concentration of chlorophyll standards by atomic absorption spectroscopy. Biochim Biophys Acta 975:384-394.

310. Santiago-Santos, M. C., T. Ponce-Noyola, R. Olvera-Ramírez, J. Ortega-López, and R. O. Cañizares-Villanueva. 2004. Extraction and purification of phycocyanin from *Calothrix* sp. Proc Biochem 39:2047-2052.

311. Bennett, A., and L. Bogorad. 1973. Complementary chromatic adaptation in a filamentous blue-green alga. J Cell Biol 58:419-435.

312. Klotz, A., E. Reinhold, S. Doello, and K. Forchhammer. 2015. Nitrogen starvation acclimation in *Synechococcus elongatus*: redox-control and the role of nitrate reduction as an electron sink. Life 5:888-904.

313. Bryant, D. A. 1982. Phycoerythrocyanin and phycoerythrin: properties and occurrence in cyanobacteria. J Gen Microbiol 128:835-844.

314. Allen, M. M., and A. J. Smith. 1969. Nitrogen chlorosis in blue-green algae. Arch Mikrobiol 69:114-120.

315. Wang, J., J. Zhu, S. Liu, B. Liu, Y. Gao, and Z. Wu. 2011. Generation of reactive oxygen species in cyanobacteria and green algae induced by allelochemicals of submerged macrophytes. Chemosphere 85:977-982.

316. Zhao, W., Z. Ye, and J. Zhao. 2007. RbrA, a cyanobacterial rubrerythrin, functions as a FNR-dependent peroxidase in heterocysts in protection of nitrogenase from damage by hydrogen peroxide in *Anabaena* sp. PCC 7120. Mol Microbiol 66:1219-1230.

317. Rastogi, R. P., S. P. Singh, D. P. Häder, and R. P. Sinha. 2010. Detection of reactive oxygen species (ROS) by the oxidant-sensing probe 2′,7′-dichlorodihydrofluorescein diacetate in the cyanobacterium *Anabaena variabilis* PCC 7937. Biochem Biophys Res Commun 397:603-607.

318. Stewart, W. D. P., and P. Rowell. 1975. Effects of L-methionine-DL-sulphoximine on the assimilation of newly fixed NH_3, acetylene reduction and heterocyst production in *Anabaena cylindrica*. Biochem Biophys Res Commun 65:846-856.

319. Lea-Smith, D. J., P. Bombelli, R. Vasudevan, and C. J. Howe. 2016. Photosynthetic, respiratory and extracellular electron transport pathways in cyanobacteria. Biochim Biophys Acta 1857:247-255.

320. Watzer, B., P. Spät, N. Neumann, M. Koch, R. Sobotka, B. Macek, O. Hennrich, and K. Forchhammer. 2019. The signal transduction protein PII controls ammonium, nitrate and urea uptake in cyanobacteria. Front Microbiol 10:1428.

321. Crawford, T. S., K. R. Hanning, J. P. Chua, J. J. Eaton-Rye, and T. C. Summerfield. 2016. Comparison of D1'- and D1- containing PS II reaction centre complexes under different environmental conditions in *Synechocystis* sp. PCC 6803. Plant Cell Environ 39:1715-1726.

322. Drath, M., N. Kloft, A. Batschauer, K. Marin, J. Novak, and K. Forchammer. 2008. Ammonia triggers photodamage of photosystem II in the cyanobacterium *Synechocystis* sp. strain PCC 6803. Plant Physiol 147:206-215.

323. Zavřel, T., P. Očenášová, and J. Červený. 2017. Phenotypic characterization of *Synechocystis* sp. PCC 6803 substrains reveals differences in sensitivity to abiotic stress. PLoS ONE 12:e0189130.

324. Dai, G. Z., B. S. Qiu, and K. Forchhammer. 2014. Ammonium tolerance in the cyanobacterium *Synechocystis* sp. strain PCC 6803 and the role of the psbA multigene family. Plant Cell Environ 37:840-851.

325. Lee, H. M., E. Flores, A. Herrero, J. Houmard, and N. Tandeau de Marsac. 1998. A role for the signal transduction protein PII in the control of nitrate/nitrite uptake in a cyanobacterium. FEBS Lett 427:291-295.

326. Sakamoto, T., and D. A. Bryant. 1998. Growth at low temperature causes nitrogen limitation in the cyanobacterium *Synechococcus* sp. PCC 7002. Arch Microbiol 169:10-19.

327. Espinosa, J., F. Rodríguez-Mateos, P. Salinas, V. F. Lanza, R. Dixon, F. de la Cruz, and A. Contreras. 2014. PipX, the coactivator of NtcA, is a global regulator in cyanobacteria. Proc Natl Acad Sci USA 111:E2423-E2430.

328. Kloft, N., and K. Forchhammer. 2005. Signal transduction protein PII phosphatase PphA is required for light-dependent control of nitrate utilization in *Synechocystis* sp. strain PCC 6803. J Bacteriol 187:6683-6690.

329. Hisbergues, M., R. Jeanjean, F. Joset, N. Tandeau de Marsac, and S. Bédu. 2000. Protein PII regulates both inorganic carbon and nitrate uptake and is modified by a redox signal in *Synechocystis* PCC 6803. FEBS Lett 463:216-220.

330. Trebst, A. 1980. Inhibitors in electron flow: tools for the functional and structural localization of carriers and energy conservation sites. Methods Enzymol 69:675-715.

331. Collier, J. L., and A. R. Grossman. 1994. A small polypeptide triggers complete degradation of light-harvesting phycobiliproteins in nutrient-deprived cyanobacteria. EMBO J 13:1039-1047.

332. Karradt, A., J. Sobanski, J. Mattow, W. Lockau, and K. Baier. 2008. NblA, a key protein of phycobilisome degradation, interacts with ClpC, a HSP100 chaperone partner of a cyanobacterial Clp protease. J Biol Chem 283:32394-32403.

333. Kato, H., T. Kubo, M. Hayashi, I. Kobayashi, T. Yagasaki, T. Chibazakura, S. Watanabe, and H. Yoshikawa. 2011. Interactions between histidine kinase NblS and the response regulators RpaB and SrrA are involved in the bleaching process of the cyanobacterium *Synechococcus elongatus* PCC 7942. Plant Cell Physiol 52:2115-2122.

334. Espinosa, J., K. Forchhammer, and A. Contreras. 2007. Role of the *Synechococcus* PCC 7942 nitrogen regulator protein PipX in NtcA-controlled processes. Microbiology 153:711-718.

335. Kato, H., T. Chibazakura, and H. Yoshikawa. 2008. NblR is a novel one-component response regulator in the cyanobacterium *Syenchococcus elongatus* PCC 7942. Biosci Biotech Bioch 72:1072-1079.

336. Baier, A., W. Winkler, T. Korte, W. Lockau, and A. Karradt. 2014. Degradation of phycobilisomes in *Synechocystis* sp. PCC6803: evidence for essential formation of an NblA1/NblA2 heterodimer and its codegradation by a Clp protease complex. J Biol Chem 289:11755-11766.

337. Li, H., and L. A. Sherman. 2002. Characterization of *Synechocystis* sp. strain PCC 6803 and delta*nbl* mutants under nitrogen-deficient conditions. Arch Microbiol 178:256-266.

338. Kloft, N., G. Rasch, and K. Forchhammer. 2005. Protein phosphatase pphA from *Synechocystis* sp. PCC 6803: the physiological framework of PII-P dephosphorylation. Microbiology 151:1275-1283.

339. Aichi, M., N. Takatani, and T. Omata. 2001. Role of NtcB in activation of nitrate assimilation genes in the cyanobacterium *Synechocystis* sp. strain PCC 6803. J Bacteriol 183:5840-5847.

340. Alfonso, M., I. Perewoska, and D. Kirilovsky. 2001. Redox control of *ntcA* gene expression in *Synechocystis* sp. PCC 6803. Nitrogen availability and electron transport regulate the levels of the NtcA protein. Plant Physiol 125:969-981.

341. Ritter, S. P. A. 2020. Redox and light derived mechanisms of environmental perception are utilized for regulation of the cyanobacterial RNA helicase *crhR*. MSc Thesis, University of Alberta, Edmonton, Alberta.

342. Mukhopadhyay, A., Z. He, E. J. Alm, A. P. Arkin, E. E. Baidoo, S. C. Borglin, W. Chen, T. C. Hazen, Q. He, H. Y. Holman, K. Huang, R. Huang, D. C. Joyner, N. Katz, M. Keller, P. Oeller, A. Redding, J. Sun, J. Wall, J. Wei, Z. Yang, H. C. Yen, J. Zhou, and J. D. Keasling. 2006. Salt stress in *Desulfovibrio vulgaris* Hildenborough: an integrated genomics approach. J Bacteriol 188:4068-4078.

343. Herschlag, D. 1995. RNA chaperones and the RNA folding problem. J Biol Chem 270:20871-20874.

344. Woodson, S. A., S. Panja, and A. Santiago-Frangos. 2018. Proteins that chaperone RNA regulation. Microbiol Spectr 6:RWR-0026-2018.

345. Cordin, O., J. Banroques, N. K. Tanner, and P. Linder. 2006. The DEAD-box protein family of RNA helicases. Gene 367:17-37.

346. Jarmoskaite, I., and R. Russell. 2014. RNA helicase proteins as chaperones and remodelers. Ann Rev Biochem 83:697-725.

347. Diges, C. M., and O. C. Uhlenbeck. 2001. *Escherichia coli* DbpA is an RNA helicase that requires hairpin 92 of 23S rRNA. EMBO J 20:5503-5512.

348. Kumar, S., G. Stecher, and K. Tamura. 2016. MEGA7: molecular evolutionary genetics analysis version 7.0 for bigger datasets. Mol Biol Evol 33:1870-1874.

349. Edgar, R. C. 2004. MUSCLE: multiple sequence alignment with high accuracy and high throughput. Nucleic Acids Res 32:1792-1797.

350. Lewis, P. O. 2003. NCL: a C++ class library for interpreting data files in NEXUS format. Bioinformatics 19:2330-2331.

351. Miller, M. A., W. Pfeiffer, and T. Schwartz. 2010. Creating the CIPRES Science Gateway for inference of large phylogenetic trees, p. 1-8. *In* Proceedings of the 2010 Gateway Computing Environments Workshop (GCE 2010). IEEE, New Orleans, LA.

352. Stamatakis, A. 2014. RAxML version 8: a tool for phylogenetic analysis and post-analysis of large phylogenies. Bioinformatics 30:1312-1313.

353. Le, S. Q., and O. Gascuel. 2008. An improved general amino acid replacement matrix. Mol Biol Evol 25:1307-1320.

354. Pattengale, N. D., M. Alipour, O. R. P. Bininda-Emonds, B. M. E. Moret, and A. Stamatakis. 2010. How many bootstrap replicates are necessary? J Comput Biol 17:337-354.

355. Letunic, I., and P. Bork. 2016. Interactive tree of life (iTOL) v3: an online tool for the display and annotation of phylogenetic and other trees. Nucleic Acids Res 44:W242-W245.

356. Micallef, L., and P. Rodgers. 2014. euler*APE*: drawing area-proportional 3-Venn diagrams using ellipses. PLoS One 9:e101717.

357. Crooks, G. E., G. Hon, J. M. Chandonia, and S. E. Brenner. 2004. WebLogo: a sequence logo generator. Genome Res 14:1188-1190.

358. Punta, M., P. C. Coggill, R. Y., Eberhardt, J. Mistry, J. Tate, C. Boursnell, N. Pang, K. Forslund, G. Ceric, J. Clements, A. Heger, L. Holm, E. L. L. Sonnhammer, S. R. Eddy, A. Bateman and R. D. Finn. 2012. The Pfam protein families database. Nucleic Acids Res 40:D290-D301.

359. Waterhouse, A. M., J. B. Procter, D. M. A. Martin, M. Clamp, and G. J. Barton. 2009. Jalview Version 2 - a multiple sequence alignment editor and analysis workbench. Bioinformatics 25:1189-1191.

360. Pause, A., N. Méthot, and N. Sonenberg. 1993. The HRIGRXXR region of the DEAD box RNA helicase eukaryotic translation initiation factor 4A is required for RNA binding and ATP hydrolysis. Mol Cell Biol 13:6789-6798.

361. Sugita, C., K. Ogata, M. Shikata, H. Jikuya, J. Takano, M. Furumichi, M. Kanehisa, T. Omata, M. Sugiura, and M. Sugita. 2007. Complete nucleotide sequence of the freshwater unicellular cyanobacterium *Synechococcus elongatus* PCC 6301 chromosome: gene content and organization. Photosynth Res 93:55-67.

362. Moreira, D., R. Tavera, K. Benzerara, F. Skouri-Panet, E. Couradeau, E. Gérard, C. L. Fonta, E. Novelo, Y. Zivanovic, and P. López-García. 2017. Description of *Gloeomargarita lithophora* gen. nov., sp. nov., a thylakoid-bearing, basal-branching cyanobacterium with intracellular carbonates, and proposal for *Gloeomargaritales* ord. nov. Int J Syst Evol Microbiol 67:653-658.

363. Turner, S., K. M. Pryer, V. P. W. Miao, and J. D. Palmer. 1999. Investigating deep phylogenetic relationships among cyanobacteria and plastids by small subunit rRNA sequence analysis. J Eukaryot Microbiol 46:327-338.

364. Dandekar, T., B. Snel, M. Huynen, and P. Bork. 1998. Conservation of gene order: a fingerprint of proteins that physically interact. Trends Biochem Sci 23:324-328.

365. Shih, P. M., D. Wu, A. Latifi, S. D. Axen, D. P. Fewer, E. Talla, A. Calteau, F. Cai, N. Tandeau de Marsac, R. Rippka, M. Herdman, K. Sivonen, T. Coursin, T. Laurent, L. Goodwin, M. Nolan, K. W. Davenport, C. S. Han, E. M. Rubin, J. A. Eisen, T. Woyke, M. Gugger, and C. A. Kerfeld. 2013. Improving the coverage of the cyanobacterial phylum using diversity-driven genome sequencing. Proc Natl Acad Sci USA 110:1053-1058.

366. Swingley, W. D., M. Chen, P. C. Cheung, A. L. Conrad, L. C. Dejesa, J. Hao, B. M. Honchak, L. E. Karbach, A. Kurdoglu, S. Lahiri, S. D. Mastrian, H. Miyashita, L. Page, P. Ramakrishna, S. Satoh, W. M. Sattley, Y. Shimada, H. L. Taylor, T. Tomo, T. Tsuchiya, Z. T. Wang, J. Raymond, M. Mimuro, R. E. Blankenship, and J. W. Touchman. 2008. Niche adaptation and genome expansion in the chlorophyll *d*-producing cyanobacterium *Acaryochloris marina*. Proc Natl Acad Sci USA 105:2005-2010.

367. Robertson, B. R., N. Tezuka, and M. M. Watanabe. 2001. Phylogenetic analyses of *Synechococcus* strains (cyanobacteria) using sequences of 16S rDNA and part of the phycocyanin operon reveal multiple evolutionary lines and reflect phycobilin content. Int J Syst Evol Microbiol 51:861-871.

368. Juteršek, M., M. Klemenčič, and M. Dolinar. 2017. Discrimination between *Synechocystis* members (cyanobacteria) based on heterogeneity of their 16S rRNA and ITS regions. Acta Chim Slov 64:804-817.

369. Nelson, W. C., Y. Maezato, Y. W. Wu, M. F. Romine, and S. R. Lindemann. 2015. Identification and resolution of microdiversity through metagenomic sequencing of parallel consortia. Appl Environ Microbiol 82:255-267.

370. Paul, R. 2014. Genome Sequencing of *Leptolyngbya* Heron Island, 2A crystal structure of phycoerythrin and spectroscopic investigation of chromatic acclimation. PhD Thesis, Arizona State University, Tempe, Arizona.

371. Wang, S., Y. Hu, M. T. Overgaard, F. V. Karginov, O. C. Uhlenbeck, and D. B. McKay. 2006. The domain of the *Bacillus subtilis* DEAD-box helicase YxiN that is responsible for specific binding of 23S rRNA has an RNA recognition motif fold. RNA 12:959-967.

372. Nishiyama, Y., D. A. Los, and N. Murata. 1999. PsbU, a protein associated with photosystem II, is required for the acquisition of cellular thermotolerance in *Synechococcus* species PCC 7002. Plant Physiol 120:301-308.

373. Gerdes, S. Y., O. V. Kurnasov, K. Shatalin, B. Polanuyer, R. Sloutsky, V. Vonstein, R. Overbeek, and A. L. Osterman. 2006. Comparative genomics of NAD biosynthesis in cyanobacteria. J Bacteriol 188:3012-3023.

374. Li, W., S. Schulman, R. J. Dutton, D. Boyd, J. Beckwith, and T. A. Rapoport. 2010. Structure of a bacterial homolog of vitamin K epoxide reductase. Nature 463:507-512.

375. Rowland, J. G., W. J. Simon, J. S. S. Prakash, and A. R. Slabas. 2011. Proteomics reveals a role for the RNA helicase CrhR in the modulation of multiple metabolic pathways during cold acclimation of *Synechocystis* sp. PCC6803. J Proteome Res 10:3674-3689.

376. Kaberdin, V. R., and U. Bläsi. 2013. Bacterial helicases in post-transcriptional control. Biochim Biophys Acta 1829:878-883.

377. Golden, S. S. 1994. Light-responsive gene expression and the biochemistry of the photosystem II reaction center, p. 693-714. *In* D. A. Bryant (ed.), The Molecular Biology of Cyanobacteria. Kluwer, The Netherlands.

378. Kim, J., P. Gamble Klein, and J. E. Mullet. 1991. Ribosomes pause at specific sites during synthesis of membrane-bound chloroplast reaction center protein D1. J Biol Chem 266:14931-14938.